INFLUENCE OF PROCESSING ON THE STRUCTURE AND PROPERTIES OF SEMI-CRYSTALLINE POLYMER SYSTEMS: 1) BIODEGRADABLE STARCH/POLY(ETHYLENE-VINYL ALCOHOL) BLENDS AND 2) POLYOLEFINIC THERMOPLASTICS

by

STEPHANIE SIMMONS

B.S., Chemical Engineering
University of Massachusetts at Amherst,
1990

Submitted to the Department of Chemical Engineering
in Partial Fulfillment of the Requirements
for the Degree of

DOCTOR OF PHILOSOPHY

at the

MASSACHUSETTS INSTITUTE OF TECHNOLOGY

June, 1995

© 1995 Massachusetts Institute of Technology
All Rights Reserved

Signature of Author .....
Program in Polymer Science and Technology, Dept. of Chemical Engineering
April 25, 1995

Certified by .....
Edwin L. Thomas, Morris Cohen Professor
Department of Materials Science and Engineering
Thesis Advisor

Accepted by: .....
Robert E. Cohen, Professor
Department of Chemical Engineering
Chairman, Committee for Graduate Students

MASSACHUSETTS INSTITUTE
OF TECHNOLOGY
JUL 10 1995
LIBRARIES
ARCHIVES

INFLUENCE OF PROCESSING ON THE STRUCTURE AND PROPERTIES OF SEMI-CRYSTALLINE POLYMER SYSTEMS: 1) BIODEGRADABLE STARCH/POLY(ETHYLENE-VINYL ALCOHOL) BLENDS AND 2) POLYOLEFINIC THERMOPLASTICS

by

STEPHANIE SIMMONS

Submitted to the Department of Chemical Engineering on April 25, 1995 in partial fulfillment of the requirements for the Degree of Doctor of Philosophy in Polymer Science and Technology

ABSTRACT

The mechanisms by which molecular parameters and processing influence the morphology and subsequent mechanical properties of semi-crystalline polymer systems were examined. Two distinct systems: 1) biodegradable starch/poly(ethylene-vinyl alcohol) blends and 2) polyolefinic thermoplastics were investigated. Processing methods which induce varying degrees of uniaxial and biaxial orientation were of prime interest. Model applications included melt fiber spinning of starch-based blends and the development of a lab-scale technique for preparing thin, equi-biaxially oriented polyolefin films for direct observation in TEM.

Starch/poly(ethylene-vinyl alcohol) blends were examined in order to establish relationships between the blend composition, processing history, and the resultant physical properties, which will assist in the subsequent development of these and similar starch-based materials for use in biodegradable thermoplastic applications (such as packaging). Three varieties of corn starches: 1) Waxy Maize (WM), 2) Native Corn (NC), and 3) high amylose Hylon VII (HY), which varied in their branch content (amylose to amylopectin ratio) and molecular weight, were employed. The starches were extrusion blended with poly(ethylene-vinyl alcohol) (EVOH) containing 56 mol% VOH over a systematic compositional range from 100% starch to 0% starch. Glycerin and water were employed as plasticizers. Wide-angle x-ray scattering, differential scanning calorimetry, scanning electron microscopy, and transmission electron microscopy (TEM) techniques were used for morphological characterization. Mechanical testing was also performed.

All starches were destructurized upon compounding and a fine dispersion was achieved via extrusion blending with EVOH. Both the Native Corn and Hylon VII blends were phase separated and also exhibited some miscibility between the polymer components as evident in EVOH melting point depression, smaller domain sizes, lower contrast between starch-rich and EVOH-rich phases, and increased resistance to moisture and enzyme etching treatments. Starches containing amylose exhibited complexation and crystallinity in the starch fraction, although most of the crystallinity in the blends was attributed to the EVOH component. Waxy maize blends were well phase separated and underwent phase coarsening as a function of time in the melt ($d \sim t^{1/8}$). At least four phases were formed in these systems: 1) amorphous starch, 2) amorphous EVOH, 3) crystalline amylose, and 4) crystalline EVOH. Phase separation between linear amylose and highly branched amylopectin is also suggested by the data. When subjecting the blends to capillary flow, orientation of both starch-rich and EVOH-rich domains was observed at various compositions with the EVOH component undergoing significantly more orientation relative to starch as evident by the presence of EVOH-rich fibrils although molecular orientation of the polymer chains was not observed.

Specific details on the use of transmission electron microscopy are given for examining the morphology of semi-crystalline, starch-based blends. Emphasis is placed

on sample preparation, contrast mechanisms, staining, and specimen sensitivity to the electron beam in order to obtain optimum electron optical operating conditions for imaging these blend specimens in TEM. Both starch and EVOH were shown to be very beam sensitive: the maximum allowable beam dosages for the crystalline fraction of these components is estimated at less than 3×10^{-3} C/cm^2 and approximately 3.5×10^{-3} C/cm^2, respectively (at 100 keV and room temperature). Both polymers encountered significant mass-thickness variations which at moderate beam dosage ($> 6.0 \times 10^{-3}$ C/cm^2) led to contrast-reversal of the blend morphology. For the starch/EVOH blends, EVOH was observed to be the matrix component even at very high starch concentrations (up to 70%). Domain sizes of starch were observed to range from less than 0.1 μm to greater than 3 μm indicating that all of the starches were destructurized in the blends. Differences in the blend structure were also observed at similar starch compositions (50%) for three corn starch varieties. Blends containing amylose appeared to be partially miscible based on contrast differences between Waxy Maize, Native Corn, and high amylose Hylon VII starch blend series. Cross-sectional TEM was demonstrated as a means to examine structural gradients in thermoplastically formed articles.

The effect of composition and starch variety on both shear and elongational flow for the starch/EVOH blends was studied using melt fiber spinning as a model application. Processability (i.e. spinnability) primarily depended upon the starch content in the blends and secondarily on starch type. Maximum spin draw ratios, λ_S, for these materials ranged from less than 1, for neat starch blends, to 215 for the EVOH/GLY control (above this limit, cohesive fracture of the filament occurred). Overall, blends containing 50% or more EVOH had sufficient elongational properties to consistently spin draw ($\lambda_S > 1$). Hylon VII blends formed consistent fibers at 30% starch content, but at compositions of 50% starch, no spinnability was observed. Waxy maize blends with as much as 70% starch had the ability to draw ($\lambda_S = 3$). Die swell increased with amylopectin content (reaching a value of 1.8 for the waxy maize/glycerol blend) and flow instabilities in the Waxy Maize blends were often observed. The Native Corn starch blends had the best overall processability in that fibers were attainable at up to 60% starch, and extrudate flow from the spinnerette was observed to be relatively stable. The effect of moisture content was examined by testing fibers as processed and after conditioning to 50% RH; a decrease in moisture content resulted in poorer flow and elongational properties for most of the blends. When fibers were subsequently cold drawn, the EVOH component was found to undergo significant molecular orientation relative to starch, which exhibited no orientation in its crystalline fraction. Most of the elongational and mechanical properties of the blend fibers were attributable to the EVOH matrix component, and interfacial debonding of the EVOH matrix from the starch-rich domains was one route to mechanical failure in items made with starch/EVOH blends. The fiber surfaces possessed a coating of the EVOH component, and appeared rough due to the presence of high modulus, relatively undeformable starch-rich domains.

Finally, a model technique for preparing thin, biaxially oriented films was developed in which a flexible substrate is employed as a 'Bubble Support' for a molten polyolefin layer which simultaneously undergoes equi-biaxial deformation and crystallization. The resulting film is thin enough for direct observation in TEM. High density polyethylene was employed to demonstrate this technique which also can be used on a wide range of semi-crystalline thermoplastics. Alteration of the experimental conditions (i.e. temperature, inflation rate, cooling time) led to a variety of observed morphologies that resulted from changes in the crystallization, relaxation, and deformation behavior of the polymer.

Thesis Supervisor: Dr. Edwin L. Thomas
Morris Cohen Professor of Materials Science and Engineering

Acknowledgments

Sincere thanks to my advisor, Prof. Edwin L. Thomas, for his guidance of my research over the years spent here at MIT. I would also like to thank Professors Robert Armstrong and Edward Merrill for serving on my thesis committee.

With regards to the starch/EVOH project, I'd like to express gratitude to A. Montana, T. Sullivan, and E. George at Novon Products, a former division of Warner-Lambert, for supplying materials, helping in the compounding of the starch-EVOH blends and for technical discussions. Stan Shimo at the EVAL Company of America was also helpful in supplying poly(ethylene-vinyl alcohol) samples. I appreciated the collaboration with Dr. Dave VanderHart that sprouted from a discussion of EVOH crystallinity at an APS meeting so long ago. Major funding for this work was provided by the United States Department of Agriculture (Grant 91-COOP-2-6108).

I'm also thankful to D. Shulz, D. Lohse, and M. Disko of Exxon for supplying materials and helping with idea of the Bubble Support apparatus. I appreciate the help Dr. Lewis Fetters at Exxon for synthesizing and characterizing polyolefin material for some work on model polyolefins not directly related to this thesis. Funding from Exxon Corporation is also appreciated.

Thanks to M. Frongillo and A. Garrett-Reed of the CMSE Electron Microscope facility for their help. Thanks also to J. Adario of the CMSE X-Ray Diffraction Facility.

In addition, acknowledgement of the National Science Foundation for a three-year graduate fellowship and the Program in Polymer Science and Technology for my first year fellowship is made.

I'm thankful for my interaction with other members of the Thomas research group. Dr. Ramon Albalak and Dr. Marcelo Villar are acknowledged for their assistance in helping me understand the rheology and processing of the starch-based systems. I thank the number of undergraduates who worked on the starch project with me: Nancy Shoendorf, Derek Rucker, Kelly Stengel, Laura Elsberg, and Javier Nazario. To the other graduate students and the post docs who spent many hours in the Thomas lab, thanks for encouraging me to finish. Special thanks to John Chen for his insight into Polymer Physics and for our Maelstrom adventures.

I thank the members of my family: my father, Charles, and my mother, Elizabeth, who taught me both persistence and the importance of hard work. I thank my sisters, Debbie and Karen, for their friendship.

Finally, I thank my best friend and husband, Walter E. Coffen, Jr. whose love, patience, and support have helped me through my years at MIT and to whom I dedicate this thesis.

Table of Contents

ABSTRACT 2

ACKNOWLEDGEMENTS 4

TABLE OF CONTENTS 5

LIST OF FIGURES 8

LIST OF TABLES 16

CHAPTER 1: Overview of Thesis 17

CHAPTER 2: Background: Structure and Properties of Starch 22

- Introduction 22
  - Starch-based Systems for Biodegradable Thermoplastic Applications 22
- What is Starch? 24
- Morphological Investigations of Starch 25
  - Morphological Techniques 25
  - Starch Morphology 29
  - Thermal Behavior of Starch 43
  - Thermoplastic Starch 49
- Blend Morphology 57
  - Starch Based Systems 60
- Conclusions 62
- References 65

CHAPTER 3: Structural Characteristics of Biodegradable Thermoplastic Starch/Poly(ethylene-vinyl alcohol) Blends 76

- Abstract 76
- Introduction 77
- Experimental 80
  - Raw Materials 80
  - Blend Compounding 81
  - Sample Preparation 83
  - Methods of Characterization 83
    - Wide-angle x-ray scattering 83
    - Thermal analysis 84
    - Scanning Electron Microscopy 85
    - Transmission Electron Microscopy 85
    - Moisture Content 86
- Results and Discussion 86
  - Observation of Extrudate (pellets) After Compounding 87
  - Wide-angle X-ray Scattering 90
    - Crystalline Phase Types 90
    - Physical Aging Studies 97
    - Temperature Dependence of WAXS 98
  - Thermal Analysis 101

The S-Transition 109
EVOH Crystallization 110
Electron Microscopy Studies 114
SEM of Untreated Fracture Surfaces 114
Blend Morphology as Observed by SEM and TEM 117
Phase Coarsening of Starch/EVOH Blends 133
SEM of Etched Filaments - Effect of Capillary Flow 136
Structural Influences on Starch/EVOH Blend Processability and Properties 141
Conclusions 143
References 145
Supplementary Tables 150

CHAPTER 4: The Use of Transmission Electron Microscopy to Study the Blend Morphology of Starch/Poly(ethylene-vinyl alcohol) Thermoplastics 157

Abstract 157
Introduction 158
Experimental 161
Materials 161
Sample Preparation 162
Instrumentation 164
Image Analysis 164
Results and Discussion 165
Beam Sensitivity of Starch and EVOH 165
Contrast Mechanisms 172
Staining of Starch-rich Domains 178
Contrast Changes as a function of Beam Dosage 180
Compositional Influence on the Morphology of NC Blends 189
Comparison of Blend Morphologies for Different Starch Types with EVOH 192
Cross-sectional TEM of a Starch/EVOH Fiber 195
Conclusions 198
References 200

CHAPTER 5: Melt Fiber Spinning of Thermoplastic Blends of Starch and Poly(ethylene-vinyl alcohol) 204

Abstract 204
Introduction 205
Fiber Spinning 208
Fiber Spinning of Blends 212
Experimental 215
Materials 215
Fiber Spinning Apparatus 216
Fiber Spinning Procedure 219
Characterization Methods 220
Results and Discussion 221
Fiber Spinning Results 222
Morphology 227
Mechanical Properties 248
Conclusions 254
References 256

Supplementary Tables 259

CHAPTER 6: Bubble Support Method for Preparing Thin, Equi-Biaxially Stretched Polyolefin Film for Direct TEM Observation 267

Abstract 267
Introduction 267
Analysis of Experiment 273
Experimental Procedure 277
Results and Discussion 279
Conclusions 296
References 297

CHAPTER 7: Conclusions/Directions for Future Work 300
Starch-Based Thermoplastics 300
Polyolefinic Thermoplastics 306

APPENDICES
Appendix A. Crystallization of Poly(ethylene-vinyl alcohol) 308
Appendix B. Starch/EVOH Blown Films 315

List of Figures

2.1. The chemical structures of amylose (AM) and amylopectin (AP) 26

2.2. Structural levels associated with native corn starch: Starch exists in the kernels of (a) corn [from Rhoades, 1993] in the form of (b) granules (5-25 μm), which consist of growth rings (120-400 nm) and a predominantly amylose core (c). Racemose packing (d) of alternating layers of crystalline and amorphous polymer chains (d ~ 8 nm) is hypothesized [from French, 1984]. A possible arrangement of components in a starch crystallite is depicted in (e) [from Galliard, 1987]. 30

2.3. Various types of ultrastructural organization within starch granules are evident depending upon the TEM preparation method employed: a) possible radial arrangement of amylose molecules, b) distribution of amorphous starch polymers, and c) arrangement of crystalline starch (amylopectin) [from Kassenbeck, 1978] 34

2.4. Kassenbeck's TEM image of corn starch depicting the crystalline periodicity of amylopectin. The racemose model for amylopectin is proposed with crystallite sizes of 62 Å (see inset) [from Kassenbeck 1978] 35

2.5. Small angle X-ray diffraction patterns from potato starch suspensions: a) native, and hydrolyzed in 2.2N HCl at 35°C for b) 1 day, c) 2 days, and d) 4 days [from Oostergetel 1989]. 36

2.6. Wide-angle x-ray diffraction patterns for 'A', 'B', 'C', and 'V' type starch crystallization [from Zobel, 1988]. On the right are schematics of WAXS patterns depicting ring intensity [from Katz, 1930]. 38

2.7. The packing of amylose chains into the unit cells of a) 'A' type starch (monoclinic: a = 21.24 Å, b = 11.72 Å, c = 10.60 Å, γ = 123.5°) and b) 'B' type starch (hexagonal: a = b = 18.5 Å, c = 10.4 Å). Upper representations depict chains along the fiber axis; the lower representations are projections of the structure onto the (a,b) plane. Closed dots indicate the presence of water molecules. Hydrogen bonding is indicated by dashed lines [from Imberty 1991]. 42

2.8. Various types of gelatinization behavior as studied by Gough and Pybus [from Banks and Greenwood 1975]. 45

2.9. DSC traces for native potato starch as a function of volume fraction of water added (G = gelatinization endotherm; M1 = melting endotherm) [from Blanshard, 1987]. 46

2.10. The dependence of the glass transition temperature on moisture content for native and pre-gelatinized wheat starch [from Zeleznak, 1987]. 48

2.11. The time and temperature ranges of various processes for modifying starch. Manufacturing of thermoplastic starch often occurs in the shaded region termed "extrusion cooking" [from Wiedmann, 1987]. 50

2.12. A simplified model of starch degradation during extrusion [from Gomez, 1984]. Conditions of shear, heat, and moisture cause starch to undergo a number of transitions form its native state. (Note: this model does not take into account changes in crystallinity or chain scission of the amylopectin fraction.) 50

2.13. WAXS spectra of corn starch extruded at 70, 95, 135, 170, 185, 200, and 225°C. a) Initial moisture content before extrusion, 22 wt%, b) After reconditioning to 30 wt% moisture content [from Mercier, 1979]. 53

2.14. SEM micrographs showing incompletely destructurized granules that are present in a) an extruded ribbon, and b) a blown film of a 50:50 corn starch/EVOH (68% VOH) blend. A Brabender single-screw extruder was employed. (Films prepared at Army Research Facility, Natick, MA). 55

3.1a. Wide-angle X-ray powder diffraction spectra for selected Waxy Maize (WM) blends compared with the EVOH control: a) EVOH/GLY, b) WM30, c) WM50, and d) WM100. 92

3.1b. Wide-angle X-ray powder diffraction spectra for selected Native Corn (NC) blends compared with the EVOH control: a) EVOH/GLY, b) NC30, c) NC50, d) NC70, and e) NC100. 93

3.1c. Wide-angle X-ray powder diffraction spectra for selected Hylon VII (HY) blends compared with the EVOH control: a) EVOH/GLY, b) HY30, c) HY50, and d) HY100. 94

3.2. Wide-angle X-ray diffraction spectra for the starches before compounding: a) Amioca Waxy Maize, b) Melojel Native Corn, and c) EKFl. Hylon VII. 95

3.3. Wide-angle X-ray diffraction spectra for the a) HY100 blend, b) NC100 blend, c) WM100 blend, and d) processing additives. 96

3.4. Wide-angle diffraction spectra of the HY100 blend taken at a) 20°C, b) at 60°C, and c) after cooling to 25°C. Note the disappearance of the peak at 22.5°. 99

3.5. Wide-angle X-ray diffraction spectra taken isothermally at various temperatures for an HY100 powder sample: a) 20°C, b) 60°C, c) 100°C, d) 150°C, and e) 230 °C. 100

3.6. DSC curves for a) first heating, b) cooling, and c) second heating cycles for the NC70 blend. Scan rates were 10°C/min. Sample was conditioned to 50% RH before testing. 103

3.7. Peak S transition temperatures as measured by DSC for the heating/cooling/heating cycles of the HY, NC, and WM model blends which were conditioned to 50% RH. Values on the right of the graph correspond to peak transition temperatures for the neat triglyceride additives. 105

3.8. Enthalpy of the "S" transition for the HY, NC, and WM model blends which were conditioned to 50% RH. 106

3.9. Peak Poly(ethylene-vinyl alcohol) transition temperatures for the heating/cooling/heating cycles of the HY, NC, and WM series of model blends which were conditioned at 50% RH. Values for Heat 1 and Heat 2 represent melting transitions. Values for Cool 1 represents EVOH crystallization. 107

3.10. Normalized EVOH transition enthalpy for the heating/cooling/heating cycles of the model blends. 108

3.11. Glycerin and moisture contents for the NC series of blends after conditioning to 50% RH for one week. 111

3.12. a) Peak melting temperatures of EVOH and b) moisture contents for the NC blends after conditioning at 0.5 and 50% RH for one week (DSC first heat cycle) 113

3.13. Scanning electron micrographs of liquid Nitrogen temperature fracture surfaces for the a) WM50, b) NC50, and c) HY50 extrudates. Images on the right side represent magnified views of the surfaces on the left. Distinct phase domains are not evident using this method. 115

3.14. Scanning electron micrographs of a.) untreated and b.) α-amylase etched fracture surfaces of a WM70 filament. Images on the right represent magnified views of the images on the left. Foaming is evident in the untreated filament. Large-scale removal of the starch-rich domains occurs during enzymatic etching. 118

3.15. Scanning electron micrographs of α-amylase etched fracture surfaces of a) WM30, b) WM50, c) WM70, and d) WM85 extrudates. Discrete starch domains are evident at compositions less than 50% starch. EVOH-rich fibrils are observable at higher starch compositions. Collapse of the WM85 filament occurred during etching and EVOH-rich filaments are present in the collected residue. 121

3.16. Scanning electron micrographs of α-amylase etched fracture surfaces of a) NC30, b) NC50, c) NC70, and d) NC85 extrudates. Discrete starch-rich domains are present in the NC30 filament. Starch removal occurs in the NC50 blend, but domains are less discrete. Etching of filaments containing more than 50% starch is less effective at distinguishing between starch-rich and EVOH-rich domains. 124

3.17. Scanning electron micrographs of α-amylase etched fracture surfaces of a) HY30, b) HY50, c) HY70, and d) HY85 extrudates. The etchant had no effect on blends containing less than 50% starch. Some texture development in blends containing more than 50% starch occurred, but domains corresponding to EVOH-rich or starch-rich compositions are not distinguishable. 126

3.18. Transmission electron micrographs of iodine stained starch/EVOH (50:50) blends: a) WM50, b) NC50, and c) HY50 extrudate sections. 129

3.19. Scanning electron micrographs of WM30 extrudate that has been held at 150°C for a) 0.01 min.. b) 0.1 min., c) 1 min., d) 10 min., e) 100 min., and f) 1000 min. Samples were etched with α-amylase aqueous solution prior to viewing in the microscope..... 134

3.20. Scanning electron micrographs of various surfaces of a WM30 filament (d = 710 μm); 1) surface, 2) axial cross-section, 3) longitudinal cross-section. Draw direction is vertical (draw ratio = 1). Images on the left are of untreated filaments (a). Images on the right (b) are the similar filaments which have been etched with α-amylase aqueous solutions..... 137

3.21. Scanning electron micrographs of various surfaces of a WM70 filament (d = 1080 μm); 1) surface, 2) axial cross-section, 3) longitudinal cross-section. Draw direction is vertical (draw ratio = 1). Images on the left are of untreated filaments (a). Images on the right (b) are the similar filaments which have been etched with α-amylase aqueous solutions..... 139

4.1. Bright field micrographs of the HY100 blend (Hylon VII high amylose starch compounded with glycerin and water). a) The morphology and electron diffraction pattern observed under low dose conditions (D ~ 9 x 10^{-4} C/cm^2). b) The same region after 20 seconds total exposure to the electron beam (D ~ 3.5 x 10^{-3} C/cm^2)..... 167

4.2. Bright field micrographs showing a microtomed section of the EVOH/GLY blend (EVOH compounded with Glycerin). a) The morphology and electron diffraction pattern observed under low dose conditions (D ~ 9 x 10^{-4} C/cm^2). b) The same region after 20 seconds total exposure to the electron beam (D ~ 3.5 x 10^{-3} C/cm^2)..... 170

4.3. Through focus series of a NC30 microtomed section: a) ΔZ ~ -13.6 μm, b) near focus, c) ΔZ ~ + 13.6 μm. Phase contrast arises as the microscope is defocused (a and c). Note that the sample undergoes beam damage as it was imaged (order of image taking and estimated total beam dosage: b) ~ 9 x 10^{-4} C/cm^2, a) ~ 1.9 x 10^{-3} C/cm^2, c) 2.8 x 10^{-3} C/cm^2)..... 176

4.4. Comparison of intensity profiles obtained from micrographs taken under similar conditions (near focus, 10kX, 4 sec. exposure, e^- dose ~ 9 x 10^{-4} C/cm2) for an unstained and iodine stained section of an NC30 blend. Contrast between the starch-rich domains (appearing at lower intensities than the EVOH matrix) increases from 0.05 to 0.11. Note also that the average intensity of the image, the optical density of the micrograph negative, decreases as it is stained (Average values are shown by the dashed line and at the left of the graph.) 181

4.5. Bright field micrographs showing an iodine stained NC30 blend section as a function of time in the beam at a current density of approximately 2.3 x 10^{-4} amp/cm^2 (at 5 kX): a) Initial exposure, t = 4 sec, D ~ 9.3 x 10^{-4} C/cm^2; b) t = 34 sec, D ~ 7.9 x 10^{-3} C/cm^2; c) t = 94 sec, D ~ 2.2 x 10^{-2} C/cm^2; d) 184 sec., D ~ 4.3 x 10^{-2} C/cm^2. Microvoids are indicated by "MV", cracks in the starch-rich phase due to microtoming are indicated by "CR" in (a). Thinner areas are observed adjacent to the starch-rich domains and are most likely due to deformation at the starch-rich/EVOH-rich interface during microtoming. The line shown in (a) represents the region selected for intensity plots displayed in figure 4.6. 182

4.6. Intensity profiles of an iodine stained NC30 sample as a function of time in the electron beam at a current density of approximately 2.3 x 10^{-4} amp/cm^2 (at 5 kX). Plots are arbitrarily shifted along the y-axis to eliminate overlapping of profiles. Note, contrast between the starch-rich and EVOH-rich domains initially increases, then falls as the total beam dosage increases. Average normalized intensities (I/Io), total beam exposure time, t, and estimated beam dosage, D, are shown at the right of the figure. 184

4.7. Bright field micrographs showing an iodine stained NC30 blend section as a function of time in the beam at a current density of approximately 2.3 x 10^{-4} amp/cm^2 (at 10 kX): a) Initial exposure, t = 4 sec, D ~ 3.7 x 10^{-3} C/cm^2; b) t = 64 sec, D ~ 6.0 x 10^{-3} C/cm^2; c) t = 124 sec, D ~ 1.1 x 10^{-1} C/cm^2; d) t = 304 sec, D ~ 2.8 x 10^{-1} C/cm^2. The line shown in (a) represents the region for intensity plots displayed in figure 4.8. 186

4.8. Intensity profiles of an iodine stained NC30 sample as a function of time in the electron beam under similar operating conditions as in Figure 4.6, but at higher magnification (at 10 kX). Plots are arbitrarily shifted along the y-axis to eliminate overlapping of profiles. Contrast decreases to zero then reverses as the specimen undergoes significant beam damage. Average normalized intensities (I/Io), total beam exposure time, t, and estimated beam dosage, D, are shown at the right of the figure. 188

4.9. Bright field electron micrographs of representative Native Corn starch/EVOH blends which were stained with iodine: a) NC15, b) NC30, c) NC50, d) NC70, and e) NC85. EVOH appears to be the matrix component even at high compositions (up to 70%) starch. Total dose per image is estimated to be less than 1 x 10^{-3} C/cm^2 190

4.10. Bright field electron micrographs showing the effect of starch type on the blend morphology for 50:50 starch/EVOH compositions: a) Waxy Maize (WM50), b) Native Corn (NC50), and c) Hylon VII (HY50) blends. As the amylose content of the starch component increases, the starch-rich domain sizes decrease and contrast between starch-rich and EVOH-rich regions decrease. 193

4.11. Bright field electron micrograph showing the near surface region of a Native Corn starch/EVOH fiber (NC50). The fiber was embedded in epoxy and stained with iodine vapor. The epoxy appears in the top of the micrograph. The EVOH component coats the fiber surface. 196

5.1. Schematic of the melt fiber spinning process. Molten polymer is forced through a spinnerette with dimensions (l_o/d_o). The extrudate is drawn at a velocity, v_f, to form a fiber of diameter, d_f. The polymer solidifies due to cooling by air flow at a distance, z, from the spinnerette. 209

5.2. Schematics of possible phase morphology arrangements for immiscible polymer blend fibers: a) side-by-side, b) sheath-core, c) matrix-fibril, d) stratified, and e) co-continuous (interpenetrating network). From D.R. Paul, 1978. 213

5.3. The Alex James One-Shot Fiber Spinning Rig: a) side view, b) front view ... 217

5.4. Schematic of a) the sample cell arrangement and b) cross-sectional view showing unmelted sample within the cell chamber. 218

5.5. Die Swell ratios as determined for the starch/EVOH blends: a) as stored, b) after conditioning at 50% RH. 225

5.6. Maximum spin draw ratios as determined for the starch/EVOH blends: a) as stored, b) after conditioning pellets at 50% RH. 226

5.7. Flat film WAXS patterns for native corn/EVOH blends: a) NC50 pellet, b) NC50 'as spun' fiber (λ_s = 11), c) cold drawn fiber (T = 110°C, λ_c = 4, λ_{total} ~ 44). For reference are: d) NC100 pellet, e) EVOH/GLY control pellet, f) comparison of scattering patterns for undrawn and drawn NC50 with NC100 and EVOH/GLY pellet references. Note: no orientation in the starch crystalline component is apparent, even after cold drawing. 228

5.8. SEM micrographs showing the surface appearance of fibers of various starch compositions and draw ratios: a) HY series, b) NC series, c) WM series. 231

5.9. SEM micrographs depicting the change in fiber surface appearance as a function of composition: a) NC50, λ_s = 23 , b) NC40, λ_s = 17 , c) NC30, λ_s =63 , d) NC15, λ_s = 95. (Draw direction vertical.) Fibril formation of the EVOH-rich phase is evident on the fiber surfaces. As starch content increases, the number of nodules and cavities present at the surface also increases. 236

5.10. TEM micrograph of a microtomed section containing a deformation zone in a NC50 blend fiber. Starch domains are stained dark with iodine vapor. 238

5.11. SEM micrograph of a NC50 fiber fracture surface resulting from mechanical behavior tests (room temperature, 50% RH). 241

5.12. TEM micrographs depicting an axial cross-sectional view of the surface region of an NC50 fiber (d = 175 μm, λ_s ~ 20). Starch is stained dark with iodine vapor. 243

5.13. SEM micrographs showing the effect of boiling water on the surface of starch/EVOH blends: a) an HY50 filament, b) an NC50 fiber, and c) a WM50 fiber. No change in the surface appearance of the HY50 filament is apparent. Nodules (~ 1 μm) are formed on the NC50 fiber. No oriented or nodular texture is apparent on the WM50 treated surface which initially exhibited EVOH-rich fibrils. 246

5.14. Mechanical behavior of selected starch/EVOH "fibers" with their corresponding draw ratios: a) HY series, b) NC series, and c) WM series. The EVOH/GLY control is shown in each plot for comparison. Testing performed after conditioning at 50% RH. 249

5.15. Mechanical properties of the starch/EVOH blend filaments (draw ratio ≤ 1) as a function of starch content: a) tensile modulus, b) tensile strength, and c) ultimate tensile modulus. 251

5.16. The effect of spin draw ratio on the tensile modulus for selected starch/EVOH blend fibers: a) 50% starch (dry basis), b) 30% starch, and c) 15% starch, EVOH/GLY control. 252

6.1. Schematic diagram of the Petermann method for preparing thin, oriented polymer films [after Petermann, 1979] 270

6.2. Bright field phase contrast (objective lens defocus ~ - 1.8 μm) transmission electron micrograph and electron diffraction pattern of a high density polyethylene 'Petermann' film. Draw direction is vertical. 271

6.3. Idealized axisymmetric deformation of a free bubble. By symmetry, the two principal directions of stress, π, are in the meridian (11) and circumferential (33) directions. Stress in the normal direction is equal to zero. 274

6.4. Schematic of the biaxial deformation experiment: a) Polymer melt is formed from a dilute solution deposited on a clamped flexible substrate. b) After shutting off the heat gun at t = 0, and waiting a period of time, t_{wait}; the substrate is inflated and the polymer deformed during the interval, $t_{inflate}$. 278

6.5. Bright-field transmission electron micrograph of a biaxially, melt drawn polyethylene film exhibiting an undeformed spherulitic morphology (t_{wait} = 0, $t_{inflate}$ = 3 s, AE = 9.3). Relaxation of the polymer chains prior to crystallization occurs after melt is deformed. 281

6.6 Bright field micrograph of a biaxially, melt drawn polyethylene film exhibiting a network of crystallized fibrils (T_i = 158°C, $T(t_{wait}$ = 2 s) ~ 136°C, $t_{inflate}$ = 3 sec, AE = 8.5). Biaxial deformation dominates the morphology of this particular film. 283

6.7. a) Magnified image of a selected area in figure 6.6. Note the distribution of fibrils approximately 70 Å in size extending in various directions and cavitated areas of the polymer film. b) Corresponding electron diffraction pattern taken normal to the film indicates a primarily planar isotropic texture. 286

6.8. a) Bright-field electron micrograph of a thicker, biaxially oriented film. exhibiting a disordered lamellar structure formed during simultaneous equi-biaxial stretching and crystallization (conc = 0.5 w/v%, Ti = 150°C, $T(t_{wait}$ = 1 s) ~ 135°C, $t_{inflate}$ = 3 s, AE = 10.6) 289

6.9. Bright-field electron micrograph of a thin polyethylene films initially exhibiting a spherulitic morphologies, but subsequently stretched to different areal elongations (T_i = 140°C, $T(t_{wait}$ = 3 s) ~ 113°C): a) $t_{inflate}$ = 1 sec., AE = 3.1; b) $t_{inflate}$ = 2 sec., AE = 7.5; c) $t_{inflate}$ = 3 sec., AE = 10.5. 282

A.1. Differential scanning calorimetry results (second heat) for poly(ethylene vinyl alcohol) as a function of vinyl alcohol content (0, 10, 18, 56, 68, 73, and 99+ mol% VOH). Scans were taken at a rate of 20°C/min (Al pans). Single melting endotherms are observed for all copolymer compositions. 312

A.2. Wide-angle x-ray diffractometry spectra for poly(ethylene-vinyl alcohol) of varying vinyl alcohol contents: a) 0 mol% (LDPE), b) 10 mol%, c) 18 mol%, d) 56 mol%, e) 68 mol%, f) 73 mol%, and g) 99+ mol% (PVOH). Corresponding Miller indices for LDPE and PVOH are shown in (a) and (g). 313

A.3. Lattice spacings for poly(ethylene-vinyl alcohol) as a function of vinyl alcohol content. Note: no samples were examined between 18 and 56% VOH. 314

B.1. Scanning electron micrographs of select starch/EVOH 'as blown' films: a) HY50, AE ~ 7.7, b) NC50, AE ~ 12.5, c) WM50, AE ~ 10; and d) NC30, AE ~ 7.7. (Specimens were coated with AuPd prior to viewing in SEM). 319

B.2. Scanning electron micrographs depicting the surface structure of the starch/EVOH blown films (shown 'as blown' in figure B.1.) after immersion in boiling water for 15 seconds: a) HY50, b) NC50, c) WM50, and d) NC30. (Specimens were dried and then coated with AuPd prior to viewing in SEM.) 321

List of Tables

2.1. Shape, Size, and Properties of Various Starch Granules [from Blanshard, 1987; Young, 1984] 27

2.2. Unit cell dimensions of amylose and amylose complexes [from Blanshard, 1987; Imberty, 1991] 41

3.1. Model Starch-Poly(ethylene-co-vinyl alcohol) Blends: Nomenclature, Composition, and Processing Parameters 82

3.2. Appearance and Flexibility of the Model Blends 88

3.3. "S" Transition DSC Data
a) High Amylose Starch (Hylon VII) Blends 150
b) Native Corn (NC) Starch Blends 151
c) Waxy Maize (WM) Starch Blends 152

3.4. Poly(ethylene-co-vinyl alcohol) Melting/Crystallization DSC Data
a) High Amylose Starch (Hylon VII) Blends 153
b) Native Corn (NC) Starch Blends 154
c) Waxy Maize (WM) Starch Blends 155
d) EVOH/Glycerin Blend 156

5.1. Optimum Spinning Conditions for the Starch/EVOH Blends (as stored, do = 762 μm). 259

5.2. Optimum Spinning Conditions for the Starch/EVOH Blends (conditioned at 50% RH, do = 762 μm) 261

5.3. Mechanical Properties: a) Hylon VII/EVOH Blends, b) Native Corn/EVOH starch Blends, c) Waxy Maize/EVOH starch Blends, and d) EVOH/GLY Control 263

B.1. Processing conditions employed during film blowing of select starch/EVOH model blends 318

Chapter 1

Overview of Thesis

Establishing the relationships between processing, structure, and physical properties is key to understanding how to improve thermoplastic products. In this thesis, semi-crystalline polymer systems that are thermoplastically prepared and processed using model techniques are investigated. Materials studied include: 1) blends of various starches with poly(ethylene-vinyl alcohol) (EVOH) for use in biodegradable thermoplastic applications, and 2) linear polyethylene to illustrate the usefulness of a model technique for preparing biaxially-stretched, melt-crystallized thin films.

Investigations of the first class of materials, starch-based thermoplastics, results from a renewed interest in the use of starch as a naturally occurring, biodegradable polymer for non-food, thermoplastic applications. Prior use of starch was limited to utilizing it as a dry filler particle (usually less than 15 wt%) in typical thermoplastic materials such as polyethylene. Within the last ten years, the ability to process starch by thermoplastic means, thus 'destructurizing' the starch granule, has resulted in the commercial production of starch-based resins and products (e.g. Ecofoam®, utensils, pens, composting bags) by a number of companies. Key to the replacement of traditional, non-degradable plastics with thermoplastic starch is the ability to process thermoplastic starch resins in standard, commercial equipment while achieving acceptable performance properties.

Currently, the limited use of starch in disposable plastics applications is attributed to difficulties in processing due to its thermo-degradation characteristics and high viscosity. In addition, the dimensional stability and mechanical properties of thermoplastic starch are often criticized due to significant moisture uptake and loss that occurs for the hydroscopic polymer constituents of starch, amylose and amylopectin, as

environmental conditions (i.e. relative humidity) change. One way of improving the processability and performance characteristics of starch has been to blend it in varying proportions with other polymers and plasticizers which possess more stable properties yet still provide some degree of biodegradability. At the time of this work, little was known about the range of microstructures that can be obtained with the different types of starch and their blends, which will directly effect their final properties. For this reason, an in-depth investigation of the blend morphology as a result of extrusion blending and after subsequent processing (e.g. fiber spinning, cold drawing, film blowing) of a systematic series of three corn starch varieties with poly(ethylene-vinyl alcohol) (EVOH) was performed. These systems were chosen as models from which to gain insight into the "thermoplastic" behavior of starch and its interaction with a synthetic polymer. In addition, the effect of blend microstructure on the mechanical and environmental properties of starch/EVOH blends was assessed. One goal of this research is to provide insight into how to control and tailor the rate of biodegradability and mechanical behavior for specific product uses.

Morphological techniques such as electron microscopy, x-ray scattering, and thermal analysis were employed to understand micro- and ultra-structural changes as a function of processing, composition, and storage conditions. Because past research has concentrated on the granular structure of starch, a methodology for examining "destructurized" starch and starch-based blends using these microstructural probes, especially transmission electron microscopy, had to be developed. Characterization of the morphology that results from extrusion blending these relatively novel systems is first performed after developing protocols for morphological techniques. Once these structures were examined, the model application of melt fiber spinning was employed as a vehicle for understanding the interaction between processing, structure, and properties. Information about the influence of flow and molecular orientation mechanisms on the structure as well as the solid state properties was derived from starch-based fibers.

Finally, the effect of orientation, phase separation, crystallization, and surface structure on the biodegradability and transport characteristics of starch/EVOH blends was considered.

In conjunction with understanding structural changes of starch/EVOH blends under unaxial orientational flow, a separate technique was developed to observe structural changes that occur when equi-biaxial stresses are applied to semi-crystalline polymer systems. The Bubble Support method was introduced as a model technique for preparing thin, equi-biaxially oriented films for direct observation in TEM. Because polyethylene has been the polymer most extensively studied in terms of its microstructure, it was employed to demonstrate the morphologies that arise using the Bubble Support method.

This dissertation is divided into chapters organized by topic. To facilitate submission for individual journal publication, most of the chapters exist as separate entities which include their own abstract, text, and reference sections.

In Chapter 2, the necessary background on starch structure and properties is presented in order to help the reader to understand the results presented on starch/EVOH blends in the following chapters. Information on the structure and properties of native starch and on extrusion cooked starch is presented. Thermodynamic and kinetic variables are discussed in terms of their effect on the morphology of starch and poly(ethylene-vinyl alcohol) blends. Morphological techniques are introduced and previous structural studies of starch using these techniques are cited as examples.

In Chapter 3, the results from a structural investigation of thermoplastic starch/poly(ethylene-vinyl alcohol) (EVOH) blends are presented. The structural changes that occurred in a systematic series of three types of corn starch (waxy maize, native corn, and Hylon VII) as each is extrusion blended with EVOH were examined. Characterization was done primarily with differential scanning calorimetry (DSC), wide-angle x-ray scattering (WAXS), and scanning electron microscopy (SEM). Overall,

various degrees of phase separation and levels of structure were observed and explained with principles from polymer science and engineering and the field of food science.

In Chapter 4, the morphological investigation of starch/EVOH blends is extended to include the technique of transmission electron microscopy (TEM). TEM has not been used extensively to study the morphology of starch, especially thermoplastically processed starch, mainly due to difficulties arising from sample preparation, staining, and specimen sensitivity. Emphasis is placed on these issues, as well as the contrast mechanisms which arise, in order to optimize the electron optical operating conditions for reliable imaging and interpretation of starch-based blends with TEM. Results from examination of the starch/EVOH blends are presented and complement the information given in Chapter 3 regarding the structural characteristics of the blends.

The processability of the starch/EVOH blends is the focus of Chapter 5. Melt fiber spinning was employed as a convenient means to study the extremes of orientation and crystallization which also occur to various extents in other thermoprocessing applications that are central to developing biodegradable packaging. Processing parameters were explored for best spinnability (i.e. maximizing spin draw ratio). Comparison of results were made with capillary rheometry studies performed by co-workers. Structural studies were performed to understand changes in blend morphology during this secondary processing procedure. Tensile properties of fibers were also measured.

A new technique to produce biaxially-oriented melt-drawn polyethylene films which are thin enough (<1000 Å) for direct viewing in TEM has been developed and is presented in Chapter 6. This method is based on modifying the Petermann [1979] method for producing uniaxially oriented film. Information from TEM on these films provides insight into the crystallization and deformation mechanisms for biaxially-oriented polyolefins which will be useful in commercial applications such as film blowing and thermoforming operations.

Finally, in Chapter 7, a summary of the entire thesis is provided, and directions for future work are outlined in terms of results from the present study.

As addenda to this thesis, the isomorphic crystallization of the ethylene and vinyl alcohol repeat units in poly(ethylene-vinyl alcohol) is investigated using WAXS, DSC, and NMR in Appendix A, and data supplementary to Chapter 5 on starch/EVOH blown films is presented in Appendix B.

Chapter 2

Background: Structure and Properties of Starch

INTRODUCTION

Since starch/poly(ethylene-vinyl alcohol) blends are considered to the greatest extent in this thesis, background information on the structure and properties of starch are given in this chapter. The basis of this section is to lay out the necessary framework for understanding results presented later in this thesis, especially in interpreting structural changes that occur in starch/poly(ethylene-vinyl alcohol) blends due to processing (i.e. extrusion, fiber spinning, film blowing). Information on the use of starch as a biodegradable thermoplastic is given by citing the relevant literature published over the past fifty years. Because starch itself is a complex system, a review of previous investigations into the morphology of native starch is presented. Next, structural changes resulting from the thermo-mechanically processing of starch are highlighted, and past studies critiqued. Issues regarding the blend morphology of starch with poly(ethylene-vinyl alcohol) are introduced. Important aspects of characterizing the morphology and properties of starch-based, semi-crystalline polymer systems are outlined.

Starch-based Systems for Biodegradable Thermoplastic Applications

Thermoplastic polymers, such as polyethylene, polypropylene, and polystyrene, are often formed into single use items such as packaging, food utensils, hygiene products, and foam chips. These polymers are employed for their economy, processability, and physical properties as well as their stability under various environmental conditions. Recent increasing awareness and concern about the impact of these non-degradable materials on the environment and in the management and treatment of solid waste has prompted legislation world-wide on regulation of plastics disposal

(such as Annex V of the MARPOL 73/78 international treaty for which dumping of non-degradable plastics at sea is prohibited). The development of biodegradable polymers to be used in disposable plastics applications is one solution to this problem [1].

Among the candidate polymers considered is starch, a biologically degradable and renewable resource that is relatively inexpensive compared to other biodegradable options (e.g. poly-D-beta hydroxybutyrate, polylactic acid) [2, 3]. In fact, formulations and processing conditions for useful applications of starch-based systems has received considerable attention in the literature over the past fifty years [4 - 41]. Typical applications of starch are agricultural films, grocery bags, disposable pens, packing peanuts, composting bags, and other single-use items. The use of starch in these applications has ranged from using unmodified and/or treated starch as filler (usually less than 15 wt%) in another polymer such as polyethylene [16], to chemically modifying starch by, for example, grafting it onto other thermoplastics [27] or through starch esterification [4, 42], to thermally and mechanically processing starch and blending it with other biodegradable polymers [43]. Extensive reviews of the use of starch as a biodegradable polymer have already been published. Recent reviews are given by Roper [2], Doane [44], Shogren [45], and others [3, 46 - 48].

Crucial to its implementation as a plastic substitute is the ability to process modified starch and starch blends by traditional thermoplastic means [49, 50]. Thermo-mechanical processing of starch to form thermoplastic items was investigated by the US Dept. of Agriculture in making films of starch and starch-synthetic polymer blends (i.e. with polyethylene-acrylic acid [17, 34, 37, 51 - 53]). Development of this technology into commercial-scale production of resins containing thermoplastic starch that can be used in standard processing equipment (e.g. injection molding equipment, film blowing apparatus) was achieved by corporations such as Novon Products, a division of Warner-Lambert, and Novamont Inc., a subsidiary of the Montedison Group in Italy. Both companies have patented compositional formulae and processing methods for making

thermoplastic starch and starch composites [29, 31, 43, 54, 55].

Thermoplastics made with starch represent a relatively new class of materials which are employed for their consumer potential. The greatest property of these systems is that they be biologically degradable fulfilling today's ecological requirement for packaging and single-use materials. However, in order to be useful, starch-based thermoplastics must also satisfy certain performance criteria which have already been set by their non-biodegradable predecessors (i.e. processability, mechanical behavior, transport properties, resistance to dissolution and swelling, and, of course, cost). In this thesis, starch/poly(ethylene-vinyl alcohol) thermoplastic blends are examined. As with any polymer system, the manner of processing effects microstucture, which, in turn, reflects back on physical properties. The key to understanding how to optimize product properties is to establish the relationships between the blend composition, processing history, and the resultant structural and physical properties of such materials.

WHAT IS STARCH?

Starch exists in the photosynthetic tissues and storage organs in plants [56], especially in cells termed plastids (namely, chloroplasts and amyloplasts). Small granules (~ 1 μm) of starch are formed in the leaves of plants during active photosynthesis from water and carbon dioxide with sunlight and chlorophyll [57]. At night, this leaf starch is broken down by enzymes into sugars (sucrose) which migrate to other parts of the plant. Some of these sugar molecules are enzymatically polymerized in the plant's seeds, tubers, and roots to form the larger granules [57] which constitute commercial starches. Starch consists of a mixture of two polymers, amylose (AM) and amylopectin (AP), both polysaccharides containing the D-glucopyranosyl repeat unit [58]. In amylose, the glucose unit is connected by α-(1,4) glucosidic linkages. In amylopectin, amylose chains are joined at branches approximately every 20 to 25 glucose units through the α-(1,6) linkage. The chemical structures of these molecules are shown

in Figure 2.1. Molecular weights of amylose range from 0.2 x 10^6 to 3 x 10^6 g/mol, while for amylopectin, from 1 x 10^6 to 6 x 10^6 g/mol. Starch is comprised of approximately 0 to 85 % amylose (fraction of polymer) depending upon its origin [21]. Smaller molecules including water (~ 10 - 20 wt% at normal atmospheric conditions), fatty substances (lipids, fats; ~ 0.9 wt%), proteins (~ 0.3 - 0.5 wt%), phosphorus (< 0.1 wt%), and ash (< 0.5 wt%) are also found in starch [57].

Commercial sources of starch include: 1) the seeds of cereal grains (corn, wheat, sorghum, and rice), 2) tubers (potato), and 3) roots (tapioca, sweet potato, and arrowroot), [57]. Through grinding and wet purification techniques [57, 59], starch granules are separated from their plant source. The size, from 2 μm for amylomaize to 175 μm for canna starch; shape, from spheres to rods; and other properties of the starch granule are highly dependent upon the plant source [59]. Differences in composition for various starch sources are emphasized in Table 2.1. In this thesis, native corn starch, waxy maize, and a high amylose corn starch (Hylon VII) are considered. Waxy maize is a variety of corn starch originating in China that contains essentially only amylopectin molecules [21] (amylose content ~ 0.8 %)[60]. It is utilized for its resistance to syneresis and its elastic, stringy properties. Hylon VII is a genetically engineered corn starch containing approximately 70 % amylose. It is resistant to swelling and forms high strength gels.

MORPHOLOGICAL INVESTIGATIONS OF STARCH

Morphological Techniques

Among the morphological techniques that are used to study the structure of starch are: 1) Light and Electron Microscopy (LM, SEM, and TEM), 2) X-Ray Scattering (SAXS and WAXS), and 3) thermal analysis (DSC). Microscopy furnishes direct, local information such as microstructure, ultrastructure, crystallinity, and orientation. X-ray scattering, a reciprocal space method, provides global information about the bulk

Amylose (linear fraction):

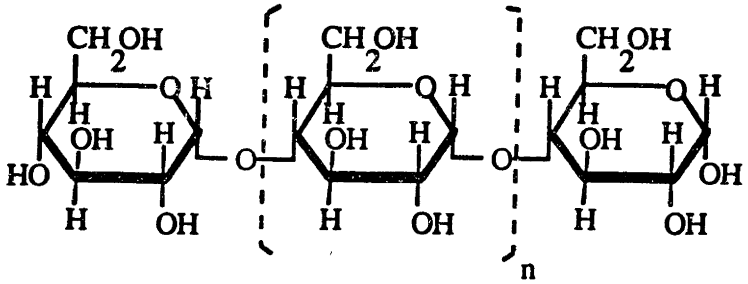

Amylopectin (branched fraction):

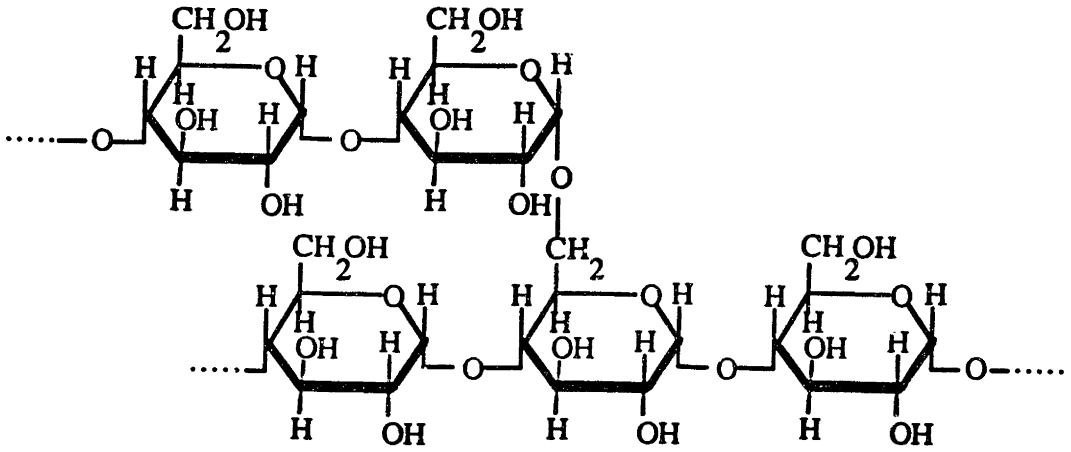

Figure 2.1. The chemical structures of amylose (AM) and amylopectin (AP).

Table 2.1. Shape, Size, and Properties of Various Starch Granules
[from Blanshard 1987; Young 1984]

Starch	Shape	Diameter	Amylose Content	Percent Crystallinity
Corn (maize)	Polyhedric	5 - 25 μm	28%	39
Potato	Ellipsoidal	15 - 100 μm	23%	25
Wheat	Lenticular	2 - 38 μm	26 - 31 %	36
Tapioca	Semi-spherical	5 - 35 μm	17 - 33 %	38
Rice	Polyhedric	3 - 8 μm	14 - 32 %	38
Amylomaize Class VII	Polyhedric	5 - 25 μm	70 - 75 %	20 - 25
Waxy Maize	Polyhedric	5 - 25 μm	0.80%	0.39

structure such as crystallinity and orientation. Short range order of the molecular constituent in starch and starch blends can be discerned using Wide Angle X-ray Scattering (WAXS) and diffraction (WAXD). Information about the long range order within polymer systems is attained using Small Angle X-ray Scattering (SAXS). Thermal analysis contributes data about the state of the material such as melting and glass transition temperatures as functions of water content, blend compatibility, and degree of crystallinity. Each of these techniques can be used characterize the structure of the native starch granule and the structural changes that occur with thermal and mechanical treatments.

Among the direct morphological techniques, light microscopy provides information about starch on the micron level. Using polarized light, birefringence studies can be performed to examine crystallinity and orientation within starch granules. Employing using Scanning or Transmission Electron Microscopy [61], information about the surface and internal structure of starch granules and thermoplastic starch can be obtained down to the 0.1 nm range.

Scanning electron microscopy (SEM) has been extensively employed to study the fine surface structure of starch since it possesses a much greater depth of focus and better resolution than the light microscope [62]. Scanning Electron Microscopy (SEM) operates under the principle that an incident beam of electrons (E ~ 1 - 30 keV) is scanned across the surface of a sample. A detector monitors the intensity of a chosen secondary signal, which is generally the emission of low energy (< 50 eV) secondary electrons. When an emitted secondary signal changes across the specimen, contrast can be observed in the displayed image (i.e. on a cathode ray tube) [63]. Generally, the starch sample is coated with a thin layer of metal (i.e. gold, gold-palladium) to render it conductive under the electron beam for conventional SEM (For field emission SEM and environmental SEM starch can be imaged without a conductive coating.) Past studies have employed SEM to monitor the changes in granular structure as a function of biosynthetic development [64],

varietal differences [65, 66], processing [67], chemical and enzymatic treatment [68, 69], and grafts with synthetic polymers [70].

Transmission Electron Microscopy (TEM) operates by passing a high energy beam of electrons (80 - 200 keV) through an extremely thin specimen (less than 100 nm for low density hydrocarbons and 20 nm for high density metals) [61]. Using an objective lens aperture, scattered electrons are separated from unscattered electrons, resulting in contrast between areas of different thickness, composition, crystallinity, and orientation [63]. Past emphasis has been placed on investigating the structural components of native granules [71 - 78]. Other studies have used electron diffraction to understand the structure of native starch granules and single crystals of amylose and amylose acetate [79 - 82].

Starch Morphology

The morphology of starch is quite complex and encompasses various structural levels. Often, various interpretations and models are used to describe starch micro- and ultra-structure. A summary of currently accepted models for corn starch morphology is presented in Figure 2.2. Starch comprises a large part of the corn kernels (figure 2.2a) in the form of polyhedrally-shaped granules that range in size from 5 to 25 μm (as shown in the scanning electron micrograph image, figure 2.2b). In the light microscope, dry starch granules appear clear and colorless with a mean refractive index of 1.5 [83]. Under polarized light, starch granules show a "Maltese-Cross" pattern [59].

The internal structure of the granule is still not well understood. Growth of the polymer chains occur around a nucleus (hilum) which is formed when a small amount of polysaccharide becomes insoluble within the seed of a plant. Dissolved sugars solidify as they are enzymatically attached to the growing polymer chains [57]. Amylopectin is formed from enzymes (synthetase and phophylase) that cause branching of the polymer chain (at the 1,6 linkage), yet relatively unbranched amylose is also formed in the

Figure 2.2. Structural levels associated with native corn starch: Starch exists in the kernels of (a) corn [from Rhoades, 1993] in the form of (b) granules (5-25 μm), which consist of growth rings (120-400 nm) and a predominantly amylose core (c). Racemose packing (d) of alternating layers of crystalline and amorphous polymer chains (d ~ 8 nm) is hypothesized [from French, 1984]. A possible arrangement of components in a starch crystallite is depicted in (e) [from Galliard, 1987].

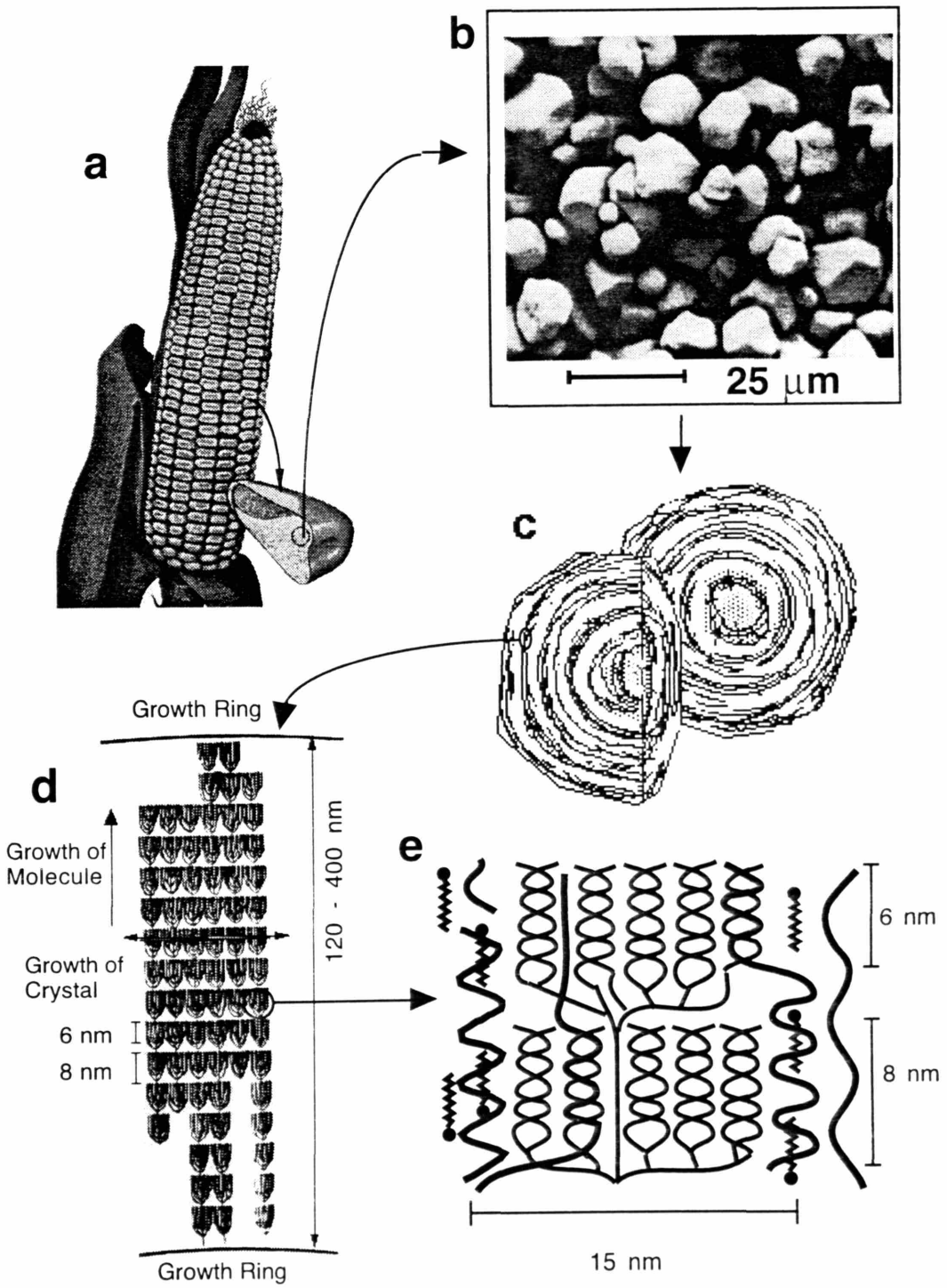
a
b
25 µm
c
Growth Ring
d
Growth of Molecule
Growth of Crystal
6 nm
8 nm
120 - 400 nm
Growth Ring
e
6 nm
8 nm
15 nm

presence of the enzyme [57]. In addition, the ratio of amylose to amylopectin increases with granule size [57]. Although the chemical structure of amylose and amylopectin has been determined with fair certainty, the manner of packing of these molecules within the starch granule remains relatively ambiguous.

In the light or electron microscope, certain starch granules exhibit concentric shells emanating from a nucleus (figure 2.2c). The exact nature of these layers (which range in size from 120 to 400 nm) are unclear since their visibility in the microscope depends upon the sample preparation procedure [84]. Generally, these shells ('growth rings') are believed to represent the daily production of starch by the plant with each ring representing the length of amylopectin molecules. At the boundary of each ring, it is likely that the starch molecules are terminated by protein linkages that exist in an amorphous zone between rings. Since this amorphous layer is most susceptible to swelling with water or to chemical or enzymatic treatment; the rings become visible [71, 72, 76]. Rings are more easily observed in waxy maize starches than in starches containing higher proportions of amylose [76]. However, with severe acid treatment, even high amylose starches exhibit concentric shells [71]. In previous TEM studies, researchers also observed dark bands splaying outward from the granule hilum (similar to '*') which was initially attributed to protidic material [85, 86]. Later, these structures were shown to be an artifact of sample preparations (i.e. folds of cut starch grains which result from defective permeation of the starch chains with inclusion material and starch water affinity) [87]. Perhaps further microscopy studies will similarly give more insight into the formation of the concentric "growth rings".

Each growth ring is believed to consist of alternating layers of crystalline and amorphous amylopectin and amylose packing normal to the its boundary. The exact structure of the amylopectin is still under dispute mainly due to differences in the experimental structural studies performed on native starch systems [59, 71 - 78]. This ultrastructure of starch granules in transmission electron microscopy is revealed only

through a series of dehydrating, embedding, sectioning, chemical treating, and staining or shadowing steps which often produce certain artifacts that limit the evaluation of transmission electron micrographs [74].

Kassenbeck [83, 88] used TEM to study the fine structure of wheat and corn starch and demonstrated the changes in structural appearance that occur with sample preparation procedures (see figure 2.3). A periodate ($NaIO_4$) treatment renders possible the chemical binding or precipitation of ions or atoms with high nuclear charge number by splitting a certain number of the glucose rings between carbon atoms 2 and 3 [73, 89]. In Kassenbeck's study, thiosemicarbazide acts on the two aldehyde groups which are formed from the above reaction and produces thiosemicarbizoles, which react with silver nitrate to form interchainal acetal bonds [83] . The latter reaction occurs mainly in the more tightly packed (less oxidized), non-crystalline regions in starch. These regions can be contrasted by the addition of osmium tetroxide and steam at 60°C. (The acetal bonds undergo reversible splitting with the liberated aldehyde and react spontaneously with OsO_4.). Crystalline regions of amylopectin can presumably be seen by negatively staining with phosphotungstic acid (PWS). Kassenbeck suggested that amylose is essentially located in the nucleus of the granule and leaches out during the chemical treatment process; the remaining structure of the granule consists of growth rings formed from the amylopectin chains. Within the growth rings, repeating radial layers with an average thickness of 62 Å were attributed to amylopectin crystallites (see Figure 2.4). Oostergetel also observed slightly larger spacings calculated using optical diffraction of TEM negatives (d ~ 90 - 100 Å) for sections of various types of starch granules prepared by wet-mashing, hydrolyzation, and negatively staining with uranyl acetate [78]. A separate study by Hizukuri and Nikuni [90] reported a tangential dimension of, tentatively, 15 nm which they attributed to the width of a crystallite.

Small angle x-ray scattering (SAXS) studies of hydrated starches also confirm the periodic spacing characteristics of native starches [91 - 94, 78] (see figure 2.5). Dry

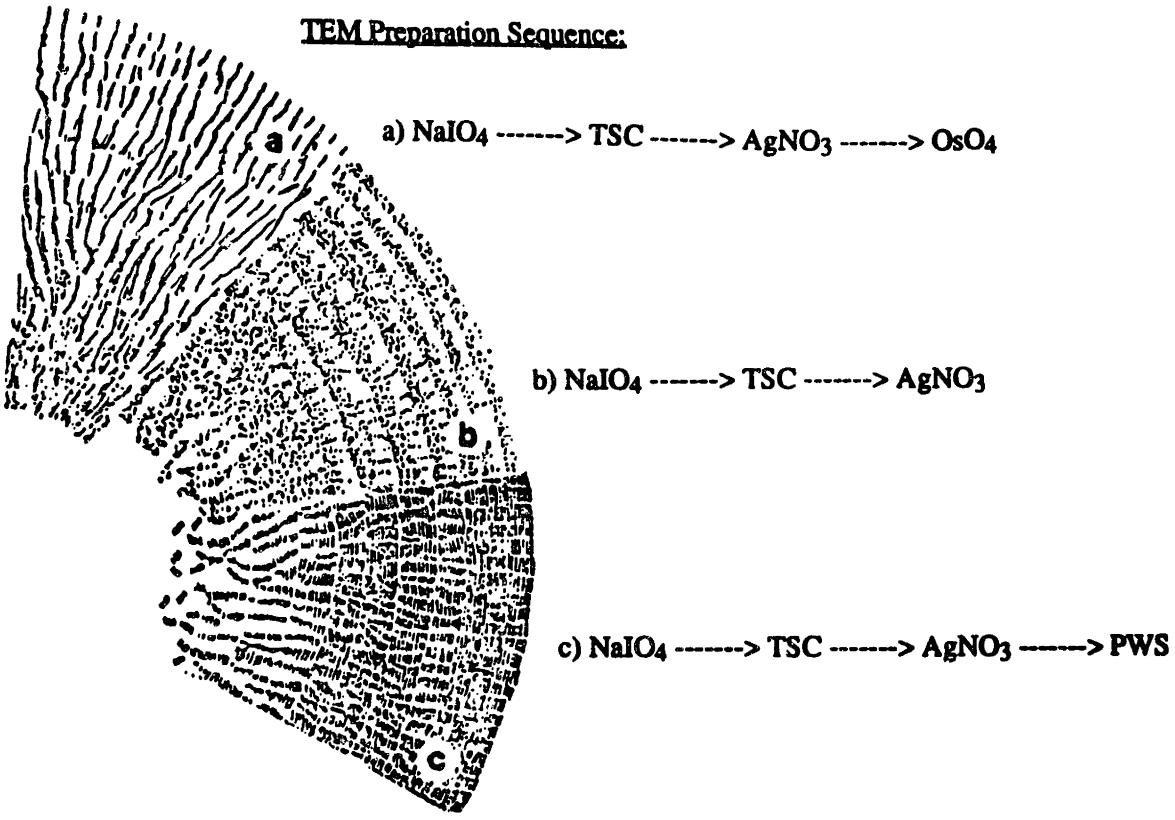

Figure 2.3. Various types of ultrastructural organization within starch granules are evident depending upon the TEM preparation method employed: a) possible radial arrangement of amylose molecules, b) distribution of amorphous starch polymers, and c) arrangement of crystalline starch (amylopectin) [from Kassenbeck, 1978].

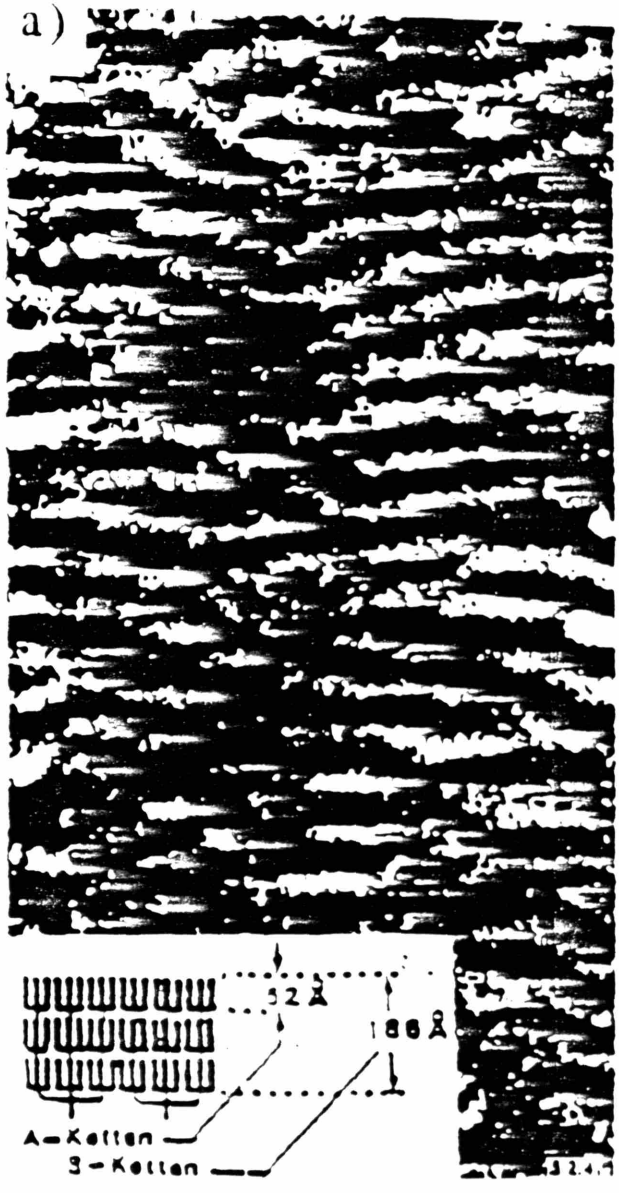

Figure 2.4. Kassenbeck's TEM image of corn starch depicting the crystalline periodicity of amylopectin. The racemose model for amylopectin is proposed with crystallite sizes of 62 Å (see inset) [from Kassenbeck 1978].

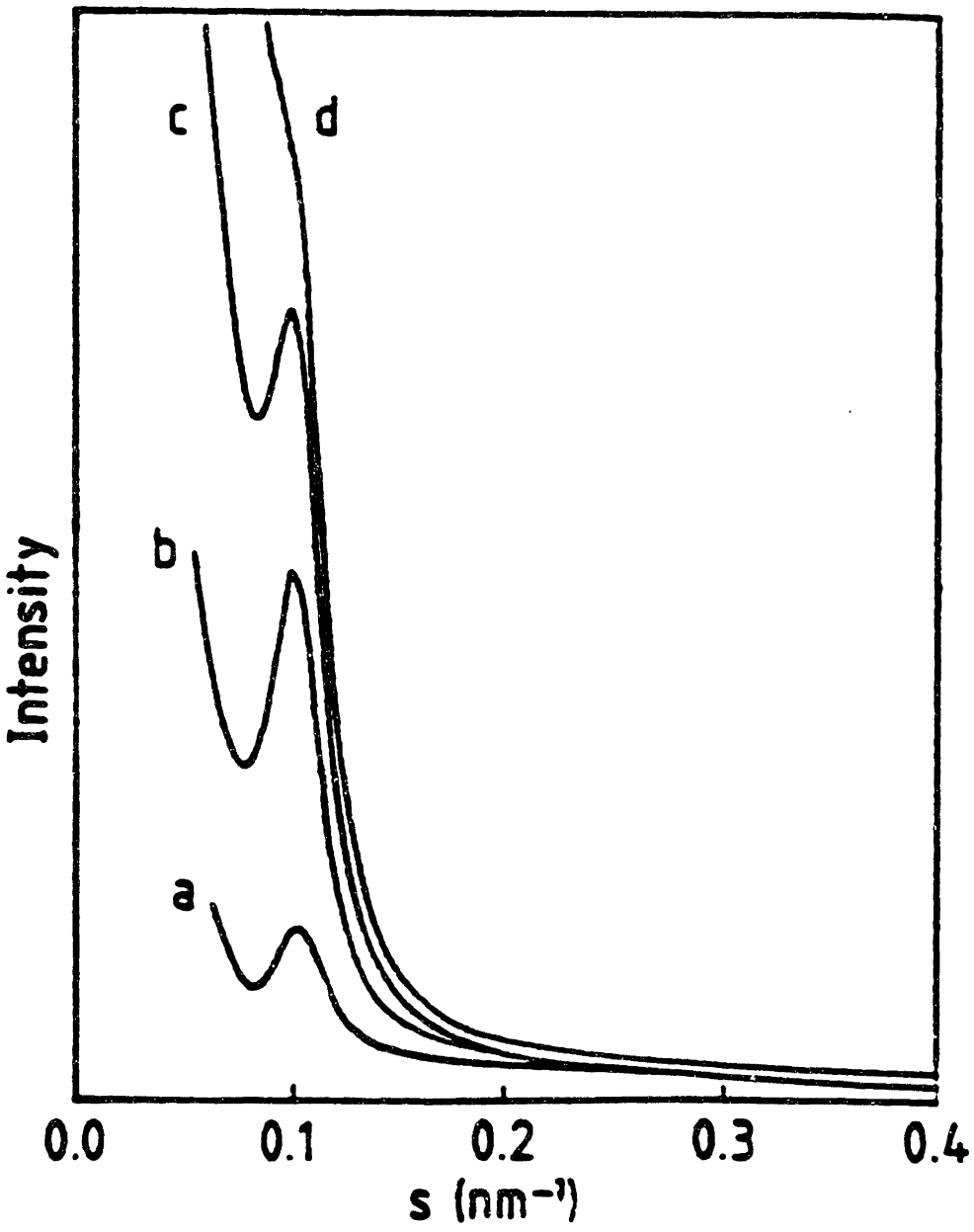

Figure 2.5. Small angle X-ray diffraction patterns from potato starch suspensions: a) native, and hydrolyzed in 2.2N HCl at 35°C for b) 1 day, c) 2 days, and d) 4 days [from Oostergetel 1989].

starches show no periodic spacings due to "the small electron density difference between amorphous and crystalline starch," [95]. However, upon hydration, the amorphous regions within the starch granule preferentially absorb water, thus lowering their electron density. From various moistened starches, Sterling determined spacings which range from 99 to 109 Å (using the Bragg relationship, $d = 2\pi/q$) [91]. A more exact value of 88.5Å was determined by Cameron and Donald who recently modeled the starch granule as "a random array of stacks of infinite lamellae embedded in a medium of specified electron density" [92]. The number of repeated lamellae in a stack was calculated to be 16, corresponding to a distance of 1600 Å, which is the "size of the relatively dense material of a growth ring in starch" [92]. It should be noted that the strong correlation of TEM and SAXS data is surprising given the expected angular dependence of this spacing (especially for Oostergetel, since different sample preparation treatments were employed).

Of the models for starch crystallization, the cluster or racemose packing of starch proposed by French is favored by most researchers (figure 2.2d) [84] given the TEM and SAXS evidence. Branching occurs at almost regular intervals (approximately every 20 - 25 repeat units) during the formation of amylopectin whose chains crystallize as they are biosynthesized. Branch points occur in the amorphous regions between crystallites. Results from both TEM and SAXS are relatively consistent with the racemose model for amylopectin. Initial studies performed by Sterling showed that crystallinity in the native granules of starch is approximately 40 %. Values for different starch types are given in Table 2.1.

Distinct wide-angle scattering patterns are observed for starches [84, 96]; patterns are shown in Figure 2.6. Generally, type 'A' patterns correspond to cereal grain starches, type 'B' to tuber, and type 'V' to complexed starches. The 'C' pattern, which is intermediate between the 'A' and 'B' patterns, is indicative of bean and other root starches [89]. Exceptions to these classifications are high amylose corn and barley starches which exhibit 'B' patterns when they possess an amylose content greater than

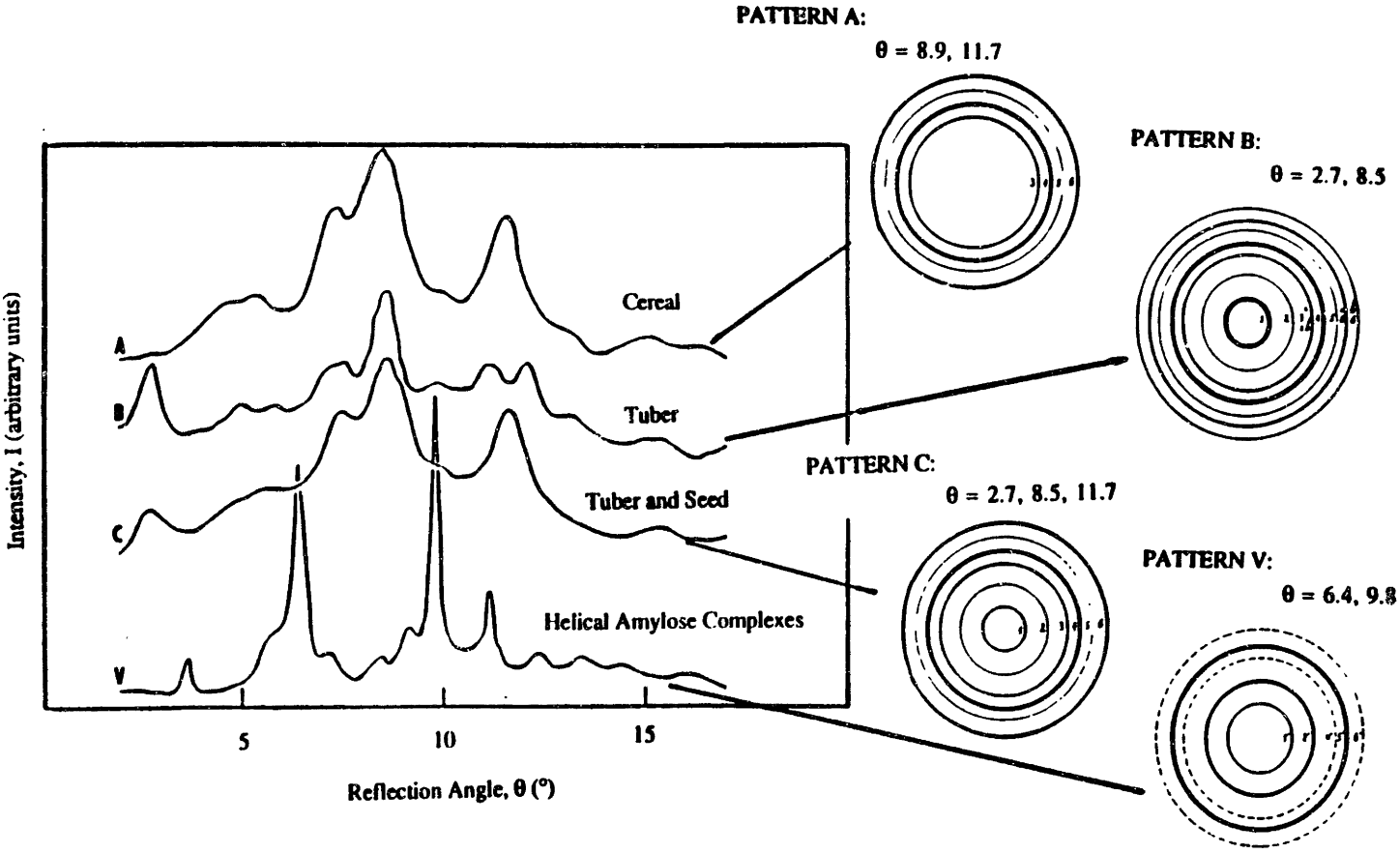

Figure 2.6. Wide-angle x-ray diffraction patterns for 'A', 'B', 'C', and 'V' type starch crystallization [from Zobel, 1988]. On the right are schematics of WAXS patterns depicting ring intensity [from Katz, 1930].

49% [97]. Recent studies have shown that the scattering patterns of starches are a function of the weight average chain length for amylopectin which contributes to most of the crystallinity in the granule [97]. Short (26), long (36), and intermediate (28) amylopectin branch lengths, give 'A', 'B', and 'C' patterns, respectively [97]. The average branch length of the amylopectin fraction is dependent upon the plant source of the starch. Starch, when it is thermally, chemically, or mechanically treated often exhibits the 'V' type pattern, which is formed upon complexing of the amylose fraction with varying nonpolar agents [98].

Crystallization is believed to proceed with granule growth either by a double helical packing of the amylose and amylopectin chains or through single helical complexing of amylose with small molecules existing in starch (figure 2.2e) [56]. Note that the schematic by Galliard grossly overrepresents the size of the actual chains with the dimensions shown in figure 2.2e. In addition, some of the branching characteristics are questionable (i.e. three branches emanating from a single $\alpha(1,6)$ linkage). Thus, this figure should only serve to be descriptive of the possible components in a starch crystallite. For instance, the possible existence of lipids at the boundaries of starch crystallites is depicted in figure 2.2e.

While the complexation of amylose and lipids may occur in certain native starches (e.g. millet), the V-type pattern is generally not observed in native corn starches. Several researchers have proposed different unit cells for the crystalline structure of starch [99 - 104]. In particular, Sarko and Wu prepared oriented 'A'-type fibers by isolating amylose from starch, acetylating the amylose, and casting it into thin films which were then cut into strips and stretched at 150°C. The oriented strips were deacetylated in alcoholic alkali and finally conditioned at 80% RH at temperatures above 85°C. 'B'-type "fibers" were prepared by exposing the deacetylated filaments to 80% RH (at room temperature) for 3 days, to 100% RH for 3 days, and finally annealing in water for 1 hr. at 90°C [89]. Based on the fiber diffraction patterns, Sarko proposed a double helical, parallel-stranded

structure for amylose with three D-glucose units per 10.4 to 10.5 Å rise in the helix (along a single strand, the repeat distance corresponds to six D-glucose units (21Å)). Note, French states that the 'A' and 'B' powder patterns from native starch granules "do not reflect precisely the same structural features as in the 'A' and 'B' fibers" of linear amylose since branched amylopectin is responsible for most of the crystallinity in the native granule [84]. In addition, anti-parallel packing of the chains was proposed, contrary to what would occur as the starch polymers are grown. Further uncertainty in structure is also due to the "inadequate amount of data, the small crystallite size, the imperfection of the crystallites, and the large unit cells" [84] that makes interpretation of x-ray data difficult.

The use of transmission electron microscopy has made it possible to obtain microdiffraction patterns of A-, B-, and V- type crystals under frozen wet conditions and yield individual diffraction spots [79, 80, 95, 105 - 108]. These results also suggest helical packing of the parallel strands of starch molecules although the unit cell dimensions and space groups are slightly different (parallel packing is also proposed). However, the number of spots is insufficient to locate the large number of atoms in the unit cell and a definite solution to the crystalline structure has not yet been experimentally attainable. Computer modeling efforts have been used to estimate structure and trial-and-error fitting to both x-ray and electron diffraction data have been performed [108 - 110]. This has resulted in a wide variety of proposed models.

Unit cell dimensions of A, B, and various starch complexes (V pattern) are shown in Table 2.2. Currently, left-handed double helices are proposed for both the A and B type crystalline patterns. A monoclinic unit cell is the accepted proposed structure for the 'A' type starch ($a = 21.24$ Å, $b = 11.72$ Å, $c = 10.69$ Å, $\gamma = 123.5°$) and a hexagonal unit cell, for the 'B' type starch ($a = b = 18.5$ Å, $c = 10.4$ Å). See figure 2.7. Determination of an exact crystal structure is complicated by changes in intensity and spacings with moisture content [109]. Shifts from 'A' to 'B' crystalline types are

Table 2.2. Unit cell dimensions of amylose and amylose complexes [from Blanshard 1987; Imberty 1991]

Structure	a (Å)	b (Å)	c (Å)	γ (°)	Helix Symmetry	Space Group	Density (g/cm^3)
Native Starch (left-handed double helices):							
A	21.24	11.72	10.69	123.5	21.38 Å repeat, 2 x 6/1	$P2_1(S)$	1.48
B	18.50	18.50	10.40	120.0	20.8 Å repeat 2 x 6/1	$P6_1$	1.45
Amylose Complexes (compact left-handed single helices):							
Va	12.97	22.46	7.91		2 1 (~ 6/5)	$P2_12_12_1$	-
Intermediate forms	13.30	23.0					-
	13.5	23.45					-
	13.55	23.5					-
Vh	12.7	23.7	8.05		6/5	$P2_12_12_1$	-
V DMSO	19.17	19.17	24.39		6/5 in 8.13 Å repeat	$P2_12_12_1$	-
Vh - iodine	13.6	23.42	8.17			$P2_1(S)$	-
Va - BuOH	26.4	27	7.92			$P2_12_12_1$	-
Vh - BuOH	13.7	25.8	8.1				-

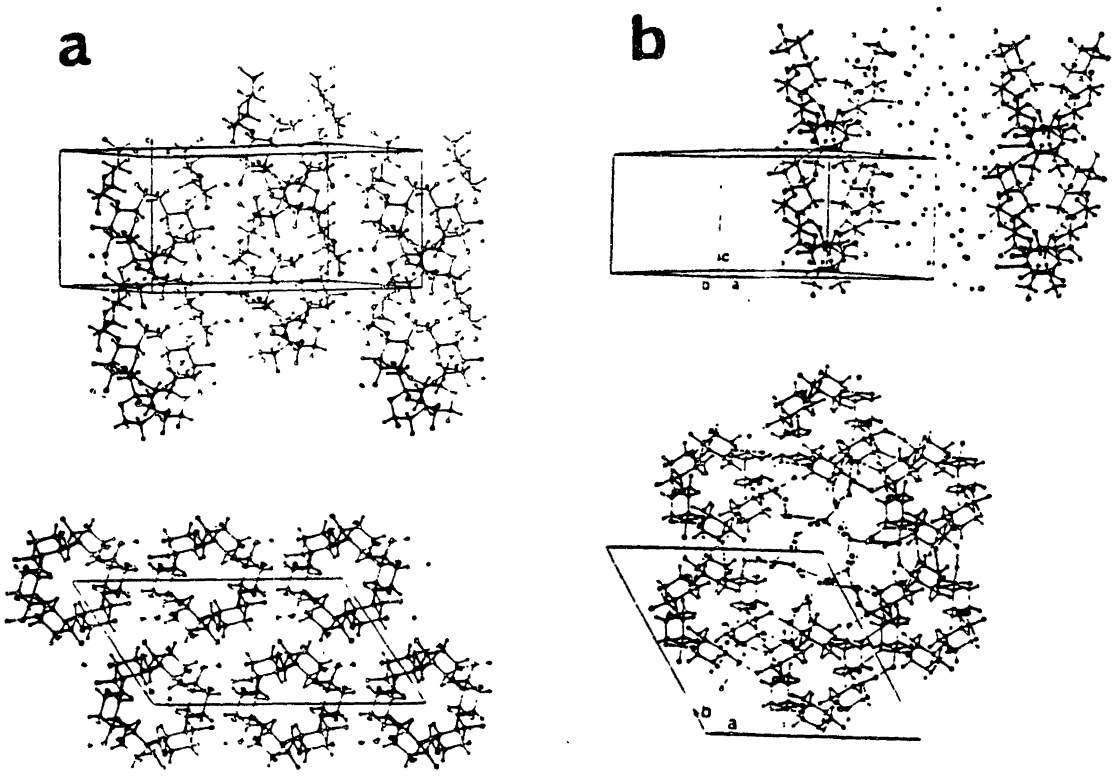

Figure 2.7. The packing of amylose chains into the unit cells of a) 'A' type starch (monoclinic: a = 21.24 Å, b = 11.72 Å, c = 10.60 Å, γ = 123.5°) and b) 'B' type starch (hexagonal: a = b = 18.5 Å, c = 10.4 Å). Upper representations depict chains along the fiber axis; the lower representations are projections of the structure onto the (a,b) plane. Closed dots indicate the presence of water molecules. Hydrogen bonding is indicated by dashed lines [from Imberty 1991].

possible depending on the amount of water present. In an 'A' type unit cell, there are only twelve glucose repeats and only a few water molecules in the unit cell; in 'B' amylose at 27% moisture, sixteen glucose repeats and from 30 to 40 water molecules are present [108]. Computer fitting of the structural packing of the starch polymers is complicated due to the "extensive flexibility" of the α(1,4) linkage and the glucose repeat itself [108].

The exact structure of the V-type crystals is similarly somewhat ambiguous and depends on the complexing agent employed. It is proposed that nonpolar molecules form the crystalline complexes by inserting themselves within the interior of left-handed amylose single helices [98]. A hydrated starch complex produces diffraction peaks which appear at 12, 6.8, and 4.4 Å as a result of reaction with such agents as aliphatic alcohols and fatty acids, certain surfactants (emulsifiers), and iodine [97]. When these complexes are dehydrated, the spacings reduce to 11.3, 6.5, and 4.3Å [97]. Other 'V' patterns appear at slightly shifted angles (due to the molecular size of the complexing agent which can extend the amylose helices from 6 to 8 glucose units per turn [98]). Examples of these agents are dimethyl sulfoxide, nitroparaffins, and branched alcohols [97].

Given the complexity of the starch granule, it is evident that exact ultrastructural features have yet to be established. What is certain is that the apparently well-ordered structure present in the native starch granule undergoes significant changes when starch is thermo-mechanically treated. An appreciation of this initial structural state is necessary to understand the morphologies that form subsequent to extrusion processing and blending with other polymers.

Thermal Behavior of Starch

Native starch undergoes a series of phase transitions when heated [111, 112]. Among these are: 1) the glass transition, 2) retrogradation, 3) gelatinization, 4) melting of

various crystallites (AM, AP, Amylose lipid complexes), and 5) degradation. Both light microscopy and differential scanning calorimetry (DSC) are often employed in the investigation of the thermal behavior of starch. With a hot stage, the light microscope has been used to study starch gelatinization, a phenomena in which the granule swells and loses its internal order [59, 89]. (The temperature at which maximum swelling of the granule takes place is referred to as the gelatinization temperature [113]). By heating starch in the presence of water, the hydrogen bonds are broken between the α-(1,4) glucosidic linkages, allowing the soluble, amorphous amylose to leach out of the granule (the amylopectin component also begins to swell). When gelatinization occurs, the 'Maltese-Cross' pattern is lost when the granule is viewed under crossed polars [114, 115]. Although the term, "gelatinization" often connotes the formation of a gel, or cross-linked network; gelatinization of starch generally results in the formation of a viscous paste which when cooled, may then form a physical network of entangled amylose molecules which are hydrogen bonded or joined by V-type crystallites. The various types of gelatinization behavior of starches are depicted in Figure 2.8.

There have been numerous studies using DSC to investigate various transitions of starch; a fairly complete summary of these studies is given by Biliaderis [116]. Blanshard [89] discusses the relationship between gelatinization and the melting points of starch granules. Whether or not the endothermic transitions are assigned to starch gelatinization or melting depends upon the temperature and moisture content (see Figure 2.9) [117]. At water contents less than 29 wt%, only melting of the crystalline regions occurs [118] (at very low moisture contents < 3 %, degradation precedes melting). Increases in the moisture content to above 44 wt% involves the overlapping of melting peaks by the gelatinization peak. At water contents of 50% or more gelatinization is the predominant thermal transition occuring. In general, gelatinization takes place at approximately 50 - 75°C whereas the melting of starch depends on moisture content.

The melting depression of starch with water content has been modeled by the

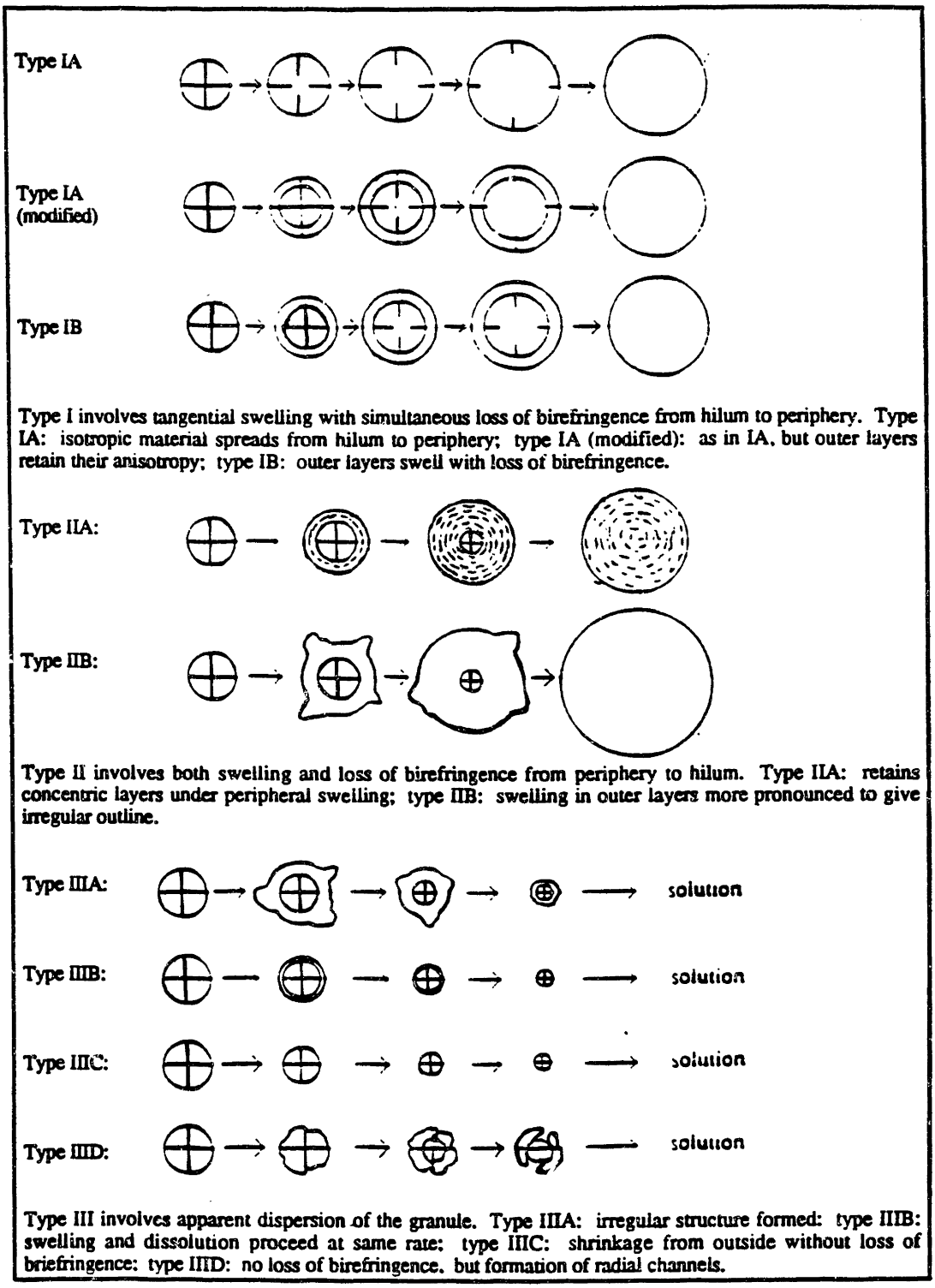

Figure 2.8. Various types of gelatinization behavior as studied by Gough and Pybus [from Banks and Greenwood 1975].

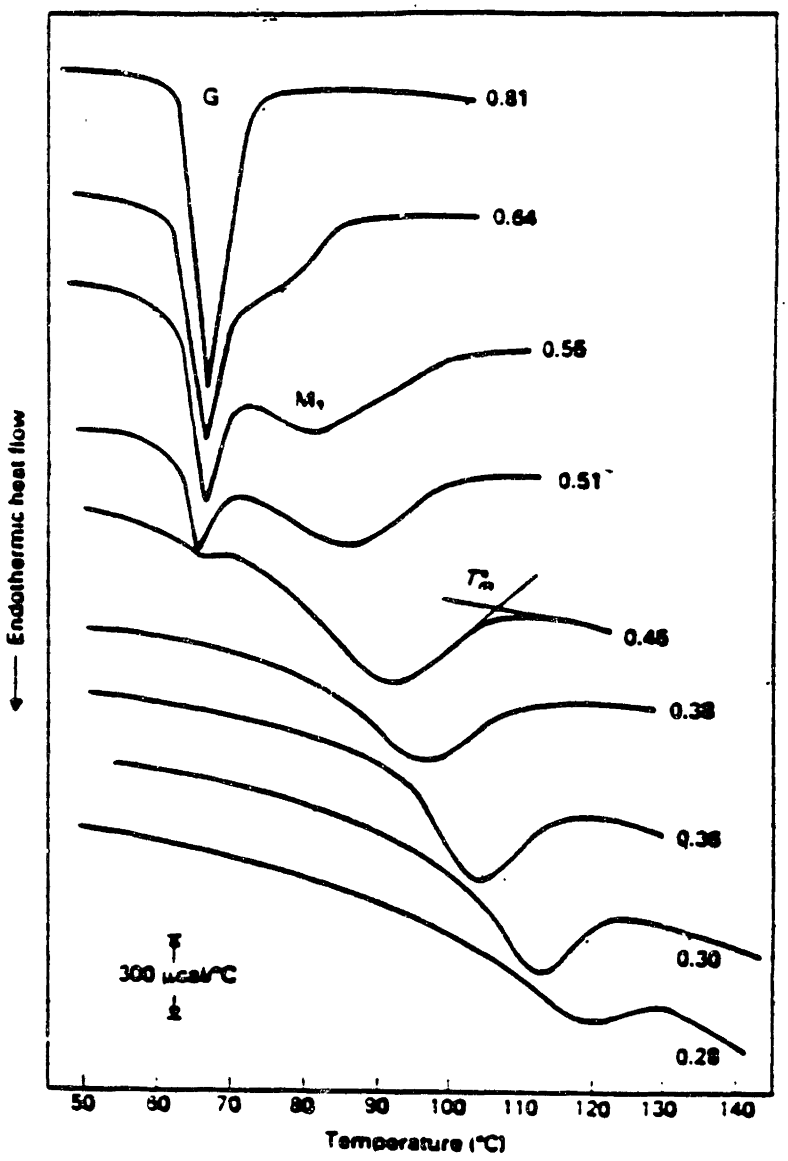

Figure 2.9. DSC traces for native potato starch as a function of volume fraction of water added (G = gelatinization endotherm; M1 = melting endotherm) [Blanshard, 1987]

Flory equation [89]:

$$\frac{1}{T_m} - \frac{1}{T_m^o} = \left(\frac{R}{\Delta H_u}\right)\left(\frac{V_u}{V_1}\right)\left(v_1 - \chi_1 v_1^2\right) \qquad (2.3)$$

where R is the gas constant, ΔH_u is the enthalpy of fusion per repeating unit, V_u/V_1 is the ratio of the molar volume of the repeating unit to the molar volume of the diluent, v_1 is the volume fraction of the diluent, and χ_1 is the Flory-Huggins polymer-diluent interaction parameter [119]. Use of this equation must be criticized since melting of the native starch crystallites (formed during the biosynthesis of amylopectin) is essentially irreversible. Most of the crystallinity associated with the re-crystallization of gelatinized starch is associated with the linear amylose component, which, in the granule, is believed to be mostly amorphous. However, one may argue that since amylopectin does crystallize to a very small extent over time, this equation can, in fact, be employed.

Retrogradation is another term used to describe changes in starch with time and has been defined to mean various behavior. In solution, the precipitation of amylose from aqueous solution is described by the term, "retrogradation" [120]. Retrogradation is also used to mean the staling of bread with time [121]. Recently, two explanations for starch "retrogradation" have been employed. Retrogradation of starch has been interpreted by food scientists to be a reversible crystallization of the amylopectin component in starch upon storage after gelatinization [120 - 125]. However, the level of crystallization is very small (WAXS peaks not much higher than noise levels) to explicitly confirm this. Others suggest that retrogradation is also attributable to physical aging which yields an endotherm at the glass transition in the DSC scans performed after periods of storage [118, 126]. Studies performed on the glass transition of wheat starch shows that it is extremely sensitive to moisture content [127, 128] (see figure 2.10) making a clear confirmation of this description of retrogradation unlikely based on thermal analysis alone.

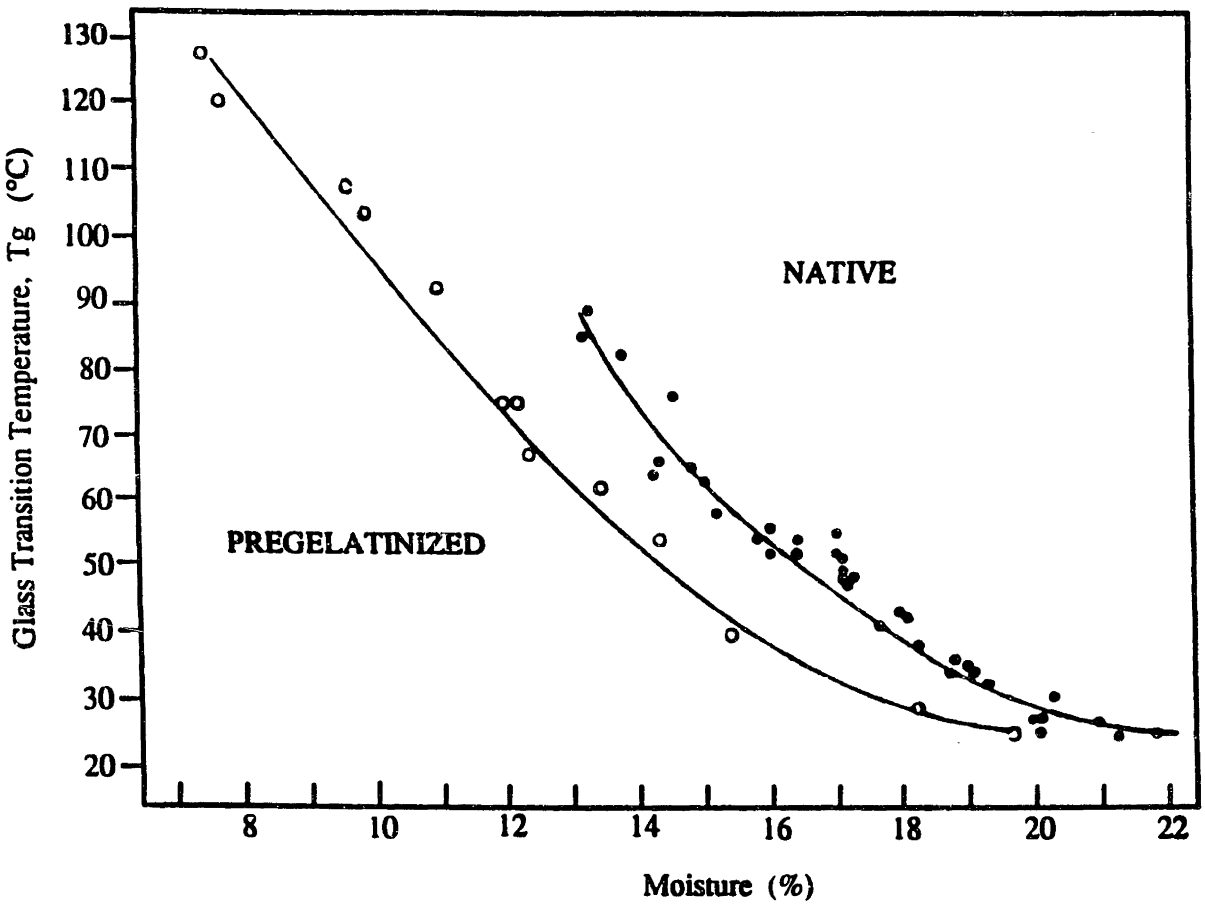

Figure 2.10. The dependence of the glass transition temperature on moisture content for native and pre-gelatinized wheat starch [Zeleznak, 1987].

Mercier and co-workers [96, 129 - 131] have shown that the granular shape of starch is not altered by gelatinization, but only becomes larger through swelling [96]. After undergoing selected heat/moisture treatment (Moisture Content (MC) =18-45 %, T = 90 to 130°C, t = 1-16 hrs), corn, wheat , and rice starches form 'V' type structures due to complexing with the fatty acids and phospholipids which naturally occur in these plant types [97]. These treated starches show higher gelatinization (and melting) temperatures and improved dispersibility in hot water [97].

Thermoplastic Starch

Although recent technology permits thermoplastic processing of starch under controlled high pressure, temperature, and moisture, starch itself cannot be considered as a typical thermoplastic polymer. The conversion of semi-crystalline native starch into a homogeneous thermoplastic is an extension of the food processing technology termed extrusion cooking [132]. A co-rotating, twin screw extruder is generally employed at higher temperature and lower residence times than those used in other food-related processes that modify starch (see Figure 2.11). During the extrusion of starch, shearing conditions produce varying effects including gelatinization (a function of water content), a bacteriological cooking effect (such as the killing of thermophile spores and the degradation of thiamine (Vitamin B1)), and the browning of starch by Maillard reactions [133, 134].

Studies on wheat and corn starches have shown that the degree of destructurization depends upon the extrusion conditions (levels of heat, shear, and moisture) at which native granules are processed [135 - 138]. A simplified model of starch degradation during extrusion presented by Gomez and Aguilera [139] is shown in Figure 2.12. While this model does not take into account the initial internal granular order, Gomez and Aquilera suggest that under extrusion conditions the starch granules can undergo a number of transitions including granular fracture, swelling, and the

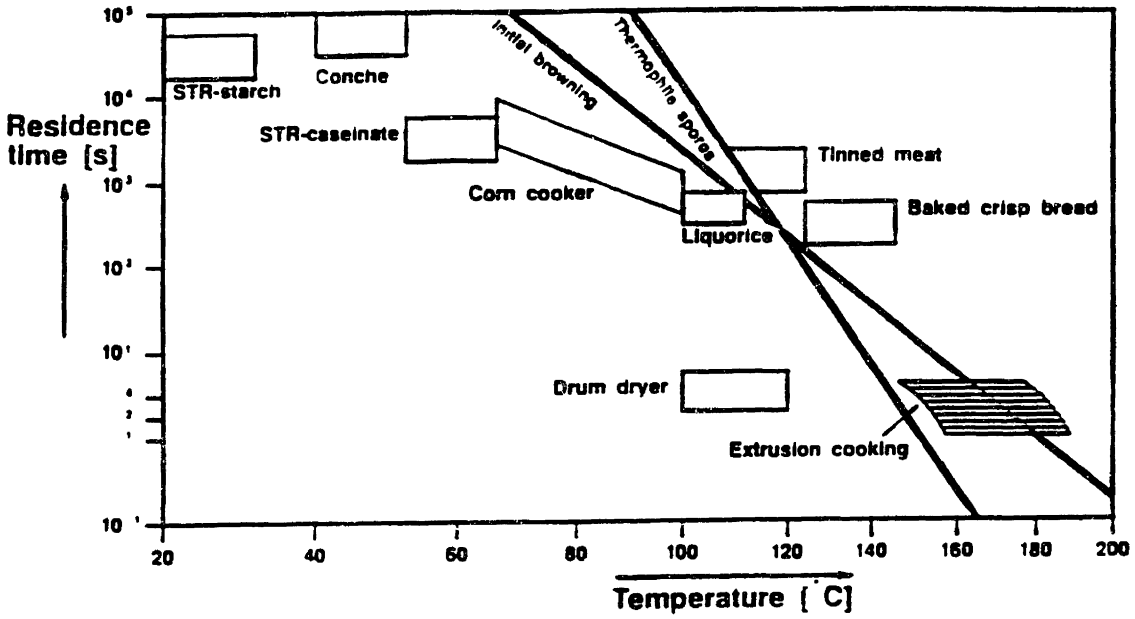

Figure 2.11. The time and temperature ranges of various processes for modifying starch. Manufacturing of thermoplastic starch often occurs in the shaded region termed "extrusion cooking" [from Wiedmann, 1987].

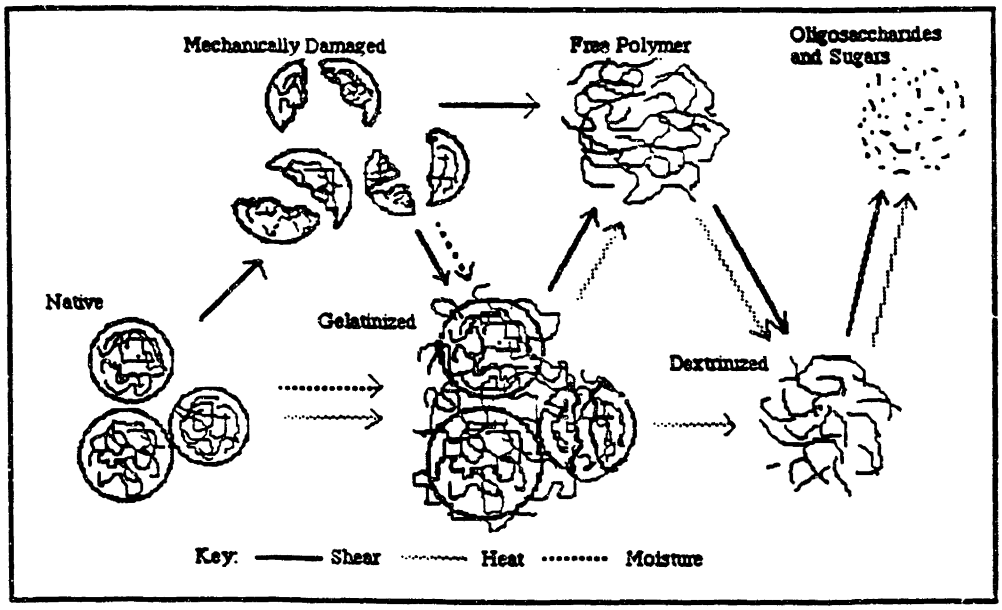

Figure 2.12. A simplified model of starch degradation during extrusion [from Gomez, 1984]. Conditions of shear, heat, and moisture cause starch to undergo a number of transitions form its native state. (Note: this model does not take into account changes in crystallinity or chain scission of the amylopectin fraction.)

formation of free polymer through a combination of shear, heat, and moisture. Detailed structural studies of the initial morphology development during low moisture extrusion processing have not yet been performed for starch and have only recently received attention for more model polymer blends [140, 141]. At higher temperatures and shear, Gomez and Aquilera suggest that the starch molecules break down and form lower molecular weight dextrins (low molecular weight, hydrolyzed chains), oligosaccharides, and eventually sugars. Starch undergoes gelatinization at high moisture contents (greater than 35% for corn starch or greater than 42% for waxy maize) and melting (under controlled pressure) at lower moisture levels [142]. In either case, melting or gelatinization of the granule is facilitated by plasticizers (i.e. water). In extrusion, the rate of destructurization is increased due to break-up of the granules by the action of shear. Higher temperatures and low moisture contents have been shown [138, 143] to decrease the viscosity during extrusion suggesting an increase in the destructurization of the starch granule and the formation of free polymer.

X-ray diffraction can be used to track morphological changes in physically modified starch via temperature, pressure, shear, and moisture treatment. For processed starch, crystallinity is dependent upon a number of variables including the degree of destructurization, the extent of orientation and flow, the cooling rate, the amount of hydrogen bonding in the final processed form, the moisture content, and the extent of aging in the presence of polyhedric alcohol plasticizers (such as glycerol) which have been shown to facilitate the crystallization of amylose molecules [60]. Previous investigations into the absolute degree of crystallinity of starch [144] have been based on a method developed by Hermans and Weidinger [145 - 147] which was first used to determine the crystallinity of cellulose.

When processed thermo-mechanically (such as through a twin-screw extruder), starch undergoes a loss of granular and crystalline structure [96]. Patterns for corn starch with an initial moisture content of 22 wt% and at extrusion temperatures ranging

from 70 to 225°C are shown in Figure 2.13. Unextruded corn starch produces the 'A'-type spectrum. As temperature is increased to 95°C, a reduction in intensity of the crystalline peaks and a broadening of the amorphous bands occur (i.e. crystallinity decreases). At 135°C, lipids initially present in the granule complex with amorphous amylose, and the 'V'-type diffraction profile is visible [129]. At higher temperatures, 185 to 225°C, a new structure, the 'E'-type, 'Extruded-type', is observed (see Figure 2.13a). Upon reconditioning the extruded starch to a 30 wt% moisture content, the 'E'-type patterns convert to the 'V'-type (see Figure 2.13b). Colonna, Buleon, and Mercier [96] explain this phenomena by stating that the structure of 'A'-type starches reorganize during extrusion into a helical complex (the 'V'-type). Upon more intense processing, the interaxial distances between the helices increase from 1.38 nm to 1.50 nm which lead to the 'E'-type structure.

Several researchers have presented data indicating that starch also undergoes significant molecular degradation (i.e. loss in molecular weight) and molecular modification as it is extrusion processed. Debranching and scission of the amylopectin and amylose molecules during mechanical shear was shown by intrinsic viscosity, water solubility, light scattering, and gel permeation experiments [129, 136, 137, 148, 149]. Recent work by Sagar [42] employing gel permeation chromatography-light scattering showed that the overall molecular weight for extrusion processed Hylon VII (2.5×10^6 g/mol) to be substantially less than the unprocessed starch (3.2×10^6 g/mol) (Conditions for processing are given in Chapter 3.). Such data was not available for the native corn or waxy maize starches due to difficulties in dissolving the amylopectin fraction [42]. One would expect greater chain breakage in these starches since the level of molecular weight reduction is thought to be greater for starches free of amylose, due to complexation of the amylose fraction with lipids. The V-amylose complexes are presumed to shield the amylose polymer from mechanical degradation [129].

Solid state properties of starch-based thermoplastics are a function of many

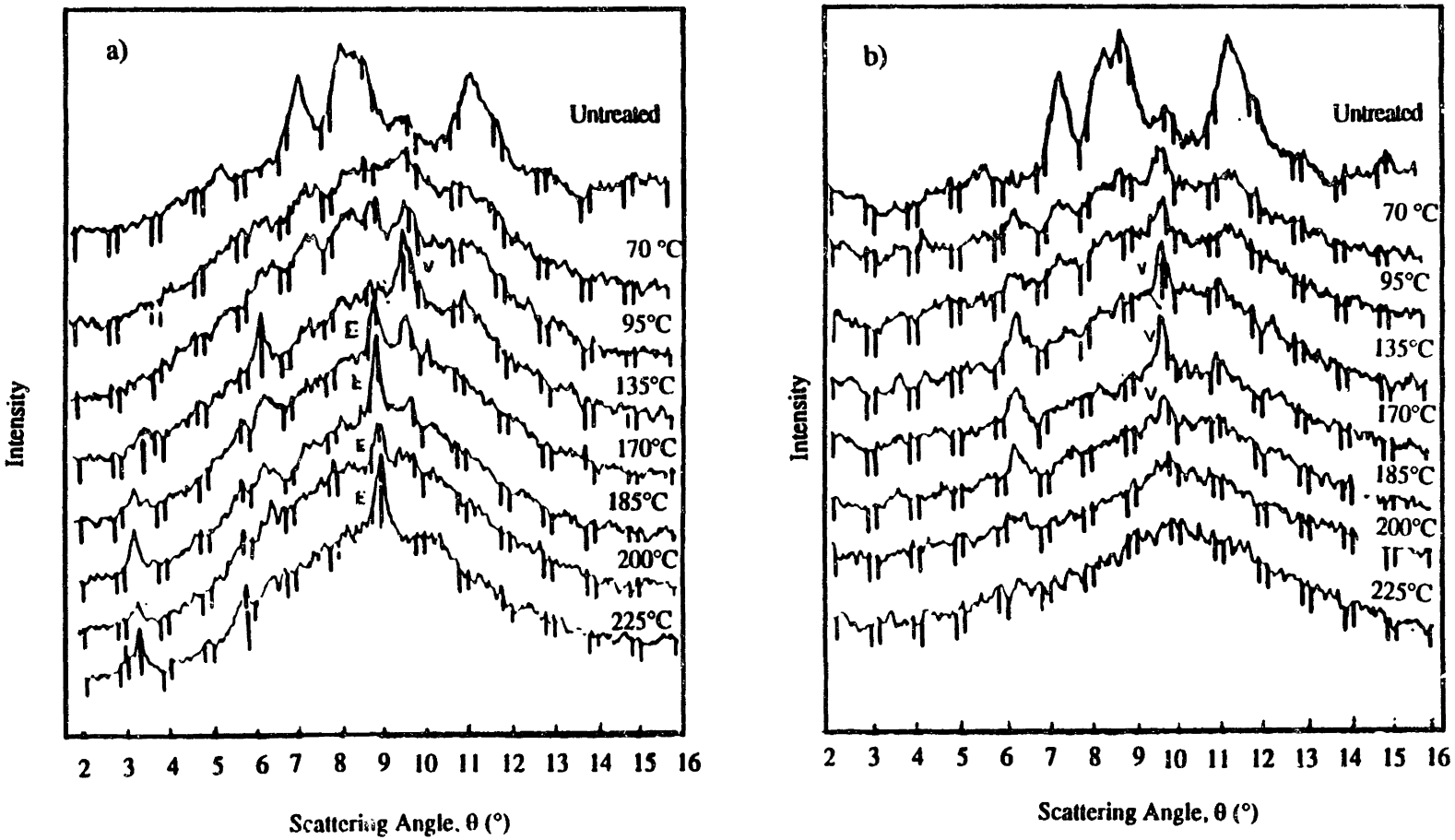

Figure 2.13. WAXS spectra of corn starch extruded at 70, 95, 135, 170, 185, 200, and 225°C. a) Initial moisture content before extrusion, 22 wt%, b) After reconditioning to 30 wt% moisture content [from Mercier, 1979].

variables; some of which include amylose content, degree of destructurization, and modification to amylose and amylopectin chain structure. Items made solely from destructurized or gelatinized starch generally have unacceptable mechanical properties and undergo dimensional changes due to significant moisture uptake and loss which varies with environmental conditions [11, 43, 150, 151]. One way of overcoming these intrinsic property deficiencies is to blend starch with other polymers in an attempt to balance an acceptable rate of biodegradability with acceptable and more stable mechanical properties for commercial plastics applications. In the present study, starch is blended with poly(ethylene-co-vinyl alcohol) (EVOH) which biodegrades although on a timescale much longer than that of starch (i.e. 1.3% mineralized in 50 days, growth of cultures in EVOH versus complete biodegradation of starch within a few days in marine environments) [48, 152]. The addition of this synthetic component serves to improve the processability, increase the toughness, and ameliorate the moisture instability of the product, but, will also decrease the overall rate of biodegradability of the system.

Granular destructurization is key to producing useful thermoplastic starch-based systems. The presence of incompletely dispersed granules (in starch-based films cast from solution) has been found to produce localized stresses which lead to a weakened film structure [11]. Melt spun fibers containing granules which have not been completely "destructurized" have shown the same behavior [39]. Previous studies on systems of starch/polyethylene [30, 153], starch/cellulose acetate [154] and even on systems of starch/EVOH [40] essentially showed evidence of relatively unchanged starch granules greater than 5 μm in size (an example of granules in a corn starch/EVOH extruded ribbon and blown film is shown in figure 2.14). In order to attain sufficient mechanical properties for intended applications, these systems would have to contain more synthetic polymer component and less starch (i.e. less than 15% in a polyethylene matrix [30]) since intact starch granules act to decrease the mechanical properties of the synthetic polymer matrix. The discrete nature of the granules, as well as any remaining

Figure 2.14. SEM micrographs showing incompletely destructurized granules that are present in a) an extruded ribbon, and b) a blown film of a 50:50 corn starch/EVOH (68% VOH) blend. A Brabender single-screw extruder was employed. (Films prepared at Army Research Facility, Natick, MA).

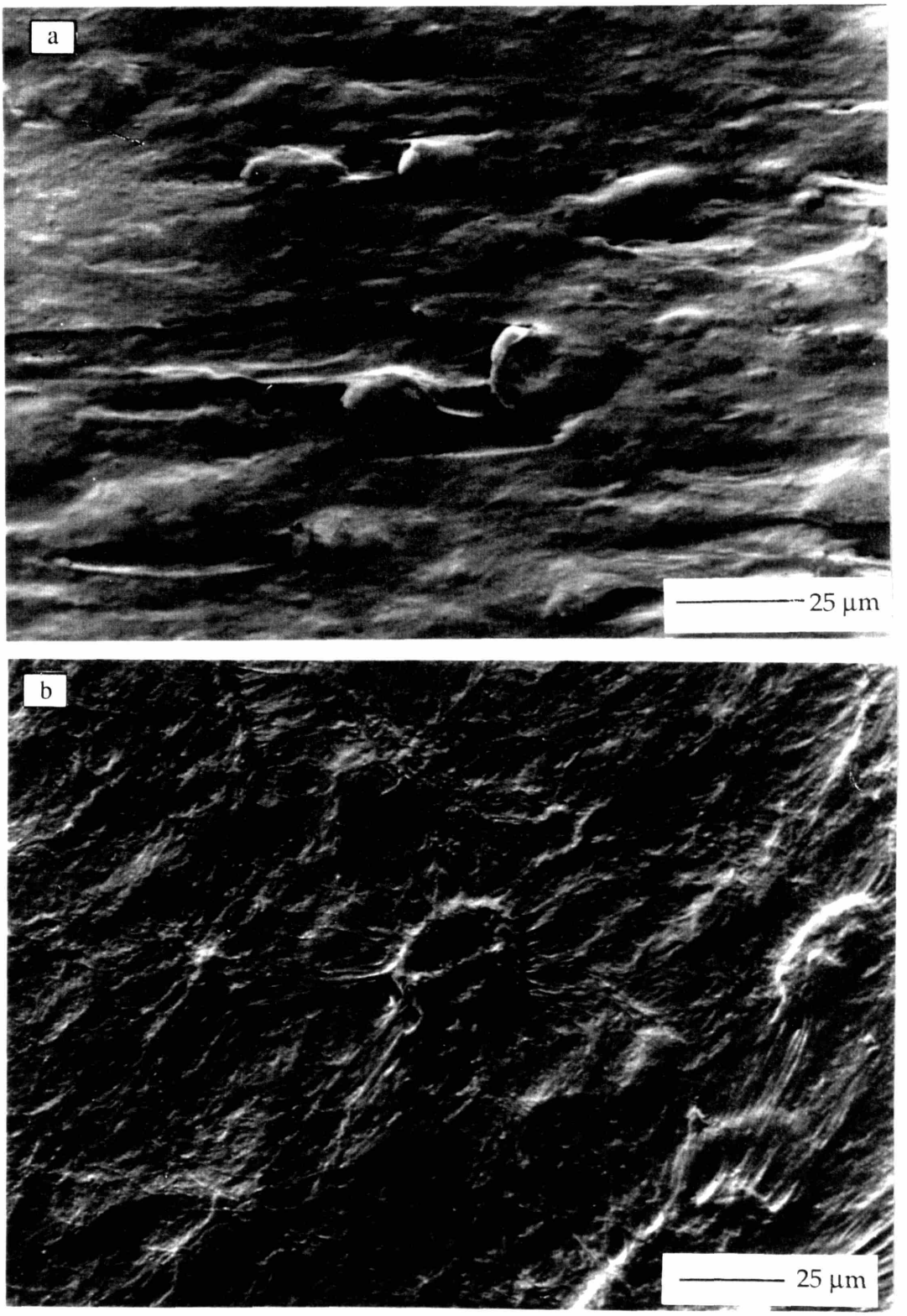
a
25 µm
b
25 µm

crystallinity of the amylopectin component (values ranging from 15-45% crystallinity have been reported by Zobel for various native starch types [97]), will restrict the rate of the biodegradation process. Thus, the focus of this study is placed on blends in which the starch is fully destructurized and more intimately mixed with poly(ethylene-vinyl alcohol) (EVOH).

BLEND MORPHOLOGY

The morphology of a thermoplastic blend made by extrusion compounding is determined by both the thermodynamics and kinetics involved in the mixing process [155]. Thermodynamically, two polymers can form a stable homogenous blend if both the free energy of mixing is negative ($\overline{\Delta G_{mix}} = \overline{\Delta H_{mix}} - \overline{T\Delta S_{mix}} < 0$) and

$$\frac{\partial^2 \overline{\Delta G_{mix}}}{\partial \phi_1^{\,2}} \geq 0 \qquad (2.1)$$

Flory-Huggins theory is often used to express the phase behavior of polymer blends [156]. In this thesis, blends of corn starch with poly(ethylene-vinyl alcohol) are considered. With the addition of plasticizer (such as glycerin and water), a description of the phase behavior can be quite complex (there are five major components to the blends). The free energy of a multicomponent systems can be expressed as:

$$\Delta G_{mix} = kT \sum_{j}^{5} \left(\frac{\phi_j}{x_j} \ln \phi_j + \sum_{i}^{j-1} \chi_{ij} \phi_i \phi_j \right) \qquad (2.2)$$

where ϕ_i and x_i, are the volume fraction and degree of polymerization of component i, respectively; χ_{ij} is the Flory-Huggins interaction parameter between components i and j.

Considering a mixture of only polymers (the major blend components), the

entropy terms, $\frac{\phi_j}{x_j} \ln \phi_j$, will generally be small (since x > 1000) and slightly negative. Often the enthalpy term is used to estimate miscibility in polymer-polymer blends and the solubility parameter approach is utilized [157]. In this case, the enthalpy of mixing is defined by [158]:

$$\Delta\overline{H_{mix}} = \frac{1}{2}\sum_{i}^{n}\sum_{j}^{n}\phi_i\phi_j\left[(\delta_i - \delta_j)^2 + 2K_{ij}\delta_i\delta_j\right] \qquad (2.3)$$

where δ_i and δ_j are the solubility parameters of components i and j, respectively. The parameter, K_{ij}, describes the departure from the geometric mean value and must be taken into account for blends with significant intermolecular interaction, (for instance, K_{ij} is negative for such favorable interpolymer interaction as hydrogen bonding). For EVOH with a vinyl alcohol content of 56 mol%, the solubility parameter is approximately 23 - 28 $(MPa)^{1/2}$ calculated by group contribution methods [159]. Similarly calculated solubility parameters for starch range from 28 to 35 $(MPa)^{1/2}$ although solubilities as high as 45 $(MPa)^{1/2}$ for starch have been reported [35]. Based on these values, immiscibility between starch and EVOH is expected. However, because of hydrogen bonding between the hydroxyl groups on starch polymers with EVOH, the parameter, K_{ij}, is likely negative, favoring miscibility. Whether or not the level of hydrogen bonding is appreciable enough to overcome the difference in solubility parameters is a question for study here (i.e. is starch is at least partially miscible with EVOH?).

In polyolefins, branching may cause immiscibility at lower temperature, although there may be more or complete miscibility at high temperature [160 - 162]. Thus, although group contribution methods predict similar solubility parameters for amylose and amylopectin (since both have the same repeat unit), the actual values are likely to be somewhat different. In fact, amylopectin is more susceptible to dissolution in some solvents (e.g. water) than amylose due to the lower intrachain hydrogen bonding

occurring for this component [59]. In addition, polydispersity in one or more of the polymer components (as is likely for both starch [42] and EVOH (MWD > 2)) may result in mutual solubility under conditions in which monodisperse samples would be immiscible [163]. Finally, one should also note that the addition of plasticizers such as water and glycerin will effect the extent of H-bonding in the blends and can alter δ_i and K_{ij}.

Experimentally, various techniques have been employed to determine if polymer-polymer pairs are compatible (i.e. miscible on a submolecular scale) [157, 164]. Polymer mixtures are often termed compatible if they exhibit single glass transition temperatures. However, this criteria of miscibility is often suspect when broadening of a single glass transition region occurs in the blend and for cases when the polymers each have glass transitions near one another. Depression of the crystallization temperature of a polymer component in a blend is also considered as a criterion for blend miscibility. Another less stringent criterion for miscibility is sample or film clarity. However, for mixtures with almost equal refractive indices, very small phase sizes, or foaming and microvoiding, this criteria is again often ambiguous. NMR is also often used to discern phase behavior; however, polymers that are compatible, but hν scattering may arise from microvoids. Finally, phase contrast or polarized light microscopy or electron microscopy is often used to discern compatibility. However, these techniques are resolution limited, and determination of miscibility may be inconclusive. It is much easier with these techniques to determine if polymers are incompatible.

Many studies have been performed on the kinetic variables involved during the blending of incompatible polymers, reviews of which are given in Paul [165] and Utracki [166]. Recently, focus has been placed on the morphology development during the extrusion compounding process for certain blends of amorphous polymers [140, 141]. Scott proposed a model of the initial morphology development resulting from extrusion blending polymers which were initially in the form of pellets [140]. The pellets are

initially sheared and form sheets or ribbons, holes then form due to interfacial instability to a degree such that a lace structure is then formed. The lace then breaks into irregularly shaped pieces that coalesce to form spherical particles [140] which are characteristic of immiscible polymer blends.

Systems more complex than rubbery incompatible systems (e.g. polystyrene-polybutadiene) have been considered, for example, semi-crystalline polymers [167] and blends of materials with significant viscosity differences [168, 169]. In these types of systems, distinct rheological regimes dependent upon the relative melting of each blend component were identified and rheological properties were characteristic of: 1) elastic solids, 2) deformable solids, 3) transition materials (fluids with suspended solid particles, fractured or semi-fluid materials, dough-like materials), and 4) viscoelastic materials [167]. Differing morphologies were expected based upon the level of processing that the blending procedure involved. Formation of droplets or fibers of a the minority polymer phase was observed depending upon the shearing conditions during extrusion blending as well as the relative viscoelastic properties, composition, particle sizes, and interfacial tensions of the polymer blend components [168, 170, 171]. The effect of shear and elongational flow on polymer blends is considered further in Chapter 5 on fiber spinning.

Starch-based Systems

The structures present in the raw materials as they are added to the extruder have been shown to influence the morphology development during the blending of two polymers [141]. The waxy maize and native corn starches employed in this study existed in their native granular form prior to the extrusion blending process. The Hylon VII grade of starch was pretreated such that it was amorphous and no longer in its granular form. It was a powder with particle size ~ 10 μm. Comparison of blends made from these varieties of starches must take into account the initial state of the starch before processing.

During thermal processing of starch granules from cereal sources, it has been documented that the amylose component will leach out of the granule at a faster rate than amylopectin [172]. In addition, amylose from corn starches easily forms complexes with the lipids present in the granule [129] during processing and is believed to be responsible for the network formation in a starch gel due to entanglements and V-amylose crystalline cross-links between linear chains which connect swollen granules [172]. Based on these results, it is therefore likely that the amylose fraction in starch will have a better chance to interact with other components such as EVOH. A morphological analysis of the starch/EVOH thermoplastic blends is required to determine if this interaction does occur.

In this research, scanning electron microscopy is used for identification of partially destructurized granules as shown in Figure 2.14 for a blown film of corn starch blended with 32 mol% EVOH in a single-screw extruder. Fracture behavior of and surface changes to starch-based fibers can also be effectively monitored using conventional SEM. To obtain information about microstructural phase behavior, cryo-fractured surfaces can be observed and well as samples which have been enzymatically etched to remove starch-rich domains

In addition, TEM is used to examine thermoplastic starch blends in which the ordered granular structure has been partially or totally eliminated. Approaches in the method of examining starch systems in TEM will depend on a number of factors. Questions like the following must be asked: What is the beam sensitivity of the polymer components to the electron beam? Are there crystalline versus non-crystalline regions which can be observed (AM, AP, or EVOH)? Are low dose procedures necessary? Will there be superstructures within a blend matrix (such as granular particles within oriented fibers)? How does water effect the observation of crystals when the sample is irradiated (does water loss destroy/alter crystals)? What is the effect of plasticizer on the visualization of microstructure (will it vaporize in a vacuum environment or when under the electron beam)? Is there direct evidence for microvoids (foaming)? What contrast

mechanisms exist to distinguish different components? Are there specific stains for amylose, amylopectin, and/or EVOH, or is there a sufficient density difference ($\rho_{EVOH} \approx$ 1.2, $\rho_{AM, AP} \approx 1.45$) to resolve these individual components? How does one prepare thin samples from bulk pellets and fibers without introducing artifacts (such as during microtoming)? Transmission electron microscopy of starch systems is therefore not trivial and technique development will be discussed in detail in this thesis.

Next, Rigaku RU200 Diffractometer operated using CuKα radiation and a Ni filter is also employed to examine thermoplastic starch-based blends. Incorporation of a heating stage within the diffractometer allowed determination of crystal transitions as a function of temperature. Additionally, an Enraf Nonius Delft Diffractis 583 (with CuKα radiation and a Ni filter) equipped with Statton camera was employed to examine crystalline changes as a function of composition and processing and orientation effects of molecular constituents (such as in starch-based fibers). Results are presented in Chapters 3 and 5.

Finally, DSC is used to determine the phase behavior of thermoplastic starch blends. Unlike starch, EVOH (44 mol% C2) undergoes nearly reversible phase transitions; it has a melting peak of 165°C and a glass transition temperature of 55 °C. Thus, EVOH is treated as a reference component in starch/EVOH blends. DSC scans of starch/EVOH blends provide information about the melting, degradation, and glass transition behavior as a function of composition which, in addition to information gained from other characterization techniques, can lead to a description of the compatibility (i.e. miscibility) of starch with EVOH.

CONCLUSIONS

The microstructural order of starch-based systems will be a function of whether the starch is in its native state, is in a processed form, or is blended with other components (such as poly(ethylene-vinyl alcohol), glycerin, and water). In this Chapter,

a relatively accepted model for native starch ultrastructure (figure 2.2) was depicted based on previous morphological studies of starch. While it is clear that the native granules of various starches possess a relatively high degree of order, the internal microstructure is still not well established. In general, crystallinity in native starch is associated with the amylopectin component (high amylose starches are less crystalline). Based on light and electron microscopy studies as well as x-ray scattering (and other techniques), the racemose model of amylopectin crystallization in native starch is currently proposed. However, given the uncertainty in the results attained with these techniques presented so far in the literature, further experimental work is necessary for true acceptance of this model. Once the initial granule order is destroyed, amylose crystallizes whereas the branched amylopectin chains remain relatively amorphous. The exact packing structures of amylose and amylopectin in crystals, which yield A-, B-, C-, and V- type x-ray and electron diffraction patterns, are still yet to be determined with complete certainty.

The effect of heat, moisture, and shear in changing starch morphology was next discussed. A very simplified model for granular destructurization during extrusion cooking was presented; the morphological changes associated with starch have not been studied in depth to define a more specific model. To date, the most structural information on starch extrusion has been provided by groups using wide-angle x-ray scattering. Differential scanning calorimetry, although often employed, is often misinterpreted by many researchers due to the number of phase transitions starch undergoes when heated [111, 112] (e.g. glass transition, retrogradation, gelatinization, melting of various crystallites (AM, AP, Amylose lipid complexes), and degradation) which vary with moisture content. A significant problem in the literature is that the terms "gelatinization" and "retrogradation" are often defined to mean different structural changes.

Although the use of starch as biodegradable polymer for certain plastics applications has been investigated over the past 50 years, relatively recent starch extrusion processing technology warrants an investigation of the structure, properties,

and subsequent processability of thermoplastic starch and thermoplastic starch-based blends. Thus, starch/poly(ethylene-vinyl alcohol) blends are studied in this thesis in terms of both thermodynamic and kinetic effects on microstructure. The effect of starch type is considered (amylose/amylopectin ratio) which is expected to lead to different blend morphologies. Reliable technique development of characterization methods (i.e. SEM, TEM, WAXS, DSC, moisture titration, and mechanical testing) are developed to eliminate as many uncertainties in determining structural changes associated with extrusion blending and subsequent thermoplastic processing (e.g. melt fiber spinning).

REFERENCES

1. D.L. Kaplan, J.M. Mayer, D. Ball, J. McCassie, A.L. Allen and P. Stenhouse, 'Fundamentals of Biodegradable Polymers', in *Biodegradable Polymers and Packaging*, C. Ching, D.L. Kaplan and E.L. Thomas, Eds. 1993, Technomic Publishing Co., Inc.: Lancaster, PA. p. 1.

2. H. Roper and H. Koch, 'The Role of Starch in Biodegradable Thermoplastic Materials,'*Starch/Starke*, **42,** 123 (1990).

3. R. Chinnaswamy and M.A. Hanna, 'Extrusion-Grafting Starch Onto Vinylic Polymers,'*Starch/Starke*, **43,** 396 (1991).

4. J.W. Mullen and E. Pacsu, 'Starch Studies: Possible Industrial Utilization of Starch Esters,'*Ind. Eng. Chem.*, **35,** 381 (1943).

5. R.L. Whistler and G.E. Hilbert, 'Mechanical Properties of Films from Amylose, Amylopectin, and Whole Starch Triacetates,'*Industrial & Engineering Chemistry*, **36,** 796 (1944).

6. I.A. Wolff, H.A. Davis, J.E. Cluskey, L.J. Gundrum and C.E. Rist, 'Preparation of Films from Amylose,'*Ind. Eng. Chem.*, **43,** 915 (1951).

7. I.A. Wolff, D.W. Olds and G.E. Hilbert, 'Triesters of Corn Starch, Amylose, and Amylopectin: Properties,'*Industrial and Eng. Chem.*, **43,** 911 (1951).

8. I.A. Wolff, D.W. Olds and G.E. Hilbert, 'Mixed Esters of Amylose,'*Ind. Eng. Chem.*, **49,** 1247 (1957).

9. R.L. Whistler and G.N. Richards, 'Fibers from Amylose Triacetate,'*Ind. Eng. Chem.*, **50,** 1551 (1958).

10. I.A. Wolff, 'Corn Amylose and Amylose Triacetate Fibers,'*Ind. Eng. Chem.*, **50,** 1552 (1958).

11. N.E. Lloyd and L.C. Kirst, 'Some Factors Affecting the Tensile Strength of Starch Films,'*Cereal Chemistry*, **40,** 154 (1963).

12. A.M. Mark and C.L. Mehltretter, 'Water-Soluble Films from Partially Acetylated High-Amylose Corn Starch,'*Die Starke*, **21,** 92 (1969).

13. F.H. Otey, A.M. Mark, C.L. Mehitretter and C.R. Russell, 'Starch-based Film for Degradable Agricultural Mulch,'*I&EC Prod. Res. And Dev.*, **13,** 90 (1974).

14. F.H. Otey, R.P. Westhoff and C.R. Russell. *Starch-based Plastics and Films*. in *Technical Symposium: Nonwoven Product Technology*. 1975.

15. F.H. Otey, R.P. Westhoff and C.R. Russell, 'Starch Graft Copolymers - Degradable Fillers for Poly(vinyl chloride) Plastics,'*I&EC Prod. Res. and Dev.*, **15,** 139 (1976).

16. G.J.L. Griffin, *J. Polym. Sci. Polym. Symp.*, **57,** 281 (1976).

17. F.H. Otey, R.P. Westhoff and C.R. Russell, 'Biodegradable Films from Starch and Ethylene-Acrylic Acid Copolymer,'*Ind. Eng. Chem. Prod. Res. Dev.*, **16,** 305 (1977).

18. F.H. Otey and R.P. Westhoff. *Biodegradable Starch-based Plastic Films for Agricultural Applications.* in *Proceedings of the 15th National Agricultural Plastics Congress.* 1980. Tucson, AZ.

19. F.H. Otey and R.P. Westhoff, 'Biodegradable Starch-Based Blown Films', in *U. S. Patent #4,337,181*, U.S.D.o. Agriculture, Ed. 1982.

20. F.H. Otey. *Starch-based Plastics and Related Products for Agriculture.* in *Proc. 17th Nat'l Agric. Plastics Congress, "Plasticulture Worldwide".* 1983. U. N. H., Manchester, NH.

21. R.L. Whistler, 'History and Future Expectations of Starch Use', in *Starch: Chemistry and Technology*, R.L. Whistler, J.N. Bemiller and E.F. Paschall, Eds. 1984, Academic Press, Inc.: New York. p. 1.

22. B.T. Nwufo, G.J.L. Griffin and K.I. Ekpenyong, 'Extrusion of Starch-Extended Water-Soluble Polyvinyl Alcohol,'*Ind. Eng. Chem. Prod. Res. Dev.*, **23,** 594 (1984).

23. W.M. Doane. *Incorporation of Starch into Plastics.* in *First Annual Corn Utilization Conference.* 1987. St. Louis, Missouri.

24. W.M. Doane, 'Starch-based Polymers for Agricultural Applications,'*Polymer Preprints*, **28,** 103 (1987).

25. F.H. Otey and W.M. Doane. *Starch-based Degradable Plastic Film.* in *Proc. of Symp. on Degrad. Plastics.* 1987. Washington, D. C.

26. F.H. Otey, R.P. Westhoff and W.M. Doane, 'Starch-based Blown Films 2,'*I&EC Research*, **26,** 1659 (1987).

27. G.F. Fanta. *Starch-Thermoplastic Polymer Composites by Graft Polymerization.* in *Corn Utilization Conference II, National Corn Growers Association.* 1988.

28. C.L. Swanson, R.P. Westhoff and W.M. Doane. *Modified Starches in Plastic Films.* in *Corn Utilization Conference II.* 1988.

29. I. Tomka, 'A Thermoplastically Processable Starch and A Process for Making It', in *PCT Patent No. WO 90/05161.* 1989.

30. W. Maddever and G.M. Chapman, 'Modified Starch-based Biodegradable Plastics', in *Plastics Engineering.* 1989. 31.

31. C. Bastioli, V. Bellotti, L. Del Gludice and R. Lombi, 'Polymer Compositions for the Production of Articles of Biodegradable Plastics Material and Methods for Their Preparation', in *European Patent Application 90110070.1*, S.r.l. Butterfly, Ed. 1990.

32. A.-C. Albertsson and S. Karlsson, 'Degradable Polyethylene-Starch Complex,'*Makromol. Chem., Macromol. Symp.*, **48/49,** 395 (1991).

33. S.M. Goheen and R.P. Wool, 'Degradation of Polyethylene-Starch Blends in Soil,'*J. Appl. Polym. Sci.*, **42,** 2691 (1991).

34. R.L. Shogren, A.R. Thompson, F.C. Felker, R.E. Harry-O'Kuru, S.H. Gordon, R.V. Greene and J.M. Gould, 'Polymer Compatibility and Biodegradation of Starch-Poly(ethylene-co-acrylic acid)-Polyethylene Blends,'*J. Appl. Polym. Sci.*, (1991).

35. R.L. Shogren, C.L. Swanson and A.R. Thompson, 'Extrudates of Cornstarch with Urea and Glycols: Structure/Mechanical Property Relations,'*Starch*, **44,** 335 (1992).

36. W.M. Doane, 'New Uses for Starch', in *New Crops, New Uses, New Markets: Industrial and Commercial Products From U.S. Agriculture*. 1992, U.S. Dept of Agriculture: Washington, D.C. p. 147.

37. G.F. Fanta, C.L. Swanson and R.L. Shogren, 'Starch-Poly(ethylene-co-Acrylic Acid) Composite Films. Effect of Processing Conditions on Morphology and Properties,'*J. Appl. Polym. Sci.*, **44,** 2037 (1992).

38. R.L. Shogren, 'Complexes of Starch with Telechelic Poly(ε-caprolactone) Phosphate,'*Carbohydrate Polymers*, **22,** 93 (1993).

39. S. Simmons, C.E. Weigand, R.J. Albalak, R.C. Armstrong and E.L. Thomas, 'Thermoplastic Processing of Starch: Melt Spinning of Starch-Based Fibers', in *Biodegradable Polymers and Packaging*, D.L. Kaplan, C. Ching and E.L. Thomas, Eds. 1993, Technomic Publishing Co.: Lancaster, PA. p. 171.

40. P.J. Stenhouse, J.M. Mayer, M.J. Hepfinger, E.A. Costa, P.A. Dell and D.L. Kaplan, 'Starch Blown Film', in *Biodegradable Polymers and Packaging*, C. Ching, D.L. Kaplan and E.L. Thomas, Eds. 1993, Technomics Publishing Co.: Lancaster, PA.

41. J.-L. Jane, S.-T. Lim and I. Paetau, 'Degradable Plastics Made from Starch andProtein', in *Biodegradable Polymers and Packaging*, C. Ching, D.L. Kaplan and E.L. Thomas, Eds. 1993, Technomic Publishing Co., Inc.: Lancaster, PA. p. 63.

42. A. Sagar, 'Modification and Characterization of Starches and Starch-Based Blends for Use as Environmentally Biodegradable Thermoplastics', Ph.D. Thesis, Massachusetts Institute of Technology (1994).

43. G. Lay, J. Rehm, R.F. Stepto, M. Thoma, J.-P. Sachetto, D.J. Lentz and J. Silbiger, 'Polymer Composition Containing Destructurized Starch', in *United States Patent No. 5,095,054*, Warner-Lambert Company, 1992.

44. W.M. Doane, 'USDA Research on Starch-Based Biodegradable Plastics,'*Starch/Starke*, **44,** 293 (1992).

45. R.L. Shogren, G.F. Fanta and W.M. Doane, 'Development of Starch Based Plastics - A Reexamination of Selected Polymer Systems in Historical Perspective,'*Starch/Starke*, **45,** 276 (1993).

46. J.-C. Huang, A.S. Shetty and M.-S. Wang, 'Biodegradable Plastics: A Review,'*Advances in Polymer Technology*, **10,** 23 (1990).

47. G. Swift, 'Directions for Environmentally Biodegradable Polymer Research,'*Acc. Chem. Res.*, **26,** 105 (1993).

48. J. Mayer and D.L. Kaplan, 'Biodegradable Materials: Balancing Degradability and Performance,'*Trends In Polymer Science*, **2,** 227 (1994).

49. H. Leitch, 'Environmental Watch: Heavy on the Starch', in *Discover*. 1990. 30.

50. D. MacKenzie, 'Italian Firm First with "Truly Biodegradable" Plastic', in *New Scientist*. 1989. 37.

51. R.L. Shogren, R.V. Greene and Y.V. Wu, 'Complexes of Starch Polysaccharides and Poly(Ethylene-co-Acrylic Acid): Structure and Stability in Solution,'*J. Appl. Polymer Sci.*, **42,** 1701 (1991).

52. R.L. Shogren, A.R. Thompson, R.V. Greene, S.H. Gordon and G. Cote, 'Complexes of Starch Polysaccharides and Poly(ethylene-co-Acrylic Acid): Structural Characterization in the Solid State,'*J. Appl. Polymer Sci.*, **47,** 2279 (1991).

53. G.F. Fanta, C.L. Swanson and W.M. Doane, 'Complexing Between Starch and Poly(ethylene-co-acrylic acid) - A Comparison of Starch Varieties and Complexing Conditions,'*Carbohydrate Polymers*, **17,** 51 (1992).

54. F. Wittwer and I. Tomka, 'Polymer Composition for Injection Molding', in *U.S. Patent #4,673,438*, W.-L. Company, Ed. 1987.

55. C. Bastioli, R. Lombi, G. Del Tredici and I. Guanella, 'A Method for the Preparation of Destructurized Strach-based Compositions Produced Thereby', in *European Patent Application*, B. S.r.l., Ed. 1990.

56. T. Galliard, ed., *Starch: Properties and Potential*. 1987, New York: John Wiley & Sons.

57. J.J.M. Swinkels, 'Sources of Starch, Its Chemistry and Physics', in *Starch Conversion Technology*, G.M.A. Van Beynum and J.A. Roels, Eds. 1985, Marcel Dekker, Inc.: New York.

58. E.L. Hirst, M.M.T. Plant and M.D. Wilkinson, 'Polysaccharides. Part XIV. The Molecular Structure of Amylose and Amylopectin', *J. Chem. Soc.*, 2375 (1932).

59. W. Banks and C.T. Greenwood. *Starch and Its Components*. 1975, Edinburgh, England: Edinburgh University Press.

60. A.H. Young, 'Fractionation of Starch', in *Starch: Chemistry and Technology*, R.L. Whistler, J.N. Bemiller and E.F. Paschall, Eds. 1984, Academic Press, Inc.: New York. p. 249.

61. E.L. Thomas, 'Electron Microscopy', in *Encyclopedia of Polymer Science and Engineering*. 1986, John Wiley and Sons, Inc.: New York. p. 644.

62. L.E. Fitt and E.M. Snyder, 'Photomicrographs of Starches', in *Starch: Chemistry and Technology*, R.L. Whistler, J.N. Bemiller and E.F. Paschall, Eds. 1984, Academic Press, Inc.: New York. p. 675.

63. D. Chescoe and P.J. Goodhew, *The Operation of Transmission and Scanning Electron Microscopes*. 1990, New York: Oxford University Press.

64. W. Banks and C.T. Greenwood, 'Molecular Properties of the Starch Components and their Relation to the Structure of the Granule,'*Annals: New York Academy of Sciences*, **210,** 17 (1973).

65. A.D. Evers and B.O. Juliano, 'Varietal Differences in Surface Ultrastructure of Endosperm Cells and Starch Granules of Rice,'*Die Starke*, 160 (1976).

66. J.-L. Jane. T. Kasemsuwan, S. Leas, H. Zobel and J.F. Robyt, 'Anthology of Starch Granule Morphology by Scanning Electron Microscopy,'*Starch/Starke*, **46,** 121 (1994).

67. C. Sterling, 'Fibrils of Starch in Potato and Curcuma,'*Die Starke*, **28,** 39 (1976).

68. K. Kanenaga, K. Kako, T. Harada, A. Koreeda, A. Harada and K. Okuyama, 'Different Behaviors Between Action of B-Subtilis α-amylase and 16% Sulfuric Acid at 32 °C to Starch Granules,'*Chemistry Express*, **4,** 519 (1989).

69. A.D. Evers and E.E. McDermott, 'Scanning Electron Microscopy of Wheat Starch,'*Die Starke*, **22,** 23 (1970).

70. G.F. Fanta, F.L. Baker, J.A. Stolp, R.C. Burr and W.M. Doane, 'Polymer Distribution in Grafted Starch Granule by Scanning Electron Microscopy,'*Die Starke*, **28,** 382 (1976).

71. M.S. Buttrose, 'Electron Microscopy of Acid-Degraded Starch Granules,'*Die Starke*, **3,** 85 (1963).

72. V.K. Muhlethaler, 'Die Ultrastruktur der Starkekorner,'**17,** 245 (1965).

73. D. Gallant and A. Guilbot, 'Electron-Microscopical Studies on the Ultrastructure of Starch Granules by the Aid of New Preparation Methods,'*Starch/Starke*, **21,** 156 (1969).

74. J.F. Chabot, J.E. Allen and L.F. Hood, 'Freeze-Etch Ultrastructure of Waxy Maize and Acid Hydrolyzed Waxy Maize Starch Granules,'*Journal of Food Science*, **43,** 727 (1978).

75. D.J. Gallant and C. Sterling, 'Electron Microscopy of Starch and Starch Products', in *Examination and Analysis of Starch and Starch Products*, J.A. Radley, Ed. 1975, Applied Sciences Publishers, Ltd.: London.

76. M. Yamaguchi, K. Kainuma and D. French, 'Electron Microscopic Observations of Waxy Maize Starch,'*J. of Ultrastructural Research*, **69,** 249 (1979).

77. A. Guilbot and C. Mercier, 'Starch', in *The Polysaccharides*, G.O. Aspinall, Ed. 1985, Academic Press, Inc.: New York.

78. G.T. Oostergetel and E.F.J. Van Bruggen, 'On the Origin of a Low Angle Spacing in Starch,'*Starch/Starke*, **41,** 331 (1989).

79. H. Chanzy, R. Vuong and J.C. Jesior, 'An Electron Diffraction Study on Whole Granule of Linterized Potato Starch,'*Starch/Starke*, **42,** 377 (1990).

80. F.P. Booy, H. Chanzy and S. A., 'Electron Diffraction Study of Single Crystals of Amylose Complexed with n-Butanol,'*Biopolymers*, **18,** 2261 (1979).

81. E.L. Welland and A.M. Donald, 'Single Crystals of V-Amylose,'*Int. J. Biol. Macromol.*, **13,** 69 (1991).

82. R.M. Gohil and R.D. Patel, 'Morphology of Amylose Acetate: Role of Intercrystalline Linkages in Polymers,'*Die Starke*, **28,** 293 (1976).

83. P. Kassenbeck, 'Beitragzur Kenntnis der Verteilung von Amylose und Amylopectin in Starkekornern,'*Starch/Starke*, **30,** 40 (1978).

84. D. French, 'Organization of Starch Granules', in *Starch*, R.L. Whistler, Ed. 1984, Academic Press, Inc.: New York p. 183.

85. R.I. Whistler and E.S. Turner, 'Fine Structure of Starch Granule Sections,'*J. Poly. Sci. (Letters)*, **18,** 153 (1955).

86. W.C. Mussulman and J.A. Wagoner, 'Electron Microscopy of Unmodified and Acid-Modified Corn Starches,'*Cereal Chemistry*, **45,** 162 (1968).

87. P.D. Gallant and A. Guibot, 'Artefacts au Cours de la Preparation de Coupes de Grains D'Amidon,'*Die Starke*, **23,** 244 (1971).

88. P. Kassenbeck, 'Electronenmikroskopischer Beitrag zur Kenntnis der Feinstrucktur der Weizenstarke,'*Die Starke*, **27,** 217 (1975).

89. J.M.V. Blanshard, 'Starch Granule Structure and Function: A Physiochemical Approach', in *Starch: Properties and Potential*, T. Galliard, Ed. 1987, John Wiley & Sons: New York.

90. S. Hizukuri and Z. Nikuni, 'Micelle Dimension of Potato Starch,'*Nature*, **180,** 436 (1957).

91. C. Sterling, 'A Low Angle Spacing in Starch,'*J. Polym. Sci.*, **56,** 510 (1962).

92. R.E. Cameron and A.M. Donald, 'A Small-Angle X-Ray Scattering Study of the Annealing and Gelatinization of Starch,'*Polymer*, **33,** 2628 (1992).

93. R.E. Cameron and A.M. Donald, 'Small Angle X-Ray Scattering and Differential Scanning Calorimetry from Starch and Retrograded Starch', in *Food Polymers, Gels and Colloids*, E. Dickinson, Ed. 1991, Royal Society of Chemistry: Cambridge, UK. p. 301.

94. R.E. Cameron and A.M. Donald, 'A Small Angle X-Ray Scattering Study of the Absorption of Water into the Starch Granule,'*Carbohydrate Research*, **244,** 225 (1993).

95. A. Buleon, M.M. Delangli, J. Brisson and H. Chanzy, 'Single Crystals of V-Amylose Complexed with Isopropanol and Acetone,'*Int. J. Biol. Macromol.*, **12,** 25 (1990).

96. P. Colonna, A. Buleon and C. Mercier, 'Physically Modified Starches', in

Starch: Properties and Potential, T. Galliard, Ed. 1987, John Wiley & Sons: New York.

97. H.F. Zobel, 'Starch Crystal Transformations and Their Industrial Importance,'*Starch/Starke*, **40,** 1 (1988).

98. G. Wulff and S. Kubik, 'Helical Amylose Complexes with Organic Complexands, 1 Microscalorimetric and Circular Dichroitic Investigations,'*Makromol. Chem.*, **193,** 1070 (1992).

99. J. Blackwell, A. Sarko and R.H. Marchessault, 'Chain Conformation in B-Amylose,'*Journal of Molecular Biology*, **42,** 379 (1969).

100. H.-C.H. Wu and A. Sarko, 'The Crystal Structure of A-Starch is it Double Helical?,'*Carbohydreate Research*, **54,** C3 (1977).

101. H.-C.H. Wu and A. Sarko, 'The Double-Helical Molecular Structure of Crystalline A-Amylose,'*Carbohydrate Research*, **61,** 27 (1978).

102. H.-C.H. Wu and A. Sarko, 'The Double-Helical Molecular Structure of Crystalline B-Amylose,'*Carbohydrate Research*, **61,** 7 (1978).

103. A. Sarko and R.H. Marchessault, *J. American Chemical Society*, **89,** 6454 (1967).

104. A. Sarko and H.-C.H. Wu, 'The Crystal Structure of A-, B-, and C-Polymorphs of Amylose and Starch,'*Starch/Starke*, **30,** 73 (1978).

105. A. Buleon, F. Duprat, F.P. Booy and H. Chanzy, *Carbohydrate Polymers*, **4,** 161 (1984).

106. H. Chanzy and R. Vuong, 'Ultrastructure and Morphology of Cystalline Polysaccharides', in *Polysaccharides: Topics in Structure and Morphologoy*, E.D.T. Atkins, Ed. 1985, VCH: Weinheim Deerfield Beach, FL.

107. A. Imberty, H. Chanzy, S. Perez, A. Buleon and V. Tran, 'New Three Dimensional Structure for A-Type Starch', *Macromolecules*, **20,** 2634 (1987).

108. A. Imberty, A. Buleon, V. Tran and S. Perez, 'Recent Advances in Knowledge of Starch Structure,'*Starch/Starke*, **43,** 375 (1991).

109. D.L. Wild and J.M.V. Blanshard, 'The Relationship of the Crystal Structure of Amylose Polymorphs to the Structure of the Starch Granules,'*Carbohydrate Polymers*, **6,** 121 (1986).

110. A.C. Eliasson, K. Larsson, S. Anderson, S.T. Hyde, R. Nesper and H.G. von Schnering, 'On the Structure of Native Starch: An Analog to the Quartz Structure,'*Starch/Starke*, **39,** 147 (1987).

111. H. Liu and J. Lelievre, 'A Differential Scanning Calorimetry Study of Melting Trnsitions in Aqueous Suspensions Containing Blends of Wheat and Rice Starch,'**17,** 145 (1992).

112. C.G. Biliaderis, C.M. Page and T.J. Maurice, 'Non-Equilibrium Melting of Amylose-V Complexes,'*Carbohydrate Polymers*, **6,** 269 (1986).

113. P.K. Hari, S. Garg and S.K. Garg, 'Gelatinization of Starch and Modified Starch,'*Starch/Starke*, **41**, 88 (1989).

114. D.J. Burt and P.L. Russell, 'Gelatinization of Low Water Content Wheat Starch - Water Mixtures: A Combined Study by Differential Scanning Calorimetry and Light Microscopy,'*Starch/Starke*, **35**, 354 (1983).

115. H. Liu and J. Lelievre, 'Effects of Heating Rate and Sample Size on Differential Scanning Calorimetry Traces of Starch Gelatinized at Intermediate Water Levels,'*Starch/Starke*, **43**, 225 (1991).

116. C.G. Biliaderis, 'Thermal Analysis of Food Carbohydrates', in *Thermal Analysis of Foods*, V.R. Harwalkar and C.-Y. Ma, Eds. 1990, Elsevier Science Publishing Co., Inc.: New York. p. 168.

117. S.S. Wang, W.C. Chiang, B. Zhao, X.G. Zheng and I.H. Kim, 'Experimental Analysis and Computer Simulation of Starch-Water Interactions during Phase Transition,'*J. Food Science*, **56**, 121 (1991).

118. R.L. Shogren, 'Effect of Moisture Content on the Melting and Subsequent Physical Aging of Cornstarch,'*Carbohydrate Polymers*, **19**, 83 (1992).

119. J.W. Donovan, 'Phase Transitions of the Starch-Water System,'*Biopolymers*, **18**, 263 (1979).

120. M.J. Miles, V.J. Morris, P.D. Orford and S.G. Ring, 'The Roles of Amylose and Amylopectin in the Gelation and Retrogradation of Starch,'*Carbohydrate Research*, **135**, 271 (1985).

121. K.J. Zeleznak and R.C. Hoseney, 'The Role of Water in the Retrogradation of Wheat Starch Gels and Bread Crumb,'*Cereal Chemistry*, **63**, 407 (1986).

122. M. Gudmundsson and A.C. Eliasson, 'Retrogradation of Amylopectin and the Effect of Amylose and Added Surfactants/Emulsifiers,'*Carbohydrate Polymers*, **13**, 295 (1990).

123. J. Longton and G.A. LeGrys, 'Differential Scanning Calorimetry Studies on the Crystallinity of Ageing Wheat Starch Gels,'*Starch/Starke*, **33**, 410 (1981).

124. T. Jankowski and C.K. Rha, 'Retrogradation of Starch in Cooked Wheat,'*Starch/Starke*, **38**, 6 (1986).

125. A. Matsunaga and K. Kainuma, 'Studies on the Retrogradation of Starch in Starchy foods; Pt. 3 Effect of the Addition of Sucrose Fatty Acid Ester on the Retrogradation of Corn Starch,'*Starch/Starke*, **38**, 1 (1986).

126. S.J. Livings, A.M. Donald and A.C. Smith, 'Ageing in Confectionary Wafers,'*Proceedings of 1992 Sutton Bovington Gasbe School*. (1992).

127. K.J. Zeleznak and R.C. Hoseney, 'The Glass Transition of Starch,'*Cereal Chemistry*, **64**, 121 (1987).

128. P.D. Orford, R. Parker, S.G. Ring and A.C. Smith, 'Effect of Water as a Diluent on the Glass Transition Behaviour of Malto-Oligosaccharides, Amylose and

Amylopectin,'*Int. J. Biol. Macromol.*, **11,** 91 (1989).

129. C. Mercier, R. Charbonniere, D. Gallant and A. Guilbot, 'Structural Modifications of Various Starches by Extrusion Cooking with a Twin Screw French Extruder', in *Polysaccharides in Food*, J.M.V. Blanshard and J.R. Mitchell, Eds. 1979, Butterworth Publ.: London. p. 153.

130. C. Mercier and P. Feillet, 'Modification of Carbohydrate Components by Extrusion Cooking of Cereal Products,'*Cereal Chemistry*, **52,** 283 (1975).

131. C. Mercier, 'Effect of Extrusion Cooking on Potato Starch Using a Twin Screw French Extruder,'*Die Starke*, **29,** 48 (1977).

132. W. Wiedmann, 'Extrusion Cooking of Starches for Semi -Products,' *Starch/Starke*, **39,** 352 (1987).

133. W. Wiedmann and E. Strobel, 'Compounding of Thermoplastic Starch with Twin-Screw Extruders', 1992, Werner-Pfleiderer Corporation.

134. W. Wiedmann, 'Principles and Applications of Starch Extrusion', 1992, Werner-Pfleiderer Corp.

135. V.J. Davidson, D. Paton, L.L. Diosady and G. Larocque, 'Degradation of Wheat Starch in a Single Screw Extruder: Characteristics of Extruded Starch Polymers,'*Journal of Food Science*, **49,** 453 (1984).

136. V.J. Davidson, D. Paton, L.L. Diosady and L.J. Rubin, 'A Model for Mechanical Degradation of Wheat Starch in a Single-Screw Extruder,'*Journal of Food Science*, **49,** 1154 (1984).

137. L.L. Diosady, D. Paton, N. Rosen, L.J. Rubin and C. Athanassoulias, 'Degradation of Wheat Starch in a Single-Screw Extruder: Mechano-Kinetic Breakdown of Cooked Starch,'*Journal of Food Science*, **50,** 1697 (1985).

138. L.S. Lai and J.L. Kokini, 'The Effect of Extrusion Operating Conditions on the On-Line Apparent Viscosity of 98% Amylopectin (Amioca) and 70% Amylose (Hylon 7) Corn Starches During Extrusion,'*Journal of Rheology*, **34,** 1245 (1990).

139. M.H. Gomez and J.M. Aguilera, 'A Physicochemical Model for Extrusion of Corn Starch,'*Journal of Food Science*, **49,** 40 (1984).

140. C.E. Scott, 'Characterization of the Reactive Polymer Blending Process', Ph.D. Thesis, University of Minnesota (1990).

141. U. Sundararaj, 'Morphology Development During Polymer Blending', Ph.D. Thesis, University of Minnesota (1994).

142. B.C. Burros, L.A. Young and P.A. Carroad, 'Kinetics of Corn Meal Gelatinization at High Temperature and Low Moisture,'*Journal of Food Science*, **52,** 1372 (1987).

143. B. Vergnes and J.P. Villemaire, 'Rheological Behavior of Low Moisture Molten Maize Starch,'*Rheol. Acta*, **26,** 570 (1987).

144. S.T. Nara, 'On the Relationship Between Specific Volume and Crystallinity of Starch,'*Starke*, **31,** 73 (1979).

145. P.H. Hermans and A. Weidinger, 'Quantitative X-Ray Investigations on the Crystallinity of Cellulose Fibers: A Background Analysis,'*J. Appl. Physics*, **19,** 491 (1948).

146. P.H. Hermans and A. Weidinger, 'X-Ray Studies on the Crystallinity of Cellulose,'*J. Polym. Sci.*, **4,** 135 (1949).

147. P.H. Hermans and A. Weidinger, 'Crystallinity of Precipitated Cellulose,'*J. Polymer Science*, **5,** 565 (1950).

148. P. Colonna, J.L. Doublier, J.P. Melcion, F. de Monredon and C. Mercier, 'Extrusion Cooking and Drum Drying of Wheat Starch. I. Physical and Macromolecular Modifications,'*Cereal Chemistry*, **1,** 538 (1984).

149. M.H. Gomez and J.M. Aguilera, 'Changes in the Starch Fraction During Extrusion-Cooking of Corn,'*Journal of Food Science*, **48,** 378 (1983).

150. R.L. Shogren, 'Effects of Moisture and Various Plasticizers on the Mechanical Properties of Extruded Starch', in *Biodegradable Polymers and Packaging*, D. Kaplan, E. Thomas and C. Ching, Eds. 1993, Technomic Publishing Co., Inc.: Lancaster, PA. p. 141.

151. G.L. Loomis, A.R. Hopkins and E.R. George, 'Starch-Based Materials', in *Biodegradable Polymers and Packaging*, C. Ching, D.L. Kaplan and E.L. Thomas, Eds. 1993, Technomic Publishing Co.: Lancaster, PA. p. 43.

152. J.E. McCassie, J.M. Mayer, R.E. Stote, A.E. Shupe, P.J. Stenhouse, P.A. Dell and D.L. Kaplan, 'Biodegradation Kinetics in Marine and Soil Systems', in *Biodegradable Polymers and Packaging*, C. Ching, D.L. Kaplan and E.L. Thomas, Eds. 1993, Technomic Publishing Co.: Lancater, PA. p. 217.

153. R.L. Evangelista, Z.L. Nikolov, W. Sung, J.-L. Jane and R J. Gelina, 'Effect of Compounding and Starch Modification on Properties of Starch-Filled Low-Density Polyethylene,'*Ind. Eng. Chem. Res.*, **30,** 1841 (1991).

154. J. Mayer, D. Kaplan and D. Vezie, 'personal communication', (1994).

155. D.R. Paul and S. Newman, eds. *Polymer Blends.*. 1978, Academic Press: New York.

156. P.J. Flory, *Principles of Polymer Chemistry*. 1953, Ithaca, NY: Cornell University Press.

157. O. Olabisi, L.M. Robeson and M.T. Shaw, *Polymer-Polymer Miscibility*. 1979, New York: Academic Press, Inc.

158. T.O. Ahn, C.K. Kim, B.K. Kim, H.M. Jeong and J.D. Huh, 'Binary Blends of Nylons with Ethylene Vinyl Alcohol Copolymers: Morphological, Thermal, Rheological, and Mechanical Behavior,'*Polymer Engineering and Science*, **30,** 341 (1990).

159. D.W. Van Krevelen, *Properties of Polymers: Their Correlation with Chemical Structure; Their Numerical Estimation and Prediction from Additive Group Contributions*. 3rd ed. 1990, New York: Elsevier Science Publishers, B. V.

160. J. Chen, M. Fone, V.N. Reddy, K.B. Schwartz, H.P. Fisher and B. Wunderlich, 'Identification and Quantitative Analysis of the Intermediate Phase in a Linear High-Density Polyethylene,'*Journal of Polymer Science: Pt. B: Polymer Physics*, **32,** (1994).

161. J. Rhee and B. Crist, 'Thermodynamics and Phase Separation in Melt Blends of Polyethylene and Model Copolymers,'*Macromolecules*, **24,** 5663 (1991).

162. J. Rhee and B. Crist, 'Phase Behavior, Morphology, and Mechanical Properties of Polyethylene-Copolymer Blends,'*Journal of Polymer Science: Part B: Polymer Physics*, **32,** 159 (1994).

163. R. Koningsveld, K. Solc and W.J. MacKnight, 'Thermodynamic Aging of Immiscible Polymer Blends,'*Macromolecules*, **26,** 6676 (1993).

164. S. Krause, 'Compatible Polymers', in *Polymer Handbook*, J. Brandrup and E.H. Immergut, Eds. 1989, John Wiley and Sons, Inc.: New York. p. VI/347.

165. D.R. Paul and J.W. Barlow, 'A Brief Review of Polymer Blend Technology', in *Multiphase Polymers*, S.L. Cooper and G.M. Estes, Eds. 1979, American Chemical Society: Washington, D. C. p. 315.

166. L.A. Utracki, *Polymer Alloys and Blends*. 1989, Munich: Hanser Publishers.

167. C.-K. Shih, D.G. Tynan and D.A. Denelsbeck, 'Rheological Properties of Multicomponent Polymer Systems Undergoing Melting or Softening During Compounding,'**31,** 1670 (1991).

168. B.D. Favis and D. Therrien, 'Factors Influencing Structure Formation and Phase Size in an Immiscible Polymer Blend of Polycarbonate and Polypropylene Prepared by Twin-Screw Extrusion,'*Polymer*, **32,** 1474 (1991).

169. C.K. Shih, 'Rheological Properties of Incompatible Blends of Two Elastomers,'**16,** 742 (1976).

170. H. Vanoene, 'Modes of Dispersion of Viscoelastic Fluids in Flow,'*Journal of Colloid and Interface Science*, **40,** 448 (1972).

171. M.V. Tsebrenko, A.V. Yudin, T.I. Ablazova and G.V. Vinogradov, 'Mechanism of Fibrillation in the Flow of Molten Polymer Mixtures', *Polymer*, **17,** 831 (1980).

172. H.J. Cornell, 'The Effect of Amylopectin on the Properties of Starch Gels,'*Die Starke*, 43 (1963).

Chapter 3

Structural Characteristics of Biodegradable Thermoplastic Starch/Poly(ethylene-vinyl alcohol) Blends

ABSTRACT

To establish relationships between the blend composition, processing history, and the resultant properties of starch-based thermoplastics, three varieties of corn starch: 1) Waxy Maize, 2) Native Corn, and 3) high amylose Hylon VII were extrusion blended with poly(ethylene-vinyl alcohol) (EVOH) containing 56 mol% VOH. Wide-angle x-ray scattering (WAXS), differential scanning calorimetry (DSC), scanning electron microscopy (SEM), and transmission electron microscopy (TEM) were used to examine the structural characteristics of the blends. All starches were destructurized upon compounding and a fine dispersion was achieved with EVOH. The Native Corn and Hylon VII blends were phase separated and exhibited some miscibility between the polymer components as evident in EVOH melting point depression, smaller domain sizes, lower contrast between phases in TEM, and increased resistance to moisture and enzyme etching treatments. Starches containing amylose exhibited complexation and crystallinity in the starch fraction, although most of the crystallinity in the blends was due to the EVOH component. Waxy Maize blends were well phase separated and underwent phase coarsening as a function of time in the melt. When subjecting the blends to capillary flow, orientation of both starch-rich and EVOH-rich domains was observed at various compositions with the EVOH component undergoing significantly more orientation relative to starch as evident by the presence of EVOH-rich fibrils. Finally, EVOH was found to coat the surfaces of filaments produced from the blends even at rather high levels of starch (70%) which is expected to somewhat stabilize these materials with respect to moisture sensitivity and slow down their initial rate of biodegradation.

INTRODUCTION

Starch has been considered as a candidate material in certain thermoplastic applications because of its known biodegradability, availability, and low cost [1, 2]. Its utilization in non-food, plastic applications has been investigated by researchers over the past fifty years [1, 3-20]. Reviews of these developments have been published by Roper [21], Doane [22], Shogren [23], and others [24-26]. Over the last few years, corporations such as Novamont Inc., a subsidiary of the Montedison Group in Italy, and the Warner-Lambert Co., Morris Plains, NJ, have commercially produced various grades of starch-based thermoplastic resin (marketed under the names, Mater-Bi® and Novon®, respectively). In the production of these materials, heat, moisture, and mechanical deformation are used to destructurize starch and blend it with various polymers and plasticizers in order to achieve a fine dispersion [4, 15, 27-29]. Typical applications of these blends are food utensils, disposable pens, packaging peanuts, composting bags, and other single-use items. Key to understanding how to optimize these product properties is establishing the relationships between the blend composition, processing history, and the resultant structural and physical properties of such materials.

Starch itself is not a true thermoplastic in the sense that it will degrade when heated and not form a melt on its own. Combining starch with plasticizers such as glycerin and water, however, will make starch behave as a thermoplastic. In this state, it can flow as a melt through an extruder and be processed in typical thermoplastic applications. Unfortunately, the mechanical properties and dimensional stability of articles made solely of thermoplastic starch are very dependent upon the relative humidity at which these articles are stored [30]. One way of overcoming this problem is to blend starch with other polymers that possess more stable properties and some degree of biodegradability. In the present study, poly(ethylene-co-vinyl alcohol) (EVOH) containing 56 mol% vinyl content was used. The addition of this synthetic component serves to improve the processability, increase the toughness, and ameliorate the moisture

instability of the product, but, will also decrease the overall rate of biodegradability of the system (EVOH biodegrades although on a timescale much slower than that of starch [26, 31]). Previous studies focusing on the injection molding and fiber spinning capabilities, physical properties, and rheology of these particular blends have been performed [30, 32, see Chapter 5]. An in-depth TEM study of the morphology of the starch/EVOH blends is presented in Chapter 4.

Since there are many sources of starch and each of these exhibits different characteristics, three different varieties of corn starch were chosen for study. These starches, which include a native corn starch and two hybrid corn starches (Waxy Maize and Hylon VII), differ in the percentage of linear amylose to branched amylopectin that exist in each starch granule and in the corresponding molecular weights of these polymer components. The blend morphology that results upon processing these starch varieties with EVOH will not only influence the mechanical properties but also the manner in which a product made from these materials degrades. For example, crystallinity will decrease the accessibility of moisture and, hence, microbes to certain areas within the blend. Also, whether or not the starch forms a continuous phase or discrete domains within the EVOH component and the size of these domains will effect both the biodegradation rate and the mechanical behavior. Finally, the biodegradation rate will be strongly affected if there is surface enrichment by one component.

The processability and properties of any thermoplastic blend will depend strongly upon the morphology that results from both the thermodynamics and kinetics involved in the mixing process [33]. The blending of different starch varieties with poly(ethylene-co-vinyl alcohol) requires the destruction of highly organized granules of the native corn and waxy maize starches or deorganization of the relatively amorphous, pre-treated high amylose particles (Hylon VII). These raw materials range in size from 5 to 25 μm. EVOH pellets of about 3 mm in diameter and 4 mm in length must be melted and thoroughly blended with the starch domains. Whether or not softening of the EVOH

phase occurs prior to, during, or after the granule destructurization and/or softening of the starch will influence the morphology of the blend upon exiting the extruder. Water (both in the "dry" materials and as a liquid feed) will cause the starch granules to swell; further destructurization occurs with the application of heat and shear. In addition, water as well as glycerin, injected into the extruder as a relatively non-volatile plasticizer, may partition unevenly between the starch and EVOH components. Processing additives, such as triglycerides, may also effect processing by lowering the interfacial tension between phases in the melt, and, hence, the final blend morphology. The number of variables involved during the compounding of starch/EVOH blends makes this a very complex process which is expected to lead to varied morphologies and associated properties.

The present study is a structural investigation of a systematic series of model blends consisting of starch, a synthetic polymer, and plasticizers, conducted using wide-angle x-ray scattering (WAXS), differential scanning calorimetry (DSC), and scanning electron microscopy (SEM). Selected results from a transmission electron microscopy (TEM) are also presented, but they are discussed in detail in Chapter 4. X-ray scattering was used to determine crystalline phase types, physical aging effects in the blends, and crystallinity changes with temperature and time. DSC was employed to explore thermal behavior (e.g. T_m, T_g of various components) and perhaps gain information on the miscibility of the blend. Electron microscopy was used to examine the morphology of the blends as a function of starch type and EVOH composition. The effect of capillary flow on certain blends was investigated using SEM to gain insight in the flow properties of the starch and EVOH components. Finally, melt phase size coarsening study was also performed to examine the stability of the melt for starch/EVOH blends. A discussion of the significance of these structural observations on the processability, biodegradability and mechanical properties of starch-based thermoplastics is presented.

EXPERIMENTAL

Raw Materials

Amioca, Melojel, and EK Fl. Hylon VII starches were supplied by National Starch and Chemical Company (Bridgewater, NJ). Amioca waxy maize (WM) is a hybrid corn starch containing essentially 100% highly branched amylopectin (M_{AP} ~ $100*10^6$ g/mole). Melojel is a native corn starch (NC) possessing 28% of linear amylose (M_{AM} ~ $1*10^6$ g/mole) and 72% amylopectin (M_{AP} ~ 50 - $100*10^6$ g/mole). Both the waxy maize and native corn starches were received in the form of granules before compounding. Hylon VII (HY) is a genetically engineered corn starch which consists of approximately 70% amylose (M_{AM} ~ $0.8*10^6$ g/mole) and 30% amylopectin (M_{AP} ~ 20 - $50*10^6$ g/mole). The Hylon VII starch, as supplied, is a fine powder that had been previously spray-dried (crystallinity in the original granules was destroyed by the use of high pressure steam). Based on intrinsic viscosity measurements performed at National Starch, $[\eta]_{0.5N\ NaOH}$ = 0.5 dl/g compared with 0.9 - 0.95 dl/g for the untreated Hylon starch. The supplier estimates that the molecular weight of the EK. Fl. Hylon VII grade is ~ $0.4*10^6$ g/mole for the amylose fraction and ~ 10 - $25*10^6$ g/mole for the amylopectin fraction [34].

Film-grade poly(ethylene-co-vinyl alcohol), EVAL E 105A, was obtained from EVAL Company of America (Lisle, IL). The EVOH contains 44 mole% ethylene, has a melt index of 12 at 210°C and a number average molecular weight, M_n, equal to 45,000. The weight to number average, M_w/M_n, is 2.22 (SEC, 90°C in dimethylacetamide/0.2 % LiBr soln., polystyrene standard) [35]. The peak melting temperature and glass transition are 165°C and 55°C, respectively, for pure EVOH. Deionized water, glycerin, and naturally occurring triglyceride additives, used as plasticizers, lubricants, release agents, and melt flow accelerators [28] were provided through the Warner-Lambert Company (Morris Plains, NJ).

Blend Compounding

Three series of blends, containing different levels of each starch and EVOH, were compounded at the Novon Research Division of Warner-Lambert in Morris Plains, NJ [30]. Nomenclature, composition, and processing conditions are summarized in Table 3.1. Ratios by weight of starch to EVOH for each series were: 100:0, 85:15, 70:30, 60:40, 40:60, 50:50, 40:60, 30:70, 15:85, and 0:100. To aid in the processing of the starch fraction, a small amount of triglycerides was added to the dry mixture (3 parts to 100 parts starch). Dry materials (starch in powder form, EVOH in pellet form, and powder additive) were mixed in a 100 L Gral Mixer prior to extrusion blending.

Compounding of this experimental series of starch/EVOH blends took place in a Leistriz Standard Model-34, twin screw, co-rotating extruder equipped with ten separate zones. Feed was added to Zone 1 through 2 ports. The dry mixture was fed, at rates of 10 to 20 kg/hr, from a hopper directly above zone 1. A twin screw outlet (for all powder blends) or a single screw (for the powder/pellet mixture) was employed to produce a constant feed throughput to the extruder. Glycerin was pumped through a liquid port at the at zone 2 at rates of 1.7 to 3.6 kg/hr such that it was approximately 15 wt% of the total feed. In addition to the feed, deionized water was added through a separate port leading to zone 2 in amounts just necessary to prevent surging (by lowering the current draw) during the extrusion of certain blends. Surging is a phenomena which occurs when there is a sudden transient rise in the current draw, usually as a result of material backing up in the feed zone or bridging in the feed hopper. At zone 8, a 200 mbar vacuum was applied for collection of volatiles (i.e. steam). The blends exited from zone 10 through the die at rates of 11 to 23 kg/hr.

Processing conditions depended upon the composition of the blend. Peak extrusion temperatures (at zones 5 and 6) ranged from 165 - 190°C, except for the NC100 blend for which lower temperatures and higher moisture levels were necessary for processing. Screw speeds ranged from 114 to 200 rpm. The blend consisting of

Table 3.1. Model Starch-Poly(ethylene-co-vinyl alcohol) Blends*: Nomenclature, Composition, and Processing Parameters

Blend	Starch:EVOH by weight	Glycerin Content (wt%)	Water Content (wt%)	Max. Extrusion Temperature (°C)	Screw Speed (RPM)	Output Flow Rate (kg/hr)
High Amylose Starch (Hylon VII) Blends:						
HY100	100:0	15.1	8.7	170	150	11.4
HY85	85:15	14.3	8.5	180	176	19.3
HY70	70:30	14.8	10.6	190	130	17.3
HY60	60:40	14.3	11.1	175	199	19.2
HY50	50:50	15.6	12.1	190	149	19.3
HY40	40:60	14.1	6.6	175	191	18.6
HY30	30:70	14.1	8.0	190	125	17.8
HY15	15:85	14.0	5.6	175	200	16.0
Native Corn Starch Blends:						
NC100	100:0	12.2	15.8	119	160	14.2
NC85	85:15	14.7	9.7	180	175	17.5
NC70	70:30	18.1	12.7	194	120	19.9
NC60	60:40	14.8	6.6	180	200	22.9
NC50	50:50	16.1	9.8	190	125	19.2
NC40	40:60	14.8	4.8	185	199	24.1
NC30	30:70	13.6	6.8	190	137	18.3
NC15	15:85	14.2	5.6	175	200	18.4
Waxy Maize Starch Blends:						
WM100	100:0	16.1	7.8	190	131	11.4
WM85	85:15	14.8	8.8	185	130	21.3
WM70	70:30	16.3	5.3	190	114	17.3
WM60	60:40	14.8	6.6	180	165	20.7
WM50	50:50	14.8	9.0	190	115	19.2
WM40	40:60	14.8	4.9	180	180	19.7
WM30	30:70	12.7	7.6	190	129	17.7
WM15	15:85	14.6	4.4	165	175	16.6
Poly(ethylene-co-vinyl alcohol) Control:						
EVOH/GLY	0:100	14.0	1.4	170	30	5.3

* Model Blends containing starch were compounded using a Leistriz (34 mm) twin screw extruder. The EVOH/GLY blend was compounded on a Haake (30 mm) extruder.

only EVOH and glycerin was compounded on a Haake extruder (30 mm, L/D = 13). Peak extrusion temperature was 170°C, screw speed was 30 rpm, and throughput was 5.3 kg/hr. All blends were pelletized upon exiting the extruder, cooled by air flow on a spiral conveyer, and collected and sealed in plastic bags.

Moisture and glycerin contents of the blends were determined after processing using titration and HPLC techniques, respectively. Further information on the processing and mechanical properties of selected blends has been published by George, Sullivan, and Park [30].

Sample Preparation

Depending upon the characterization technique, blends were examined as extruded (pellet form), as pulverized (powder form), or after undergoing secondary processing (filament form). Pellets were pulverized using a Fritsch Pulverisette (Model 14701) cryogenic grinder with a 0.5 μm screen. Filaments were prepared by placing pellets in an Alex James One-Shot® fiber spinning apparatus, heating to 150°C, and extruding the blend through a spinnerette (D = 0.03" (763 μm), L/D = 3) at approximate shear rates of 40 to 140 s^{-1}.

Because moisture content was found to vary depending upon the relative humidity (RH) at which the blend was stored, certain samples were conditioned by placing the pellets in closed chambers at room temperature and varying RH (produced from solutions of differing ratios of glycerin to water) for at least one week [36]. Humidity and temperature were recorded using a Testoterm 6100 thermohygrometer.

Methods of Characterization

Wide-Angle X-Ray Scattering

Wide angle x-ray scattering (WAXS) patterns of blends were collected using a Rigaku automated standard powder diffractometer attached to a Rigaku RU 300 rotating

anode generator with a copper anode assembly. A Nickel beta filter was employed for all scans. The generator was operated at 50 kV and 200 mA. Powder from pulverized pellets were mounted on a glass slide by first making a suspension of the sample in collodion/amyl acetate, depositing the suspension on the slide, and allowing the liquid to evaporate. The glass slide was mounted in the diffractometer. A detector slit of 0.5°, scatter slit of 0.5°, and receiving slit of 0.3 were employed. Samples were scanned over the 2θ range from 2 to 50° (step size = 0.01°). The scan rate employed was fixed by the analysis sought: 1) 1° for determining accurate d-spacing determination, 2) 2° for estimating the degree of crystallinity, and 3) 10° for surveying a particular blend. The degree of crystallinity was estimated for the neat blends by using the crystallinity determination module in the Rigaku software which employed Ruland's method [37][38]. Values of atomic and Compton scattering factors for the atoms comprising each polymer were taken from the International Tables of Crystallography [39].

Hot stage WAXS was performed on a Rigaku RU 200 wide-angle powder diffractometer using the Rigaku High Temperature X-Ray Diffractometer Attachment (Model CN231181). A scan rate of 2°/min was employed. Heating of the specimen took place in a nitrogen atmosphere, and ice water was used as the coolant system. Samples were heated at approximately 10°/min to fixed temperatures ranging from 20°C to 230°C and remained at each temperature for the length of the scan (typically 20 minutes).

Thermal Analysis

Thermal analysis of the samples was performed under nitrogen using a Perkin-Elmer DSC-7 fitted with an Intracooler II. The DSC was calibrated using indium and zinc standards. High pressure, stainless steel capsules were employed to suppress volatile loss and sample degradation. Approximately 25 mg of material (cut pellets) was heated from -65°C to 200 °C, cooled to -65°C, and heated again to 230°C at a rate of

10°C/min for each trial. DSC trials were run after conditioning each sample at 50% RH or < 1% RH for at least one week. Titration was carried out concurrently with each DSC trial and a corresponding moisture content recorded for each sample.

Scanning Electron Microscopy (SEM)

Preparation of samples for SEM included fracturing filaments or pellets immediately after they had been immersed in liquid nitrogen for 1 to 5 minutes (depending on samples thickness). Surfaces were imaged as fractured or after etching out of the starch component. For etching, samples were placed in either aqueous solutions containing α-amylase (27 units/mg. solid from Asperillus oryzae, Sigma Chemicals) or a control solution of distilled water. Both solutions were adjusted to a pH level of 6.9 using a sodium phosphate buffer (Sigma Chemicals). These solutions were heated at 37°C for 6 hours. Samples were then rinsed with distilled water and allowed to dry overnight on filter paper. Samples were mounted on aluminum stubs with conductive tape and sputter-coated with gold palladium. A Cambridge StereoScan Scanning Electron Microscope was employed at a voltage of 10 keV. Images were recorded with Polaroid P/N 55 film.

Transmission Electron Microscopy (TEM)

Extrudates from the compounding process were microtomed to thicknesses below 1000 Å at temperatures from -20 to 15 °C using a Reichert-Jung FC4E cryo-ultramicrotome. Prior to viewing in TEM, certain sections were placed in a stainer containing elemental iodine (Mallinckrodt Specialty Chemicals) and exposed to iodine vapor for one hour to preferentially stain the amorphous starch-rich fraction. A JEOL 200 CX TEMSCAN electron microscope was employed at 200 keV to image the samples. Because of the sensitivity of both starch and EVOH to the electron beam, samples were imaged using low dose techniques [40]. Images were obtained at relatively

low magnification (5 to 10 kX) by first focusing on an area, translating to an adjacent area, and recording a 2 to 4 second exposure with Kodak SO-163 image plates. Details on this technique are given in chapter 4.

Moisture Content

Average moisture content of the samples was determined using a Mettler DL18 Karl Fischer Titration System. Between 0.100 and 0.150 g. of material was placed in a Mettler DO301 oven heated to a temperature of 200°C. Sample mass was recorded on a Mettler AE240 balance. Grade 5 dry Nitrogen purge gas was passed through the oven at a rate of 200 ml/min. and into the beaker containing reagent grade methanol where titration takes place. Hydranol Composite 5 (Fischer Chemical) was used as the titrant. A period of 20 minutes from sample insertion in the oven to the time of titration occurred to permit sufficient vaporization of the moisture in the sample. After the automatic titration process was complete, a value for water content was recorded based on the initial sample mass.

RESULTS AND DISCUSSION

A structural investigation of starch/poly(ethylene-vinyl alcohol) blends was performed in order to gain insight into how well these materials will behave as biodegradable thermoplastics. First, the visible appearance of the blends after exiting the extruder and upon storage will give us an initial indication of the blend structure and stability of the blends from which to motivate more detailed studies (e.g. Do chemical reactions as evident by color changes occur? Does melt fracture, swelling, or foaming of the extrudate take place? Are the blends opaque indicating crystallization and/or phase separation? Are the blends at equilibrium? Do the materials change in opacity as a function of storage condition and time? Does plasticizer leach out of the pellets?). Next, wide-angle x-ray scattering (WAXS) is performed to discern the crystalline phase types

occurring in each blend, if physical aging occurs (such as through retrogradation of the starch fraction), and if crystalline phase transformations occur as a function of temperature (The use of flat film WAXS to explore orientation effects is presented in Chapter 5. No orientation was observed for the extrudate and filament samples employed in this study.) Through the use of differential scanning calorimetry (DSC), the thermal behavior of the blends can be analyzed for glass transitions, melting/crystallization behavior, and indications of miscibility. Examination of the blends with scanning electron microscopy (SEM) allows us to determine if micron scale phase separation is occurring through observations of blend surfaces as fractured or enzymatically etched. Once the effectiveness of SEM is determined for observing the morphology of certain starch/EVOH blends, orientation of phase domains as a function of shear (in capillary flow) can be established as well as the stability of the blend structure in the melt. Finally, TEM is a useful technique for understanding differences in phase separation between different starch varieties with EVOH since sub-micron details can be explored. By combining information attainable with these structural characterization techniques, we can then predict and explain results from processability and property tests (e.g. fiber spinning results, mechanical behavior of the blends, and biodegradation rates).

Observation of Extrudate (pellets) After Compounding

Observations of the appearance and flexibility of the model blends are listed in Table 3.2. The blends containing amylose were deep amber or yellow in color indicating that certain degradation and Maillard browning reactions occurred [41-43]. The WM100 blend appeared clear indicating that such reactions were not prevalent in this system. As the EVOH content was increased, the materials appeared whiter and more opaque suggesting phase separation and crystallization of the synthetic component. Exposure to a saturated water atmosphere turned pellets from all blends opaque, except for the HY100, HY85, and NC100 blends. Pure EVOH does not take up significant moisture

Table 3.2. Appearance and Flexibility of the Model Blends

Blend	Color	Clarity	Texture	Foaming	Flexibility (180° Bend)
High Amylose Starch (Hylon VII) Blends:					
HY100	Amber	Translucent	Melt Fracture	No	No, split occurs
HY85	Amber	Translucent	Smooth	No	No, split occurs
HY70	Yellow	Translucent	Smooth	No	Yes
HY60	Yellow	Translucent	Smooth	No	Yes
HY50	Yellow	Translucent	Smooth	No	Yes
HY40	Yellow	Translucent	Smooth	No	Yes
HY30	White	Translucent	Smooth	No	Yes
HY15	White	Translucent	Smooth	No	Yes
Native Corn Starch Blends:					
NC100	Yellow	Translucent	Smooth	No	Yes
NC85	Yellow	Translucent	Smooth	No	Yes
NC70	Yellow/white	Translucent	Mostly smooth	No	Yes
NC60	Yellow/white	Translucent	Smooth	No	Yes
NC50	White/yellow	Opaque	Smooth	No	Yes
NC40	White/yellow	Opaque	Smooth	No	Yes
NC30	White	Opaque	Smooth	Slight	Cracks on surface
NC15	White	Opaque	Smooth	No	Yes
Waxy Maize Starch Blends:					
WM100	Clear	Translucent	Melt Fracture	No	No, Brittle
WM85	Clear	Translucent	Melt Fracture	No	No
WM70	Clear	Translucent	Melt Fracture	No	Split occurs
WM60	White	Translucent	Melt Fracture	No	Yes
WM50	White	Opaque	Melt Fracture	Yes	Yes
WM40	White	Opaque	Melt Fracture	No	Yes
WM30	White	Opaque	Melt Fracture	Yes	Yes
WM15	White	Opaque	Melt Fracture	No	Yes
Poly(ethylene-co-vinyl alcohol) Control:					
EVOH/GLY	White	Opaque	Smooth	Smooth	Yes

(< 3%) and remains clear when saturated with water; however, the EVOH/GLY control sample becomes opaque and absorbs up to 8% moisture [44]. This increase in moisture level may enhance the refractive index difference between crystalline domains (which exclude plasticizer) and amorphous domains (which with glycerin is known to absorb water) making the EVOH/GLY blend appear opaque. Similar behavior is believed to occur in the starch/EVOH blends.

Surface observation of the WM100 and HY100 extrudates showed irregularities which may be due to melt fracture [45]. Melt fracture is a phenomena associated with the elastic instability of a polymer to flow and is usually associated with shear stresses above 10^5 Pa [46]. It was not observed in the NC100 material which is probably due to the high level of moisture present (thus lower shear) during the compounding of this particular blend. Melt fracture was apparent in all of the Waxy Maize blends and was probably due the level of branching and lower amount of entanglements in this starch component. None of the Native Corn or Hylon VII blends with EVOH showed evidence of melt fracture upon exiting the extruder, however.

Visible foaming at the die was generally not a problem since conditions were optimized to eliminate this phenomena. Conditions to suppress foaming included lowering the amount of water injected into the extruder and replacing it with a fixed amount of glycerin, a lower vapor pressure component; venting of water vapor from the extruder two zones before reaching the die; and setting the temperature at the die from 90 to 95°C, which is lower than the boiling temperature of water at atmospheric pressure (glycerin was not expected to contribute to the foaming process since its boiling point is 290°C). Despite these efforts, a small amount of foaming was observed in certain blends (i.e. NC30, WM50, and WM70) .

A viscous fluid was observed to migrate to the surface of some pellets as they were stored. The composition of the fluid is believed to be mainly glycerin from its consistency and from the fact that it has a lower vapor pressure than water, thus making it

less likely to evaporate from the surface. Blends exhibiting this coating were generally high in EVOH content, greater than 70 % for the waxy maize and native corn starch blends. The fluid was also observed on the surface of all the Hylon VII blends. These observations seem to indicate that the partitioning coefficient for glycerin and water was higher for blends containing amylopectin than those containing amylose or EVOH. It may also mean that glycerin and/or water was excluded from the crystalline domains of EVOH or amylose-complexes thus lowering the apparent partitioning coefficient for these domains. Measurements of the glycerin content via HPLC did not show a significant drop in plasticizer levels for the blends higher in EVOH content; however, values for the bulk glycerin content may be biased due to the glycerin on the surface of the pellets [30].

Wide-Angle X-Ray Scattering

Wide-angle x-ray scattering (WAXS) provides information about the short range order of the molecular constituents in polymer blends; levels and types of crystallinity is can be determined by this technique. WAXS of starches has been often used to classify starch by their distinct powder patterns (e.g. A, B, C types of native starches) [47-49]. When starch is thermally, chemically, or mechanically treated, it often exhibits the 'V' type pattern, which is formed upon complexing of amylose or amylopectin with varying agents (usually non-polar molecules which insert themselves within the interior of the polymer helices) [48]. Thus, WAXS can be used to track morphological changes in starch as it has been extruded under varied heat, shear, and moisture levels [50, 51], as a function of aging, and, with the use of a hot stage, after heating to various temperatures.

Crystalline Phase Types

Blends were first surveyed after compounding to determine the crystalline phase types that existed after initial processing. WAXS scans of representative compositions of the three types of starch blends, taken at a scan rate of 2θ of 10°/min, are shown in

Figure 3.1. Peaks associated with the poly(ethylene-co-vinyl alcohol) component were evident at 2θ equal to 10.8, 20.4, 21.7. These results indicate that a portion of the EVOH fraction was forming a distinct crystalline phase for which the melting points as determined by DSC occur over the range 120 to 150 °C. The level of crystallinity measured via WAXS is estimated to be 16 +/- 3% for the EVOH/GLY control sample. For blends containing starch, the estimation of crystallinity levels via WAXS using Ruland's method[37] is more difficult since some of the peaks corresponding to the amylose complex overlap with the EVOH peaks. Scattering associated with the EVOH crystalline phase became less apparent, expectedly, as the starch content is increased. The Waxy Maize blends, which contain only amylopectin, did not show crystallinity associated with the starch fraction (figure 3.1a). For the blends containing amylose, crystallinity associated with the starch fraction was apparent from peaks occurring at 12.9, 16.6, 18.3, 19.7, and 22.4° for the Hylon VII and Native Corn starch blends (figure 3.1b and 3.1c). In order to help understand the changes which occurred in the structure of the starch fraction during the extrusion blending process, the results of WAXS scans taken of the raw starch materials are shown in Figure 3.2. The native corn and waxy maize raw starches yielded WAXS patterns that are representative of the 'A'-type pattern documented in the literature [52-54]. These patterns also indicated that these starches existed in granular form and that the amylopectin fraction is responsible for most of the sample's crystallinity. The Hylon VII starch exhibited a WAXS spectrum typical of a completely amorphous polymer. This is consistent with the fact that the Hylon VII starch granules had been steam treated and all crystallinity was destroyed prior to compounding.

The WAXS spectra of the neat starch blends are shown in Figure 3.3; the scan of the triglyceride additives is also shown in this figure for comparison. After compounding the starch with glycerin, water, and the triglyceride additives at high temperature (as listed in Table 1), scans taken of these materials exhibited markedly different structures. The

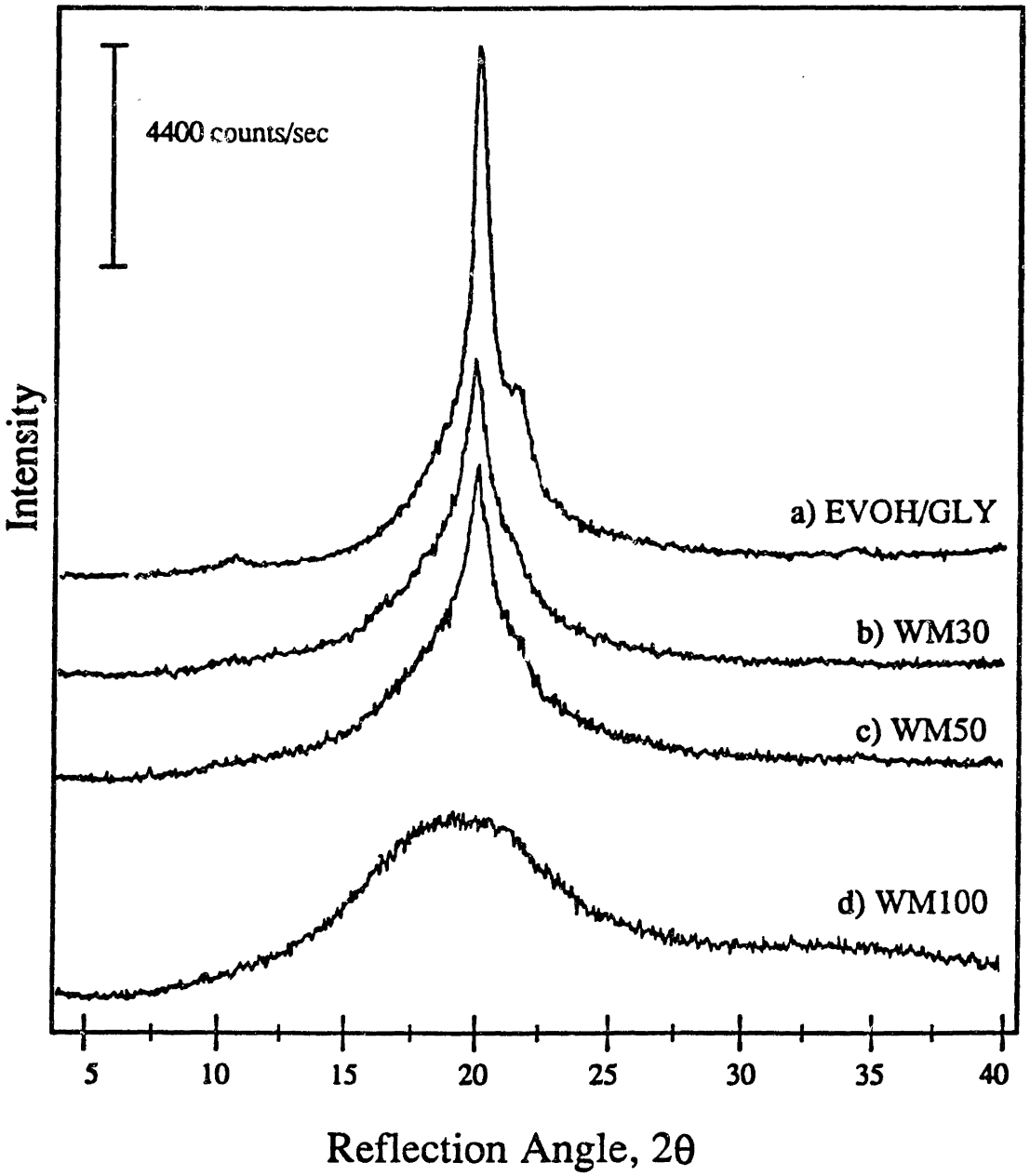

Figure 3.1a. Wide-angle X-ray powder diffraction spectra for selected Waxy Maize (WM) blends compared with the EVOH control: a) EVOH/GLY, b) WM30, c) WM50, and d) WM100.

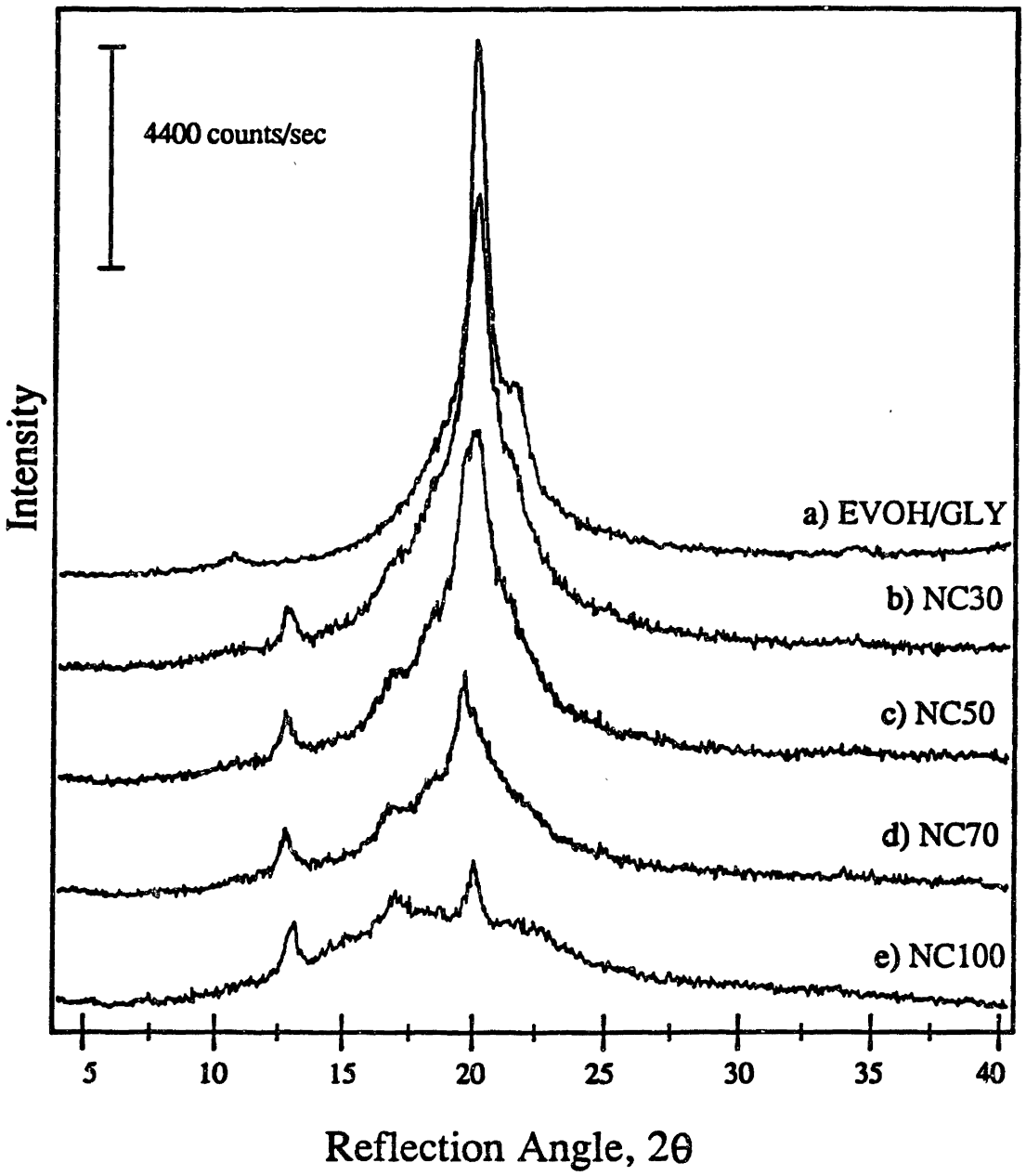

Figure 3.1b. Wide-angle X-ray powder diffraction spectra for selected Native Corn (NC) blends compared with the EVOH control: a) EVOH/GLY, b) NC30, c) NC50, d)NC70, and e) NC100.

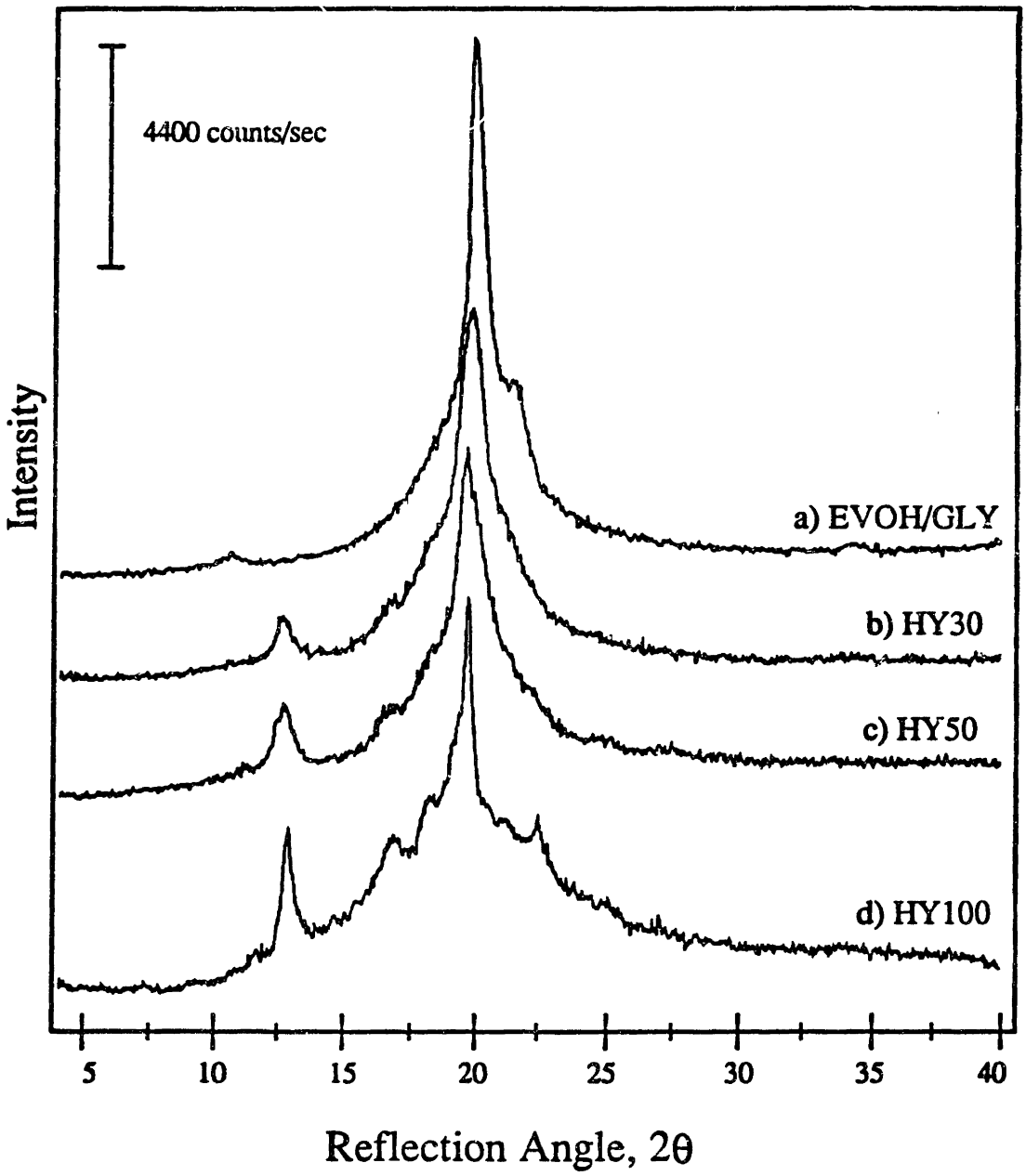

Figure 3.1c. Wide-angle X-ray powder diffraction spectra for selected Hylon VII (HY) blends compared with the EVOH control: a) EVOH/GLY, b) HY30, c) HY50, and d) HY100.

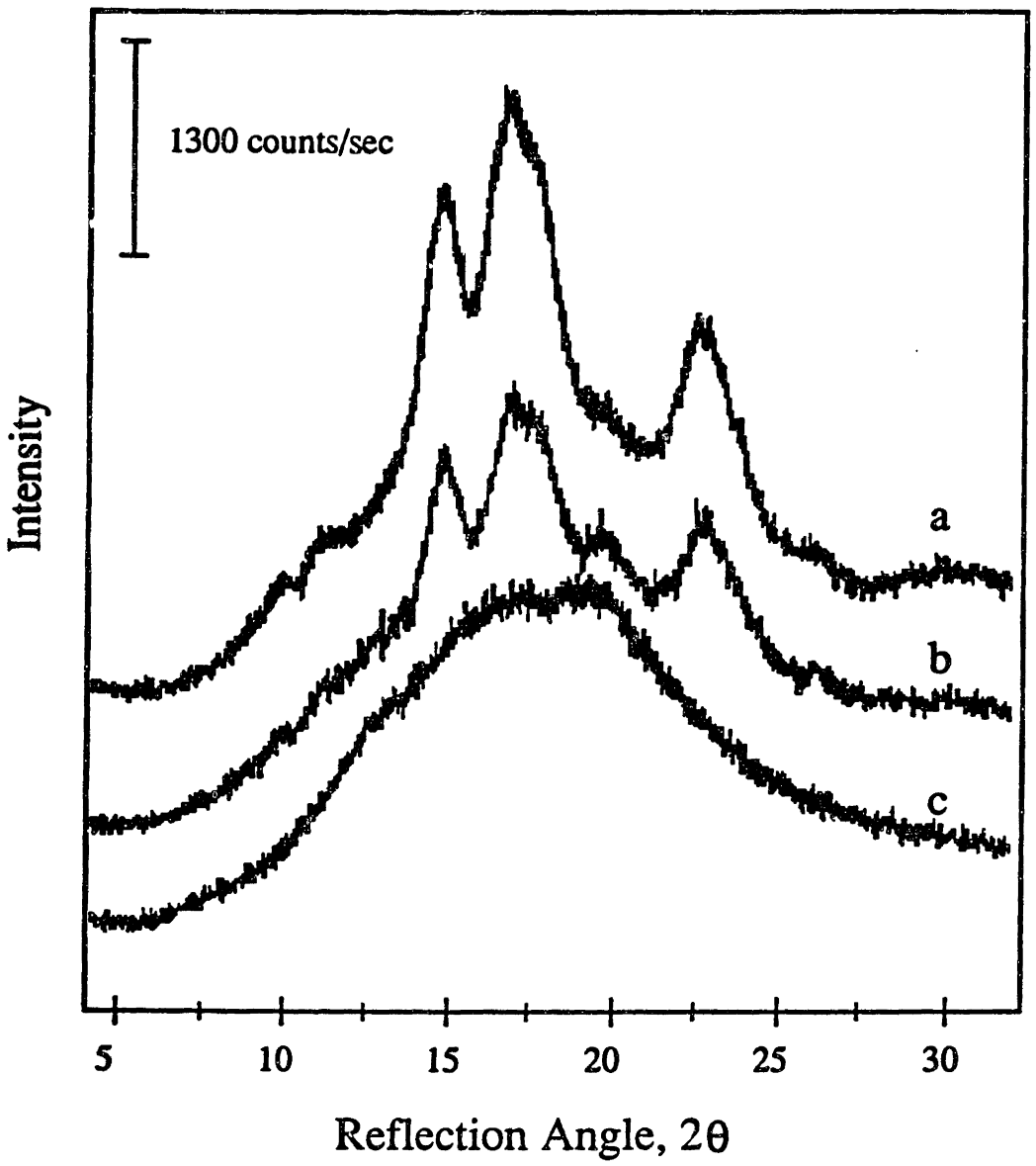

Figure 3.2. Wide-angle X-ray diffraction spectra for the starches before compounding: a) Amioca Waxy Maize, b) Melojel Native Corn, and c) EKFl. Hylon VII.

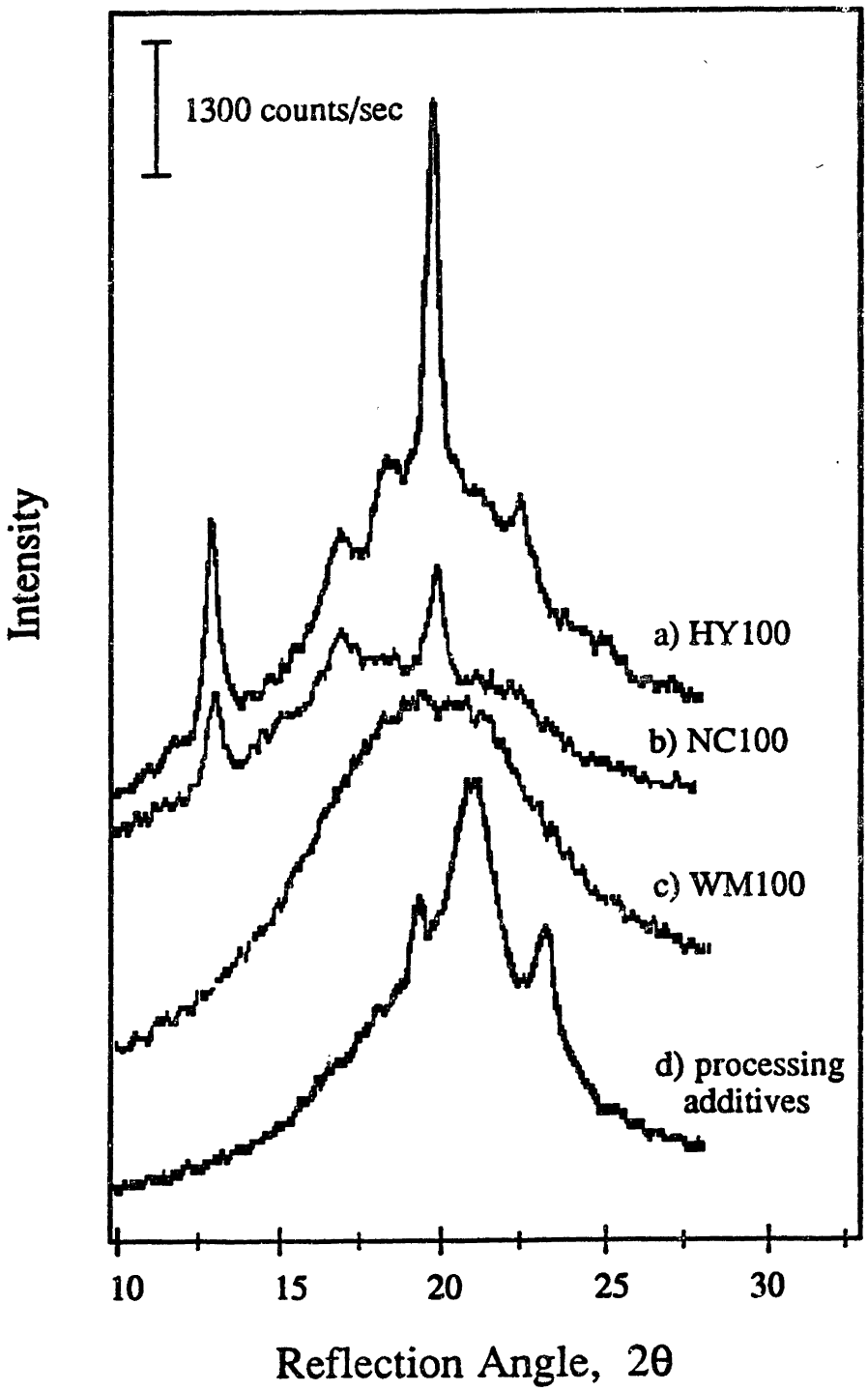

Figure 3.3. Wide-angle X-ray diffraction spectra for the a) HY100 blend, b) NC100 blend, c) WM100 blend, and d) processing additives.

waxy maize starch, which was initially highly crystalline, exhibited only amorphous scattering. Conversely, the Hylon VII starch, initially amorphous, exhibited peaks associated with a crystalline component. The peaks at 2θ equal to 12.9, 16.6, 18.3, 19.7, and 22.4° can be attributed to the amylose complex which forms between the linear starch fraction and certain fatty acids and triglycerides which also occur naturally in the starch granule [48]. The estimated crystallinity for the HY100 blend was 10 +/- 2 %. These peaks did not correspond to scattering from the triglyceride additives (peaks of which are measured at 5.7, 19.3, 21.0, 23.2); however, from DSC data, it is hypothesized that at least one of the additives may have formed complexes with the amylose fraction (in addition to the complex formation that occurs between lipids naturally present in the starch granule [55]). The Native Corn blend series also showed peaks at similar angles indicating the formation of similar amylose complexes. The ratio of the peak areas in the NC100 sample to its amorphous scattering was less than that observed for the HY100 material; hence, crystallinity is less than 5% for this material. Finally, the Waxy Maize starch blends, in which the waxy maize component initially showed an A-type crystalline pattern, exhibited essentially no crystallinity, only a broad region of amorphous scattering was observed. Again, peaks associated with the triglyceride additive were not visible from the WAXS scans. Overall, these results indicated that the amylose formed a second distinct crystalline phase in the starch/EVOH blends through complexation and that essentially all of the branched amylopectin fraction remained amorphous after thermo-mechanical processing.

Physical Aging Studies

In order to discern if certain changes occur in the level and/or type of crystallinity as a function of time, WAXS of newly compounded blends and blends which were allowed to age over time were collected. Results of scans taken for blends after one week indicate only a slight increase in starch crystallinity for the NC and HY series, otherwise

no noticeable difference in the spectra is observed. Patterns remain relatively constant for powder samples which were tested after 6 months and 1 year after compounding and appear similar to those in Figure 3.1. It should be noted that the as processed moisture content was maintained by storing samples in several layers of polyethylene and foil wrapping and that variations in the spectra are not due to fluctuations in water content.

Waxy maize blends have been documented in the literature to undergo crystallization over time. This retrogradation phenomena is thought to be responsible for the staling of bread [56]. Usually the crystallization of amylopectin is facilitated by the presence of water in amounts greater than 14%. A slight 2θ peak has been measured around 20° by others for waxy maize gels that have been aged over a period of days to weeks. Wide-angle X-ray diffraction measurements for the WM100 blend (with ~ 8 % moisture) do not show evidence of a peak that is discernible from the background scatter, even after 2 years of aging. Patterns taken are similar to those in figures 3.1a and 3.3.

Temperature Dependence of WAXS

In order to complement the DSC analysis and detect transitions attributed to the crystalline fraction of the starch in the blends, WAXS was performed on the HY100 blend at various temperatures. Pulverized pellets of the HY100 blend were mounted on glass slides and heated to various temperatures at rates of approximately 10°C/min. Signal was monitored at 2θ equal to 20.8° during the heating cycle to determine if significant shifts in intensity occurred. When the desired temperature was attained, the temperature ramping cycle was stopped and a WAXS scan was taken over a period of 15 to 20 minutes (see figures 3.4 and 3.5). One should note also the decrease in signal from data shown in previous figures. The signal-to-noise levels are lower due to the hardware of the hot stage attachment (i.e. Beryllium windows, Platinum heater).

The first trial consisted of taking a scan at 20°C (slightly below room temperature due to the coolant), heating to 60 °C, taking a scan, then cooling the sample down to

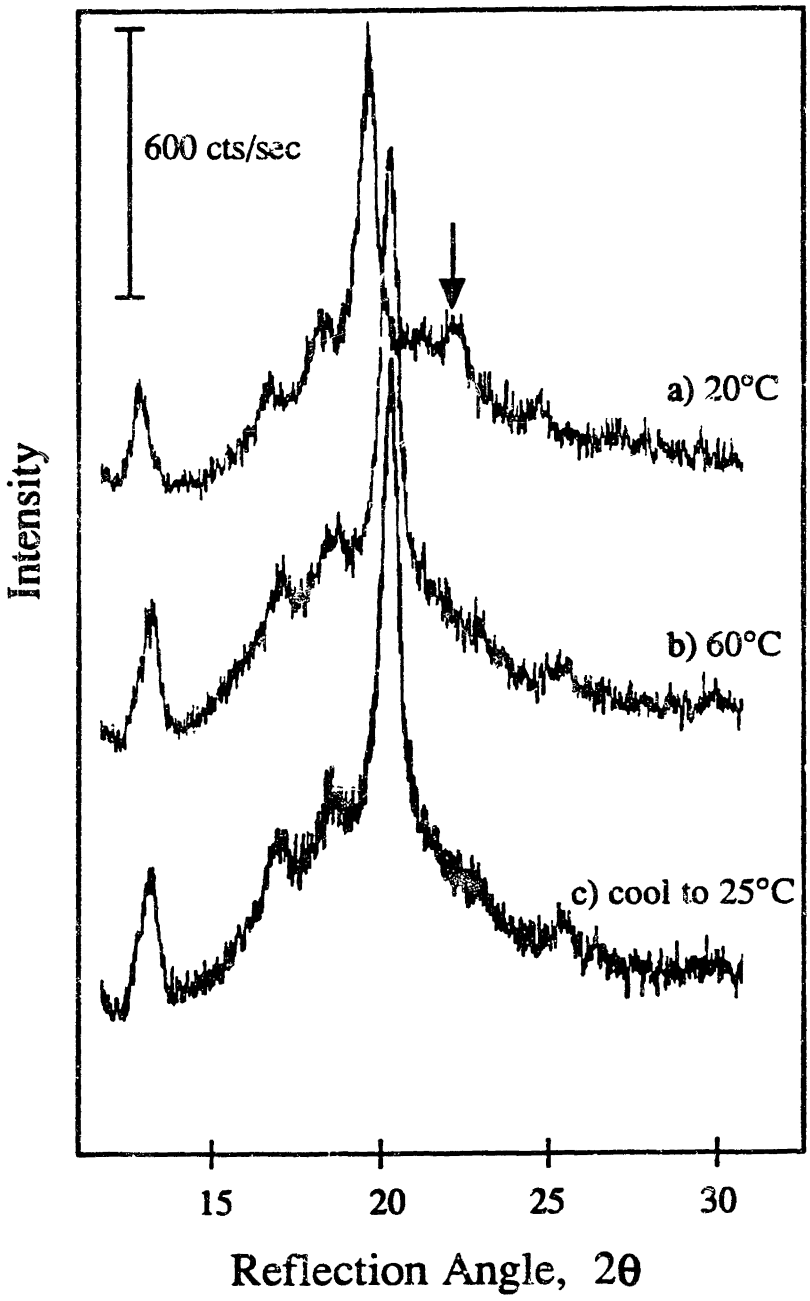

Figure 3.4. Wide-angle diffraction spectra of the HY100 blend taken at a) 20°C, b) at 60°C, and c) after cooling to 25°C. Note the disappearance of the peak at 22.5°.

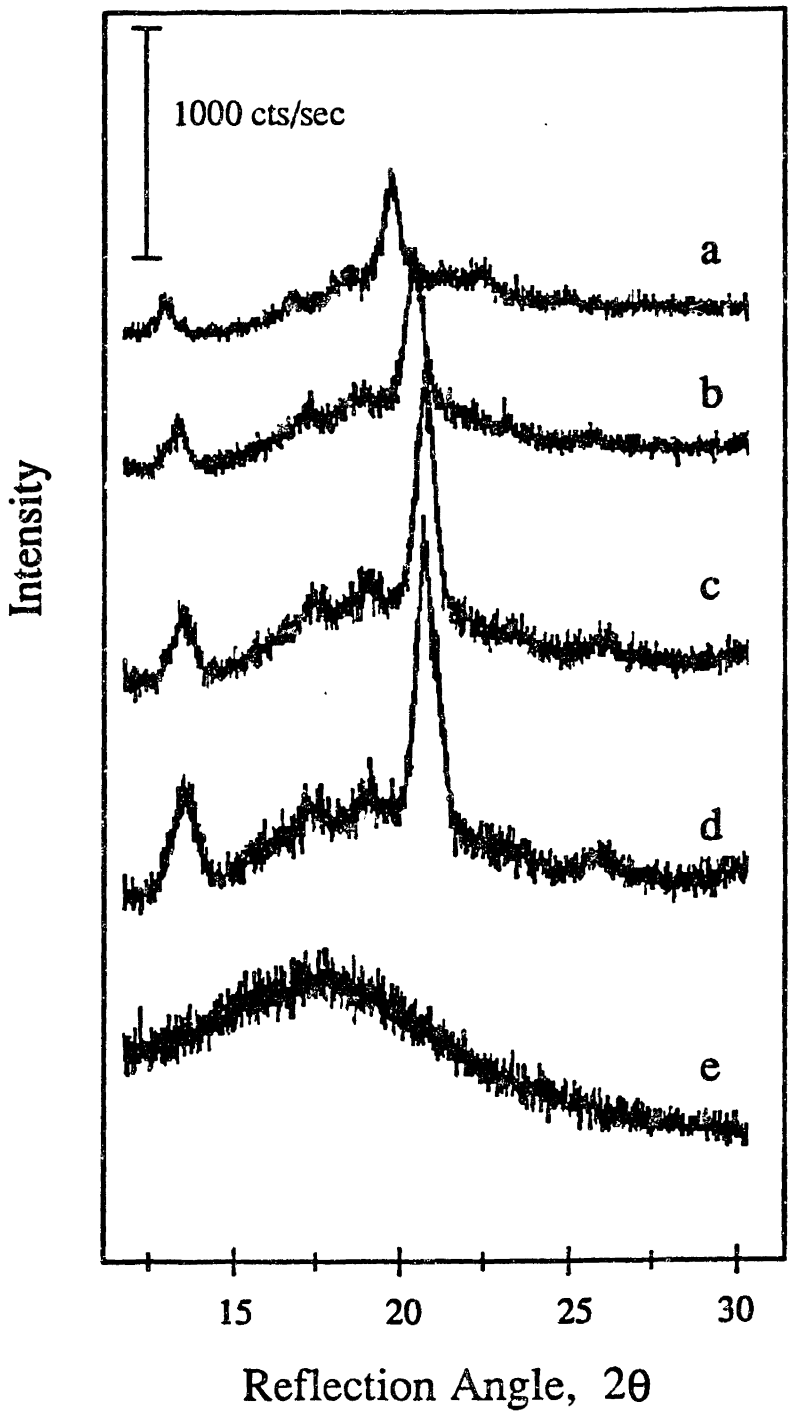

Figure 3.5. Wide-angle X-ray diffraction spectra taken isothermally at various temperatures for an HY100 powder sample: a) 20°C, b) 60°C, c) 100°C, d) 150°C, and e) 230 °C.

room temperature (25°C) and taking a new scan. Results are shown in Figure 3.4. There is a noticeable increase in the scattering intensity of the crystalline peaks which must indicate a shifting to a higher level of crystallinity (i.e. annealing at 60°C) and an overall decrease in the chain to chain lateral spacing within the amylose crystallite. The initial scan at 20°C corresponded closely with values for 2θ taken for the V type patterns recorded by Mercier and others [50, 57, 58]. The shifting in the scattering peak angles represent a shifting in the spectra from a hydrated form to a dry form of the V-complex. This increase in peak intensity and level of order, can also be attributed to a decrease in the moisture level of the sample that results from drying of the sample over the course of heating [59]. The shift from the hydrated form to the dried form of the V-amylose complex represents shifts in the seven residue left helical packing of 1.38 to 1.31 nm between helices [50]. The disappearance of a small peak at 2θ equal to 22.4° also occurs upon heating the sample to 60°C; this peak could possibly be attributed to melting of any crystallized starch which would produce an A or B crystal type [60-62].

A second experiment was undertaken in which the HY100 sample was heated from 20°C to various temperatures (60, 100, 150, and 230 °C) at which the isothermal scans were taken; see Figure 3.5. Again, an increase in the scattering intensity for each WAXS spectra was observed due to drying of the starch sample. A shift to a higher scattering angle was observed, even to a higher angle in the 100 and 150 °C cases from that of 60°C trial. This behavior seemed to indicate that the sample was drying out, forming a more closed packed crystal. The crystalline scattering peaks associated with the amylose complex exist until 230°C. It was at this point that the sample completely degraded and the crystalline pattern was no longer visible (i.e. V-amylose melting occurs near the degradation point of the sample).

Thermal Analysis

In the previous section, EVOH, amylose, and amylopectin are shown to be semi-

crystalline to different degrees. Differential scanning calorimetry was employed to discern thermal transitions (e.g. melting, crystallization, glass transitions) and to gain some information on the miscibility between starch and EVOH. As described in the experimental section, three scans for each sample were performed. Since plasticizers, especially water, will migrate out of the sample during heating, the first heat values for melting temperature will give the best indication of the influence of the plasticizers on the melting point and glass transition for the blend. Cooling and second heating cycles provide more information on reversible transitions by erasing any prior thermal histories associated with the sample.

A typical heat/cool/heat cycle is shown in figure 3.6 for a NC70 blend (mass = 20.86 mg) conditioned in a 50% relative humidity chamber. The moisture content of this sample was measured to be 5.0 %. In the first heat, a small endothermic peak ($\Delta H = 0.8$ J/g) was observed at an onset temperature of 56°C with a peak at 60.5°C. A second endotherm associated with the melting of poly(ethylene-vinyl alcohol) cystallites occurred with an onset temperature of 121.5 °C and a peak temperature of 133 °C ($\Delta H = 10.8$ J/g). A shift in the heating curve, associated with the glass transition of starch, was not readily apparent in this scan. It may have been obscured by the baseline or the smaller endothermic transition. After 2 minutes of holding at 200 °C, the cool cycle was started. At the scan rate of -10°C/min, crystallization of the EVOH occurred at an onset temperature of 98.5 °C and a peak temperature of 94 °C. The enthalpy of transition for the EVOH crystallization was 9.9 J/g. The smaller, low temperature, endotherm was again apparent is this blend with an onset temperature of 38 °C and a peak temperature of 35 °C ($\Delta H = 0.74$ J/g). Finally, after holding for 2 minutes at -65 °C, the sample was re-heated. In the second heating cycle, transitions similar to the first heat were observed although slightly shifted in temperature. For the small endotherm, the onset occurred at 48 °C with a peak at 52°C which was lower than the measured temperature in the first heating cycle. The EVOH melting transition began at 125 °C and peaked at 134°C. This

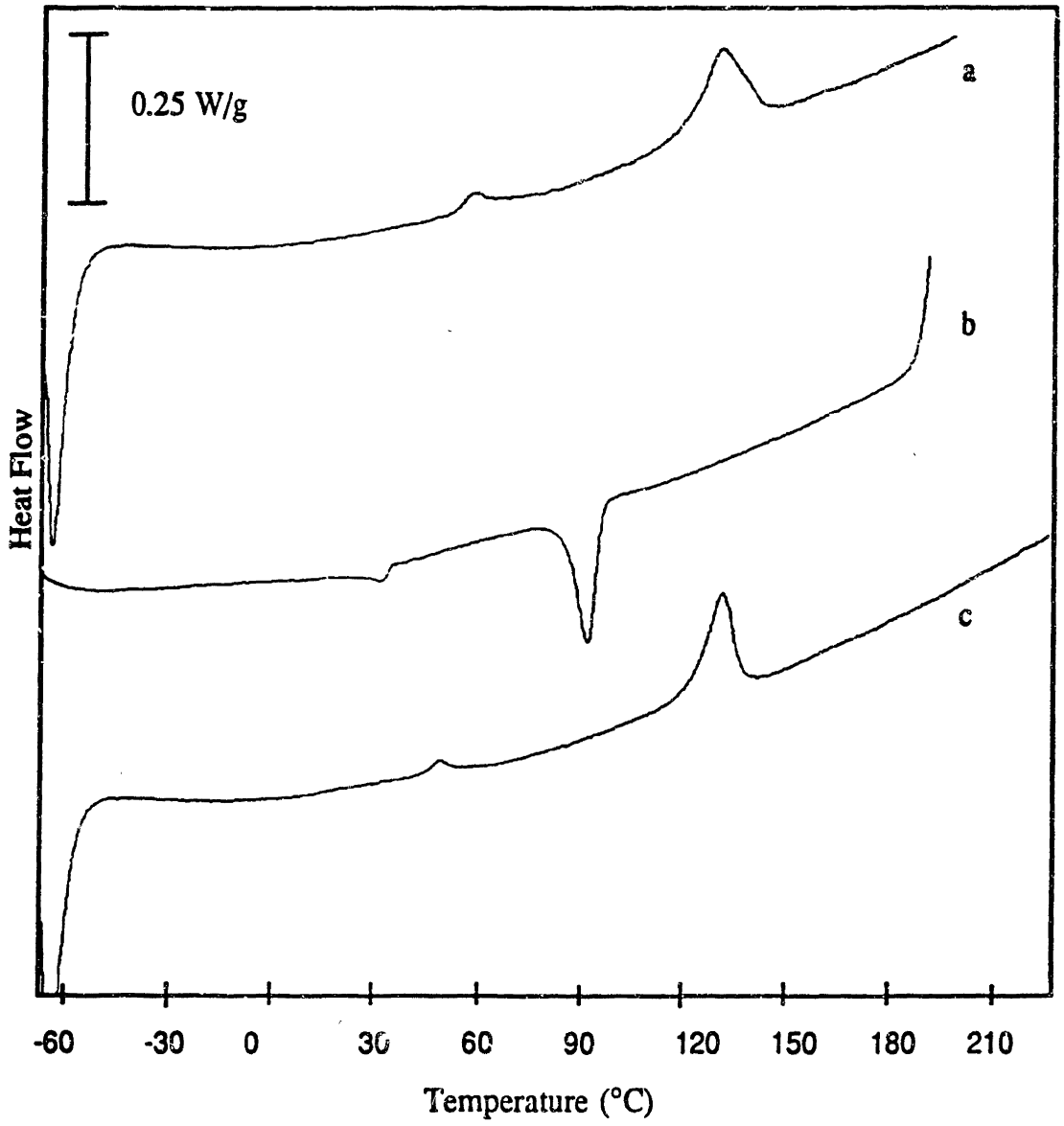

Figure 3.6. DSC curves for a) first heating, b) cooling, and c) second heating cycles for the NC70 blend. Scan rates were 10°C/min. Sample was conditioned to 50% RH before testing.

endotherm is much sharper than in the first heat and was slightly shifted to a higher temperature, implying a more narrow distribution of somewhat larger crystal sizes and melting within a purer phase. Overall, the enthalpies associated with both transitions were lower than those values measured from the first heat. The EVOH peak has a ΔH equal to 8.5 J/g, and, for the lower temperature transition, ΔH equals 0.7 J/g. These two transitions were observed in every blend which contained both starch and EVOH. Further cooling and heating cycles yield reproducible results.

DSC results for the series of blends are shown in given in Tables 3.3. and 3.4 and Figures 3.7, 3.8, 3.9, and 3.10. Each blend was conditioned for at least one week at 50% RH; moisture and glycerin contents for each component are shown in figure 3.11 (a linear relationship with starch content is evident). In figures 3.7 and 3.8, values for temperature and enthalpy are given for the lower temperature transition. In order to clarify the discussion, the term "S-transition" will be used to designate this transition since it is only present in DSC scans taken with blends containing starch. This transition occurred over the range of 40 to 65°C. In Figures 3.9 and 3.10, the endotherm corresponding to the melting of the EVOH component is presented. The normalized enthalpy of this transition was determined in order to roughly estimate the percentage of the EVOH component which had crystallized. For blends containing EVOH, the heating runs yielded endotherms which correspond to the melting of EVOH crystals. Temperatures ranged from 120 to 152 °C depending upon composition and storage conditions. Smaller multiple transitions were also observed in these systems that were extremely dependent on moisture content. These transitions are most likely related to the glass transition of the starch and EVOH, but the transitions often overlapped with the S-transition. For this reason and because of the low signal to noise level of the glass transition, we do not attempt to quantitatively describe this data here.

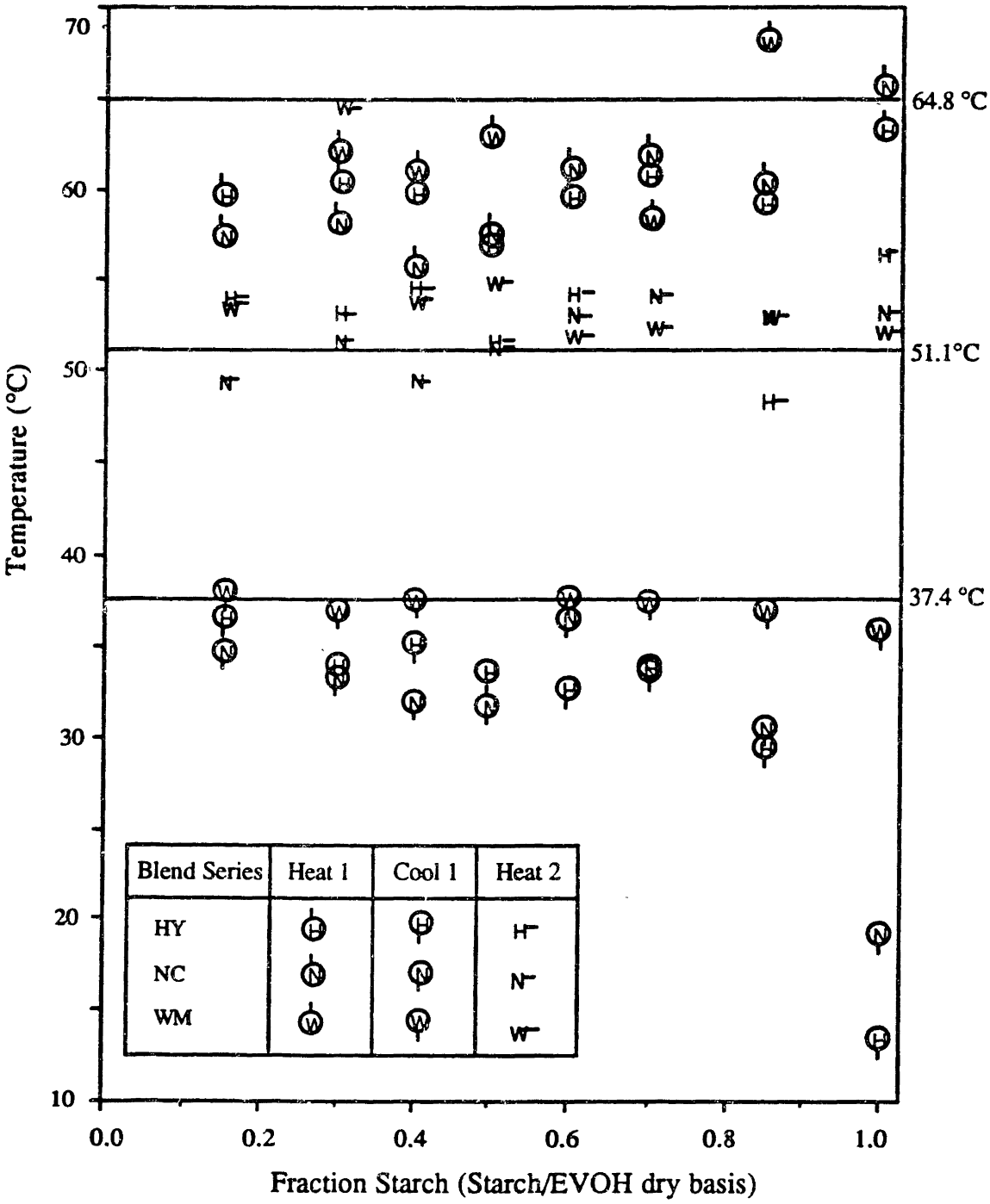

Figure 3.7. Peak S transition temperatures as measured by DSC for the heating/cooling/heating cycles of the HY, NC, and WM model blends which were conditioned to 50% RH. Values on the right of the graph correspond to peak transition temperatures for the neat triglyceride additives.

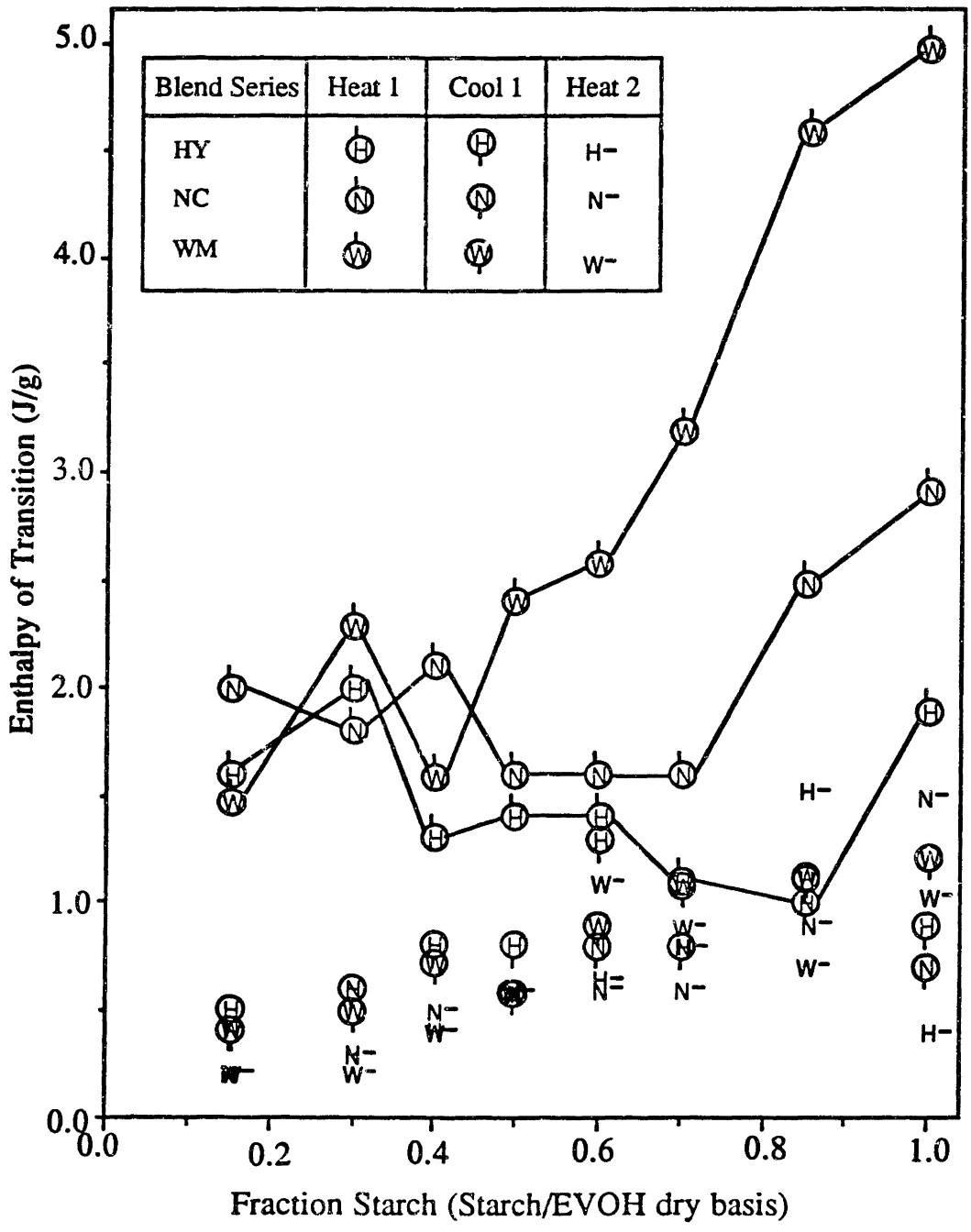

Figure 3.8. Enthalpy of the "S" transition for the HY, NC, and WM model blends which were conditioned to 50% RH.

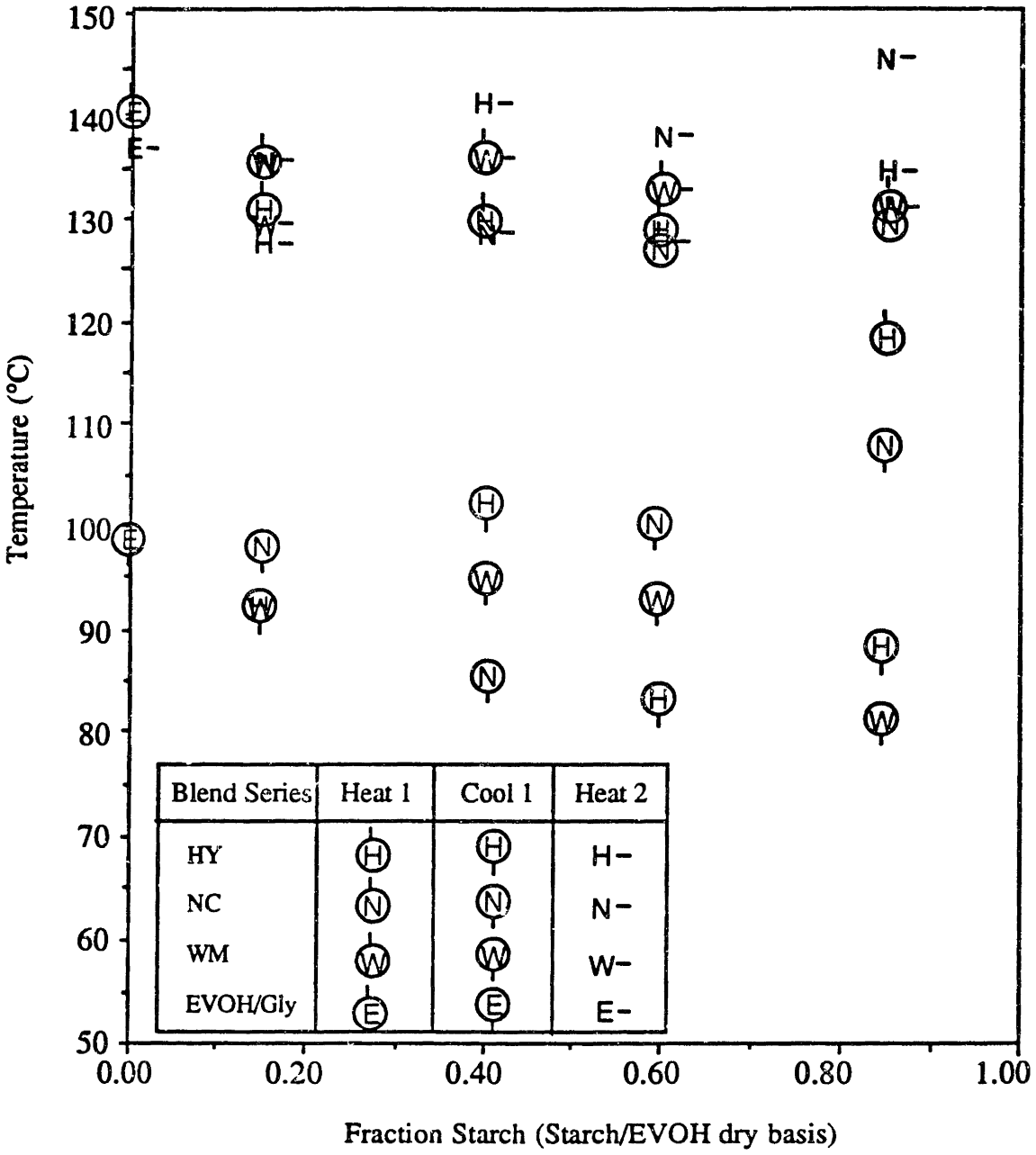

Figure 3.9. Peak poly(ethylene-vinyl alcohol) transition temperatures for the heating/cooling/heating cycles of the HY, NC, and WM series of model blends which were conditioned at 50% RH. Values for Heat 1 and Heat 2 represent melting transitions. Values for Cool 1 represents EVOH crystallization.

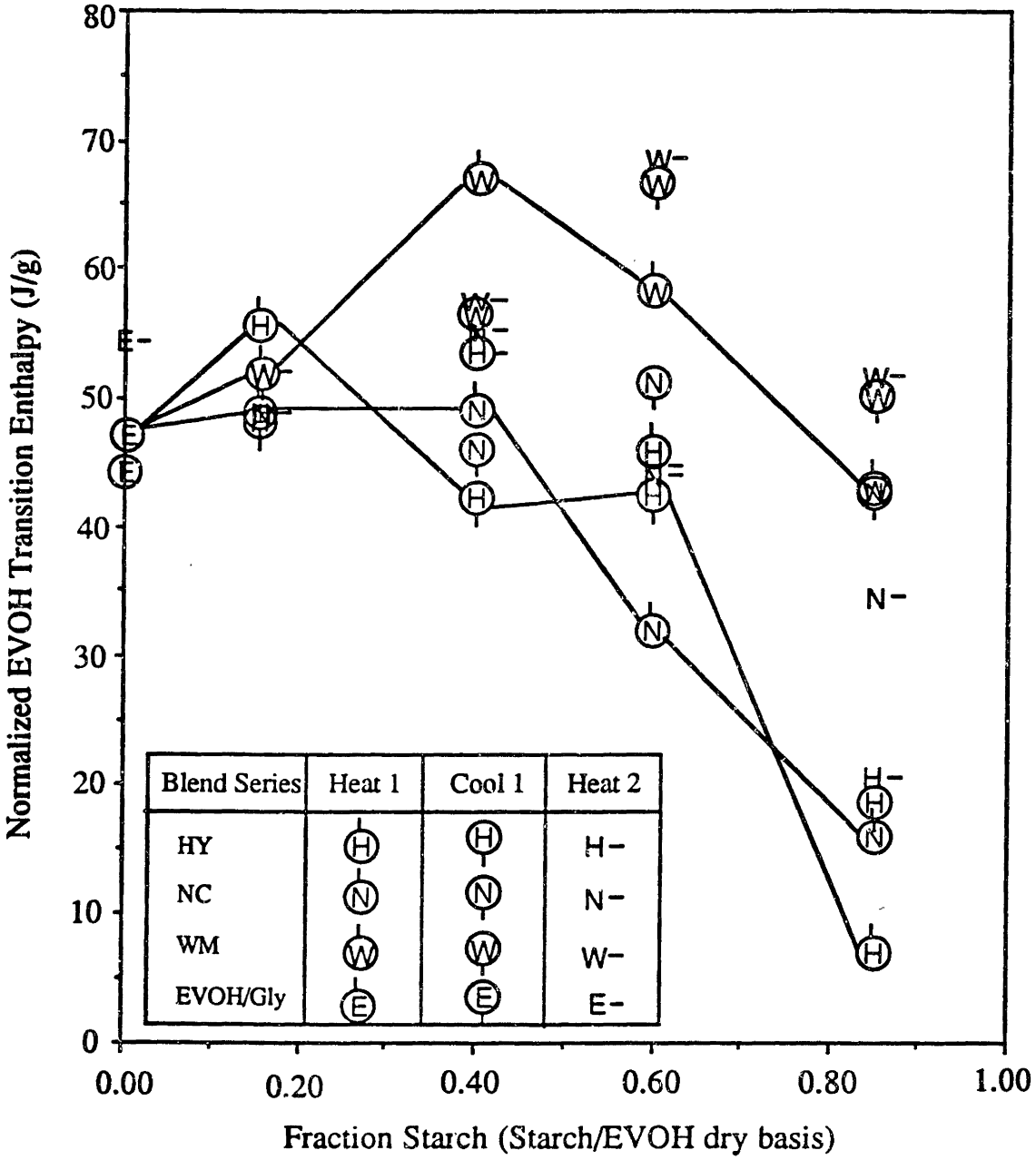

Figure 3.10. Normalized EVOH transition enthalpy for the heating/cooling/ heating cycles of the model blends.

The S-Transition

The S-transition ($\Delta H < 4$ J/g) that occurs between 50 and 70 °C may be attributed to any of a number of factors which include melting of the amylopectin fraction [63], amylose-complex melting due to plasticizer effects, glass transition as influenced by physical aging [64], and perhaps crystallization of the processing additives. The disappearance of a small WAXS peak near 60°C in the HY100 at $2\theta \sim 22.5°$ may suggest melting of a retrograded starch that yields an A or B x-ray diffraction pattern [62]. Hot stage WAXS showed that amylose-complex melting occurred at temperatures above 200°C, which is much higher than the measured S-transition. Peak temperatures for the heating/cooling/heating cycles for the starch/EVOH blends are displayed in Figure 3.7. DSC of the triglyceride additives yielded reproducible melting transitions that occurred in the range from 42 to 65°C. Values obtained for the first heat, cooling, and second heat are represented by lines drawn across the composition range. The first heat transition was slightly lower than that measured for the neat triglyceride additive. The cooling and second heating cycle yielded values for temperature that roughly approximated that of the pure triglycerides. We can thus conclude that the S transition observed in this temperature range is primarily due to the additive.

A note should be made regarding the enthalpy of these transitions, however. Figure 3.8 displays the enthalpy associated with the S transition for the series of starch blends (values from the first heating cycle are connected by lines). The enthalpy determined from the cooling and second heating cycle was similar and increased, as expected, nearly linearly with triglyceride composition. In the first heating cycle, however, the enthalpy of transition increased at a greater rate as the starch content increased for the native corn and waxy maize blends. In addition, the enthalpy of this transition for the first heat was also much higher than in the cooling and second heating cycles for all of the starch blends (i.e. all of the S-transition in the first heat cannot be due

to triglyceride alone). This difference suggests that the lower temperature endotherm between 55 and 60°C is partially due to the melting of retrograded starch.

EVOH Crystallization

From WAXS, it was shown that the EVOH component in the starch blends crystallized. Since the glass transitions of both starch and EVOH components are hard to distinguish from DSC, we turned our attention to the EVOH melting/crystallization transition in order to gain information on the miscibility of these components (i.e. an increase in melt miscibility will lead to a depression in the melting point). The effect of starch type on the crystallization behavior of the EVOH component is shown in Figure 3.9 which shows the peak melting temperature for the heating / cooling / heating cycles for each blend conditioned to 50% RH. Overall, the EVOH melting points in the Hylon VII and Native Corn starch blends generally occurred at lower temperatures possibly indicating increased miscibility in the melt between the amylose-containing starch types with EVOH.

DSC measurements have shown that the melting point of EVOH decreases as the amount of starch in a blend is increased. Usually this depression will provide evidence for melt miscibility, however, up to 30% of the total blend consists of glycerin and water plasticizers which can both act to depress the melting point of the EVOH component. In order to estimate the effect of the plasticizers on the melting point depression, the following comparison is made. First, values for moisture and glycerin content for the three blend series are shown in Figure 3.11. Overall, the glycerin content is relatively constant among the blends (~ 15 wt%). The addition of glycerin causes about a 15°C decrease in the crystallization temperature of EVOH (from 165°C to approximately 150°C). Since the glycerin level in the blends is relatively constant, the melting point should stay relatively constant for the blends if starch and EVOH are completely immiscible in the melt (assuming uniform partitioning of plasticizer between the

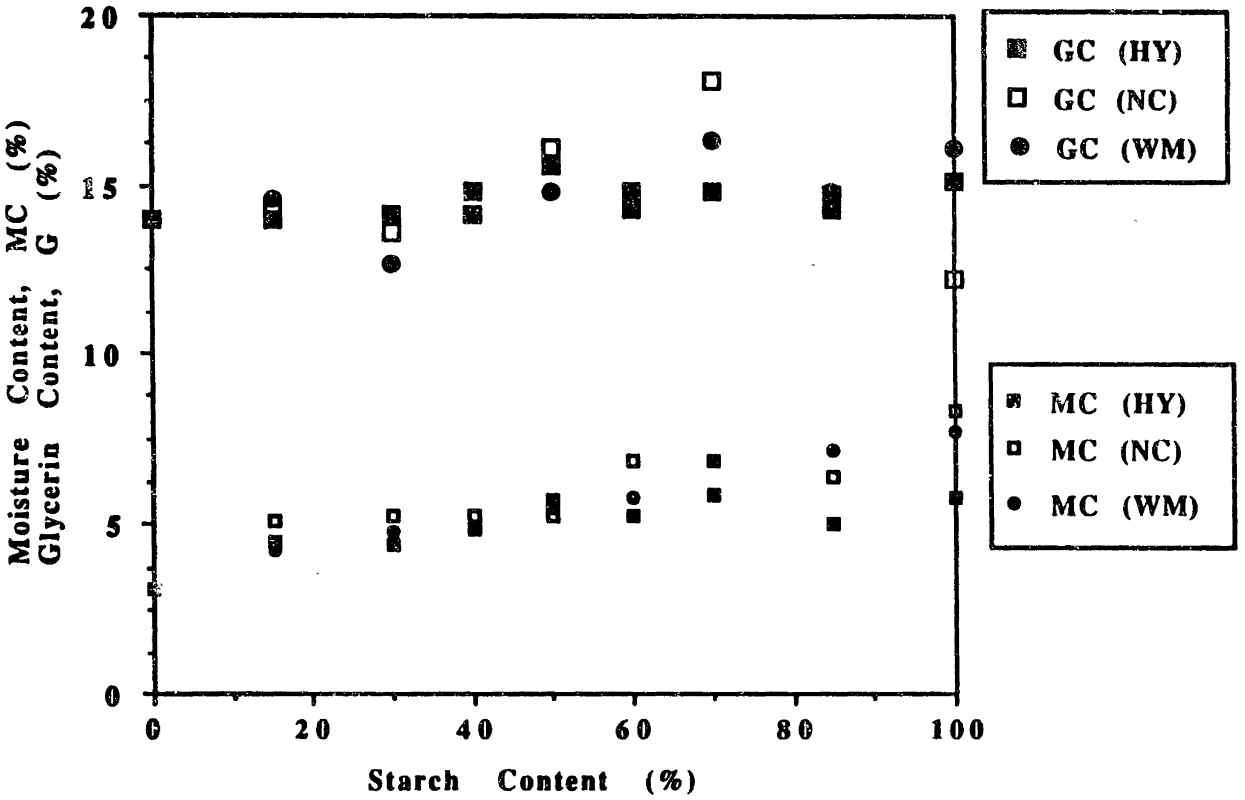

Figure 3.11. Glycerin and moisture contents for the NC series of blends after conditioning to 50% RH for one week.

respective types of polymer domains). At 50% RH, the amount of moisture contained in each of the starch varieties is relatively constant, but increases with starch content (from 3 to 8 %). Since melting points follow an inverse behavior with plasticizer content, one might assume that the melting point depression is due solely to increased levels of water. However, in Figure 3.12, the peak melting temperatures for the EVOH melting transition (first heat) and corresponding moisture contents are shown at 50% RH and 0.5% RH. (At 0.5% RH, the blends contain less than 2% moisture and moisture content does not increase with starch content.). At both humidity levels, the blends show an approximately 10° decrease in peak melting temperatures over the composition range of 0 to 85% starch. The difference in melting points ranges from 10 to 15°C and is a linear function of the increase in moisture levels at higher relative humidity. Thus, from DSC measurements of the blends, about 10°C depression in the melting point of EVOH is attributable to glycerin and from 10 to 15°C depression in the melting point at 50% RH is due to the water in the starch/EVOH blends (note: the presence of glycerin increases the water uptake of the EVOH component). The presence of WM starch leads to less than a 5°C depression, NC starch, up to 10°C, and the HY starch, up to 15°C for the blends at 50% RH. Thus, miscibility *does* increase as the amylose content in the starch blends increases. Although temperatures from the second and third scans in DSC, in most cases, yield more accurate information since the thermal histories of each blend are made constant, migration of glycerin and water within and out of the blends may cause significant changes in the temperature of crystallization and melting (up to 25°C). Thus, values for first heat are the most reliable and tell us the most information about the blend.

The transition enthalpy, normalized to the amount of EVOH in the blend in order to assess crystallinity levels, is plotted in Figure 3.10 as a function of starch content. If there is no effect on the level of crystallization of the starch or plasticizers, the values for normalized transition enthalpy should be constant. Values for the first heat (connected dots) show an increase in EVOH crystallinity up to 40% starch content. This behavior

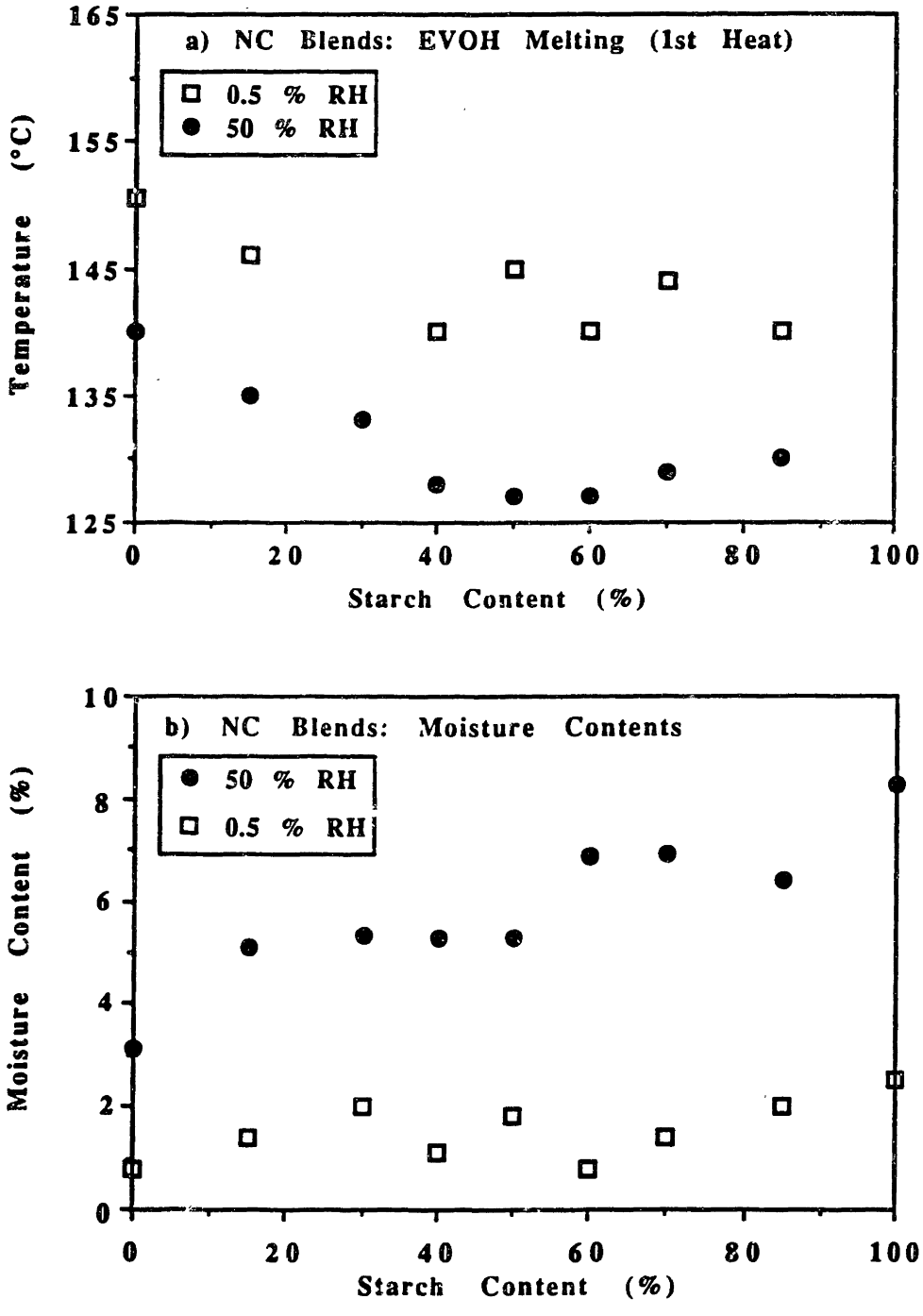

Figure 3.12. a) Peak melting temperatures of EVOH and b) moisture contents for the NC blends after conditioning at 0.5 and 50% RH for one week (DSC first heat cycle).

was not as dramatic for the second heating and cooling cycles and is probably a result of the initial thermal history of the blend during compounding and storage. Crystallinity subsequently dropped off at starch contents above 50% for the HY and NC blends as evident in all of the heating and cooling cycles. Higher transition temperatures and values of enthalpy may indicate increased phase separation between the starch and EVOH components; the purer the EVOH phase, the more it will crystallize. Overall, the waxy maize blends showed the highest transition temperatures and transition enthalpies indicating that the two polymer components are well phase separated. DSC results for the NC and HY blends seem to indicate that there is some miscibility between the starch and EVOH in the HY and NC blends.

Electron Microscopy Studies

SEM of Untreated Fracture Surfaces

Electron microscopy was next performed to obtain information on the phase morphology of the starch/EVOH blends. First, the untreated fracture surfaces were examined with scanning electron microscopy (SEM). Representative blend fracture surfaces for the WM50, NC50, and HY50 blends are shown in Figure 3.13. SEM showed no evidence of the original waxy maize or native corn starch granules such as are evident in thermoplastics employing starch as a filler [65-67]. Brittle fracture bands were visible in all blends. Starch-rich or EVOH-rich domains were not directly evident on the fracture surfaces. Small tufts (< 0.2 μm), visible on the NC50 sample, are indicative of some ductility prior to fracture. These regions appear bright in the micrographs due to charging of the specimen. Some small voids (< 0.5 μm) were evident in the WM, NC, and HY blends; these may be attributed to a small amount of foaming during the processing of the blends.

Overall, examination of the fracture surface does not lead to much insight into the phase behavior of the particular blends. Because no distinct phases were evident, one

Figure 3.13. Scanning electron micrographs of liquid Nitrogen temperature fracture surfaces for the a) WM50, b) NC50, and c) HY50 extrudates. Images on the right side represent magnified views of the surfaces on the left. Distinct phase domains are not evident using this method.

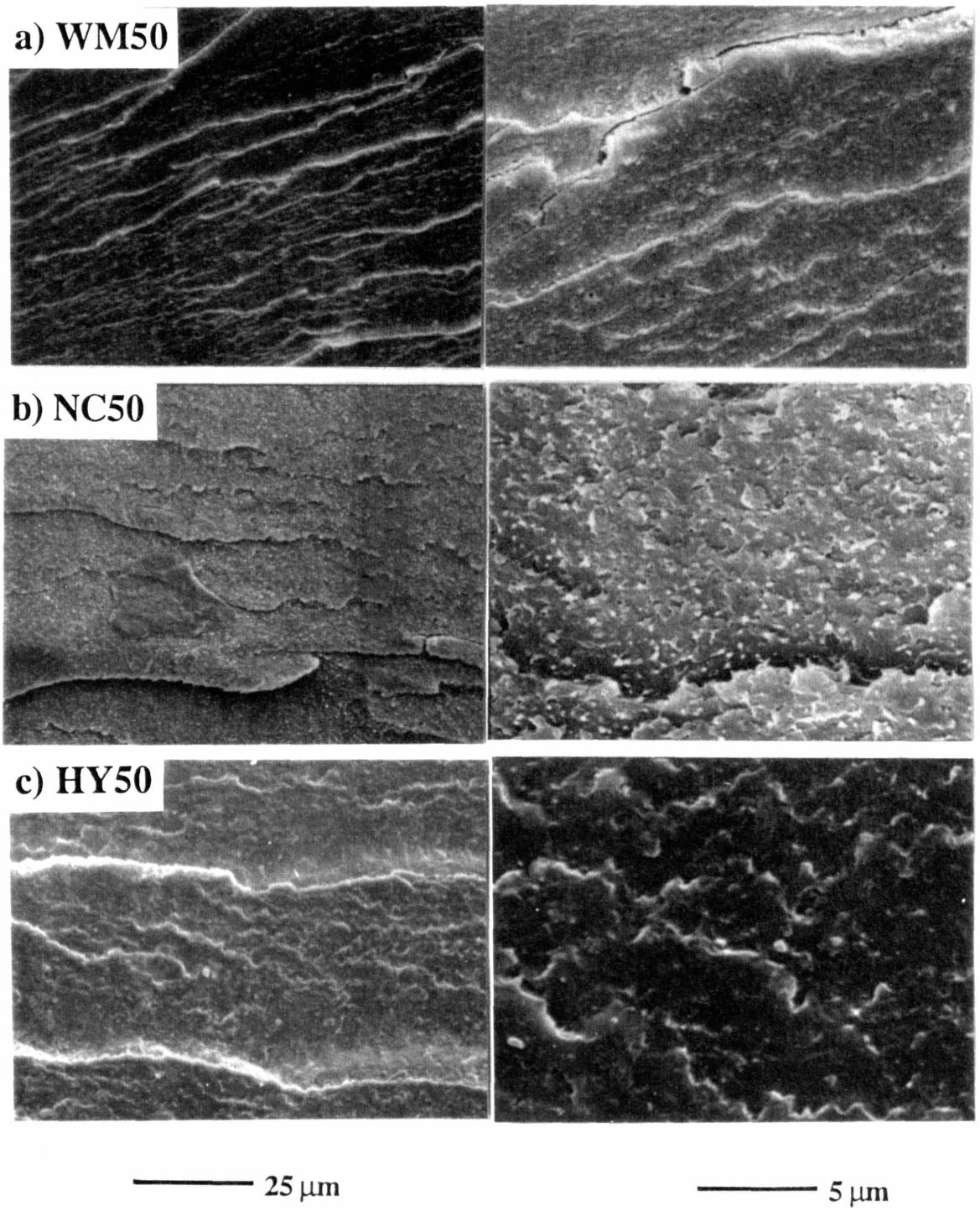
a) WM50
b) NC50
c) HY50
25 μm
5 μm

might propose that there is considerable miscibility between the sample phases. However, similarities in the mechanical properties of the EVOH and starch components at low temperature will yield similar fracture behavior even for completely incompatible materials. In addition, there may be good interfacial adhesion between the polymer components. Finally, since the glass transition of the both components is probably near or above room temperature, a relaxation of a more "rubbery" component (as the sample heats up to room temperature after cryo- fast fracture) that would provide a distinction between the rubbery and plastic domains does not occur [68].

Blend Morphology as Observed by SEM and TEM

In order to distinguish between starch and EVOH-rich domains, etching away of one component or preferential staining is necssary. In the SEM study, enzymatic etching [69] was employed according to the procedure outlined in the experimental section. The α-amylase enzyme attacks the α(1,4) glycosidic linkage in both amylose and amylopectin facilitating their removal from the blend structure into an aqueous solution. For TEM imaging, iodine vapor is used to provide the required levels of contrast to discern starch-rich domains from EVOH-rich areas. Both techniques yielded useful information about the blend morphology of the starch/EVOH blends.

SEM micrographs of untreated and etched surfaces of WM70 filaments are shown in Figure 3.14. In Figure 3.14a, an untreated WM70 showed evidence of small voids, probably due to foaming during processing. In Figure 3.14b, the etched WM70 filaments exhibited significant removal of the starch-rich fraction. The volume removed, as determined by image analysis, was less than 70%, however, since some of the waxy maize was encapsulated (even at this composition) and was therefore not accessible to the etchant. (Note that weight loss determination of volume removal was not possible due to unknown partitioning of the water and glycerin components after the etching procedure).

Figure 3.14. Scanning electron micrographs of a.) untreated and b.) α-amylase etched fracture surfaces of a WM70 filament. Images on the right represent magnified views of the images on the left. Foaming is evident in the untreated filament. Large-scale removal of the starch-rich domains occurs during enzymatic etching.

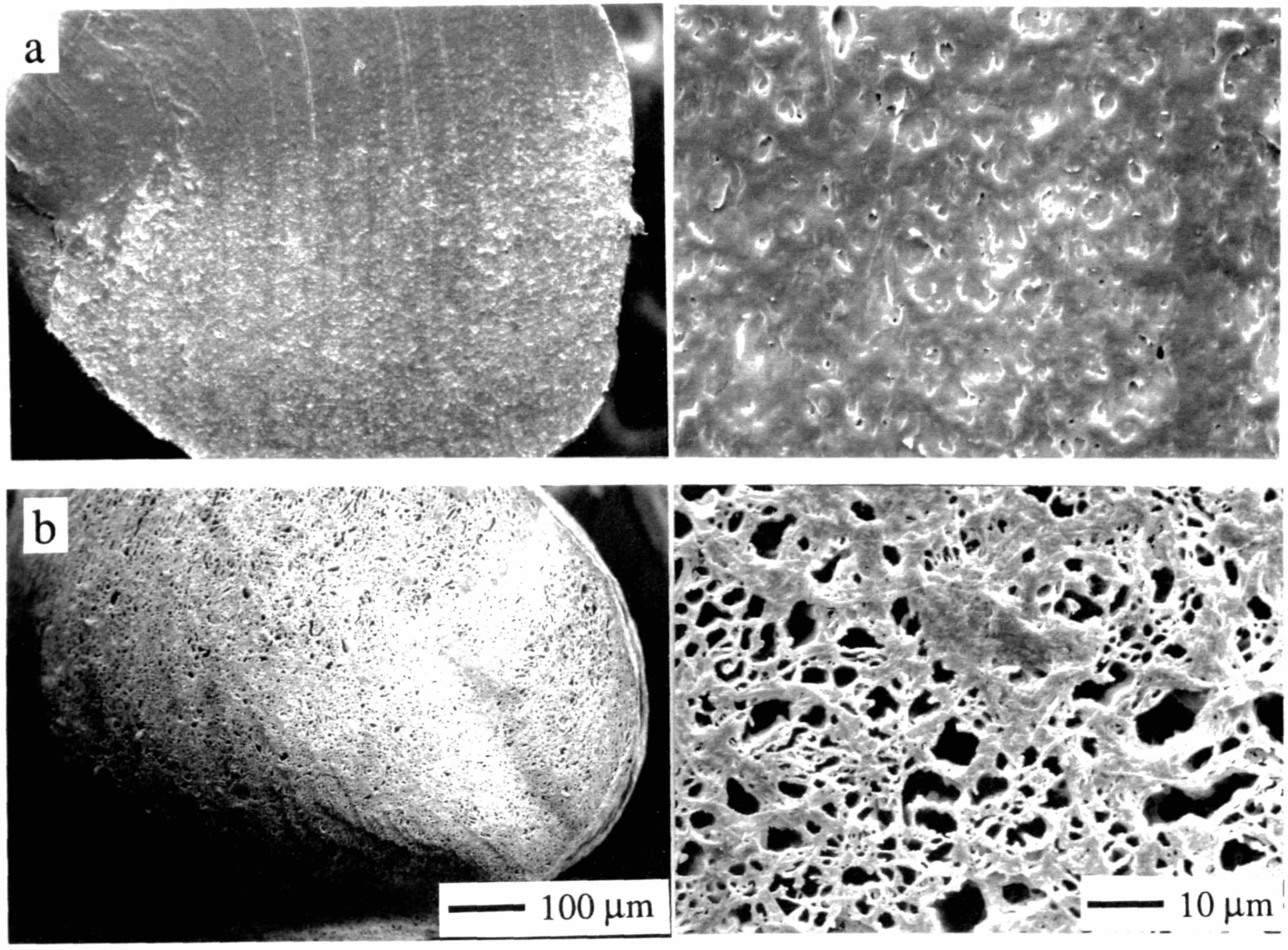
a
b
100 µm
10 µm

Results of etching filaments of representative waxy maize, native corn, and Hylon VII blends are shown in Figures 3.15, 3.16, and 3.17, respectively. The morphology of the waxy maize blends was most effectively revealed by etching. In Figure 3.15a, the etched WM30 blend exhibited approximately spherical cavities which ranged in size from 0.1 to 4 μm. In some areas, smaller domains in the process of coalescing were observed. Slightly smaller, yet more numerous, domains were visible in the WM50 sample. These domains ranged in size from 0.05 to 3 μm in size and were shaped like prolate spheroids. In both cases, the EVOH component seemed to comprise most of the matrix structure of the blend.

More extensive removal of the starch-rich domains was observed for the case of the WM70 sample (figure 3.15b). Because starch was the majority component in this blend, one would have expected complete collapse of the filament which has been etched. Due to incomplete etching, one can conclude that this partial removal is that of accessible starch-rich domains and that the EVOH-rich domains contribute to most of the matrix of this particular blend and may even encompass large starch-rich domains. Fibril-like threads approximately 0.4 to 0.7 μm in diameter were visible on the etched surface and appeared to be intertwined among each other and the remaining unetched bulk sample. It should be noted that these fibrils form during flow through the capillary and would therefore be oriented predominantly along the longitudinal direction of the filament. Fibrils observed in this axial cross-sectional view have most likely folded over upon drying of the etched filament. These observations lead us to propose that a co-continuous morphology forms at this composition since the EVOH-rich domains were distributed throughout the blend structure even though EVOH was the minority component. The fact that the EVOH domains appeared as fibrils indicates that there has been a significant amount of orientation within the melt as it passed through the spinnerette which became quenched in as the filament cooled.

Figure 3.15. Scanning electron micrographs of α-amylase etched fracture surfaces of a) WM30, b) WM50, c) WM70, and d) WM85 extrudates. Discrete starch domains are evident at compositions less than 50% starch. EVOH-rich fibrils are observable at higher starch compositions. Collapse of the WM85 filament occurred during etching and EVOH-rich filaments are present in the collected residue.

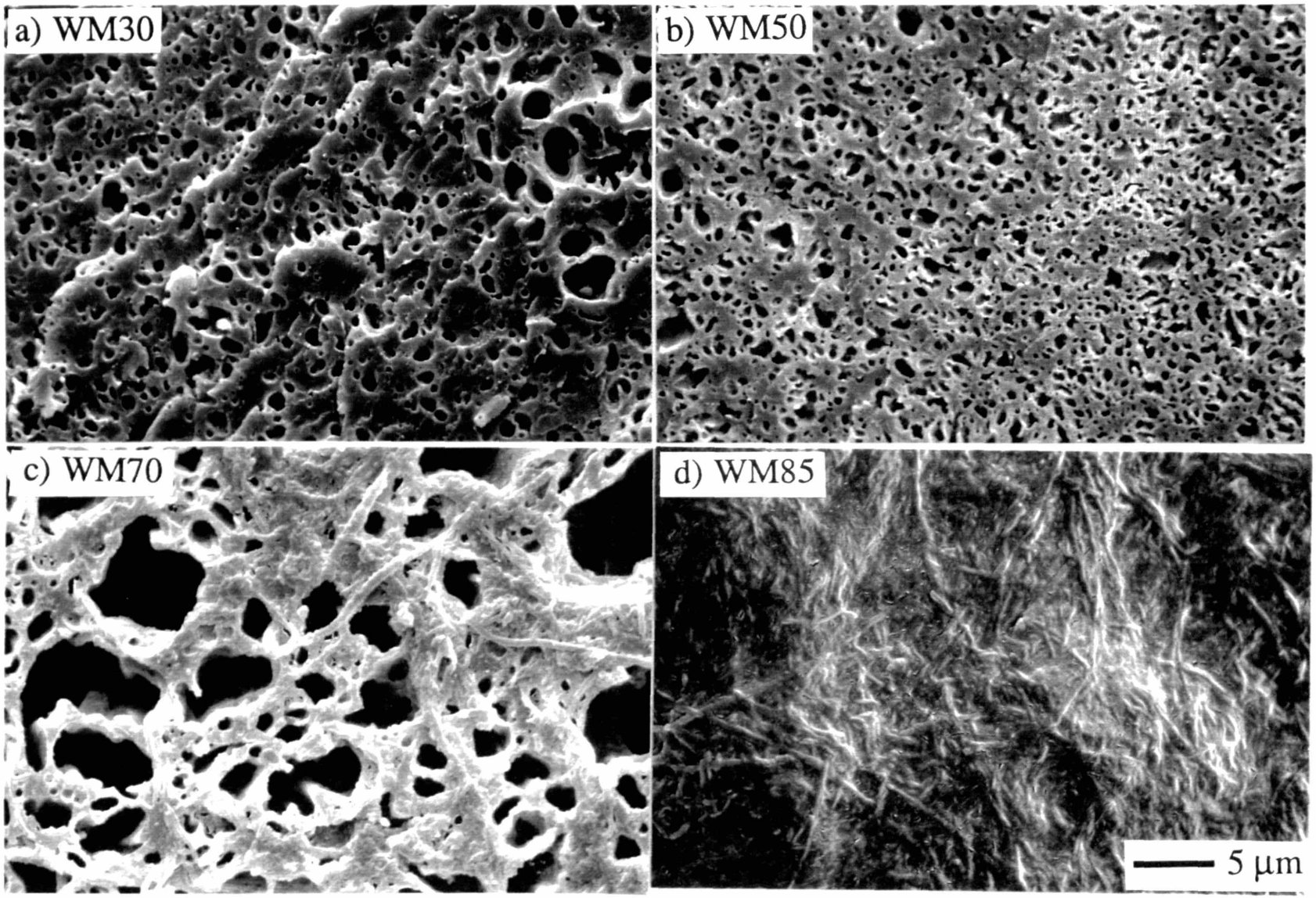
a) WM30
b) WM50
c) WM70
d) WM85
5 µm

In Figure 3.15d, the result of etching the WM85 filament is shown. In this case, the filament collapsed during the etching treatment. EVOH-rich fibrils approximately 0.35 μm in diameter and of lengths greater than 5 μm remain after etching. At this composition, the starch-rich phase formed a matrix in which the minority EVOH component experienced extensive orientation in the WM85 blend during capillary flow through the spinnerette.

Etching of the native corn starch blends was less effective. Removal of the starch-rich domains was apparent for the NC blends containing less than 50% starch, but only erosion of the filament fracture surface was observed for the NC70 and NC85 filaments. For the NC30 and NC50 blends, roughly spherical domains were visible after etching. These cavities ranged in size from 0.05 to 3 μm (figure 3.16 (a, b)). The surfaces of the NC70 and some areas of the NC85 filament appear nodular which may result from drying of a previously swollen filament (figure 3.16 (c, d)). Note, these results are somewhat reminiscent of etching starch-based films and fibers with boiling water [70][71].

Little morphological information was obtainable from etching of the Hylon VII blends. No differences between unetched and etched HY30 and HY50 filaments was observed (figure 3.17 a,b). The dark areas appearing in the micrograph were most likely due to holes in the gold-palladium coating which were observed due to loss of volatiles (i.e. water vapor, scission products) from the blend during exposure to the electron beam [72]. The HY70 and HY85 blends also did not show much etching behavior (3.18 c, d), but some changes in the surface structure most likely attributable to swelling and subsequent drying of the structure were evident.

Since the α–amylase etchant will attack the α(1,4) glycosidic linkage and not the α(1,6) linkage, it was not expected that the waxy maize blends would etch the most easily. The native corn series showed some removal of the starch-rich domains at compositions less than 50% starch, but, at higher compositions, little etching was

Figure 3.16. Scanning electron micrographs of α-amylase etched fracture surfaces of a) NC30, b) NC50, c) NC70, and d) NC85 extrudates. Discrete starch-rich domains are present in the NC30 filament. Starch removal occurs in the NC50 blend, but domains are less discrete. Etching of filaments containing more than 50% starch is less effective at distinguishing between starch-rich and EVOH-rich domains.

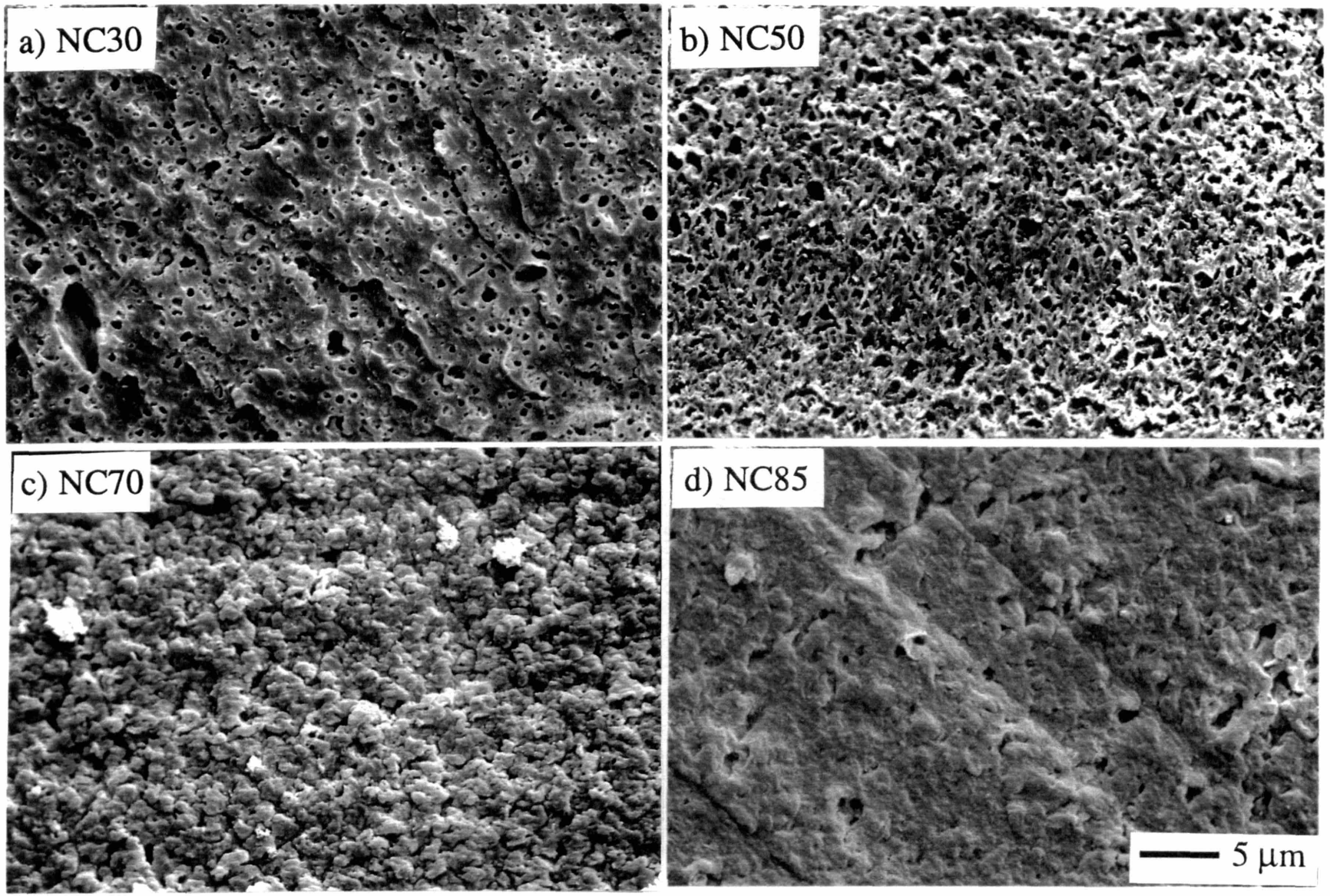
a) NC30
b) NC50
c) NC70
d) NC85
5 µm

Figure 3.17. Scanning electron micrographs of α-amylase etched fracture surfaces of a) HY30, b) HY50, c) HY70, and d) HY85 extrudates. The etchant had no effect on blends containing less than 50% starch. Some texture development in blends containing more than 50% starch occurred, but domains corresponding to EVOH-rich or starch-rich compositions are not distinguishable.

a) HY30
b) HY50
c) HY70
d) HY85
5 µm

observable. Surprisingly, the Hylon VII blends with almost all α(1,4) linkages showed the most resistance to etching. This can be understood in terms of the accessibility of the etchant to the starch, crystallinity of starch, and the use of water as a carrier for the enzyme etchant. The extent of etching relies on the susceptibility of the blend to the penetration of the aqueous carrier phase. The diffusion of water and access of the water soluble enzymes into a blend is expected to be less for a miscible starch-EVOH region than for a pure starch domain. Therefore, compatibility of starch with the EVOH component may diminish some of the ability of the blend to etch and domains will become less evident. Also, if certain components are crystalline, etching will be retarded in the crystalline regions compared to the amorphous regions. At lower compositions of the starch component, the fraction of domains accessible to the etchant decreases and the fraction of isolated clusters increases, thus making etching less effective. Treatment of the 100% starch blends with water showed complete collapse of the WM100 filament, swelling of the NC100, and slight swelling of the HY100 filaments. Treating the same blends with enzyme solution results in breakup of the WM100 and NC100 filaments and slight swelling of the HY100 filament. Because of the sensitivity of the waxy maize to water, etching of the starch-rich domains in the WM blends can be carried out even in the control water solution. The addition of the enzyme, however, has resulted in greater removal of polymer, possibly by scissioning any chains that have become entangled and allowing lower molecular weight chains to be carried into solution. Studies by others [73] have also demonstrated that the susceptibility of native granules is dependent upon the relative amounts of amylose and amylopectin present in the starch; high-amylose varieties are less readily attacked by enzymes (because of increased H-bonding and retrogradation [74, 75]) whereas waxy maize varieties are most susceptible.

Transmission electron microscopy provided more detailed information the blend morphology of the starch/EVOH blend and is treated specifically in Chapter 4. Micrographs of the WM50, NC50, and HY50 blends are shown in Figure 3.18 which

Figure 3.18. Transmission electron micrographs of iodine stained starch/EVOH (50:50) blends: a) WM50, b) NC50, and c) HY50 extrudate sections.

a
b
c
1 µm

illustrate the existence of distinct starch-rich domains for each of the starch varieties employed in this study (iodine stained, starch-rich domains appear dark against the lighter EVOH-rich matrix via mass thickness contrast). For the Waxy Maize blend (WM50), a phase separated structure reminicent of an incompletely mixed incompatible polymers was observed (Figure 3.18a). Oriented droplets ranging from 0.05 μm to approximately 5 μm in length were visible with L/D values averaging 1.8 +/- 0.5 (smallest droplets are least oriented, as expected). Irregularities in droplet shape and the fact that these droplets exhibited some preferred orientation indicates that optimum blending between the two polymer components has not been achieved during the extrusion process [76]. Smaller light phase domains appear within the darker regions indicating the formation of composite droplets. Domain sizes are consistent with those observed in SEM for the etched WM50 blend (figure 3.15b).

Unlike in the WM50 blend, no composite droplets were observed in the NC50 blend (figure 3.18b). The EVOH-rich, lighter area, appeared continuous throughout the sections indicating that this component (or a mixture of mostly EVOH and some of the starch fraction) forms the matrix. Starch-rich domains were visible as discrete domains ranging in size from approximately 0.05 μm to 1.2 μm. Although the electron densities of the waxy maize and native corn starches are similar, the contrast between the starch-rich domains and the blend matrix is lower. This fact may indicated that the the amylose fraction in the Native Corn starch may be partially miscible with the EVOH fraction.

Finally, the HY50 blend exhibits a finer dispersion of smaller starch-rich domains ($d < 0.25$ μm) distributed throughout a gray matrix (figure 3.18c). Overall, HY blends are more difficult to visualize due to the lower initial contrast level between the starch-rich and EVOH-rich domains which quickly fades as the sample is observed in TEM. This lower contrast as well as finer domain sizes provides evidence for even greater levels of miscibility between the starch and EVOH components. The presence of visibly discrete

starch-rich domains, however, indicates that, for the most part, all the starch types in this study are somewhat immisicible with EVOH.

The addition of EVOH will effect the extent to which the starch component will be sheared during the extrusion process. Rheological measurements from Villar, Thomas, and Armstrong [32] can be used to further understand our structural observations. Capillary viscometry measurements showed that the viscosity of the blends generally decreases as the EVOH content increases (except for the WM blends). At 150 °C and a shear rate of 100 sec^{-1}, EVOH, WM100, NC100, and HY100 have viscosities of 900, 320, 1000, and 5100 Pa-s, respectively. At compositions of more than 50% EVOH, the viscosity of the blends tends to approach that of neat EVOH. Villar proposed that the starch molecules experience lower stress at these compositions, and undergo less chain scission during the compounding process. This behavior will have direct consequences on the mixing behavior between the starch and EVOH components. SEM on the WM series has shown that distinct starch-rich domains are evident for the 30, 50, and 70% compositions. For WM50, the blend structure is similar to that of traditional incompatible polymer blends wheras for blends with high starch contents, the minority EVOH component appeared to be well distributed throughout the starch matrix For the NC blends, discrete starch domains were evident at compositions less than 50% starch; however, no discrete phases were evident in SEM (Further TEM of the NC series, shows that, similar to the WM blends, EVOH is finely dispersed in blends high in starch content [Chapter 4]). For the Hylon VII blends, the viscosity of the starch is much higher than that of the EVOH component; however, finer mixing of the phases is evident. As demonstrated in the viscometry data, incorporation of EVOH into the blend lowers the viscosity of the material even at relatively high amylose content. This observation is consistent with the results of this morphology study in which the Hylon VII and EVOH appear to have the most interaction.

Phase Coarsening of Starch/EVOH Blends

A study was performed on the WM30 blend pellets in order to understand more about the stability of the phase structure of starch blends in the melt. This property is extremely relevant to processing applications such as injection molding, film blowing, and fiber spinning where holding time in the melt becomes very important. Pellet sections (~ 25 mg) were heated in the DSC (in high pressure capsules, with a nitrogen purge) to 150°C at a rate of 10°C/min, held at that temperature for 0.01, 0.1, 1.0, 10, 100, and 1000 minutes, and cooled at the maximum DSC-7 cooling rate (set to 500°C/min). DSC results showed consistent sample to sample melting behavior. The samples were then removed from the DSC capsules, placed in liquid nitrogen for one minute, and then immediately fractured using a razor blade to initiate the crack. One section was viewed in SEM as fractured. The other section of each fracture was etched with α-amylase before viewing in the SEM. Both sections were coated with Au-Pd before imaging in the microscope.

As shown in Figure 3.19, domain growth of the waxy maize-rich fraction was observed. However, images of the some of the control samples show voids inherent in the pellets which may have formed during their initial processing or in the thermal treatment. These voids (from volatile foaming) may have facilitated the etching behavior of some of the pellets, resulting in artifacts inherent in the observed systems. Because of this inherent phenomena, a quantitative analysis of the domain growth will be in error. Estimates of average void size as a function of time are: 0.9, 1.2, 1.5, 1.5, 2.8, and 3.8 +/- 0.2 μm over the time range; this behavior does not follow Ostwald ripening kinetics for nucleation and growth of minority phase domains (i.e. $d \neq t^{1/3}$) as has been observed for other polymer blends [77]. Instead, a slower rate of coarsening ($d \sim t^{1/8}$) is observed which may be a result of the initial phase sizes present upon exiting the extruder, diffusional properties of the starch-domains at 150°C (partially due to the high molecular

Figure 3.19. Scanning electron micrographs of WM30 extrudate that has been held at 150°C for a) 0.01 min., b) 0.1 min., c) 1 min., d) 10 min., e) 100 min., and f) 1000 min. Samples were etched with α-amylase aqueous solution prior to viewing in the microscope.

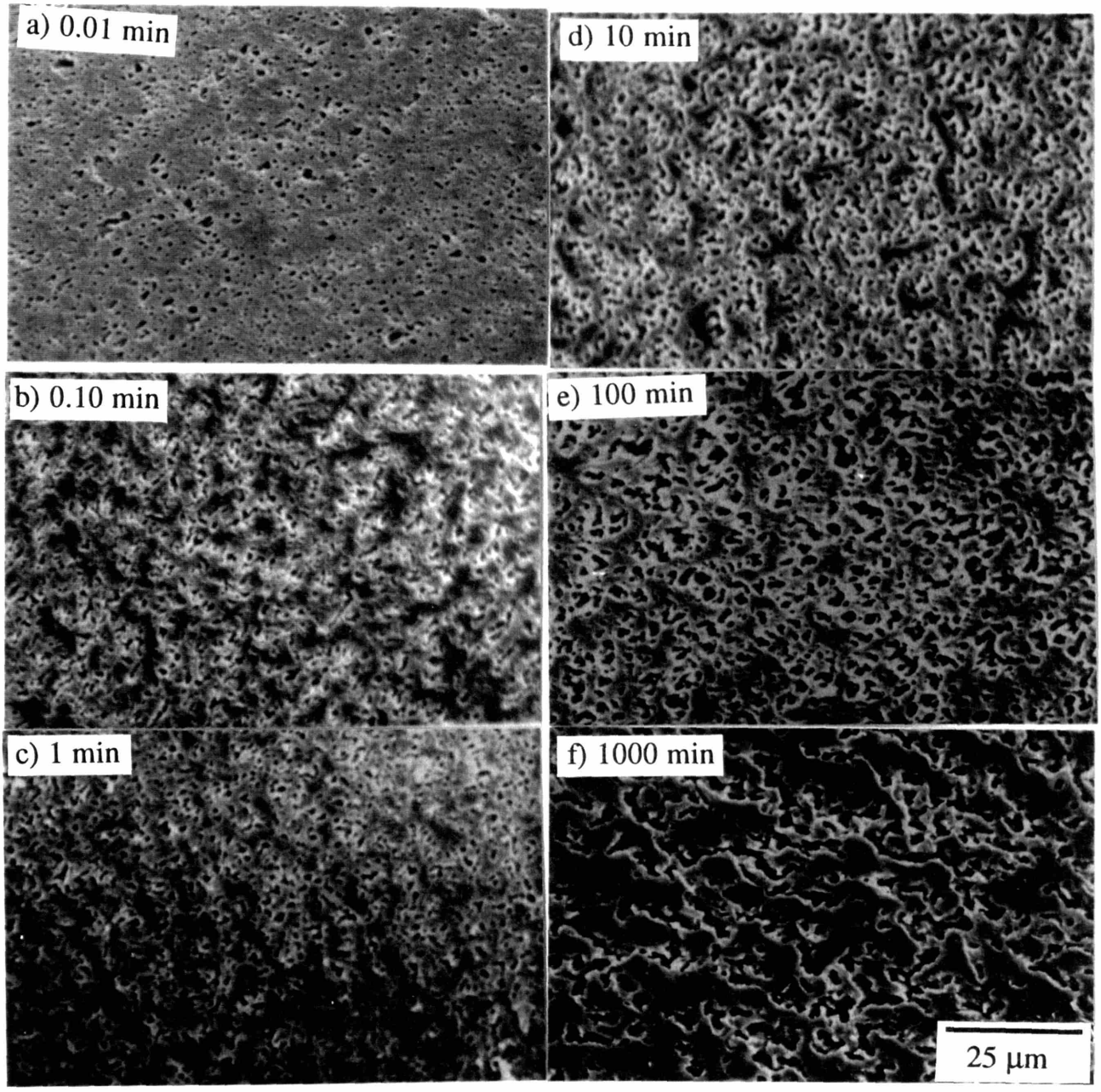
a) 0.01 min
d) 10 min
b) 0.10 min
e) 100 min
c) 1 min
f) 1000 min
25 µm

weight of the starch component), interfacial effects involving the processing additives, partial miscibility of components, and plasticizer migration in the blend.

SEM of Etched Filaments - Effect of Capillary Flow

In order to gain some insight on the bulk morphological structure that forms when molten starch/EVOH blends are forced through a capillary to form a filament, the surfaces, axial cross-sections, and longitudinal cross-sections of certain filaments were examined. Results for the WM30 and WM70 blends are shown in Figures 3.20 and 3.21, respectively. On the left side of each figure are untreated surfaces; on the right side are the results of enzymatically etching the filament (with exposed surfaces) following the procedure given previously.

The etching procedure appeared to have little effect on the outside surfaces of starch/EVOH filaments. The WM30 filament surface was highly textured with nodular and oblong protuberances ranging in size from 1 to 10 microns which indicate inhomogeneity in the sample flow (figure 3.20a). Etching with enzymatic solution does not appear to dramatically change the appearance of the filament surface although some oblong holes (up to 5 μm long) and cracks extending along the flow direction are visible. Sharking or ribbing of the WM70 filament surface was observed (figure 3.21a); this was a result of unstable flow through the spinnerette [46]. The etched WM70 filament also possessed some holes and grooves but its appearance was still strongly reminiscent of the original filament.

As evident in Figures 3.20b and 3.21b which show the axial cross-sections of the filaments, some foaming had occurred in the WM30 blend and more extensively in the WM70 filament . Both fracture surfaces appear very different after etching. In the axial cross-sectional view, the WM30 filament contained approximately circular domains ranging in size from 0.2 to 3 μm (figure 3.20b). The WM70 filament possessed many irregularly shaped domains that ranged in size from 0.5 to 17 μm. The longitudinal

Figure 3.20. Scanning electron micrographs of various surfaces of a WM30 filament (d = 710 μm); 1) surface, 2) axial cross-section, 3) longitudinal cross-section. Draw direction is vertical (draw ratio = 1). Images on the left are of untreated filaments (a). Images on the right (b) are the similar filaments which have been etched with α-amylase aqueous solutions.

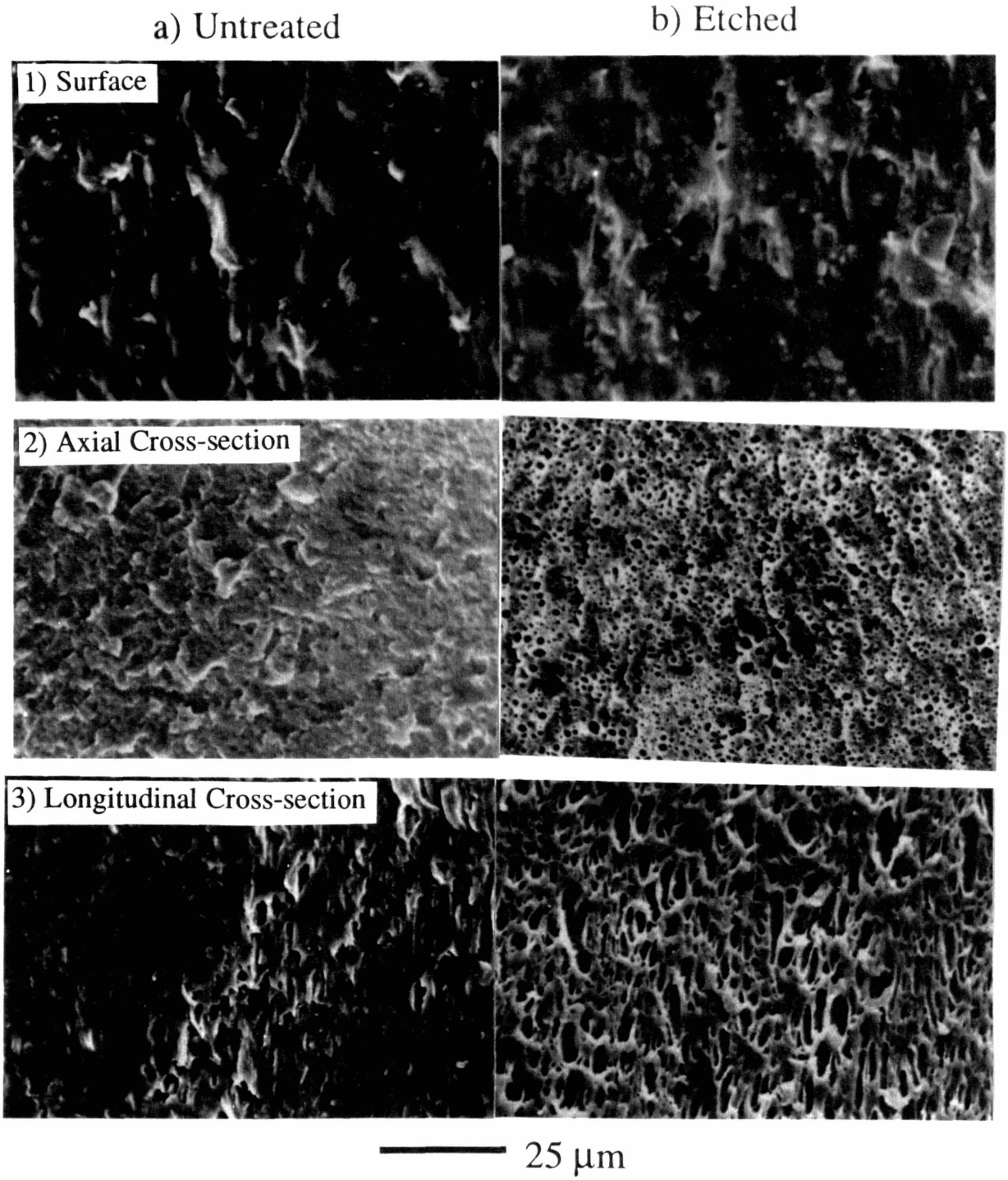
a) Untreated
b) Etched
1) Surface
2) Axial Cross-section
3) Longitudinal Cross-section
25 μm

Figure 3.21. Scanning electron micrographs of various surfaces of a WM70 filament (d = 1080 μm); 1) surface, 2) axial cross-section, 3) longitudinal cross-section. Draw direction is vertical (draw ratio = 1). Images on the left are of untreated filaments (a). Images on the right (b) are the similar filaments which have been etched with α-amylase aqueous solutions.

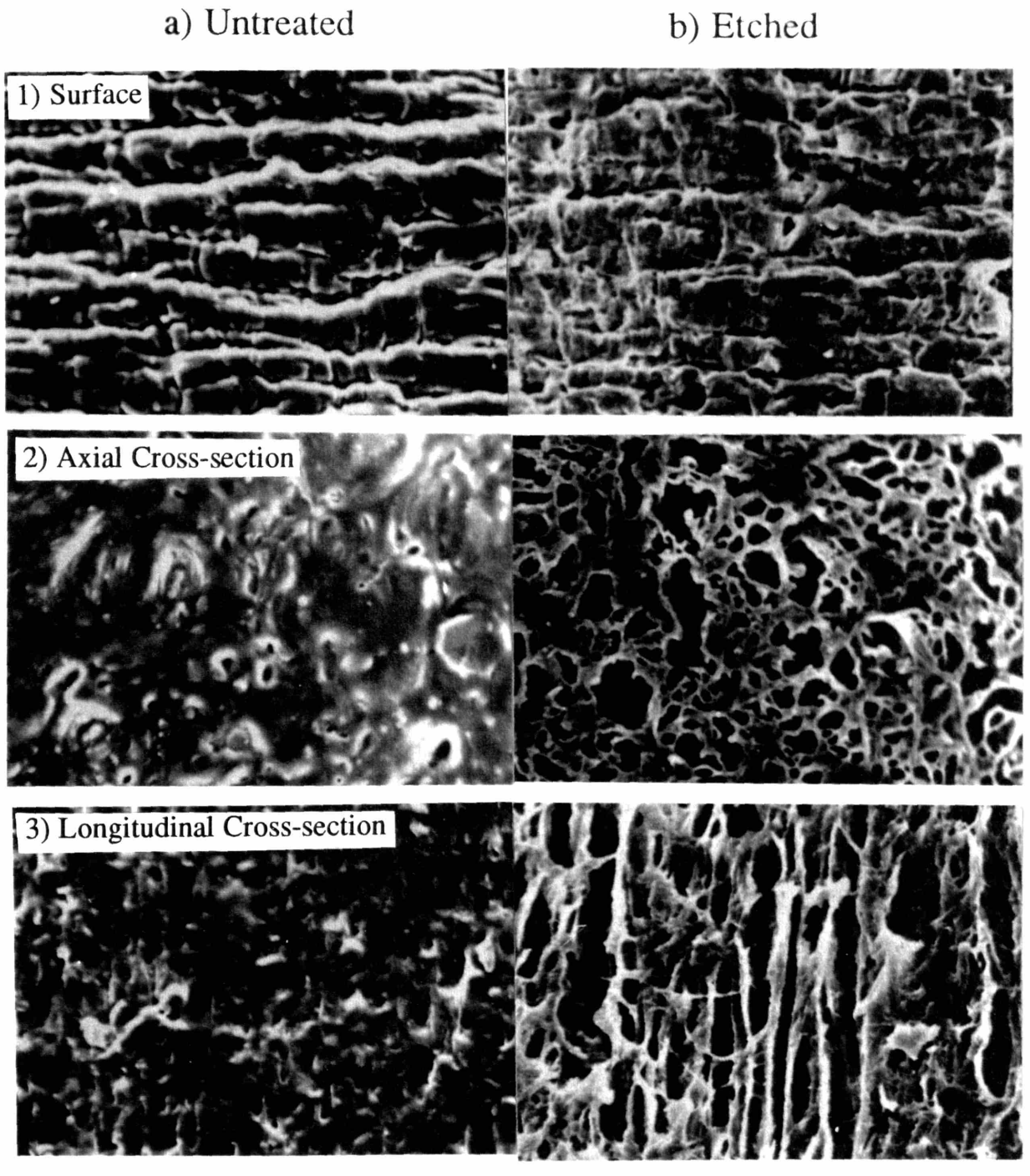
a) Untreated
b) Etched
1) Surface
2) Axial Cross-section
3) Longitudinal Cross-section
25 μm

cross-sectional view of the WM30 filament indicated that the starch-rich domains were ellipsoidal in shape and are aligned along the fiber axis. Values for L/D range from 1 to greater than 10. Phase inversion appears to occur in the WM70 sample. Here, the EVOH phase forms long thread-like particles. These threads are connected together horizontally possibly indicating a co-continuous structure since the minority EVOH component appears to extend throughout the length of the sample. It should be noted that there is no evidence from flat film WAXS that the EVOH or starch phases are oriented; this result indicates that, though the phases are oriented, the molecules contained in the domains have relaxed.

Structural Influences on Starch/EVOH Blend Processability and Properties

During the compounding of the model series of blends, adequate amounts of plasticizer (glycerin and water) as well as sufficient levels of heat and shear allowed for the destructurization of the initial granules. SEM and TEM showed no trace of intact native granules for all of the waxy maize and native corn starch blends. X-ray and thermal analysis confirmed that the starch component formed a molten phase during the compounding process as evident in the loss of crystallinity in the amylopectin component. Partial miscibility of the amylose fraction is also suggested due to etching behavior and melting point depression of the EVOH component. The distribution and connectivity of starch-rich phase domains which are smaller than granule size will alter the transport processes leading to biodegradation of the blend.

Crystallinity in the NC and HY blends occurs in both the EVOH and starch domains. An increase in crystallinity will lower the rate of biodegradation for these types of blends. As noted from the etching studies, the aqueous solutions do not penetrate the HY extrudates or filaments and the α-amylase does not readily etch the starch phase from the bulk structure. Similar results should occur with microbial attack. In solution, amylose, more than amylopectin, undergoes a phenomena called retrogradation in which

interchain hydrogen bonding between polymer chains causes them to precipitate out of aqueous solutions [78] This action of the amylose chains would serve to exclude plasticizer from "retrograded" regions. Plasticizer was observed on the outer surface of the Hylon VII blends which seems to confirm this hypothesis. Retrogradation of amylopectin is also documented to occur but much more slowly over time [74, 78]. This process contributes to the small endotherm observed in DSC between 55 and 60°C for the NC and WM blends (Note, most of this endotherm is attributed to the additive, however) and will increase the brittleness and slow the rate of biodegradation for these blends.

Under certain processing conditions (i.e. filament formation), EVOH has been shown to primarily coat the blend surfaces as evident in the enzymatic etching experiment (similar results are evident in studies employing cross-sectional TEM of starch/EVOH fibers as shown in Chapter 5). EVOH is more moisture resistant and less biodegradable than starch. Articles made with this coating will therefore be less moisture sensitive and initially more resistant to microbial attack.

The mechanical properties of starch/EVOH blends will also depend the distribution of starch-rich and EVOH-rich phases. Smaller and well distributed phase domains will lead to mechanical behavior that is more consistent with a blend of two components (i.e. load is distibuted over a wider area). Conversely, large domains of starch will more likely act as points of concentration for stress, resulting in mechanical failure at lower tensile stresses. Thus, blends can contain higher amounts of destructurized starch rather than dry starch granule filler. If miscibility exists between starch and EVOH, the interfacial adhesion between phases may improve, and debonding of domains leading to failure is expected to decrease. Finally, blends containing more amylose are more likely to be stronger partially due to the larger amount of linear, crystallizable polymer present. The mechanical behavior of the starch/EVOH blends is explored in more detail in Chapter 5.

CONCLUSIONS

The extrusion blending of three varieties of corn starch with poly(ethylene-vinyl alcohol) to produce a biodegradable thermoplastic resin was investigated by examining the structural characteristics of the resulting blends. The corn starches, Waxy Maize (WM), Native Corn (NC), and high amylose Hylon VII (HY), varied in their branch content (amylose to amylopectin ratio) and molecular weight. The starches were blended with poly(ethylene-vinyl alcohol) containing 56 mol% VOH over a systematic compositional range from 100% starch to 0% starch (control sample). Glycerin and water were employed as plasticizers.

X-ray, thermal analysis, and electron microscopy results indicated that the WM and NC granules were destructurized during the extrusion process (The HY starch was pre-treated prior to blending), and a polymer-polymer blend was formed with the EVOH component. All of the blends showed evidence of phase separation between starch and EVOH. The Native Corn and Hylon VII blends, in particular, appeared to be partially miscible as evident from EVOH melting point depression beyond the effects due to the two plasticizers alone, smaller domain sizes, and lower contrast between phases in TEM. Blends containing amylose exhibited crystalline scattering patterns associated with the amylose complex in WAXS, although most of the crystallinity was due to the EVOH component.

Whereas Waxy Maize blends are most susceptible to moisture and enzyme etching treatments, the Native Corn and Hylon VII blends show more resistance to swelling, dissolution, and degradation due to increased levels of crystallinity, H-bonding in the starch fraction, smaller phase sizes, and partial miscibility with the EVOH component. SEM was thus most useful for studying WM blends and NC blends with starch contents of 50% or less. More morphological information was attainable with TEM (using iodine as a stain for starch) in which distinct starch-rich and EVOH-rich domains were clearly evident for all three starch types. Starch-rich domain sizes decreased as the amylose

content of the starch component was increased (i.e. $d_{WM50} > d_{NC50} > d_{HY50}$) and contrast between phases decreased indicating increased miscibility between the polymer components.

The influence of time in the melt and shear (capillary) flow on the phase morphology for select Waxy Maize blends was then examined since this series yielded the most structural information with SEM. Waxy maize-rich domains undergo phase coarsening as a function of time in the melt although much slower than Ostwald ripening kinetics ($d \sim t^{1/8}$). Orientation of both starch-rich and EVOH-rich domains, but not polymer molecules, was observed at various compositions; EVOH underwent significant orientation relative to starch as evident by EVOH-rich fibrils in blends with a large amount of starch. Little etching was observed on the filament surfaces indicating that EVOH is coating the specimen as it is extruded through a capillary.

REFERENCES

1. R.L. Whistler, 'History and Future Expectations of Starch Use', in *Starch: Chemistry and Technology*, R.L. Whistler, J.N. Bemiller and E.F. Paschall, Eds. 1984, Academic Press, Inc.: New York. p. 1.

2. W.M. Doane, 'New Uses for Starch', in *New Crops, New Uses, New Markets: Industrial and Commercial Products From U.S. Agriculture.* 1992, U.S. Dept of Agriculture: Washington, D.C. p. 147.

3. J.W. Mullen and E. Pacsu, 'Starch Studies: Possible Industrial Utilization of Starch Esters,'*Ind. Eng. Chem.*, **35,** 381 (1943).

4. I. Tomka, 'A Thermoplastically Processable Starch and A Process for Making It', in *PCT Patent No. WO 90/05161.* 1989.

5. F.H. Otey, R.P. Westhoff and C.R. Russell. 'Starch-based Plastics and Films' in *Technical Symposium: Nonwoven Product Technology.* 1975.

6. F.H. Otey, R.P. Westhoff and C.R. Russell, 'Biodegradable Films from Starch and Ethylene-Acrylic Acid Copolymer,'*Ind. Eng. Chem. Prod. Res. Dev.*, **16,** 305 (1977).

7. R.P. Westhoff, W.F. Kwoleck and F.H. Otey, 'Starch-Polyvinyl Alcohol Films - Effect of Various Plasticizers,'*Starch/Starke*, **31,** 163 (1979).

8. G.F. Fanta, R.C. Burr and W.M. Doane, 'Polymerization of Alkyl Acrylates and Alkyl Methacrylates with Starch,'*Journal of Applied Polymer Science*, **25,** 2285 (1980).

9. F.H. Otey and R.P. Westhoff. 'Biodegradable Starch-based Plastic Films for Agricultural Applications. in Proceedings of the 15th National Agricultural Plastics Congress'. 1980. Tucson, AZ.

10. F.H. Otey. 'Starch-based Plastics and Related Products for Agriculture'. in *Proc. 17th Nat'l Agric. Plastics Congress, "Plasticulture Worldwide".* 1983. U. N. H., Manchester, NH.

11. W.M. Doane. 'Incorporation of Starch into Plastics'. in *First Annual Corn Utilization Conference.* 1987. St. Louis, Missouri.

12. W.M. Doane, 'Starch-based Polymers for Agricultural Applications,'*Polymer Preprints*, **28,** 103 (1987).

13. G.F. Fanta. 'Starch-Thermoplastic Polymer Composites by Graft Polymerization'. in *Corn Utilization Conference II, National Corn Growers Association.* 1988.

14. C.L. Swanson, R.P. Westhoff and W.M. Doane. 'Modified Starches in Plastic Films'. in *Corn Utilization Conference II.* 1988.

15. C. Bastioli, V. Bellotti, L. Del Gludice and R. Lombi, 'Polymer Compositions for the Production of Articles of Biodegradable Plastics Material and Methods for Their Preparation', in *European Patent Application 90110070.1*, S.r.l. Butterfly, Ed. 1990.

16. R.L. Shogren, R.V. Greene and Y.V. Wu, 'Complexes of Starch Polysaccharides and Poly(Ethylene-co-Acrylic Acid): Structure and Stability in Solution,'*J. Appl. Polymer Sci.*, **42,** 1701 (1991).

17. R.L. Shogren, A.R. Thompson, R.V. Greene, S.H. Gordon and G. Cote, 'Complexes of Starch Polysaccharides and Poly(ethylene-co-Acrylic Acid): Structural Characterization in the Solid State,'*J. Appl. Polymer Sci.*, **47,** 2279 (1991).

18. R.L. Shogren, A.R. Thompson, F.C. Felker, R.E. Harry-O'Kuru, S.H. Gordon, R.V. Greene and J.M. Gould, 'Polymer Compatibility and Biodegradation of Starch-Poly(ethylene-co-acrylic acid)-Polyethylene Blends,'*J. Appl. Polym. Sci.*, (1991).

19. C. Ching, D.L. Kaplan and E.L. Thomas, eds. *Biodegradable Polymers and Packaging*. . 1993, Technomics Publishing Co.: Lancaster, PA.

20. D. Trimmell, C.L. Swanson and R.L. Shogren, 'Extrusion Processing of Granular Starch-g-Poly(methyl acrylate): Effect of Extrusion Conditions on Morphology and Properties,'*J. Appl. Poly. Sci.*, **48,** 1665 (1993).

21. H. Roper and H. Koch, 'The Role of Starch in Biodegradable Thermoplastic Materials,'*Starch/Starke*, **42,** 123 (1990).

22. W.M. Doane, 'USDA Research on Starch-Based Biodegradable Plastics,'*Starch/Starke*, **44,** 293 (1992).

23. R.L. Shogren, G.F. Fanta and W.M. Doane, 'Development of Starch Based Plastics - A Reexamination of Selected Polymer Systems in Historical Perspective,'*Starch/Starke*, **45,** 276 (1993).

24. J.-C. Huang, A.S. Shetty and M.-S. Wang, 'Biodegradable Plastics: A Review,'*Advances in Polymer Technology*, **10,** 23 (1990).

25. G. Swift, 'Directions for Environmentally Biodegradable Polymer Research,'*Acc. Chem. Res.*, **26,** 105 (1993).

26. J. Mayer and D.L. Kaplan, 'Biodegradable Materials: Balancing Degradability and Performance,'*Trends In Polymer Science*, **2,** 227 (1994).

27. F. Wittwer and I. Tomka, 'Polymer Composition for Injection Molding', in *U.S. Patent #4,673,438*, Warner-Lambert Company, 1987.

28. G. Lay, J. Rehm, R.F. Stepto, M. Thoma, J.-P. Sachetto, D.J. Lentz and J. Silbiger, 'Polymer Composition Containing Destructurized Starch', in *United States Patent No. 5,095,054*, Warner-Lambert Company, 1992.

29. C. Bastioli, R. Lombi, G. Del Tredici and I. Guanella, 'A Method for the Preparation of Destructurized Starch-based Compositions Produced Thereby', in *European Patent Application*, B. S.r.l., 1990.

30. E.R. George, T.M. Sullivan and E.H. Park, 'Thermoplastic Starch Blends with a Poly(Ethylene-co-Vinyl Alcohol): Processability and Physical Properties,'*Polymer Engineering and Science*, **34,** 17 (1994).

31. J.E. McCassie, J.M. Mayer, R.E. Stote, A.E. Shupe, P.J. Stenhouse, P.A. Dell and D.L. Kaplan, 'Biodegradation Kinetics in Marine and Soil Systems', in *Biodegradable Polymers and Packaging*, C. Ching, D.L. Kaplan and E.L. Thomas, Eds. 1993, Technomic Publishing Co.: Lancaster, PA. p. 217.

32. M.A. Villar, E.L. Thomas and R.C. Armstrong, 'Rheological Properties of Thermoplastic Starch and Starch/Poly(ethylene-co-vinyl alcohol) Blends,'*Polymer*, (submitted 1994).

33. D.R. Paul and S. Newman, eds. *Polymer Blends*. . 1978, Academic Press: New York.

34. R. Billmers, personal communication, National Starch Co., Bridgewater, NJ (1994).

35. R. Dolfinger, unpublished data (1993).

36. 'Constant Test Atmospheres over Aqueous Solutions', in *Deutsche Normen*. 1981.

37. W. Ruland, 'X-Ray Determination of Crystallinity and Diffuse Disorder Scattering,'*Acta Cryst.*, **14**, 1180 (1961).

38. L.E. Alexander, *X-Ray Diffraction Methods in Polymer Science*. 1969, New York: John Wiley & Sons, Inc.

39. C.H. MacFillavry and G. Riech, eds. *International Tables for X-Ray Crystallography*. . Vol. 3. 1968, The Kynoch Press: Birmingham, England.

40. D.L. Misell, *Image Analysis, Enhancement and Interpretation*. Practical Methods in Electron Microscopy, ed. A.M. Glauert. Vol. 7. 1978, New York: North-Holland Publishing Company.

41. L.L. Buckholz Jr., 'The Role of Maillard Technology in Flavoring Food Products,'*Cereal Foods World*, **33**, 547 (1988).

42. W. Wiedmann and E. Strobel, 'Compounding of Thermoplastic Starch with Twin-Screw Extruders', 1992, Werner-Pfleiderer Corporation.

43. W. Wiedmann, 'Principles and Applications of Starch Extrusion', 1992, Werner-Pfleiderer Corp.

44. L. Elsberg, unpublished results (1993).

45. C.E. Weigand, 'Thermoplastic Processing of Starch and Starch-Based Systems', M.S. Thesis, Massachusetts Institute of Technology (1992).

46. Z. Tadmor and C.G. Gogos, *Principles of Polymer Processing*. 1979, New York: John Wiley & Sons.

47. A. Sarko and H.-C.H. Wu, 'The Crystal Structure of A-, B-, and C-Polymorphs of Amylose and Starch,'*Starch/Starke*, **30**, 73 (1978).

48. H.F. Zobel, 'Starch Crystal Transformations and Their Industrial Importance,'*Starch/Starke*, **40,** 1 (1988).

49. P. Muhrbeck, 'On Crystallinity in Cereal and Tuber Starches,'*Starch/Starke*, **43,** 347 (1991).

50. C. Mercier, R. Charbonniere, D. Gallant and A. Guilbot, 'Structural Modifications of Various Starches by Extrusion Cooking with a Twin Screw French Extruder', in *Polysaccharides in Food*, J.M.V. Blanshard and J.R. Mitchell, Eds. 1979, Butterworth Publ.: London. p. 153.

51. P. Colonna, J.L. Doublier, J.P. Melcion, F. de Monredon and C. Mercier, 'Extrusion Cooking and Drum Drying of Wheat Starch. I. Physical and Macromolecular Modifications,'*Cereal Chemistry*, **1,** 538 (1984).

52. J.R. Katz, 'Abhandlungen zur Physihalichen Chemie der Starke und der Brothereitung', in *Zeitshrift fur Physikalische Chemie*, W. Ostwald and J.H. Van't Hoff, Eds. 1930, Akademische Veraggellschaft M.B.H.: Leipzig.

53. H.-C.H. Wu and A. Sarko, 'The Crystal Structure of A-Starch is it Double Helical?,'*Carbohydrate Research*, **54,** C3 (1977).

54. H.-C.H. Wu and A. Sarko, 'The Double-Helical Molecular Structure of Crystalline A-Amylose,'*Carbohydrate Research*, **61,** 27 (1978).

55. T.J. Schoch, 'Non-carbohydrate Substances in the Cereal Starches,'*J. Amer. Chem. Soc.*, **64,** 2954 (1942).

56. P.L. Russell, 'A Kinetic Study of Bread Staling by Differential Scanning Calorimetry: The Effect of Painting Loaves with Ethanol,'*Starch/Starke*, **35,** 277 (1983).

57. P. Colonna, J. Tayeb and C. Mercier, 'Chapter 9: Extrusion Cooking of Starch and Starchy Products', in *Extrusion Cooking*, C. Mercier, P. Linko and J.M. Harper, Eds. 1989, American Association of Cereal Chemists, Inc.: St. Paul, MN. p. 247.

58. C. Mercier, R. Charbonniere, Grebaut and J.F. Gueriviere, 'Formation of Amylose-Lipid Complexes by Twin-Screw Extrusion Cooking of Manioc Starch,'*Cereal Chemistry*, **57,** 4 (1980).

59. M. Ahmed and J. Lelievre, 'Effect of Various Drying Procedures on the Crystallinity of Starch Isolated from Wheat Grains,'*Starch/Starke*, **30,** 78 (1978).

60. J.R. Katz, *Baker's Weekly*, **81,** 34 (1934).

61. R.D. Dragsdorf and E. Varriano-Marston, *Cereal Chem.*, **57,** 310 (1980).

62. K.J. Zeleznak and R.C. Hoseney, 'Characterization of Starch from Bread Aged At Different Temperatures,'*Starch/Starke*, **39,** 231 (1987).

63. J. Longton and G.A. LeGrys, 'Differential Scanning Calorimetry Studies on the Crystallinity of Aging Wheat Starch Gels,'*Starch/Starke*, **33,** 410 (1981).

64. R.L. Shogren, 'Effect of Moisture Content on the Melting and Subsequent Physical Aging of Cornstarch,'*Carbohydrate Polymers*, **19,** 83 (1992).

65. R.L. Evangelista, Z.L. Nikolov, W. Sung, J.-L. Jane and R.J. Gelina, 'Effect of Compounding and Starch Modification on Properties of Starch-Filled Low-Density Polyethylene,'*Ind. Eng. Chem. Res.*, **30,** 1841 (1991).

66. R.P. Westhoff, F.H. Otey, C.L. Mehltretter and C.R. Russell, 'Starch-filled Polyvinyl Chloride Plastics: Preparation and Evaluation,'*Ind. Eng. Chem. Prod. Res. Dev.*, **13,** 123 (1974).

67. G.J.L. Griffen, 'Biodegradable Fillers in Thermoplastics,'*Adv. Chem. Ser.*, **134,** 156 (1974).

68. L. Engel, H. Kingele, G.W. Ehrenstein and H. Schaper, *An Atlas of Polymer Damage: Surface Examination by Scanning Electron Microscope.* 1981, Englewood Cliffs, NJ: Prentice-Hall, Inc.

69. P. Bernfield, 'Amylases, α and β,'*Methods in Enzymol.*, **1,** 149 (1955).

70. C. Bastioli. 'Mater-Bi: Properties and Biodegradability' in *Environmentally Degradable Polymers: Technical, Business, and Public Perspectives (August 13-15, 1991).* 1991. Chelmsford, MA.

71. S. Simmons, C.E. Weigand, R.J. Albalak, R.C. Armstrong and E.L. Thomas, 'Thermoplastic Processing of Starch: Melt Spinning of Starch-Based Fibers', in *Biodegradable Polymers and Packaging*, D.L. Kaplan, C. Ching and E.L. Thomas, Eds. 1993, Technomic Publishing Co.: Lancaster, PA. p. 171.

72. L. Reimer, 'Irradiation Changes in Organic and Inorganic Objects,'*Laboratory Investigation*, **14,** 344 (1965).

73. A.D. Evers, 'Chapter 4: Cereal Starches and Proteins', in *Food Microscopy*, J.G. Vaughan, Ed. 1979, Academic Press: New York. p. 139.

74. M.J. Miles, V.J. Morris, P.D. Orford and S.G. Ring, 'The Roles of Amylose and Amylopectin in the Gelation and Retrogradation of Starch,'*Carbohydrate Research*, **135,** 271 (1985).

75. M. Gudmundsson and A.C. Eliasson, 'Retrogradation of Amylopectin and the Effect of Amylose and Added Surfactants/Emulsifiers,'*Carbohydrate Polymers*, **13,** 295 (1990).

76. D.R. Paul and S. Newmann, eds. *Polymer Blends.* . Vol. 1. 1978, Academic Press, Inc.: New York.

77. F.M. Mirabella Jr., 'Phase Separation and the Kinetics of Phase Coarsening in Commercial Impact Polypropylene Copolymers,'*J. Poly. Sci. Pt. B Poly. Phys. Ed.*, **32,** 1205 (1994).

78. H.J. Cornell, 'The Effect of Amylopectin on the Properties of Starch Gels,'*Die Starke*, 43 (1963).

Table 3.3a. "S" Transition DSC Data: High Amylose Starch (Hylon VII) Blends

Blend	Starch:EVOH by weight	Water Content at 50% RH	DSC Cycle	Onset Temperature (°C)	Peak Temperature (°C)	Transition Enthalpy (J/g)	Normalized ΔH (J/g add)
HY100	100:0	5.8	Heat 1.	57.0	63.1	1.9	78.1
			Cool 1.	17.3	13.6	0.9	36.8
			Heat 2.	49.6	53.3	0.4	17.4
HY85	85:15	5.0	Heat 1.	43.9	49.3	1.0	46.5
			Cool 1.	34.6	29.7	1.1	50.7
			Heat 2.	34.5	38.4	0.7	33.2
HY70	70:30	5.9	Heat 1.	54.7	60.8	1.1	65.1
			Cool 1.	38.4	33.9	0.8	43.9
			Heat 2.	50.0	54.2	0.8	46.8
HY60	60:40	5.3	Heat 1.	50.8	59.7	1.4	92.7
			Cool 1.	36.2	32.6	1.3	86.1
			Heat 2.	50.0	54.4	0.7	45.0
HY50	50:50	5.7	Heat 1.	46.8	56.9	1.4	113.5
			Cool 1.	36.5	33.5	0.8	61.6
			Heat 2.	48.0	51.6	0.6	44.6
HY40	40:60	4.9	Heat 1.	51.6	59.8	1.3	124.7
			Cool 1.	38.6	35.1	0.8	82.4
			Heat 2.	51.2	54.6	0.4	34.4
HY30	30:70	4.4	Heat 1.	50.9	60.4	2.0	261.1
			Cool 1.	37.9	33.9	0.6	76.1
			Heat 2.	50.2	53.2	0.3	35.4
HY15	15:85	4.5	Heat 1.	51.9	59.7	1.6	475.5
			Cool 1.	40.5	36.7	0.5	140.9
			Heat 2.	50.9	53.7	0.2	47.0

Table 3.3b. "S" Transition DSC Data: Native Corn (NC) Starch Blends

Blend	Starch:EVOH by weight	Water Content at 50% RH	DSC Cycle	Onset Temperature (°C)	Peak Temperature (°C)	Transition Enthalpy (J/g)	Normalized ΔH (J/g add)
NC100	100:0	8.3	Heat 1.	60.3	65.7	2.9	118.2
			Cool 1.	22.9	19.3	0.7	29.4
			Heat 2.	51.9	56.6	1.5	60.1
NC85	85:15	6.4	Heat 1.	54.6	60.4	2.5	121.4
			Cool 1.	35.2	30.4	1.0	46.8
			Heat 2.	48.8	53.1	0.9	44.0
NC70	70:30	6.9	Heat 1.	56.1	61.8	1.6	93.1
			Cool 1.	37.8	33.6	0.8	49.3
			Heat 2.	49.7	54.3	0.6	36.0
NC60	60:40	6.9	Heat 1.	55.3	61.2	1.6	106.3
			Cool 1.	40.1	36.4	0.8	50.8
			Heat 2.	48.9	52.9	0.6	39.6
NC50	50:50	5.3	Heat 1.	52.0	57.4	1.6	130.7
			Cool 1.	35.0	31.8	0.6	51.1
			Heat 2.	47.5	51.4	0.6	47.1
NC40	40:60	5.3	Heat 1.	47.1	55.8	2.1	203.3
			Cool 1.	35.1	32.0	0.8	75.0
			Heat 2.	45.8	49.6	0.5	53.3
NC30	30:70	5.3	Heat 1.	51.3	58.1	1.8	227.7
			Cool 1.	36.2	32.9	0.6	72.9
			Heat 2.	47.4	51.5	0.3	37.7
NC15	15:85	5.1	Heat 1.	48.8	57.4	2.0	591.5
			Cool 1.	38.2	34.8	0.4	108.9
			Heat 2.	47.1	49.6	0.2	44.1

Table 3.3c. "S" Transition DSC Data: Waxy Maize (WM) Starch Blends

Blend	Starch:EVOH by weight	Water Content at 50% RH	DSC Cycle	Onset Temperature (°C)	Peak Temperature (°C)	Transition Enthalpy (J/g)	Normalized ΔH (J/g add)
WM100	100:0	7.7	Heat 1.	55.7	63.1	5.0	208.1
			Cool 1.	38.8	35.9	1.2	48.5
			Heat 2.	45.9	52.3	1.0	41.4
WM85	85:15	7.2	Heat 1.	55.0	68.3	4.6	219.6
			Cool 1.	39.5	37.0	1.1	52.5
			Heat 2.	50.3	53.2	1.5	72.6
WM70	70:30	6.9	Heat 1.	50.2	58.4	3.2	182.9
			Cool 1.	39.9	37.3	1.0	57.5
			Heat 2.	48.7	52.6	0.9	50.6
WM60	60:40	5.8	Heat 1.	52.8	59.6	2.6	232.7
			Cool 1.	39.8	37.6	0.9	78.7
			Heat 2.	48.3	52.1	1.1	94.9
WM50	50:50	5.5	Heat 1.	56.4	63.1	2.4	188.7
			Cool 1.	36.5	32.5	0.6	45.4
			Heat 2.	50.5	55.2	0.6	44.6
WM40	40:60	4.9	Heat 1.	51.0	61.2	1.6	157.9
			Cool 1.	40.4	37.4	0.7	65.1
			Heat 2.	51.2	54.0	0.4	37.5
WM30	30:70	4.8	Heat 1.	55.0	62.1	2.3	295.0
			Cool 1.	40.0	37.2	0.5	60.5
			Heat 2.	64.3	64.7	0.2	23.2
WM15	15:85	4.3	Heat 1.	49.9	59.6	1.5	451.4
			Cool 1.	41.3	38.0	0.4	109.2
			Heat 2.	52.0	54.1	0.2	50.2

Table 3.4a. Poly(ethylene-vinyl alcohol) Melting/Crystallization DSC Data: High Amylose Starch (Hylon VII) Blends

Blend	Starch:EVOH by weight	Water Content at 50% RH	DSC Cycle	Onset Temperature (°C)	Peak Temperature (°C)	Transition Enthalpy (J/g)	Normalized ΔH (J/g EVOH)
HY100	100:0	5.8	Heat 1.			-	
			Cool 1.			No transition	
			Heat 2.			-	
HY85	85:15	5.0	Heat 1.	113.4	118.1	0.9	7.1
			Cool 1.	98.4	87.8	2.3	18.7
			Heat 2.	105.1	132.6	2.5	20.4
HY70	70:30	5.9	Heat 1.	112.7	124.8	6.2	25.5
			Cool 1.	84.9	79.6	6.9	28.5
			Heat 2.	113.4	125.0	6.9	28.6
HY60	60:40	5.3	Heat 1.	115.3	128.5	14.8	45.6
			Cool 1.	88.0	82.8	13.6	42.0
			Heat 2.	115.0	127.6	14.2	43.7
HY50	50:50	5.7	Heat 1.	113.4	125.8	15.2	38.2
			Cool 1.	93.5	88.9	16.8	42.2
			Heat 2.	115.1	129.0	18.8	47.1
HY40	40:60	4.9	Heat 1.	116.6	129.1	16.5	33.3
			Cool 1.	108.2	102.0	20.9	42.2
			Heat 2.	128.1	140.9	20.9	42.2
HY30	30:70	4.4	Heat 1.	115.7	131.5	27.7	48.0
			Cool 1.	102.5	97.1	29.6	51.2
			Heat 2.	120.3	135.5	29.3	50.7
HY15	15:85	4.5	Heat 1.	114.6	131.8	39.4	55.6
			Cool 1.	99.4	93.2	34.1	48.1
			Heat 2.	114.2	130.5	36.8	51.9

Table 3.4b. Poly(ethylene-vinyl alcohol) Melting/Crystallization DSC Data: Native Corn (NC) Starch Blends

Blend	Starch:EVOH by weight	Water Content at 50% RH	DSC Cycle	Onset Temperature (°C)	Peak Temperature (°C)	Transition Enthalpy (J/g)	Normalized ΔH (J/g EVOH)
NC100	100:0	8.3	Heat 1.		-		
			Cool 1.		No transition		
			Heat 2.		-		
NC85	85:15	6.4	Heat 1.	123.8	129.8	1.9	16.0
			Cool 1.	115.0	107.8	5.1	42.3
			Heat 2.	139.6	146.8	4.2	34.5
NC70	70:30	6.9	Heat 1.	124.9	128.8	5.2	22.7
			Cool 1.	113.3	107.2	12.2	53.1
			Heat 2.	138.0	146.4	8.7	38.1
NC60	60:40	6.9	Heat 1.	119.7	126.9	10.4	32.0
			Cool 1.	105.2	99.8	16.6	51.0
			Heat 2.	128.5	137.5	13.8	42.5
NC50	50:50	5.3	Heat 1.	116.9	127.5	19.9	50.1
			Cool 1.	96.8	91.7	21.0	52.7
			Heat 2.	121.6	133.2	19.8	49.8
NC40	40:60	5.3	Heat 1.	115.7	127.8	24.2	49.1
			Cool 1.	91.1	85.4	22.7	46.0
			Heat 2.	114.9	127.3	27.2	55.2
NC30	30:70	5.3	Heat 1.	118.1	132.6	29.6	50.8
			Cool 1.	97.9	91.7	28.6	49.1
			Heat 2.	118.7	132.5	32.7	56.1
NC15	15:85	5.1	Heat 1.	118.1	135.2	34.7	49.0
			Cool 1.	103.6	97.8	35.0	49.6
			Heat 2.	116.2	131.5	39.5	55.9

Table 3.4c. Poly(ethylene-vinyl alcohol) Melting/Crystallization DSC Data:
Waxy Maize (WM) Starch Blends

Blend	Starch:EVOH by weight	Water Content at 50% RH	DSC Cycle	Onset Temperature (°C)	Peak Temperature (°C)	Transition Enthalpy (J/g)	Normalized ΔH (J/g EVOH)
WM100	100:0	7.7	Heat 1.		-		
			Cool 1.		No transition		
			Heat 2.		-		
WM85	85:15	7.2	Heat 1.	124.1	131.6	5.2	42.9
			Cool 1.	97.1	81.9	6.1	50.5
			Heat 2.	124.1	130.7	6.2	51.6
WM70	70:30	6.9	Heat 1.	124.8	132.5	6.9	28.8
			Cool 1.	96.0	89.8	12.2	51.2
			Heat 2.	124.4	132.2	12.3	51.4
WM60	60:40	5.8	Heat 1.	125.3	132.6	6.8	28.3
			Cool 1.	99.7	93.9	16.0	66.7
			Heat 2.	124.6	133.5	16.5	68.7
WM50	50:50	5.5	Heat 1.	128.1	137.6	10.7	26.4
			Cool 1.	119.8	110.4	26.7	65.8
			Heat 2.	144.2	154.6	23.4	57.6
WM40	40:60	4.9	Heat 1.	124.4	137.0	33.1	67.3
			Cool 1.	102.2	95.5	27.7	56.2
			Heat 2.	125.3	136.7	27.9	56.8
WM30	30:70	4.8	Heat 1.	122.2	136.6	30.7	52.1
			Cool 1.	101.6	95.1	31.1	52.9
			Heat 2.	123.3	136.0	34.9	59.4
WM15	15:85	4.3	Heat 1.	119.6	134.8	36.8	52.1
			Cool 1.	99.9	93.0	35.1	49.8
			Heat 2.	118.5	133.1	36.3	51.6

Table 3.4d. Poly(ethylene-vinyl alcohol) Melting/Crystallization DSC Data: EVOH/Glycerin Blend

Blend	Starch:EVOH by weight	Water Content at 50% RH	DSC Cycle	Onset Temperature (°C)	Peak Temperature (°C)	Transition Enthalpy (J/g)	Normalized ΔH (J/g EVOH)
EVOH/GLY	0:100	3.1	Heat 1.	121.7	140.4	46.9	56.3
			Cool 1.	106.8	99.3	44.5	53.4
			Heat 2.	118.8	137.2	54.4	65.3

Chapter 4

The Use of Transmission Electron Microscopy to Study the Blend Morphology of Starch/Poly(ethylene-vinyl alcohol) Thermoplastics

ABSTRACT

Transmission electron microscopy (TEM) is demonstrated to be a useful technique for examining the morphology of complex systems such as thermoplastic starch/poly(ethylene-vinyl alcohol) (EVOH) blends. Emphasis is placed on sample preparation, contrast mechanisms, staining, and specimen sensitivity to the electron beam in order to obtain optimum electron optical operating conditions for imaging these blend specimens in TEM. Both starch and EVOH were shown to be very beam sensitive: the maximum allowable beam dosages for the crystalline fraction of these components is estimated at less than 3×10^{-3} C/cm^2 and approximately 3.5×10^{-3} C/cm^2, respectively. Both polymers encountered significant mass-thickness variations which at moderate beam dosage ($> 6.0 \times 10^{-3}$ C/cm^2) led to contrast-reversal of the blend morphology. For the starch/EVOH blends, EVOH was observed to be the matrix component even at very high starch concentrations (up to 70%). Domain sizes of starch were observed to range from less than 0.1 μm to greater than 3 μm indicating that all of the starches were destructurized in the blends. Differences in the blend structure were also observed at similar starch compositions (50%) for three corn starch varieties. Blends containing amylose appeared to be partially miscible based on contrast differences between Waxy Maize (WM), Native Corn (NC), and high amylose Hylon VII (HY) starch blend series. Finally, cross-sectional TEM was demonstrated as a method of examining structural gradients in thermoplastically formed articles (e.g. a starch/EVOH melt-spun fiber).

INTRODUCTION

Key to understanding both the flow characteristics and physical properties of polymer blends is the determination of their blend morphology. Often a goal is to detemine number and volume fraction of certain phases at a given blend composition, gain information on the domain size, shape, and connectivity of these phases, and detect if and where crystallization and orientation in a blend are occuring. Transmission electron microscopy (TEM) can be an especially useful technique in attaining this information by allowing the experimenter to view sub-micron scale domains without removal of components, through the use of mass thickness, diffraction, and phase contrast mechanisms. Electron diffraction on selected areas in addition to dark field operation can be performed to examine crystalline regions. Also, cross-sectional TEM allows one to observe gradients in structure from the surface to interior regions of a bulk sample. Despite these advantages of transmission electron microscopy, obtaining meaningful and believable results often provides a challenge to the polymer morphologist due to the difficulty in obtaining thin specimens with sufficient contrast, overcoming the radiation sensitivity of the polymer samples, and in interpreting images taken under specific electron optical conditions [1]. In this chapter, we give details on the use of transmission electron microscopy to investigate the microstructure of blends consisting of thermoplastic starch and poly(ethylene-vinyl alcohol). Because of the difficulty in preparing microtomed samples, staining components preferentially, and imaging these systems in TEM, past use of this technique in examining thermoplastic starch-based blends has been quite limited.

Starch, processed thermoplastically, can be employed as a biodegradable alternative in certain polymer applications (e.g. disposable packaging, cups, utensils, composting bags, etc.). Thermoplastic starch refers to granular starch which has been 'destructurized' [2, 3] forming a mixture of its polymer constituents (amylose and

amylopectin) and the various proteins, lipids, and smaller molecules (such as water) that are also contained in the starch granule. To attain better processability and to increase the level of mechanical stability and moisture resistance to the final product, starch is often extrusion blended with another polymer component, in our particular case, with poly(ethylene-vinyl alcohol) (EVOH) and with plasticizers such as glycerin and water. The blend composition can be then tailored to yield the required flow and physical properties necessary for further thermoplastic processing such as injection molding, fiber spinning, or film blowing.

In Chapter 3, scanning electron microscopy (SEM) provided general information about the bulk phase structure in starch-EVOH blends in which accessible starch-rich phase domains had been removed. The extent of information achievable with SEM on these blends was quite limited due to the varied susceptibility of different starch types to the enzyme etchant. Also, the addition of an aqueous carrier for the etchant caused swelling and deformation of the blend as it was etched, likely changing the overall morphology. Others have used light microscopy to image starch-EVOH blends [4], however, the domain sizes observed were roughly the size of native starch granules (~10 to 25 μm).

TEM has been used to investigate the structure of granular starch, starch gels, and single crystals of amylose complexes. In the past, emphasis has been placed on investigating the structural components of native granules [5 - 8]. Because of the similarity of amylose and amylopectin in chemical composition and electron density, differentation between these components is not easily achieved in TEM (In fact, no differentiation between the two polymers in the microstructure of starch gels has been observed [9].) The internal structure of starch granules is revealed only through a complex and lengthy series of dehydrating, embedding, sectioning, chemical treating, and staining or shadowing steps which often produce artifacts that limits the interpretability of transmission electron micrographs [6]. Such structural development

studies examined the growth rings of various types of starches by methods such as staining with potassium permanganate, enzymatically treating with α-amylase, partially degrading by acid treatment (linterization), and/or shadowing with metals [10 - 13]. A study performed by Kassenbeck sucessfully revealed the fine structure of wheat and maize starches by using periodate, thiosemicarbazide, silver nitrate, and osmium tetroxide staining agents to distinguish the crystalline from non-crystalline regions in the starch granules [14, 15]. Kassenbeck established that amylose is essentially located in the nucleus of the granule and is surrounded by growth rings formed by amylopectin chains which undergo crystallization into alternating radial layers approximately 62 Å thick (i.e. the rasemose model). A summary of the extensive and varied specimen preparation techniques for studying the native starch granules by TEM is given by Gallant and Sterling [16] and Blanshard [17].

The often ambiguious results of these initial studies (attributed mostly to granule folding during sample preparation) were later overcome by an embedding and microtoming procedure developed by Chanzy [18]. Granule sections were observed under frozen hydrated conditions by TEM in diffraction mode [18]. Without staining, the locations of granules in TEM could only be determined through diffraction and comparision with an optical micrograph under cross polars of the same sample showing the 'Maltese-Cross' patterns indicating the presence of starch granules. The electron diffraction of these potato starch samples were typical of B type starch and exhibited fiber diffraction patterns for the central sections and strongly arced or continuous ring diagrams for noncentral or tangential sections of the granule [18]. Further electron diffraction studies have been performed by this group and others on single crystals of amylose [19, 20] and amylose acetate [21].

In this study, TEM is performed on biodegradable blend materials produced from the thermoplastic processing of starch in which the ordered granular structure has been partially or totally eliminated. We seek to image the microstructure that results

from extrusion blending, fiber spinning, film blowing, and injection molding, three varieties of corn starch (differing in amylose/amylopectin ratio) with another polymer, poly(ethylene-vinyl alcohol). Due to the moisture sensitivity of starch and the presence of plasticizers in the blend, special steps are taken during the microtoming and sample preparation process. Next, the beam sensitivity of both starch and EVOH is established and steps are taken to minimize damage of the sample as it is exposed to the electron beam. Contrast mechanisms, which include mass-thickness, diffraction and phase contrast, between starch and EVOH-rich domains are considered as well as the effect of partial blend miscibility on the observed structures. The choice of a selective stain to enhance contrast between the starch and poly(ethylene-vinyl alcohol) components, both of which are very similar in their chemical composition, is addressed. Structural changes which occur to the blends as they are imaged using the electron microscope are then established. Finally, having obtained a reliable method of preparing and then imaging starch/poly(ethylene-vinyl alcohol) blends, we present the blend morphology of the blends as a function of composition, compare the morphology of different starch varieties in blends with EVOH, and observe the blend structure that arises at the near surface region of a melt-spun starch/EVOH fiber.

EXPERIMENTAL

Materials

Amioca Waxy Maize (WM, 100% amylopectin), Melojel Native Corn starch (NC, 72% amylopectin), and Hylon VII (HY) a high-amylose starch, were obtained from National Starch and Chemical Co. (Bridgewater, NJ). Naturally occuring triglyceride additives were pre-mixed with the starch fraction in small amounts (3 wt% to the starch fraction) to aid in processing. Poly (ethylene-vinyl alcohol) (EVALCA E105A), containing 56 mol% vinyl alcohol groups, was supplied by EVALCA Co. (Lisle, IL). Glycerin (15% by weight of the total feed) was injected into the extruder

during processing. A limited amount of water was also added and removed during processing in order to reduce torque build-up in the extruder. Nomenclature of each blend is presented as "starch type: percent of starch" (i.e. NC30 refers to a blend containing a 30:70 ratio by weight of Melojel Native Corn starch to EVOH; see Chapter 3).

We sought to characterize these materials as polymer-polymer blends (i.e. starch-rich or EVOH-rich domains). However, given the complex nature of these materials (i.e. three polymer components which are each crystallizable, two plasticizers, and various small molecules), we must take into account the effect of plasticizers and various small molecule additives in addition to the likely presence of orientation from processing in analyzing the overall morphology. For this reason, blends containing only starch or only EVOH with plasticizer (vic. glycerin and water) were examined first to determine structural features observable in either polymer. Next, blends of starch with EVOH were examined.

Sample Preparation

Bulk polymer samples require microtoming into sections that are thin enough so that the electron beam can pass through the specimen thus forming an image in the TEM [22]. For polymer-polymer blends, the shape, size, and distribution of the polymer phases also define limits to the specimen thickness. Ideally, specimens should be thinner than the thickness of the phase domains one seeks to image and there should be no overlapping of domains in projection. Otherwise, only uncorrelated fluctuations in the observed projected images are detected and individual domains cannot be readily discerned (such as for the case of a large volume fraction (>30%) of randomly distributed domains which are small in comparison to the specimen thickness [23]).

Microtoming is usually performed at a temperature lower than the polymer glass transition temperature. For starch, Tg is a strong function of the relative humidity at

which it is stored and can range from below room temperature to greater than 200 °C [24]. For pure EVOH, Tg occurs at 55 °C. The presence of glycerin and water in the blends will serve to lower these transitions, and these small molecule components may partition unevenly between the polymeric components. An accurate determination of the glass transition temperatures for the blends via differential scanning calorimetry was difficult due to the low signal to noise of the Tg transition and the overlapping temperatures of multiple endothermic transitions for the blends [see Chapter 3]. A Reichert-Jung FC4E cryo-ultramicrotome was employed for preparing sections using a sample temperature setting of -20 to 15°C and a knife temperature from -20 to 0°C. Cutting temperatures were optimized with respect to the mechanical characteristics of each blend; usually, specimen and knife temperatures decreased as the EVOH level increased.

Samples were cut with a razor prior to placing them in the sample holder. A trapezoidal mesa (< 0.2 mm per side) was trimmed with the microtome using a glass knife following procedures detailed in the literature [25]. A 35° diamond (Diatome®) knife was used to cut sections using the microtome setting of 30 to 50 nm. Samples were carefully collected from the knife with an eyelash tool and deposited onto a droplet of ethanol placed on a either a 400 or 600 mesh copper grid (Ted Pella, Inc., Redding, CA). The grids were blotted on filter paper to remove any excess ethanol. It must be stressed that no water was used during the microtoming process to eliminate swelling of the starch fraction (ethanol showed no interaction with any of the starch blends). Grids containing sample sections were placed overnight in a dessicator containing 8 mesh anhydrous calcium sulfate (W. A. Hammond Drierite Co., Xenia, OH). Prior to viewing in TEM, certain sections were placed in a stainer containing elemental iodine (Mallinckrodt Specialty Chemicals) and exposed to iodine vapor for one hour to preferentially stain the amorphous starch-rich fraction. In addition, certain sections were coated with a thin layer of carbon (< 50 Å)using a Ladd vacuum

evaporator (Ladd Research Industries, Inc., Burlington, VT) to improve the electrical and thermal conductivity as well as the rigidity of the sections in the TEM.

Instrumentation

A JEOL 200 CX TEMSCAN electron microscope was employed at 100 to 200 keV to image the samples. The spherical aberration coefficient and focal length of the objective lens were 6.7 mm and 5.0 mm, respectively. Objective apertures of 20 and 40 μm diameters, corresponding to 0.10 and 0.17 $Å^{-1}$ cut off values in reciprocal space were most often employed. Because of the sensitivity of both starch and EVOH to the electron beam, samples were imaged using low dose techniques and employing a small condenser aperture (200 μm) and small spot size [1, 22, 26 - 28]. Images were obtained at relatively low magnification (5 to 10 kX) by first focusing on an area, translating to an adjacent area, and recording a 2 to 4 second exposure with Kodak SO-163 image plates.

Image Analysis

Selected negatives were digitized using a UMAX UC630 scanner with transparency attachment. Adobe Photoshop® was used for digitizing the images at 300 or 600 dpi over a range of gray scales from 0 to 255 (0 = black, 255 = white). Optical densities corresponding to measured gray scales were obtained through calibration of the scanner with a Kodak Q-14 Gray Scale (20 density steps at 0.1 density increments). Digitized images were saved as TIFF files which were imported into the NIH Image program (Version 1.35) for analysis of domain size and intensity. Intensity profile plots were determined from various micrographs to quantify image contrast and its dependence on microscope operating conditions and on beam damage.

RESULTS AND DISCUSSION

To characterize polymer blends, one seeks to apply morphological descriptors to the structures observed in transmission microscopy. These descriptors include the number of phases, volume fraction of each phase, and composition; the domain sizes, shapes, and connectivity; and whether or not crystallization or orientation occurs. Accurate determination of these descriptors requires both an understanding of the imaging mechanisms of the electron microscope and the particular changes the imaging process may have on the appearance of the structure of the sample.

The observation of a starch/poly(ethylene-vinyl alcohol) blend in the TEM is not as trivial as for a simple blend system, for example, a polystyrene/polybutadiene blend in which one primarily uses amplitude mass-thickness contrast to discern the relatively large (> 1 μm) unstained polystyrene domains from polybutadience domains heavily stained with osmium tetroxide. For this reason, we highlight the following issues involved in the imaging of starch/EVOH blends: 1) the beam sensitivity of both starch and poly(ethylene-vinyl alcohol), 2) the contrast mechanisms involved in discerning starch from EVOH domains, and 3) contrast changes as a function of electron beam exposure. These issues are important to the interpretation of blend morphology as a function of composition and starch-type. Finally, the usefulness of TEM as a technique to examine gradients in structure (i.e. a starch-based fiber) is presented.

Beam sensitivity of Starch and EVOH

Organic materials undergo radiation damage when exposed to the electron beam. The degree of damage is related to the total dose, D, the product of beam current density, j (amps/cm^2), and irradiation time, t [29]. For polymers, the main effects of radiation damage are cross-linking and chain scission. Both occurrances generally result in loss of mass through the volatilization of gases produced from these reactions

(e.g. H_2, CH_4, CO, CO_2, H_2O). The geometry of the sample and the cross-section of the electron beam in combination with the beam intensity will also cause changes in the specimen due to secondary thermal effects (e.g. loss of crystallinity, desorption of substances such as water, and decomposition) and charging effects with strong electric fields (e.g. specimen motion and curling of sections).

In order to understand the effect of beam damage on the starch/EVOH blends, TEM was performed on the HY100 and the EVOH/GLY blends. This initial study was performed to gain information about the crystalline nature of each blending component and the nature of beam damage. It should be noted that a starch/EVOH blend does not represent a superposition of the two pure components since different partitioning of plasticizers (i.e. glycerol, water) and some polymer-polymer mixing may occur. Figure 4.1a. depicts the morphology of unstained HY100 as imaged under low dose conditions using an estimated electron dose of approximately 9×10^{-4} C/cm^2. Figure 4.1b shows the influence of beam damage on the sample which has been exposed to the beam for an additional 20 seconds. With increasing electron dose, the HY100 shows significant dimensional changes including the enlargment of voids, mass loss, and the formation of a rippled texture. The lighter oblong areas, with major axes approximately 0.1 to 0.2 μm in size, which are observed in figure 4.1a, are barely visible in the beam damaged sample. The diffraction pattern for the HY100 blend was difficult to record due to both multiple scattering and the limited amount of crystallinity which will lower the extent of diffraction contrast attainable from this sample. Faint rings corresponding to a V-amylose complex were nevertheless visible providing evidence for crystallinity (see inset figure 4.1a). At the operating voltage of 200 keV, the electron beam lifetime of the V-amylose crystals in HY100 was estimated to be less than a quarter of that of stretch-oriented PE film (an accurate value was difficult to determine), and, therefore, the maximum allowable beam dosage for V-amylose crystals is estimated to be less

Figure 4.1. Bright field micrographs of the HY100 blend (Hylon VII high amylose starch compounded with glycerin and water). a) The morphology and electron diffraction pattern observed under low dose conditions (D ~ 9 x 10^{-4} C/cm^2). b) The same region after 20 seconds total exposure to the electron beam (D ~ 3.5 x 10^{-3} C/cm^2).

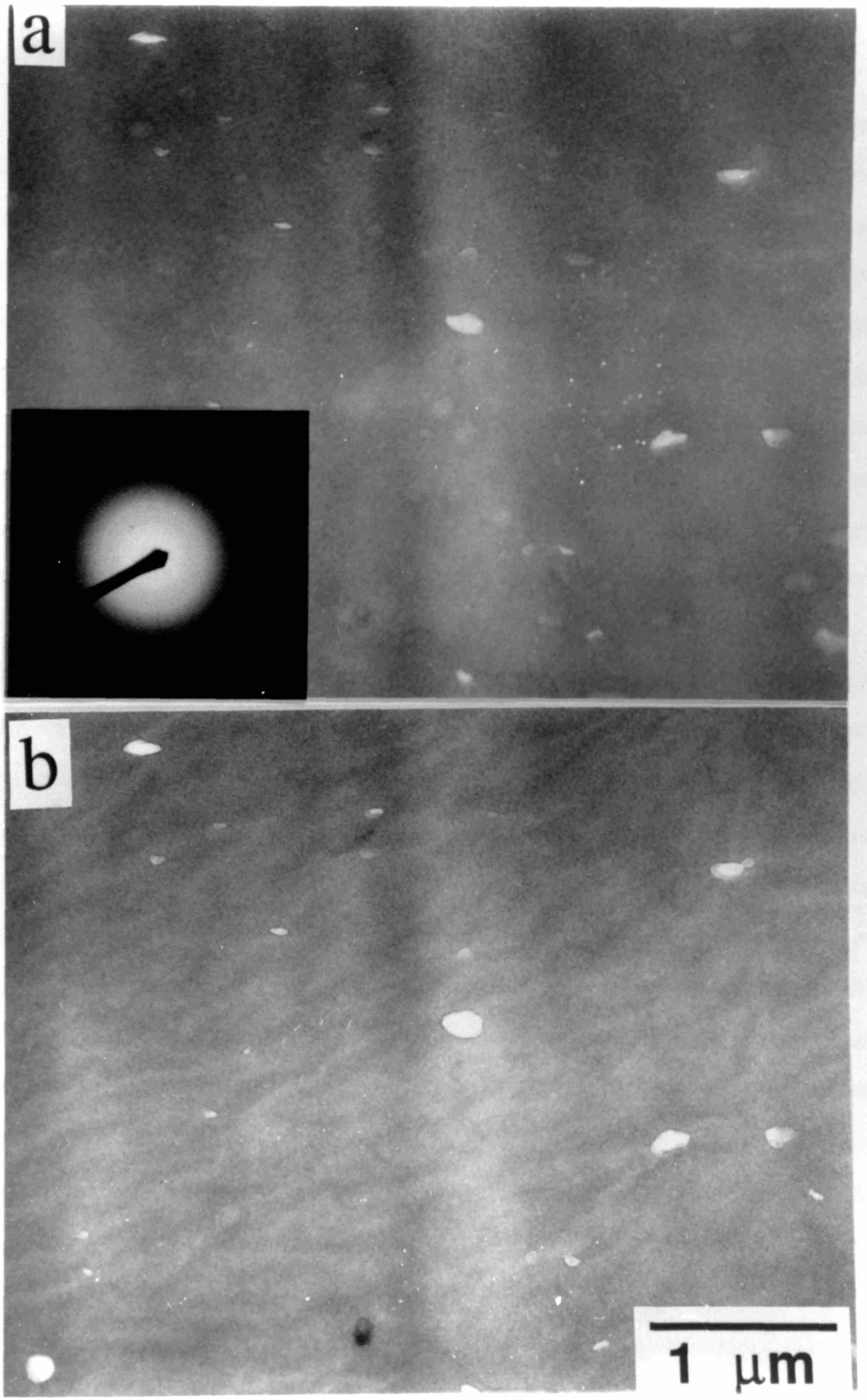
a
b
1 μm

than 3 x 10^{-3} C/cm^2 (based on the total end point dose for polyethylene crystals at 200 keV and 20°C).

A different beam damaged morphology was observed for EVOH (see figure 4.2). What initially appeared as a relatively homogenous material (figure 4.2a), the EVOH/GLY blend developed a mottled texture as the sample became damaged (figure 4.2b). The ring-like domains (~ 1 μm in size) which form may indicate the out of plane buckling of small EVOH spherulites due to beam effects [30]. A banded spherulitic texture as observed in more typical semi-crystalline polymers was not observed for the EVOH/GLY material. Crystallinity, however, was readily apparent in the diffraction pattern (see inset, figure 4.2a) and corresponds to data taken by x-ray diffraction [Chapter 3]. The crystal lifetime for EVOH containing 44 mol% vinyl content corresponded to a maximum allowable beam dosage of approximately 3.5 x 10^{-3} C/cm^2, which indicates that EVOH is slightly less radiation sensitive than starch.

The observed morphology of both starch and EVOH is thus highly dependent upon the amount of beam dose that each receives (i.e. both components are very sensitive to the electron beam). Studies by Reimer [29] showed that only 50% of the initial mass remained for starch and polyvinyl alcohol remained after long term electron irradiation at a current density of 0.3 x 10^{-6} amp/cm^2. (In other words, electron beam damages principally through chain scission and crosslinking and results in mass loss up to 50% via irradiation for starch.) Using a simple rule of mixtures, only 60% of the initial mass of EVOH containing 56% vinyl alcohol repeat units is expected to remain after exposure to the maximum allowable beam dose. For polyethylene, which retains 80% of its initial mass, mainly cross-linking occurs and mass loss is attributed to the formation of H_2 gas [29]. For polymers containing alcohol groups, chain scission at the -COH residue is favored and H_2, CO, and H_2O gases are formed [29]. Loss of crystallinity, cross-linking, and chain scission will result in both density and thickness variations in the polymers as they are imaged. The structural appearance of radiation

Figure 4.2. Bright field micrographs showing a microtomed section of the EVOH/GLY blend (EVOH compounded with Glycerin). a) The morphology and electron diffraction pattern observed under low dose conditions (D ~ 9 x 10^{-4} C/cm^2). b) The same region after 20 seconds total exposure to the electron beam (D ~ 3.5 x 10^{-3} C/cm^2).

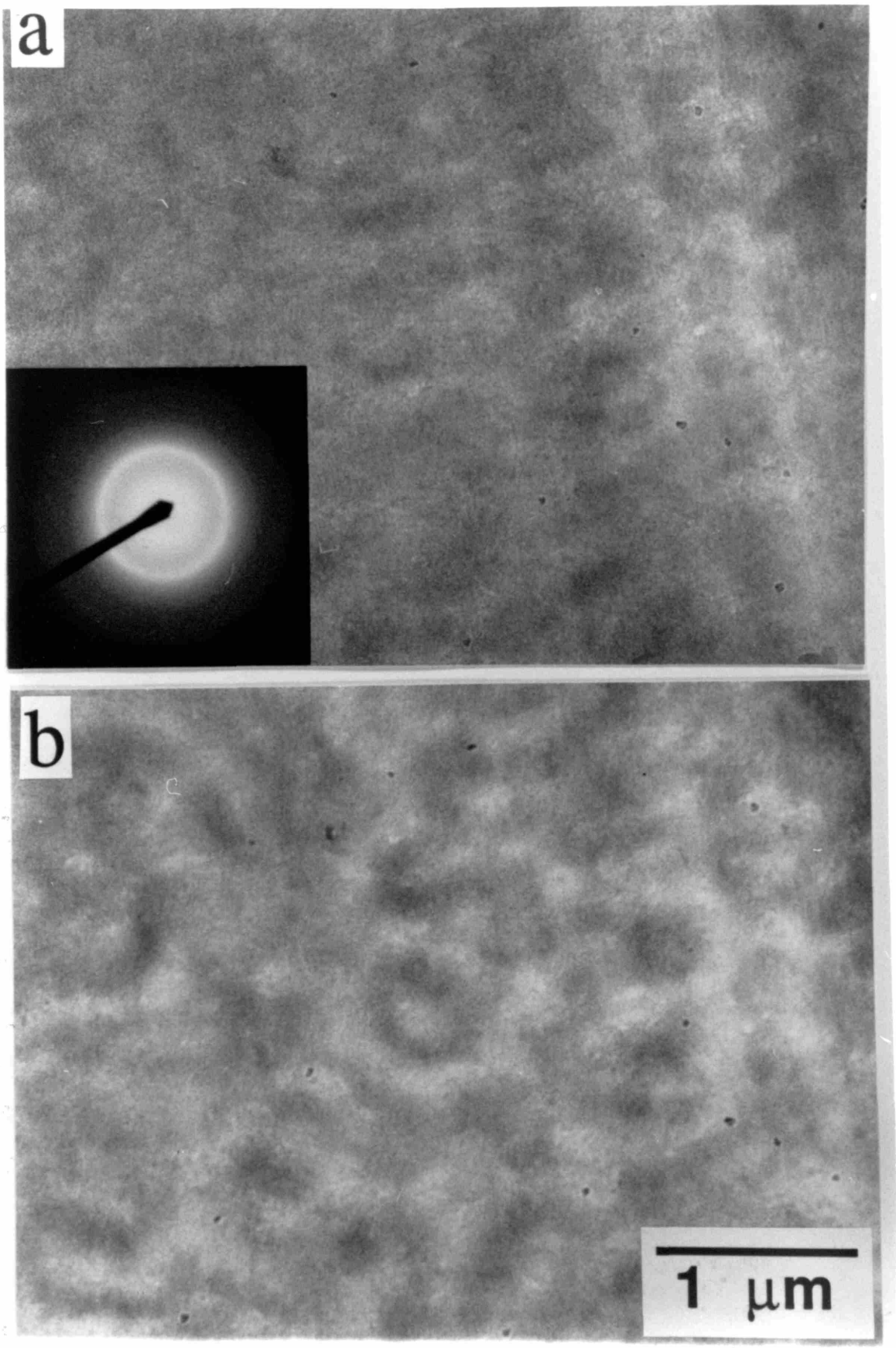
a
b
1 μm

sensitive polymer blends will change since the mass-thickness contrast between phase domains is altered during TEM imaging. For this reason, micrographs depicting the starch/EVOH blend morphologies were taken under low dose conditions (i.e. 5 to 10 kX magnification with minimum beam exposure, $< 1 \times 10^{-3}$ C/cm^2) by focusing on an area, then translating to a new area to take the exposure. In this way, structural changes to the specimen are minimized.

Contrast Mechanisms

Contrast arises in TEM due to spatial variations in the phase and amplitude of the specimen transmission function, $\Psi(\mathbf{r})$, as incident electrons interact with the sample. Details on the image formation and contrast mechanisms using TEM can be found in various references in the literature [22, 26, 31, 32]. In this section, we address contrast mechanisms and discuss the relevance of each type of contrast in interpreting TEM images of the starch/EVOH blends.

Amplitude contrast (mass-thickness or diffraction contrast) results from loss of electrons from the image by scattering outside of the objective aperture. For samples that scatter incoherently in bright field (i.e. no diffraction contrast), mass-thickness contrast arises from differences in the fraction of the incident beam intensity, I_o, which is collected by the objective aperture for different domains (which extend completely across the film thickness) of density, ρ, and thickness, t. This intensity, I, also depends on the optics through the choice of beam energy, E_o and objective aperture size, α; parameters which define the effective mass scattering cross-section, Sp. The value of I, at location i, is defined by:

$$I(E_o, \alpha)_i = I_o \, e^{-S_p(E_o,\alpha)\rho t_i} \qquad (4.1)$$

The level of contrast, C, in bright field mode, resulting from mass-thickness differences between two components at adjacent locations 1 and 2, can be expressed as (for $I_1 > I_2$):

$$C = \frac{I_1 - I_2}{I_1} = \frac{e^{-S_p\rho_1 t_1} - e^{-S_p\rho_2 t_2}}{e^{-S_p\rho_2 t_2}} \qquad (4.2)$$

For Sp of approximately 3.5 x 10^{-3} m^2/mg and a constant ($t_1 = t_2$) estimated thickness of 1000 Å, the initial contrast, C, between starch ($\rho \sim 1.45$ g/cm^3) and EVOH ($\rho \sim 1.15$ g/cm^3) is approximately 0.08 indicating that through mass-thickness differences, starch and EVOH-rich domains should be initially discernible. Image analysis performed on a near focus unstained NC30 blend (30% native corn starch/70% EVOH) yielded a value for contrast of 0.05 between unstained starch-rich and EVOH-rich domains. This lower value of contrast may indicate partial miscibility between the starch and EVOH fractions which would result from a decrease in density for the starch-rich domains and a density increase in the EVOH-rich areas. A quantification of the level of miscibility between the starch and EVOH fractions by using measured contrast values was considered but not achieved to due the effects of beam damage on the samples.

Diffraction contrast results from scattering outside the objective aperture by crystalline regions which are properly oriented for diffraction. Diffraction contrast is often used to map out the displacement fields, defects, or textures present in crystalline samples (e.g. see Chacko, Adams, and Thomas [33]). The diffracted intensity depends on the local deviations of the crystal lattice planes from the Bragg angle [22], as follows:

$$I(s) \cong |F(hkl)|^2 \frac{\sin^2 \pi s t}{\sin^2 \pi s} \qquad (4.3)$$

where F(hkl) is the structure factor for the (hkl) reflection and t is the crystal thickness. The diffracted intensity falls off to zero at less than one degree of misorientation (vic. as **s** becomes greater than or less than 0). Diffraction contrast occurs in regions where the Bragg condition is satisfied and, in bright field mode, these regions appear darker in the TEM image than areas where $\mathbf{s} \neq 0$, since $I = I_0 - I(\mathbf{s})$; when the objective aperture is set to collect electrons scattered under a certain Bragg condition (i.e. dark field mode), these areas appear bright. Because of the relatively low levels of crystallinity in the EVOH and starch materials and the rapid loss of crystallinity due to electron exposure, diffraction contrast is not a significant contrast mechanism for the starch-EVOH systems. Phase contrast depends on the phase shift of the transmitted wave which is a function of the electron microscope transfer function and the object function, $\Psi(\mathbf{r})$, of the specimen [23, 31, 32]. In bright field, image phase contrast can be represented by the the inverse Fourier transform of the product of the microscope transfer function, $A(\mathbf{K}) \sin \chi(\mathbf{K})$, and the Fourier transform of the specimen object function, $\Psi(\mathbf{r})$:

$$C_{phase} = \frac{I(\mathbf{r}) - I_{ave}}{I_{ave}} = F^{-1}[2\, A(\mathbf{K}) \sin \chi(\mathbf{K})\, F\psi(\mathbf{r})] \qquad (4.4)$$

The electron microscope transfer function, modulates object frequences in the image, where $A(\mathbf{K}) = 1$ /0 inside/outside the objective aperture and

$$\chi(\mathbf{K}) = \pi \lambda (\Delta Z)\, \mathbf{K}^2 + \frac{\pi}{2} C_s \lambda^3 \mathbf{K}^4 \qquad (4.5)$$

ΔZ and C_s are the defocus and spherical aberration coefficients of the objective lens.

$\Psi(\mathbf{r})$ is proportional to the product of the inner potential, $\phi(\mathbf{r})$, and the sample thickness:

$$\Psi(\mathbf{r}) = \frac{\pi}{\lambda V_o} t\, \bar{\phi}(\mathbf{r}) \qquad (4.6)$$

where λ is the wavelength of the electron, V_0 is the accelerating voltage, and t is the specimen thickness. The mean inner potential, $\bar{\phi}$, can be estimated from the sample density, ρ, and f_i, the electron-scattering factor at zero angle of the ith atom of the basic structural unit of molecular weight, M:

$$\bar{\phi} = 69 \frac{\rho}{M} \sum_i f_i \qquad (6)$$

Using values of $f_H(0) = 0.221$, $f_C(0) = 1.024$, $f_O(0) = 0.840$ in p-units [34], the mean inner potential was calculated to be roughly 7.2 - 7.3 volts for various types of starch (ρ ~ 1.45 - 1.47 g/cm^3, M = 161 g/mol) and 7.3 volts for EVOH (56 mol% VOH, ρ ~ 1.15 g/cm^3, M ~ 37 g/mol), respectively. This result indicates that one probably cannot discern between unstained starch and EVOH domains through phase contrast.

To illustrate the contrast mechansims occuring between starch and EVOH, a through focus series taken of a blend containing a native corn starch/EVOH ratio of 30:70 (NC30 blend) is shown in Figure 4.3. The minority component starch-rich domains appear dark in the micrograph against the lighter EVOH-rich matrix background. One should note that the near focus image (Figure 4.3b) was taken first at an exposure of 4 sec (~ 9.3 x 10^{-4} C/cm^2), and shows some evidence of beam damage as evident in the the texture which had developed in the matrix. Subsequent beam damage occurs for the underfocus and overfocus images so the level of contrast is changing between domains and figure 4.3 should only serve to illustrate the primary mechanisms of contrast. The near focus image shows definite contrast between darker, starch-rich domains, indicating that mass-thickness effects are primarily responsible for differences in the appearance of domains. The underfocus (ΔZ ~ -13.6 μm) and overfocus images (ΔZ ~ + 13.6 μm) provide finer details from the phase contrast which arises from non-zero values of the microscope transfer function; negative values of defocus adds to mass thickness contrast whereas positive values oppose mass-thickness

Figure 4.3. Through focus series of a NC30 microtomed section: a) $\Delta Z \sim -13.6$ μm, b) near focus, c) $\Delta Z \sim +13.6$ μm. Phase contrast arises as the microscope is defocused (a and c). Note that the sample undergoes beam damage as it was imaged (order of image taking and estimated total beam dosage: b) ~ 9×10^{-4} C/cm^2, a) ~ 1.9×10^{-3} C/cm^2, c) 2.8×10^{-3} C/cm^2).

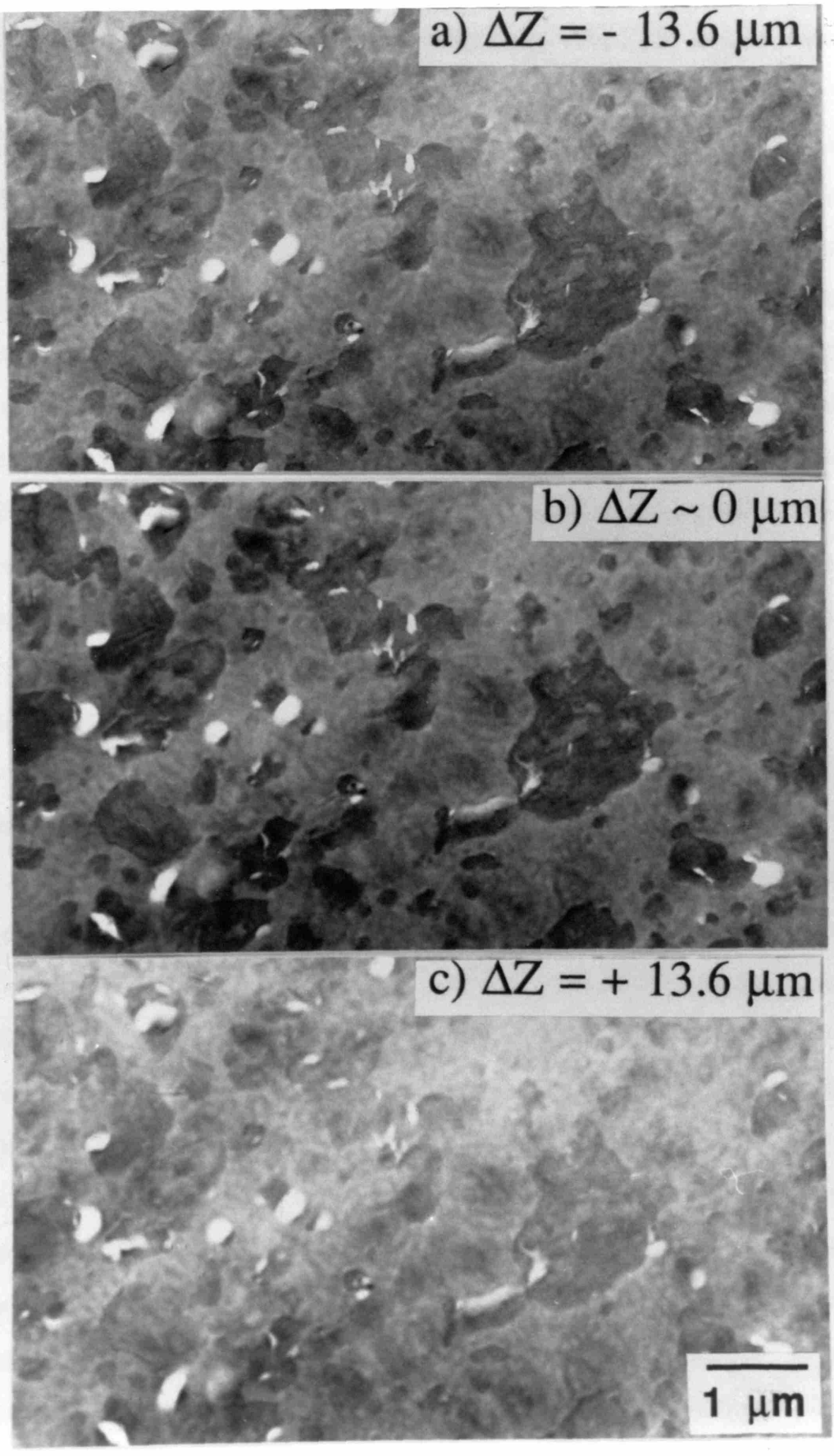
a) ΔZ = - 13.6 μm
b) ΔZ ~ 0 μm
c) ΔZ = + 13.6 μm
1 μm

contrast. Defocusing reveals microtome cutting lines, voids, and distinct domain boundaries to be more clearly discernible in figure 4.3a.

At low to medium resolution, amplitude contrast generally dominates the overall image contrast with phase contrast providing finer details when defocusing the microscope [26]. The spatial frequency of the NC30 sample is highly complex and starch-rich domains vary over the range from 0.1 to greater than 1 μm in size. Phase contrast may add definition to the observed image by highlighting differences that occur in the microtoming characteristics of each phase (at $\Delta Z \sim +/- 13600$, contrast is enhanced for lower frequency objects, $d > 0.08$ μm). Although the sample is semi-crystalline, the measured and calculated densities of amorphous and crystalline EVOH at a composition which contains 56 mol% VOH are very similar ~ 1.15 [35]. Similar densities for thermoplastic starch and V-amylose crystals are also reported (~ 1.4 g/cm^3 [36]). Finally, beam damage which affects specimen composition, density and thickness will influence values for the inner potential.

Staining of the Starch-rich Domains

To improve contrast between the starch and EVOH domains it is desirable to use a specific heavy metal stain (so as to increase the electron density of one phase). Since starch and EVOH have essentially the same chemical constituents (both contain C-O, O-H, C-H, and C-C groups), finding a stain which would distinguish between the two components in TEM provided a challenge. Stains considered were osmium tetroxide (OsO_4), ruthenium tetroxide (RuO_4), uranyl acetate (UA), ruthenium red (RR), and iodine. Of these stains, OsO_4 and UA are negative stains, concentrating into regions of high free volume. Neither of these stains have been shown to react with polysaccharide chains specifically. Uranyl acetate has been used in the past with some success in obtaining structural information through TEM of starch gels [37, 38] and starch and starch blend thin sections in which the granule has not been completely

destructurized [7, 39]. Previous work has shown that RR, although it seems a prime candidate for polysaccharide staining [40] has been shown to be unreactive with neutral polysaccharides [41]. Iodine is a positive stain for amylose and amylopectin, forming a complex within the helical starch polymer chains [42]. Samples were microtomed and stained with osmium tetroxide, ruthenium tetroxide, uranyl acetate, and ruthenium red, but no increased contrast between components was readily apparent. However, iodine was found to predominantly stain the starch-rich domains.

Iodine is known [43] to physically absorb into the amorphous regions of semi-crystalline polymers such as polyethylene. Iodine also forms chemical complexes by binding in linear sequences within the interiors of amylose, amylopectin, and poly(vinyl alcohol) helices [42, 44 - 51]. Generally, this complexing behavior occurs for starches that are not highly crystalline (i.e. already V-amylose complexed starches will not react with the iodine) [42]. Staining of the bulk extrudate (pellets) for 4 hours with iodine resulted in a color change from translucent yellow to dark violet for thermoplastic starch pellets and only a slight change from clear to light yellow for the neat EVOH blend (indicating little to no complex formation in this component). The different staining behavior provides a means for enhancing the mass thickness contrast between starch-rich and EVOH-rich regions in electron microscopy. Any physi-sorbed iodine will vaporize in the vacuum chamber of the electron microscope and in the electron beam due to sample heating[5]; complexed iodine will be less volatile, but as starch is irradiated it is likely that with the ensuing structural changes to the starch, the iodine stain will be lost. Again, low dose procedures are critical in obtaining useful information from TEM.

To confirm that the use of iodine promotes contrast between starch and EVOH, micrographs taken under similar conditions for unstained and stained NC30 sections were digitized and analyzed. For the unstained sample, the average contrast, C, was determined to be 0.05. For the stained sample, the average contrast increased to 0.11,

indicating that the iodine stain is preferential to the starch-rich domains. Intensity profiles of showing the effect of the iodine stain on the NC30 sample are shown in Figure 4.4. It should be noted that the iodine also penetrates the EVOH matrix, as evident in the overall shift to lower optical density of the negative, but it does not penetrate into the EVOH-rich matrix to the degree that it complexes with the starch.

Contrast Changes as a function of Beam Dosage

Given the results of the beam sensitivity study performed on the neat starch and EVOH materials, we next determined the effect of beam dose on the structure of starch-EVOH blends. In Figure 4.5, a series of micrographs of the NC30 blend (previously stained for one hour with iodine) are displayed as a function of time at a specific beam current density (~ 2.3 amps/cm^2). A line profile plot showing the changes in contrast as a function of beam dosage is shown in Figure 4.6.

Figure 4.5a depicts the initial structure of the NC30 blend at a defocus of ~ 13.6 μm taken at a magnification of 5 kX and exposure time 4 sec. (Note, contrast is artificially enhanced with the use of high contrast print paper.) The dark, starch-rich domains (less than 0.1 to 1.2 μm) are easily discernible against a gray background. Contrast calculated from intensity analyses is 0.11. Holes and thin regions appearing bright in the micrographs are present either adjacent to or within the starch-rich domains. These areas may be attributed to microvoiding within the blend due to foaming of plasticizer (mainly water) during the extrusion blending process. Cracks observed within the starch-rich domains may have occured during microtoming due to the brittle properties of the starch component. Microtome cutting lines are also visible. The matrix itself possesses a slightly mottled texture which could be due to the presence of small starch-rich domains which are less than the thickness of the film or due to initial beam damage to the EVOH component. The following set of micrographs seem to indicate that the latter scenario is valid.

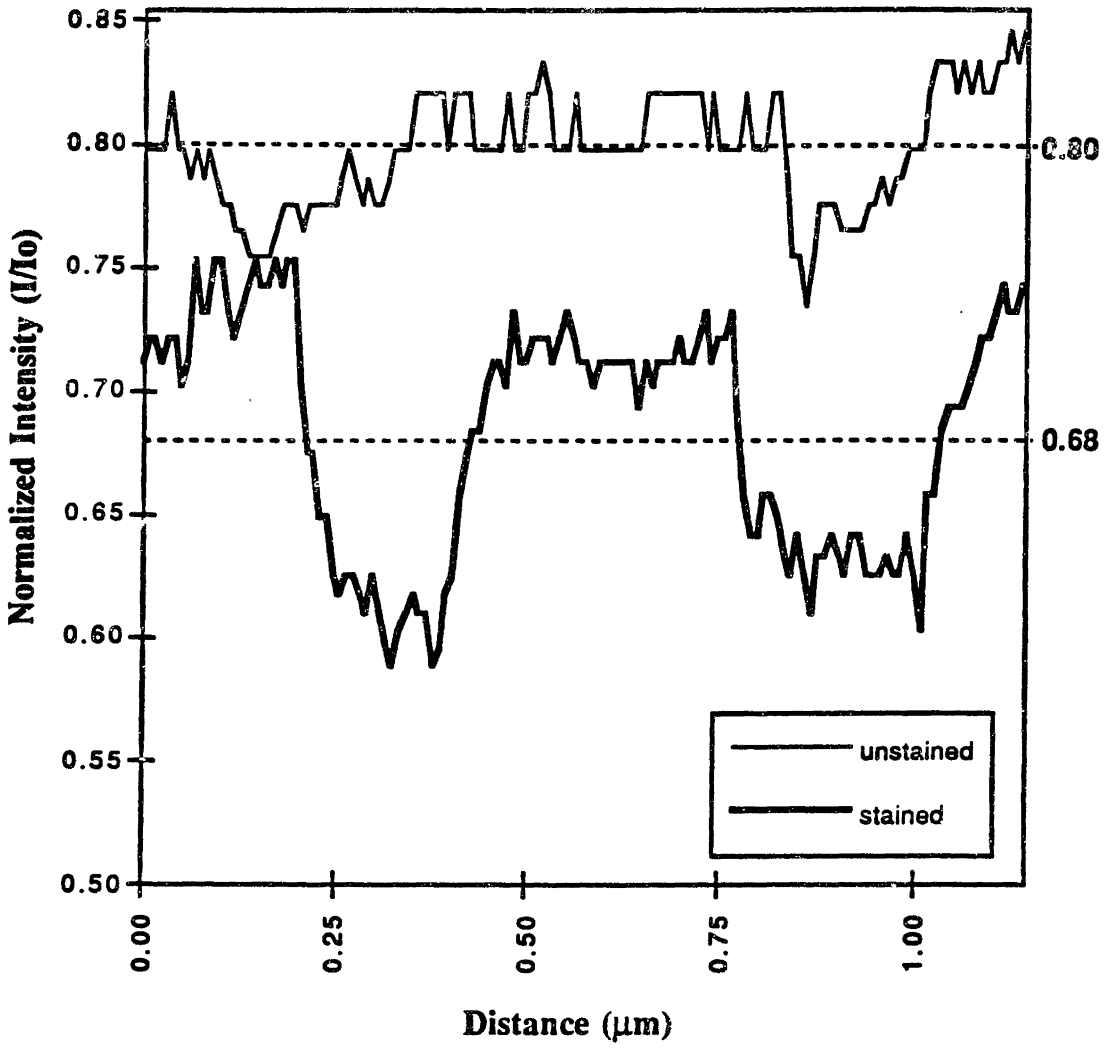

Figure 4.4. Comparison of intensity profiles obtained from micrographs taken under similar conditions (near focus, 10kX, 4 sec. exposure, e^- dose ~ 9 x 10^{-4} C/cm2) for an unstained and iodine stained section of an NC30 blend. Contrast between the starch-rich domains (appearing at lower intensities than the EVOH matrix) increases from 0.05 to 0.11. Note also that the average intensity of the image, the optical density of the micrograph negative, decreases as it is stained (Average values are shown by the dashed line and at the left of the graph.).

Figure 4.5. Bright field micrographs showing an iodine stained NC30 blend section as a function of time in the beam at a current density of approximately 2.3 x 10^{-4} amp/cm^2 (at 5 kX): a) Initial exposure, t = 4 sec, D ~ 9.3 x 10^{-4} C/cm^2; b) t = 34 sec, D ~ 7.9 x 10^{-3} C/cm^2; c) t = 94 sec, D ~ 2.2 x 10^{-2} C/cm^2; d) 184 sec., D ~ 4.3 x 10^{-2} C/cm^2. Microvoids are indicated by "MV", cracks in the starch-rich phase due to microtoming are indicated by "CR" in (a). Thinner areas are observed adjacent to the starch-rich domains and are most likely due to deformation at the starch-rich/EVOH-rich interface during microtoming. The line shown in (a) represents the region selected for intensity plots displayed in figure 4.6.

a
M
V
V
M
b
c
d
2 µm

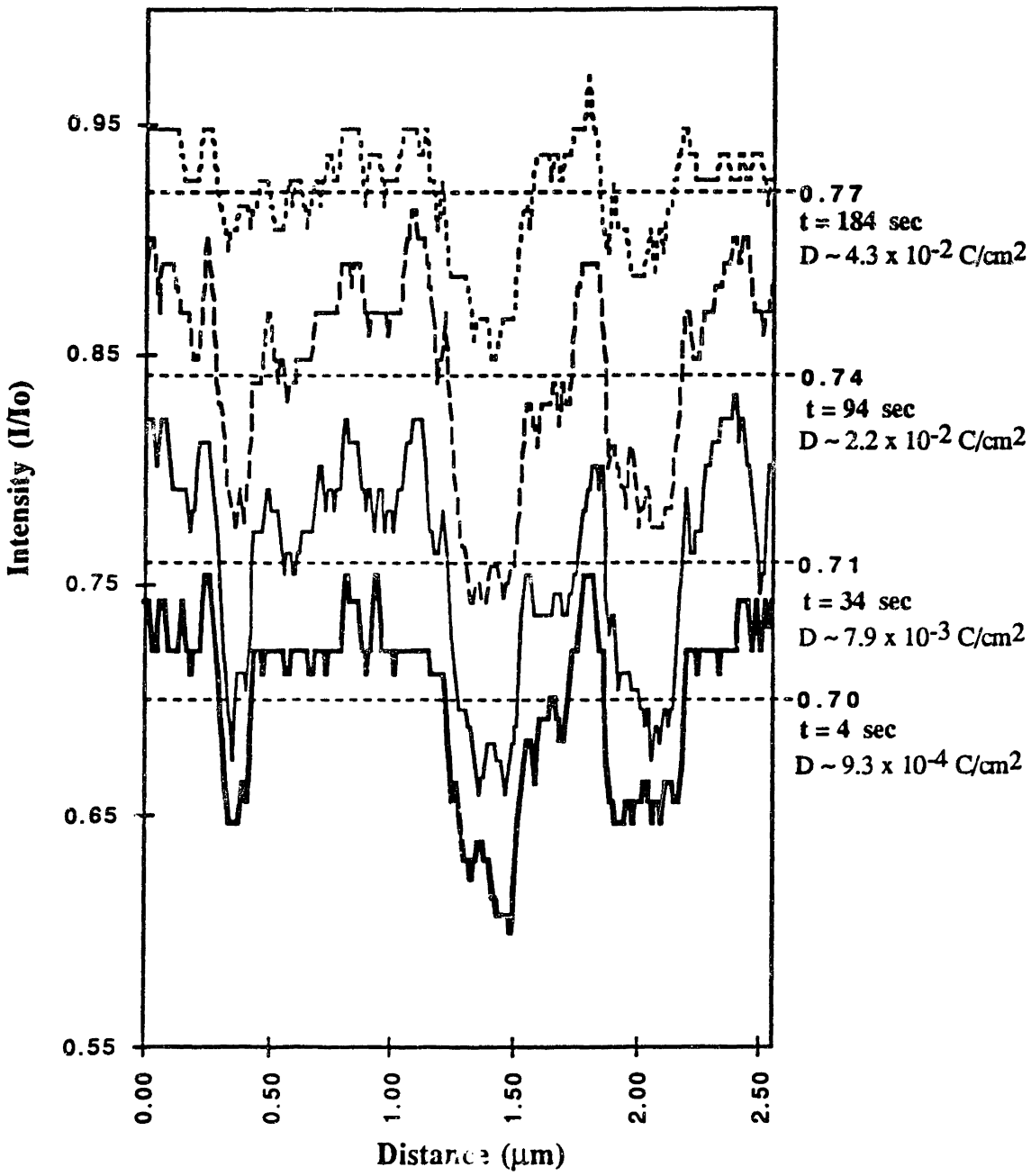

Figure 4.6. Intensity profiles of an iodine stained NC30 sample as a function of time in the electron beam at a current density of approximately 2.3 x 10^{-4} amp/cm^2 (at 5 kX). Plots are arbitrarily shifted along the y-axis to eliminate overlapping of profiles. Note, contrast between the starch-rich and EVOH-rich domains initially increases, then falls as the total beam dosage increases. Average normalized intensities (I/Io), total beam exposure time, t, and estimated beam dosage, D, are shown at the right of the figure.

As the section is irradiated it undergoes mass-loss such that the average measured intensity of the exposed film increases (i.e. I/I_0 -> 1). After 30 seconds beam exposure (figure 4.5b), the NC30 blend shows an increase in the mottling in the matrix and a loss of the light boundary surrounding the starch-rich domains. Overall the average contrast increases slightly (C = 0.14) which may be due to the loss of physi-sorbed iodine from amorphous areas of the EVOH-rich region. Figure 4.5c is similar to the above figure after 90 seconds of beam exposure although contrast between the starch and EVOH regions begins to decay (C = 0.12). After 180 second of beam exposure, contrast between these domains decreases to approximately 0.06 (figure 4.5d). As the starch-rich regions are irradiated, they undergo loss of crystallinity which would release the complexed iodine and change the mass-thickness contrast between the starch and EVOH-rich regions. Also visible in Figure 4.5d are alternating bands of light and dark gray in the EVOH-rich matrix. These bands (repeating ~ 140 nm) form as different regions in the EVOH-rich matrix are irradiated and are therefore probably not due to the presence of starch-rich domains.

If the microscope is operated at higher magnification, M_2, under the same beam intensity (i.e. such that the optical density of the exposed film is similar for a given fixed exposure time), the specimen dose increases by a factor of $(M_2/M_1)^2$ [26]. Figures 4.7 and 4.8 depict more dramatic contrast changes over a region of the NC30 for micrographs taken under similar conditions as in Figure 4.6, but at the higher magnification of 10 kX. As the sample experiences these moderate doses, the initial contrast measured as 0.08, reduces to zero after only one minute exposure. Increasing beam dosage results in an inversion of contrast that at 2 minutes is noticable (C = -0.03) and after 5 minutes the inverted level of contrast becomes similar to that of the initial image (C = -0.08). Imaging these starch-based systems under normal TEM conditions (or at higher magnifications) will cause this contrast-reversal to occur sooner and lead to a definite misinterpretation of the blend morphology. Knowing the changes in the

Figure 4.7. Bright field micrographs showing an iodine stained NC30 blend section as a function of time in the beam at a current density of approximately 2.3 x 10^{-4} amp/cm^2 (at 10 kX): a) Initial exposure, t = 4 sec, D ~ 3.7 x 10^{-3} C/cm^2; b) t = 64 sec, D ~ 6.0 x 10^{-3} C/cm^2; c) t = 124 sec, D ~ 1.1 x 10^{-1} C/cm^2; d) t = 304 sec, D ~ 2.8 x 10^{-1} C/cm^2. The line shown in (a) represents the region for intensity plots displayed in figure 4.8.

a
b
c
d
1 μm

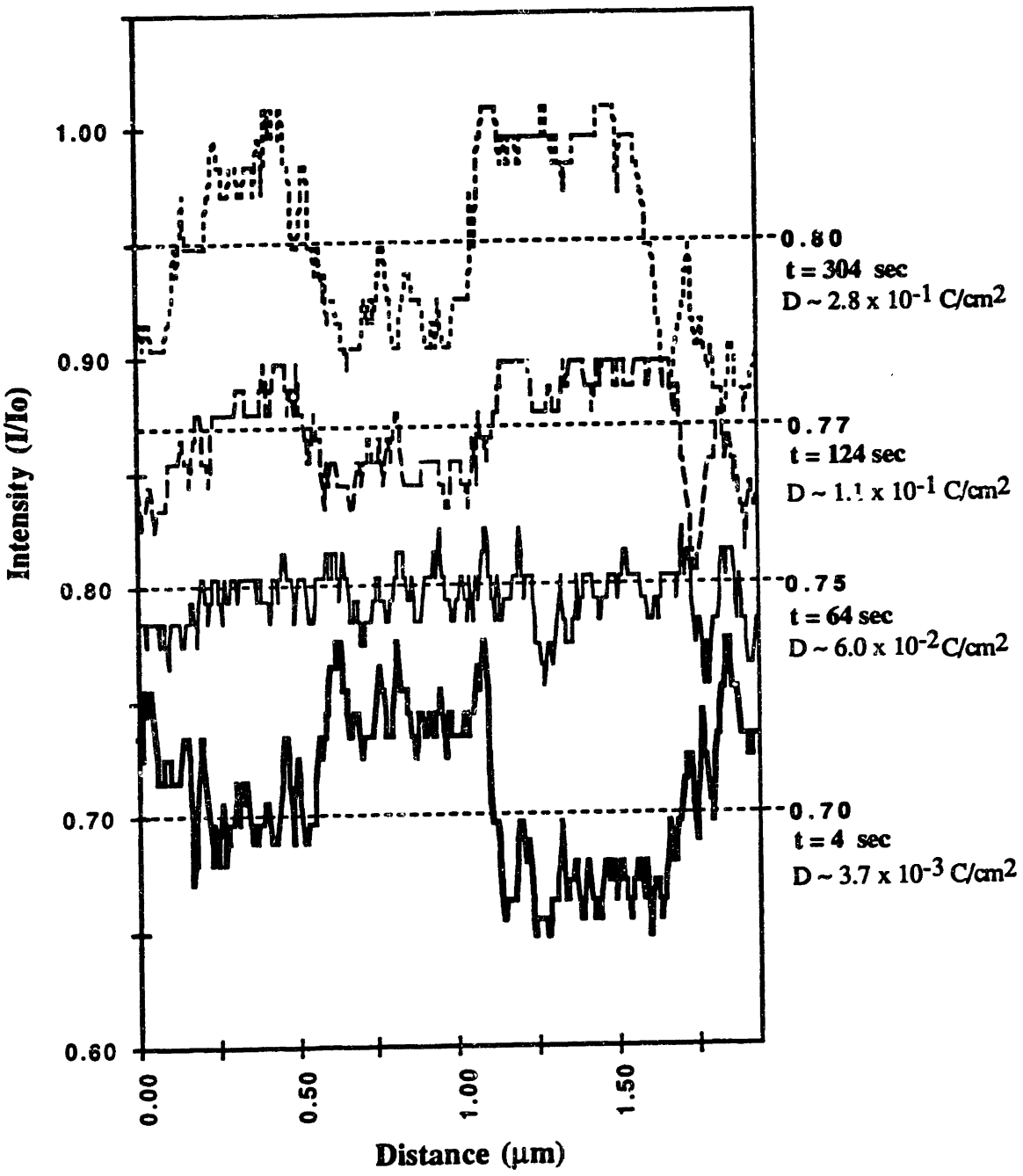

Figure 4.8. Intensity profiles of an iodine stained NC30 sample as a function of time in the electron beam under similar operating conditions as in Figure 4.6, but at higher magnification (at 10 kX). Plots are arbitrarily shifted along the y-axis to eliminate overlapping of profiles. Contrast decreases to zero then reverses as the specimen undergoes significant beam damage. Average normalized intensities (I/Io), total beam exposure time, t, and estimated beam dosage, D, are shown at the right of the figure.

structure that can occur in starch-EVOH blends as they interact with the electron beam, one should be cautious in interpreting results without understanding the electron-optical conditions at which they were imaged. After optimizing the electron optical conditions for the NC30 blend, we next employ TEM to observe the morphology of starch/EVOH blends comprised of various compositions and starch types.

Compositional Influence on the Morphology of NC Blends

The morphology of the native corn starch and EVOH blends (NC series) that forms following extrusion blending is shown in Figure 4.9. It should be noted that the blends were microtomed nearly perpendicular to the extrusion direction. The morphology shown in Figure 4.6a for the NC15 blend is similar to that observable in more typical phase-separated polymer blends (droplets in a matrix). The starch forms discrete domains which range in size from 0.2 to up to 3 μm in diameter in an EVOH-rich matrix. Increasing the starch composition to 30% relative to EVOH, results in the microstructure observed before for the NC30 blend. The size distribution of starch-rich domains is again varied but ranges from less than 0.1 μm to 1.2 μm. The discrete nature of the starch-rich domains is again visible in the NC50 material (and of the same size scale as the NC30 material) although now the area fraction of starch-rich domains is higher and the distance between any two domains is less than 0.5 μm (figure 4.6c). At a majority composition of the starch component (70% starch, 30% EVOH by weight), the NC70 blend begins to show a complex morphology. The intermaterial dividing surface between the starch-rich and EVOH-rich domains tends to have positive curvature towards the EVOH component at even up to 70% starch. This structure indicates that the EVOH component is well distributed throughout the blend and is still acting as a matrix component. In the larger dark areas, however, small (~ 0.25 μm) droplet-like gray inclusions, corresponding to EVOH-rich domains, are visible. This morphology can thus be described as discrete composite domains with starch as the

Figure 4.9. Bright field electron micrographs of representative Native Corn starch/EVOH blends which were stained with iodine: a) NC15, b) NC30, c) NC50, d) NC70, and e) NC85. EVOH appears to be the matrix component even at high compositions (up to 70%) starch. Total dose per image is estimated to be less than 1 x 10^{-3} C/cm^2.

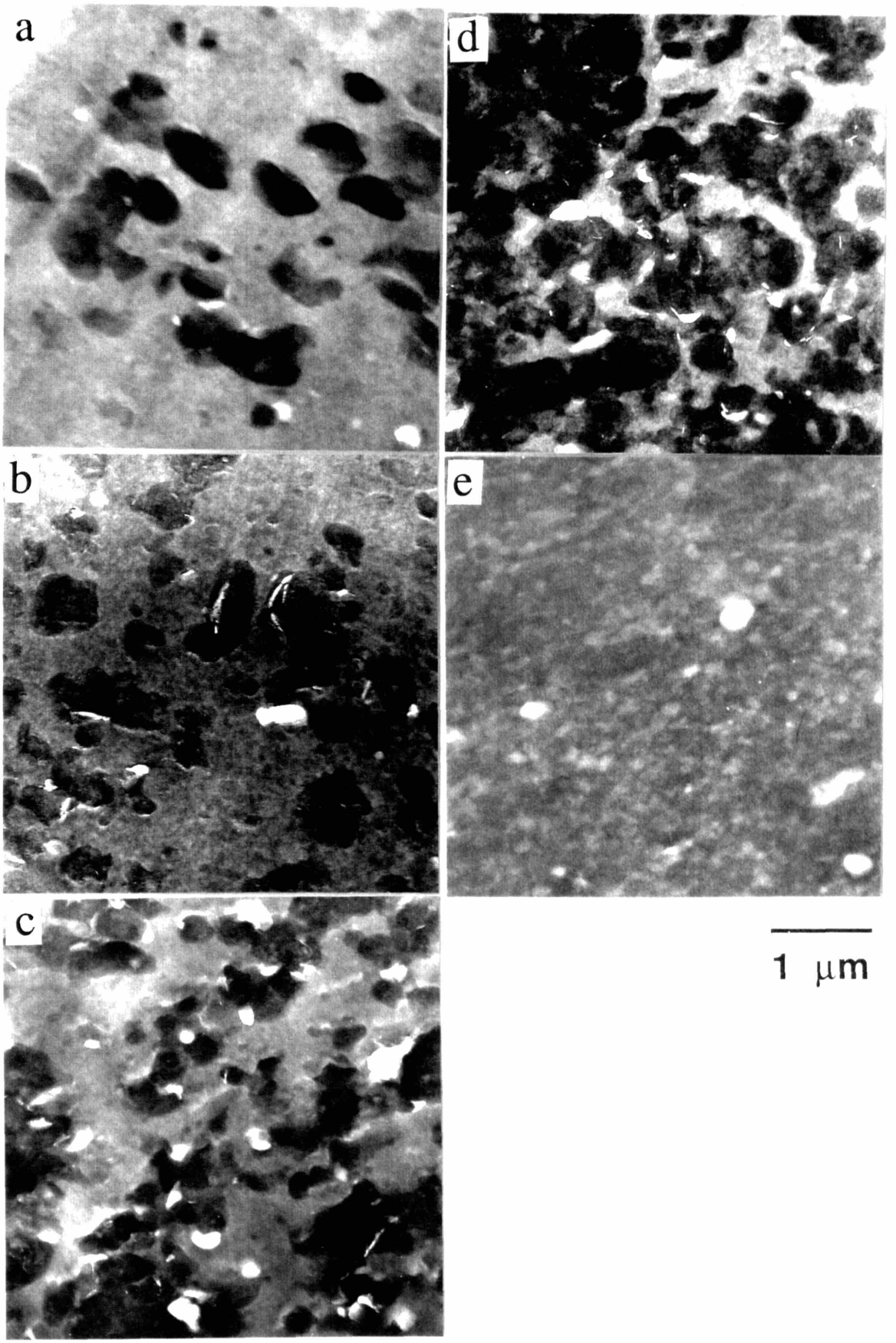
a
d
b
e
c
1 μm

majority component within a minority matrix phase of predominantly EVOH. Finally, as the starch content is increased even further (85 % starch to 15% EVOH), light gray regions less than 0.3 μm in width were observed to be uniformly distributed throughout the NC85 extrudate section. Dark gray domains approximately 0.2 to 0.5 μm were also observed. This system appeared to be phase separated, but the minority EVOH-rich component forms much smaller and well distributed domains within a mottled starch-rich matrix.

Comparison of Blend Morphologies for Different Starch Types with EVOH

Extrudate, in the form of pellets, was microtomed and observed in TEM to discern differences in the phase structure for blends of each starch type. Micrographs were taken of the 50% starch blends, since these are illustrative and provide easy visualization of both the starch and EVOH components. Figure 4.10 shows three distinct types of morphology for the three types of 50/50 starch/EVOH blends. As shown in Figure 4.10a, excellent contrast exists between the iodine-stained, starch-rich, dark phase, and EVOH-rich, light phase, regions for the Waxy Maize blend (WM50). At 50/50 composition, the EVOH is a continuous phase, starch is discrete. Oriented droplets ranging from 0.05 μm to approximately 5 μm in length were visible with L/D values averaging 1.8 +/- 0.5 (smallest droplets are least oriented, as expected). Irregularities in droplet shape and the fact that these droplets exhibited some preferred orientation indicates that optimum blending between the two polymer components has not been achieved during the extrusion process [52]. Smaller light phase domains appear within the darker regions indicating the formation of composite droplets. Overall, a very complex phase separated structure reminicent of an incompletely mixed incompatible polymers was observed for the WM50 blend [52].

The morphology of the NC50 blend extrudate appears quite different (see Figure 4.10b). Dark, ellipsoidally-shaped domains with major axes of approximately

Figure 4.10. Bright field electron micrographs showing the effect of starch type on the blend morphology for 50:50 starch/EVOH compositions: a) Waxy Maize (WM50), b) Native Corn (NC50), and c) Hylon VII (HY50) blends. As the amylose content of the starch component increases, the starch-rich domain sizes decrease and contrast between starch-rich and EVOH-rich regions decrease.

a
b
c
1 μm

0.05 μm to 1.2 μm were distributed within a lighter matrix. Unlike in the WM50 blend, no composite droplets were observed. The EVOH-rich, lighter area, appeared continuous throughout the sections indicating that this component (or a mixture of mostly EVOH and some of the starch fraction) forms the matrix. Starch-rich domains were visible as discrete domains within this matrix. Although the densities of the waxy maize and native corn starches are similar, the contrast between the starch-rich domains and the blend matrix is lower. This fact may indicated that the the amylose fraction in the Native Corn starch may be partially miscible with the EVOH fraction.

Finally, the HY50 blend exhibits a finer dispersion of smaller starch-rich domains distributed throughout a gray matrix (figure 4.10c). Domain sizes are less than 0.25 μm; however, an accurate determination of domain sizes is difficult due to the number the small and finely dispersed domains. Significant microvoiding is also observed in this material. Overall, HY blends are more difficult to visualize due to the lower initial contrast level between the starch-rich and EVOH-rich domains which quickly fades as the sample is observed in TEM. Since densities of the three starch types are similar (1.45 - 1.47 g/cm^3), mass-thickness contrast differences would yield lower initial contrast values for the HY blends than for the NC or WM blends if the amylose fraction were partialy miscible with EVOH.

Cross-sectional TEM of a Starch/EVOH Fiber

Besides being useful in determining the bulk morphology of the blends as compounded, TEM is useful in examining structural differences that might occur due to subsequent processing such as fiber spinning. A micrograph shown in figure 4.11 displays the near surface region of an NC50 melt spun monofilament [see Chapter 5]. The diameter of this fiber is 175 μm with a draw ratio of 20. After drying the filament in a dessicator for 24 hours, the fiber was embedded in epoxy, and microtomed perpendicular to the draw direction. Sections were then stained for one hour with

Figure 4.11. Bright field electron micrograph showing the near surface region of a Native Corn starch/EVOH fiber (NC50). The fiber was embedded in epoxy and stained with iodine vapor. The epoxy appears in the top of the micrograph. The EVOH component coats the fiber surface.

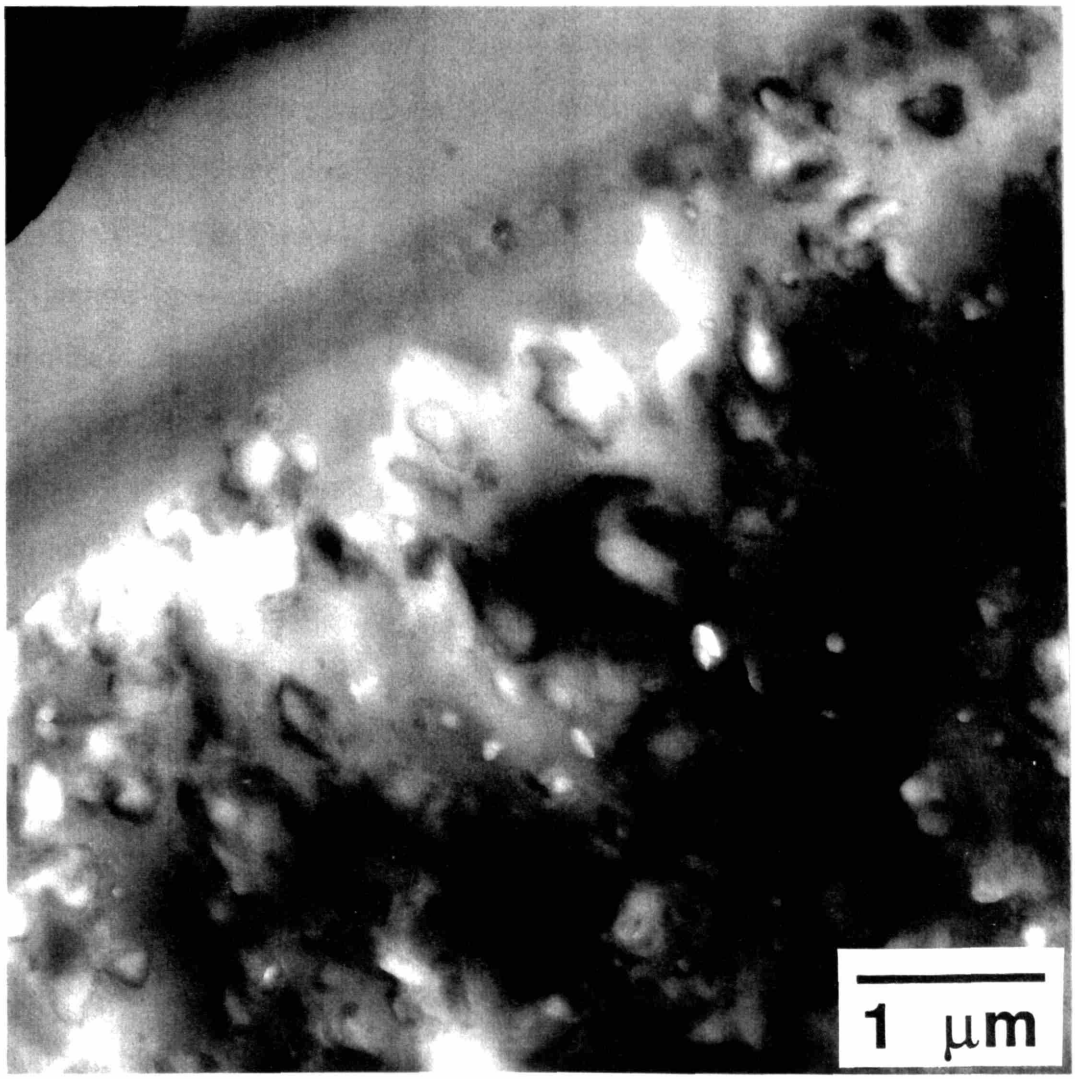
1 μm

iodine. The dark region appearing on the top left corner of the micrograph is the epoxy, a knife mark is visible as a diagonal line near the top edge of the fiber. A gradient structure is visible at the fiber surface as evident by the light band approximately 1 μm wide that traces the surface of the fiber, this light band becomes progressively darker as it approaches the interior of the fiber. This region is predominantly unstained EVOH. A number of inclusions ranging in size from less than 0.1 micron to approximately 0.5 μm are also visible in the micrograph which are starch-rich areas. The lightest areas evident in the micrograph correspond to microvoids.

The EVOH-rich surface layer on the fiber can be explained by considering the fiber spinning process. As the lower viscosity component in the melt, the EVOH fraction may adhere to the walls of the spinnerette capillary, coating the filament as it exits the spinnerette. When the fiber is drawn, EVOH is still present on the surface but a roughness develops due to the presence of the starch fractions which have a low elongational viscosity and limit the overall draw properties (and hence, final diameter) of the fiber. This surface morphology as observed by TEM is critical in interpreting biodegradability and transport properties since degradation and diffusion will be retarded at the EVOH-rich surface of the fiber.

CONCLUSIONS

Transmission electron microscopy (TEM) has been shown to be a useful technique in examining the morphology of complex systems such as thermoplastic starch/poly(ethylene-vinyl alcohol) (EVOH) blends. Before sucessful imaging and correct interpretation of micrographs can be achieved, however, one must understand the contrast mechanisms, beam sensitivity of the sample, and optimum electron optical operating conditions for imaging the specimen in TEM. First, a method of preparing a thin section is developed which does not produce artifacts in the blend morphology (e.g. water causes the starch fraction to swell). Next, the structural changes that occur

to the respective blend components as a function of beam dose and methods of limiting beam damage to the specimen are determined (usually by operating under low dose conditions). Maximum allowable beam dosage for reliable imaging of starch blends was less than 3 x 10^{-3} C/cm^2 and for EVOH, ~ 3.5 x 10^{-3} C/cm^2. An understanding of the contrast mechanism between components is then attained, and if necessary, a selective stain is chosen to improve mass-thickness contrast. Although a small amount of contrast was observed in the Native Corn starch/EVOH blend (C = 0.05), it was enhanced through the use of iodine to preferentially stain the starch fraction. In addition, possible contrast changes occuring between phase domains in the blendmust be evaluated as a function of beam dosage. For the starch/EVOH system, contrast was shown to initially increase then decrease as the sample was exposed to the electron beam. At moderate electron beam dosages greater than 6 x 10^{-3} C/cm^2, contrast reversal between the starch-rich and EVOH-rich regions was observed to occur. Image interpretations at high dosage without such detailed knowledge of the contrast mechanisms would lead to erroneous conclusions.

Once the difficulties encountered with imaging the specimen are overcome, TEM becomes very useful in determining blend morphology. For the starch/EVOH system, EVOH was observed to be the matrix component even at very high starch concentrations (up to 70%). The average size and distribution of domains was observed to change as the starch content was varied. Differences in the blend structure were also observed at similar starch compositions (50%) for three corn starch varieties. Blends containing amylose appeared to be at least partially miscible based on contrast differences between the WM, NC, and HY blend series. Microvoiding of plasticizer during the extrusion blending process was also evident at the periphery of starch-rich regions. Finally, cross-sectional TEM was demonstrated as a method of examining structural gradients in blends such as the presence of a 1 μm thick EVOH layer at the outer surface of a melt-spun starch/EVOH fiber.

REFERENCES

1. E.L. Thomas, 'Transmission Electron Microscopy of Polymers', in *Structure of Crystalline Polymers*, I.H. Hall, Ed. 1984, Elsevier Appl. Science Publishers, Ltd.: New York. p. 79.

2. G. Lay, J. Rehm, R.F. Stepto, M. Thoma, J.-P. Sachetto, D.J. Lentz and J. Silbiger, 'Polymer Composition Containing Destructurized Starch', in *United States Patent No. 5,095,054*, W.-L. Company, Ed. 1992.

3. C. Bastioli, R. Lombi, G. Del Tredici and I. Guanella, 'A Method for the Preparation of Destructurized Strach-based Compositions Produced Thereby', in *European Patent Application*, B. S.r.l., Ed. 1990.

4. P.A. Dell and W.G. Kohlman, 'Effects of Water Content on the Properties of Starch/Poly(ethylene-vinyl alcohol) Blends,'*Journal of Applied Polymer Science*, **52,** 353 (1994).

5. D.J. Gallant and C. Sterling, 'Electron Microscopy of Starch and Starch Products', in *Examination and Analysis of Starch and Starch Products*, J.A. Radley, Ed. 1975, Applied Sciences Publishers, Ltd.: London.

6. J.F. Chabot, J.E. Allen and L.F. Hood, 'Freeze-Etch Ultrastructure of Waxy Maize and Acid Hydrolyzed Waxy Maize Starch Granules,'*Journal of Food Science*, **43,** 727 (1978).

7. M. Yamaguchi, K. Kainuma and D. French, 'Electron Microscopic Observations of Waxy Maize Starch,'*J. of Ultrastructural Research*, **69,** 249 (1979).

8. A. Guilbot and C. Mercier, 'Starch', in *The Polysaccharides*, G.O. Aspinall, Ed. 1985, Academic Press, Inc.: New York.

9. K. Kanenega, A. Koreeda, A. Harada, K. Okuyama and T. Harada, 'Similarity of Electron Micrographs between Amylose and Amylopectin in Gelatinized Starch,'*Chemistry Express*, **12,** 781 (1989).

10. M.S. Buttrose, 'Submicroscopic Development and Structure of Starch Granules in Cereal Endosperms,'*J. Ultrastructural Research*, **4,** 241 (1960).

11. M.S. Buttrose, 'Electron Microscopy of Acid-Degraded Starch Granules,'*Die Starke*, **3,** 85 (1963).

12. R.I. Whistler and E.S. Turner, 'Fine Structure of Starch Granule Sections,'*J. Poly. Sci. (Letters)*, **18,** 153 (1955).

13. W.C. Mussulman and J.A. Wagoner, 'Electron Microscopy of Unmodified and Acid-Modified Corn Starches,'*Cereal Chemistry*, **45,** 162 (1968).

14. P. Kassenbeck, 'Electronenmikroskopischer Beitrag zur Kenntnis der Feinstrucktur der Weizenstarke,'*Die Starke*, **27,** 217 (1975).

15. P. Kassenbeck, 'Beitragzur Kenntnis der Verteilung von Amylose und Amylopectin in Starkekornern,'*Starch/Starke*, **30,** 40 (1978).

16. D. Gallant and A. Guilbot, 'Electron-Microscopical Studies on the Ultrastructure of Starch Granules by the Aid of New Preparation Methods,'*Starch/Starke*, **21,** 156 (1969).

17. J.M.V. Blanshard, 'Starch Granule Structure and Function: A Physiochemical Approach', in *Starch: Properties and Potential*, T. Galliard, Ed. 1987, John Wiley & Sons: New York.

18. H. Chanzy, R. Vuong and J.C. Jesior, 'An Electron Diffraction Study on Whole Granule of Linterized Potato Starch,'*Starch/Starke*, **42,** 377 (1990).

19. F.P. Booy, H. Chanzy and S. A., 'Electron Diffraction Study of Single Crystals of Amylose Complexed with n-Butanol,'*Biopolymers*, **18,** 2261 (1979).

20. E.L. Welland and A.M. Donald, 'Single Crystals of V-Amylose,'*Int. J. Biol. Macromol.*, **13,** 69 (1991).

21. R.M. Gohil and R.D. Patel, 'Morphology of Amylose Acetate: Role of Intercrystalline Linkages in Polymers,'*Die Starke*, **28,** 293 (1976).

22. E.L. Thomas, 'Electron Microscopy', in *Encyclopedia of Polymer Science and Engineering*. 1986, John Wiley and Sons, Inc.: New York. p. 644.

23. E.J. Roche and E.L. Thomas, 'Defocus Electron Microscopy of Multiphase Polymers: Use and Misuse,'*Polymer*, **22,** 333 (1981).

24. K.J. Zeleznak and R.C. Hoseney, 'The Glass Transition of Starch,'*Cereal Chemistry*, **64,** 121 (1987).

25. N. Reid and J.E. Beesley, *Sectioning and Cryosectioning for Electron Microscopy*. Practical Methods in Electron Microscopy, ed. A.M. Glauert. Vol. 13. 1991, New York: Elsevier Science Publ. B. V.

26. D.L. Misell, *Image Analysis, Enhancement and Interpretation*. Practical Methods in Electron Microscopy, ed. A.M. Glauert. Vol. 7. 1978, New York: North-Holland Publishing Company.

27. E.L. Thomas, 'Electron Microscopy of Radiation Sensitive Polymers', in *Developments in Electron Microscopy and Analysis*, J.A. Venables, Ed. 1975, Academic Press, Inc.: New York.

28. W.W. Adams, 'An Electron Microscopy and X-Ray Scattering Investigation of the Deformation Morphology of Solid State Extruded Fibers and Melt-Drawn films of Polyethylene', Ph.D. Dissertation, University of Massachusetts (1984).

29. L. Reimer, 'Irradiation Changes in Organic and Inorganic Objects,'*Laboratory Investigation*, **14,** 344 (1965).

30. A. Keller, 'Radiation Effects and Crystallinity in PE and Paraffins', in *Developments in Crystalline Polymers - I*, D.C. Bassett, Ed. 1982, Applied Sciences Publishers: Englewood, NJ. p. 37.

31. K. Hansen, *Advances in Optical and Electron Microscopy*, ed. R. Barer and V.E. Cosslett. Vol. 4. 1971, London: Academic Press.

32. H.P. Erickson, *Advances in Optical and Electron Microscopy*. Vol. 5. 1973, London: Academic Press.

33. V.P. Chacko, W.W. Adams and E.L. Thomas, 'Imaging of Polyethylene Films by Diffraction Contrast,'*Journal of Materials Science*, **18,** 1999 (1983).

34. B.K. Vainshtein, E. Feigl and J.A. Spink, eds. *Structure Analysis by Electron Diffraction.* . 1964, Pergamon Press: Oxford (UK).

35. T. Matsumoto, K. Nakamae, N. Ogoshi, M. Kawasoe and H. Oka, 'Vinyl Alcohol Copolymers,'*Kobunshi Kagaku*, **28,** 610 (1971).

36. A. Buleon, M.M. Delangli, J. Brisson and H. Chanzy, 'Single Crystals of V-Amylose Complexed with Isopropanol and Acetone,'*Int. J. Biol. Macromol.*, **12,** 25 (1990).

37. Y. Kanzawa, A. Koreeda, A. Harada and T. Harada, 'Electron Microscopy of the Gel-Forming Ability of Polysaccharide Food Additives,'*Agricultural Biological Chemistry*, **53,** 979 (1989).

38. K. Kanenaga, K. Kako, T. Harada, A. Koreeda, A. Harada and K. Okuyama, 'Different Behaviors Between Action of B-Subtilis α-amylase and 16% Sulfuric Acid at 32 °C to Stach Granules,'*Chemistry Express*, **4,** 519 (1989).

39. R. Dombrowksi, Personal Communication (1992).

40. E. Murano, S. Paoletti, A. Cesaro and R. Rizzo, 'Ruthenium Red Complexation with Ionic Polysaccharides in Dilute Aqueous Solutions: Chirooptical Evidence of Stereospecific Interaction,'*Analytical Biochemistry*, **187,** 120 (1990).

41. B. Reimann, 'Zur Verwendbarkeit von Rutheniumrot als elektronenmikroskopisches Kontrastierungsmittel,'*Mikroscopie*, **16,** 224 (1961).

42. W. Banks and C.T. Greenwood, *Starch and Its Components*. 1975, Edinburgh, England: Edinburgh University Press.

43. L.C. Sawyer and D.T. Grubb, *Polymer Microscopy*. 1987, New York: Chapman and Hall.

44. M. Noltemeyer and W. Saenger, 'X-ray Studies of Linear Polyiodide Chains in α-Cyclodextrin Channels and a Model for the Starch-Iodine Complex,'*Nature*, **259,** 629 (1976).

45. T. Hirai, M. Hirai, S. Hayashi and T. Ueki, 'Study of the Conformational Change of Amylose Induced by Complexation with Iodine Using Synchrotron X-ray Small-Angle Scattering,'*Macromolecules*, **25,** 6699 (1992).

46. M. Hirai, T. Hirai and T. Ueki, 'Effect of Branching of Amylopectin on Complexation with Iodine as Steric Hindrance,'*Polymer*, **35,** 2222 (1994).

47. H. Takamiya, Y. Tanahasi, T. Matsuyama, T. Tanigami, K. Yamaura and S. Matsuzawa, 'On the Poly(vinyl alcohol)-Iodine Complexes,'*Journal of Applied Polymer Science*, **50,** 1807 (1993).

48. Y.-S. Choi and K. Miyasaka, 'X-Ray Study on the Structure of the Poly(vinyl alcohol)-Iodine Complex,'*Polymer Journal*, **23,** 977 (1991).

49. Y.-S. Choi and K. Miyasaka, 'Structure of Poly(vinyl alcohol)-Iodine Complex Formed in the Amorphous Phase of Poly(vinyl alcohol) Films,'*Journal of Applied Polymer Science*, **48,** 313 (1993).

50. Y.-S. Choi and K. Miyasaka, 'Structure and Prooerteies of Poly(Vinyl Alcohol)-Iodine Complex Formed in the Cyrstal Phase of Poly(Vinyl Alcohol) Films,'*Journal of Applied Polymer Science*, **51,** 613 (1994).

51. T. Yokota and Y. Kimura, 'Iodine-Poly(vinyl alcohol) Interactions, 5) Realeasing Mechanism of I^- and I_2 in the Decomposition Process of the Blue Complex,'*Makromol. Chem.*, **194,** 295 (1993).

52. D.R. Paul and S. Newmann, eds. *Polymer Blends.* Vol. 1. 1978, Academic Press, Inc.: New York.

Chapter 5

Melt Fiber Spinning of Thermoplastic Blends of Starch and Poly(ethylene-vinyl alcohol)

ABSTRACT

The thermoplastic processability of corn starch and poly(ethylene-vinyl alcohol) (EVOH) blends by melt fiber spinning was investigated to understand the fundamental relationships between processing history, microstructure, and physical properties. The effect of composition and starch variety on both shear and elongational flow for these blends was of prime interest. Processability (i.e. spinnability) primarily depended upon the starch content in the blends and secondarily on starch type. Maximum spin draw ratios, λ_S, for these materials ranged from less than 1, for neat starch blends, to 215 for the EVOH/GLY control. Overall, blends containing 50% or more EVOH had sufficient elongational properties to consistently spin draw ($\lambda_S > 1$). Hylon VII blends formed consistent fibers at 30% starch content, but at compositions of 50% starch, no spinnability was observed. Waxy maize blends with as much as 70% starch had the ability to draw ($\lambda_S = 3$). Die swell increased with amylopectin content (reaching a value of 1.8 for the waxy maize/glycerol blend) and flow instabilities in the waxy maize blends were often observed. Overall, the native corn starch blends had the best processability in that fibers were attainable at up to 60% starch and extrudate flow from the spinnerette was observed to be relatively stable. Wide-angle x-ray studies showed that the EVOH component undergoes significant orientation, whereas the extensibility of the starch-rich domains is very low, especially for any crystalline fraction. Most of the elongational and mechanical properties of the blend fibers are attributable to the EVOH matrix component, and debonding of the EVOH matrix from the starch-rich domains is one route to failure in items made with starch/EVOH blends. Microscopic

investigations also revealed that the EVOH component coats the fiber surfaces, which are rough due to relatively undrawn starch-rich inclusions.

INTRODUCTION

The use of large quantities of starch in biodegradable applications requires that it be both processable and, as a load bearing component, possess acceptable mechanical properties. In previous studies, the injection molding capabilities as well as other physical properties for starch-synthetic polymer systems have been explored [1, 2]. In this study, we seek to further examine the processability and mechanical properties of the starch/EVOH blends by employing the model application of fiber spinning. In addition, the morphological analyses presented in Chapters 3 and 4 are extended to consider the effects of elongational flow on the blend structure.

Fiber spinning was chosen since it incorporates important process variables beyond those encountered in injection molding and extrusion. The elongational flow behavior ("drawability") of starch and starch blends is of key interest since these properties are critical to the largest market area of biodegradable polymers, packaging (i.e. films and thermoformed items). The orientation and crystallization of starch and its blends provide potential insight into film blowing applications where high orientation and possible crystallization under rapid deformation and cooling may occur. Fibers also provide an experimental basis for determining the upper bounds on the mechanical properties attainable with starch, since the microstructure is straightforward to manipulate via systematic changes of fiber process variables (spin draw ratio, cold draw ratio, etc.). Finally, rapid conditioning at various relative humidities and investigation of surface dependent properties such as biodegradability and dissolution testing should be facilitated due to the high surface area to volume ratio of fibers.

Amylose and amylopectin, the major components of starch, are not typical thermoplastic polymers; they can only be thermoplastically processed under controlled

high pressure, temperature, and moisture conditions. These polymers are highly sensitive to molecular degradation during processing due to their low thermal conductivity and high viscosity, which require high mechanical energy input through shear and pressure to cause them to flow [3]. During the extrusion of starch, an irreversible phase transformation from the native semicrystalline granular structure to an amorphous melt phase occurs. Interaction of lipids and other fatty acids with the amylose fraction also occurs during processing causing a semi-crystalline V-complex to form upon cooling. This "destructurized" starch generally possesses unstable product properties due to moisture uptake and loss. As early as 1944, Whistler [4] pointed out that starch possesses poor film and fiber-forming characteristics due to the presence of the branched amylopectin fraction, which, in native corn starch, composes approximately 70% of the starch granule [5]. The presence of incompletely destructurized granules (in films cast from solution) has also been found to produce localized stresses which lead to a weakened film structure [6].

Thermoplastic blends of destructurized starch, a synthetic polymer, and low volatility plasticizers have been found to possess the fluidity and thermal stability necessary to form consistently drawn fibers, although the degree of biodegradability may be lessened depending on the choice of synthetic polymer [7, 8]. In addition, the solid state properties of starch-based blends will be strongly influenced by their composition. Previous studies have shown that the linear amylose fraction of starch yields stronger and more flexible films than does the branched amylopectin fraction [9], and that there is a nonlinear, positive correlation between tensile strength and amylose content [6]. It has also been determined that the water binding capacity of starch decreases with increased amylose content, possibly due to the increased hydrogen bonding between and within amylose chains which reduces the number of hydroxyl groups available to water [10]. Thus, mechanical stability over a range of humidities should exist for high amylose starch blends. Finally, films prepared from acid-modified

and oxidized starches display a modest (approximately 20%) improvement in tensile strength at high humidities (65%RH) from that achieved by unmodified starches [6].

To date, relatively few studies have been performed on the thermoplastic processing of starch and starch blends, especially in terms of understanding the influence of flow, cooling rate, and molecular orientation. In particular, very few studies have been published on fiber spinning characteristics [7, 11, 12]. In order to draw a consistent fiber consisting solely of starch (or amylose), chemical modification is required. In the 1940s, early research showed the possibilities of producing oriented filaments and solution-cast films of starch fractions converted to acetates [13 - 15]. Mechanical properties were evaluated for industrial applications [4], although no wide-range commercial use of unsupported starch films developed. From the 1940s to the 1970s, focus was placed on the organization within the native granule. For x-ray studies of the basic packing in the crystalline state, oriented filaments were produced from starch esters. These were subsequently deacetylated, forming amylose fibers for crystallographic study [16 - 20]. In the 1960s, other studies [6, 21 - 23], concentrated on determining how starch variety, degree of granular modification, polymer and plasticizer additives, and humidity affect the tensile strength and ultimate elongation of starch and starch-based films cast from aqueous solution. An ongoing effort, which started during the 1970s at the United States Department of Agriculture's Northern Regional Research Laboratory, has focused on producing starch-based biodegradable plastics for agricultural mulch and other disposable applications [9, 24 - 29]. Molded and blown films were made from aqueous dispersions or grafts of starch and such polymers as poly(ethylene-co-acrylic acid), poly(vinyl alcohol), and poly(vinyl chloride). Recent environmental awareness and legislation during the 1980s and 1990s has produced an increased effort in developing biodegradable materials to replace classical non-degradable polymers for certain products which resulted in the commercial production of "biodegradable" starch-based resins by companies such as

Warner-Lambert and Novamont [30].

The melt processability, spinnability, and final solid state structural and physical properties of model thermoplastic, starch-poly(ethylene-vinyl alcohol) blends were evaluated in this study. Different blends were spun at two different moisture levels in the pellets: 1) as stored and 2) as conditioned in a 50% relative humidity (RH) chamber. Certain fibers were analyzed with wide-angle x-ray scattering (WAXS), scanning electron microscopy (SEM), and transmission electron microscopy (TEM) to understand the morphological characteristics of the as-spun and cold-drawn fibers. Finally, mechanical testing of the fibers "as spun" and after conditioning back to 50% RH levels was performed. Tensile properties were evaluated in terms of blend composition and processing history for each sample.

FIBER SPINNING

Fiber spinning is a structuring process in which a polymer fluid is forced through a spinnerette to form an extrudate which then undergoes simultaneous melt stretching, cooling, and solid-state drawing to form an anisotropic fiber of much smaller diameter. Fibers can be spun from the melt (melt spinning) or from solution (dry or wet spinning). In this study, melt spinning is considered; a schematic of this process is shown in Figure 5.1. A polymer is heated to its molten state and extruded through a spinnerette at a specified temperature, T_o, and velocity, v_o. The spinnerette is essentially a small capillary with a length to diameter ratio, l_o/d_o, of less than 5. The shape of the spinnerette part is usually designed to minimize elastic instabilities at the entrance flow region [31]; in Figure 5.1, a "wine glass" design is shown. As the polymer exits the spinnerette, it may undergo swelling due to strain recovery (a delayed elastic effect), although with melt stretching the extent of swelling is lessened [31]. The polymer is cooled, in this case by air flow, until it solidifies at some distance, z, below the spinnerette exit. Stretching occurs as the polymer is collected on a take-up

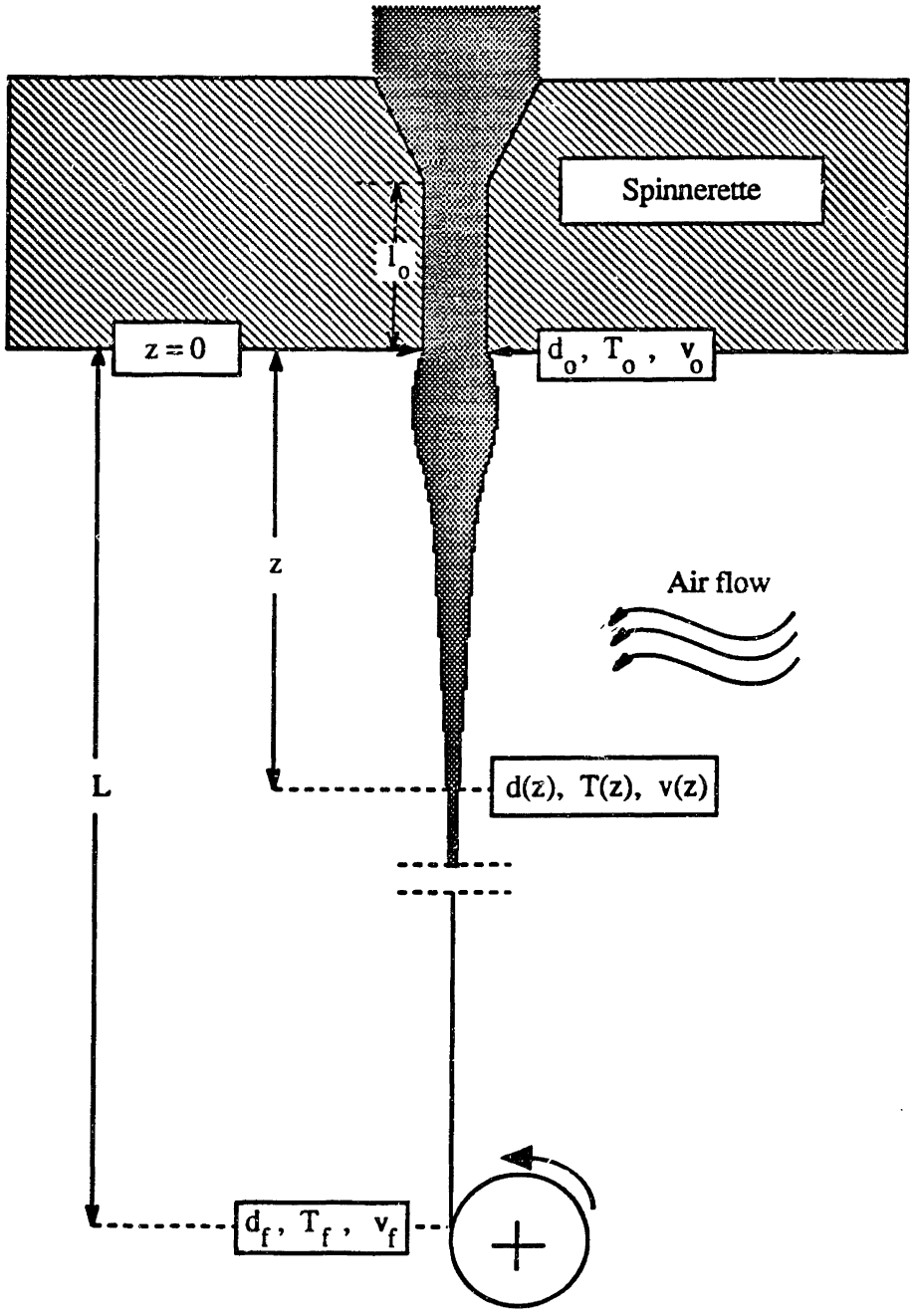

Figure 5.1. Schematic of the melt fiber spinning process. Molten polymer is forced through a spinnerette with dimensions l_o/ d_o. The extrudate is drawn at a velocity, v_f, to form a fiber of diameter, d_f. The polymer solidifies due to cooling by air flow at a distance, z, from the spinnerette.

reel placed at a distance, L, from the spinnerette orifice. The velocity of the take-up reel, v_f, is set such that the collected fiber has a diameter of, d_f. The extent of stretching that the polymer experiences is described by the spin draw ratio, λ_s, which is the ratio of the take-up velocity, v_f, to that of the velocity of the melt at the spinnerette exit, v_o [32]. Assuming that the density of the fiber is constant, the spin draw ratio can be defined as:

$$\lambda_s = \frac{v_f}{v_o} \approx \frac{A_o}{A_f} = \left(\frac{d_o}{d_f}\right)^2 \qquad (5.1)$$

where A_o and A_f , are the cross-sectional areas of the extrudate and fiber, respectively; and d_o and d_f, are their respective diameters. To separate out the effects of die swell on the determination of spin ratio, A_o and d_o are usually taken to be the area and diameter of the spinnerette capillary.

Whether or not a polymer system will form consistent fibers is dependent upon key process variables involved in spinning. Of most importance in the forming of fibers are the properties of the material itself (e.g. chemical composition, molecular structure, entanglement density, elongational viscosity, and crystallizability) [33]. A consistent fiber will be formed provided that the material possesses spinnability and does not exhibit draw resonance under the conditions at which it is spun. Spinnability is defined as the ability of polymer melts to be drawn without breaking (due to necking or cohesive fracture) [31]. Take-up velocity and draw ratio are controlled by the viscoelastic deformation and relaxation characteristics of a particular polymer. Draw resonance occurs due to melt flow instabilities which lead to a periodic variation in the diameter of the fiber over the draw down length [31]. Both spinnability and draw resonance depend upon the melt strength (extensional viscosity) of the polymer [33].

Other primary variables which influence the fiber quality include: 1) the extrusion temperature, T_o; 2) the dimensions and number of spinnerette orifices, d_o, l_o,

n; 3) the mass outflow, W; 4) the length of the spinning path, L; 5) the take-up velocity, v_f; and 6) the cooling conditions. Based on the continuity equations, these variables will determine what extrusion velocity, the average diameter of the fiber, and achievable spin-draw ratio. The primary variables will influence the texture and physical properties of the as-spun fiber through the kinematics and dynamics of the spinning process [33]. For instance, the viscosity of the melt and the flow behavior are dependent upon the extrusion temperature. This temperature as well as the cooling conditions (heat transfer coefficient, cooling medium temperature, etc.) will effect the solidification process of the polymer filament. Altering the take-up velocity will change the amount of tension applied to the fiber, hence, influencing the elongational flow of the material perhaps leading to draw resonance. Overall, the effects of non-isothermal spinning on the draw resonance of polymer systems is not fully understood. If the polymer solidifies before encountering the take-up reel, no resonance occurs [31].

In order to increase the orientation of the polymer chains within a fiber, a secondary structuring process, termed cold drawing, is often performed. Cold drawing occurs at a lower temperature than that at which the filament was melt-spun; usually between the glass transition temperature and the melting temperature of the polymer [31]. The as-spun fiber is stretched at this temperature by feeding it to a second take-up reel. After cold drawing, the fiber's strength is often significantly improved [31]. The extent of this secondary stretching process is described by the cold draw ratio, λ_c, which is similar in definition to the spin draw ratio:

$$\lambda_c = \frac{v_2}{v_1} \approx \frac{A_1}{A_2} = \left(\frac{d_1}{d_2}\right)^2 \qquad (5.2)$$

where v_1 and v_2 are the linear velocities of the feed and take-up reels, respectively. A_1 and A_2 are the cross-sectional areas of the fiber before and after cold drawing. respectively; d_1 and d_2 are the undrawn and drawn fiber diameters, respectively.

Fiber Spinning of Blends

The addition of a second polymer or the addition of plasticizer will effect the processing, structure development, and final properties of a melt-spun fiber. Polymer blends historically have been used to improve some property of the fiber that is not adequate with only one component. For instance, one may want to improve the rheological or mechanical properties, change the optical properties or appearance of a fiber, make a particular fiber dyeable, or produce lower cost fibers. The effect of plasticizers will be to lower the viscosity and, hence, improve the flow properties of the polymer system. Plasticizers will also lower the glass transition, thus making the fiber less brittle. The effect of each process variable on the morphology and properties will be compounded by interactions of the polymer with the added components.

Typical structures of immiscible blend fibers include the side-by-side, sheath-core, and matrix-fibril morphologies [34] as shown in figure 5.2a, b, and c, respectively. The side-by-side morphology, in which each side of the fiber is composed of a separate polymer, is often used where self-crimping characteristics or high extensibility is necessary as in textile applications. The sheath-core morphology, in which one polymer encases the other, is useful for dyeing or environmentally stabilizing the fiber. Special processing equipment is usually required to form these two structural types. The matrix-fibril morphology, however, results upon fiber spinning of a random phase separated blend in typical fiber spinning equipment. Depending upon the flow conditions through the spinnerette and composition, a stratified blend morphology, instead of the matrix-fibril, may form [35] (Figure 5.2d). In addition, at intermediate compositions and under certain rheological conditions, a co-continuous or interpenetrating network morphology may form (Figure 5.2e). This structure may also be a result of spinodal decomposition of miscible polymers which cross the single to two phase boundary [34] during the spinning process. Given previous morphological results on the starch/EVOH blends [Chapters 3 and 4], we would expect the matrix-

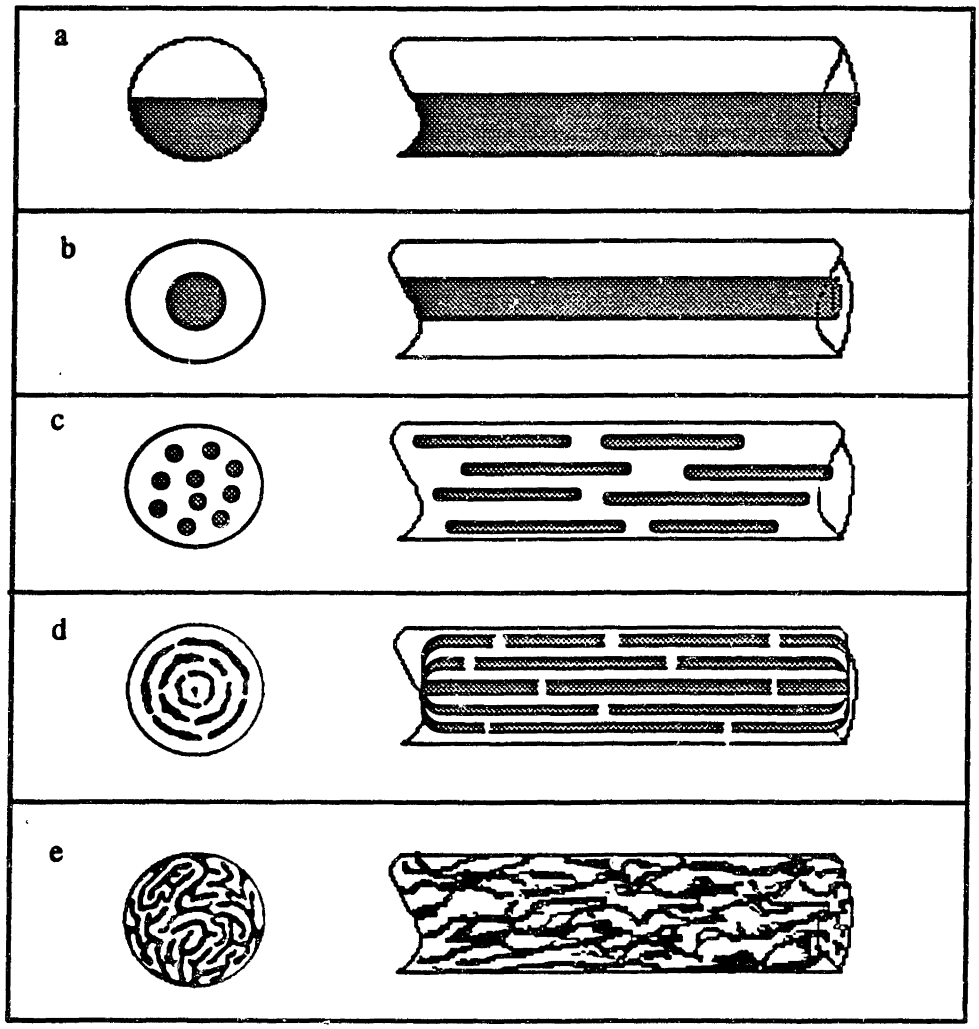

Figure 5.2. Schematics of possible phase morphology arrangements for immiscible polymer blend fibers: a) side-by-side, b) sheath-core, c) matrix-fibril, d) stratified, and e) co-continuous (interpenetrating network). From D.R. Paul, 1978.

fibril morphology, or its variations, such as the stratified or co-continuous morphologies, to exist in many of the starch-EVOH blends.

The stability of the blend melt is a critical factor in the production of melt-spun fibers. The blends should be well-mixed prior to entering the spinnerette (such as prior mixing in a twin-screw extruder). Ideally, the blend pellets should be re-extruded to achieve a fine dispersion in the melt spinning instrument [34]. In addition, a reduced residence time in the melt is recommended to lessen morphological changes associated with phase domain coalescence, chemical reactions, and degradation phenomena that may occur in the barrel region of the fiber spinner.

Once the blend pellets are melted, pressure is exerted on the system causing the blend to flow through the capillary of the spinnerette. Here, the blend experiences stresses that cause droplet break-up, a phenomena competing with the thermodynamic tendency for dispersed droplets to coalesce. The morphology in the spinnerette will depend upon the relative values for viscosity of the polymer components, their interfacial tension, the shear stress, and droplet size [35]. As the blend approaches the spinnerette orifice, it experiences a rapid acceleration and undergoes elongational flow. The relative viscosity and elasticity of each blend component at this state will effect the extension ratios (i.e. L/D) for fibril formation within the matrix component [34].

Chain orientation induced during drawing will increase the rate and level of crystallinity of semi-crystalline polymers; however, partial miscibility in the melt state of a blend will lower the rate and amount of crystallinity associated with each component since rapid transport away from growing crystals of the non-crystallizable component inhibits crystallization. The location at which crystallization/solidification occurs along the spinline will influence the draw properties of the blend. As mentioned in the previous section, draw resonance is eliminated if solidification occurs before the take-up reel. Finally, the interfacial adhesion between components may limit the extensibility of one component, or, in other cases, voids may form and surface

roughness may increase if one component draws more readily than the other [34].

The addition of plasticizers serves to improve the flow properties of a polymer, and the mechanical properties of the resulting fiber. One of the problems occasionally encountered during fiber-spinning is the foaming of the extruded filaments. This phenomenon is due to the flashing of plasticizers, mainly water in this study, that become superheated as the pressure within the melt suddenly drops to atmospheric pressure. Foaming is possible since the temperature of the extrudate remains initially above both the glass transition temperature of the polymer and the boiling point of water at the lower (~ 1 atm) pressure. Foaming may be reduced by decreasing the amount of plasticizers, by lowering the extrusion temperature and by extruding into an enclosure kept at a pressure above the vapor pressure of the plasticizer at the extrusion temperature. Finally, the partitioning of the plasticizer components between phases must be considered when trying to understand the overall processing, structure, and property characteristics of a polymer-polymer blend fiber.

EXPERIMENTAL

Materials

Blends consisting of three varieties of corn starch were extrusion blended with EVOH containing 56 mol% vinyl alcohol content (Grade EVAL E105A, EVALCA Co., Lisle, IL). Amioca waxy maize (WM), a starch containing essentially 100% amylopectin; Melojel, a native corn starch (NC) possessing approximately 30% amylose; and Hylon VII (HY), a hybrid corn starch consisting of approximately 70 % amylose, were supplied by National Starch Co., Bridgewater, NJ. Compounding of this experimental series took place at the Novon Products Division of Warner-Lambert, Co., Morris Plains, NJ [1]. In order to improve subsequent processing into melt-spun fibers, glycerin was added as a plasticizer in the amount of 15 % of the total weight to all of these blends during the extrusion process. Water was also added during compounding.

Finally, naturally occurring triglyceride additives were pre-mixed with the starch fraction in small amounts (3 wt% to the starch fraction) to aid in processing. Details on the blend compounding of these materials are given in Chapter 3 (Table 3.1).

Fiber Spinning Apparatus

Fiber spinning of the blends was performed using a batch, lab-scale device manufactured by Alex James and Associates, Inc., Greenville, SC. A schematic representation of the One-Shot® fiber spinner is shown in Figure 5.3. Polymer pellets are held in a cylinder which is placed into a 'melt head'. A motor drives an actuator which forces the piston to extrude the melt through the single-orifice spinnerette. As the monofilament exits the spinnerette, it passes through a quench cabinet through which air flow is controlled. One meter below the spinnerette exit, the fiber is collected on take-up reel at controlled linear velocity. A control panel on the left side of the spinner allows one to regulate the actuator direction and speed, the temperature of the melt head, and fan speed. Indicators display thermocouple readings for the melt head and cylinder (sample) temperature.

A close-up of the sample cell and spinnerette is shown as a schematic in Figure 5.4. A single hole spinnerette is employed of 0.03" (762 μm) and L/D equal to 3 is joined to the cell using four bolts. A screen gasket is placed between the spinnerette and cell to filter out large impurities. Up to approximately 50g. of sample (pellets) is placed into the cell and the steel piston (1" ID) is immediately inserted after filling the chamber (to eliminate moisture changes due to atmospheric conditions). A brass jam nut seals the piston to the sample cell. The pull-out hole (shown in Figure 5.4a) for a holder rod allows the user to insert and remove the cell from the melt-head. In the melt head, the approximate temperature of the sample is monitored by inserting a thermocouple into the "thermocouple hole" of the cell.

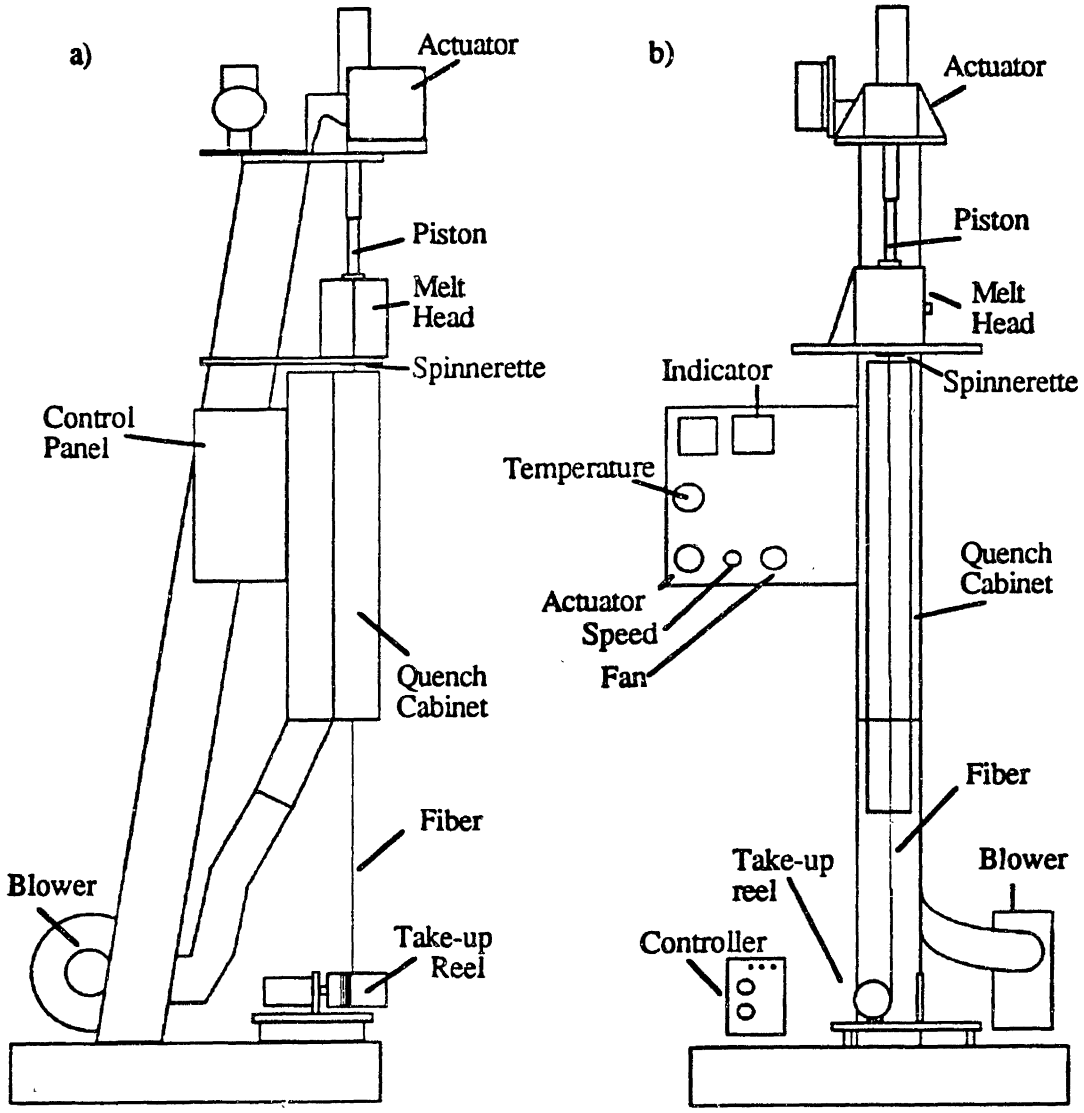

Figure 5.3. The Alex James One-Shot Fiber Spinning Rig: a) side view, b) front view.

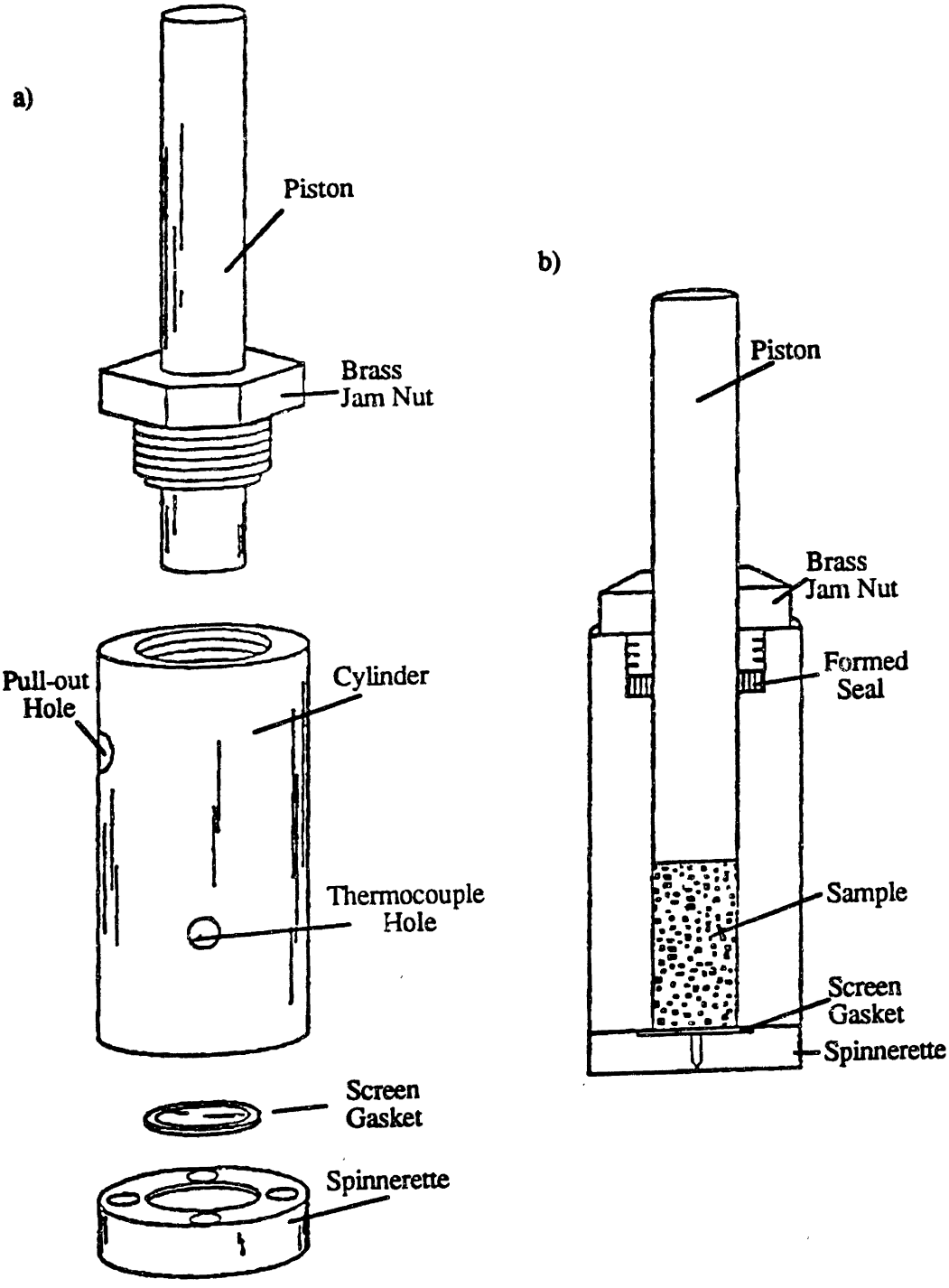

Figure 5.4. Schematic of a) the sample cell arrangement and b) cross-sectional view showing unmelted sample within the cell chamber.

Fiber Spinning Procedure

Trials were performed with pellets obtained from the compounding process (either as stored or after conditioning to 50% RH for at least one week). Approximately 50g. of each blend was placed into the sample cell for each spinning run. The spinnerette of inside diameter 762 μm (0.03") was employed for runs used to survey the spinnability of the blends. The melt head temperature was initially set to 160°C (the sample temperature, measured by the thermocouple placed adjacent to the barrel was approximately 150°C, which is above the peak EVOH melting temperature for the blends as measured by DSC [see Chapter 3]). Slight pressure was placed on the piston as each sample was heated. Once the measured temperature reached equilibrium, if the sample did not flow through the spinnerette, the temperature of the melt head was raised by ten degrees in steps until sample was observed to flow out of the spinnerette. If foaming or steam was observed at the spinnerette orifice, the temperature of the melt head was subsequently lowered to eliminate this phenomena. After molten extrudate was observed to exit the spinnerette and an acceptable temperature condition was reached, the actuator was set to 4.0. It was observed that the plunger speed varied according to the flow properties of the melt, so its velocity was determined by measuring the vertical travel of the plunger as a function of time.

After flow conditions were optimized, the piston speed and velocity of the filament was determined. These values were used to estimate volumetric flowrate, Q, through the spinnerette. Apparent shear rates, $\dot{\gamma}_a$, were approximated by:

$$\dot{\gamma}_a = \frac{4\,Q}{\pi\,R^3} \qquad (5.3)$$

where R is the inner radius of the spinnerette. The shear rates for which data on the power-law exponent, n, was available from rheometric measurements [2] were corrected using the Rabinowitsch equation:

$$\dot{\gamma}_c = \frac{4Q}{\pi R^3}\left(\frac{3n+1}{n}\right) \qquad (5.4)$$

Once a steady state was achieved, the undrawn extrudate (defined as the filament) was taped to the take-up reel and blends were screened for spinnability by slowly increasing the velocity of the take-up reel. Air flow was used to cool certain blends, often making them more spinnable. Those blends which could draw were collected on the take-up reel. Maximum spinnability was determined by collecting the fibers (drawn extrudate) at a velocity just under that at which they were observed to fracture. Spin draw ratio was calculated using equation 5.1 from at least ten different sections of the fiber. Die swell was determined by taking the ratio of the undrawn filament diameter to the spinnerette diameter. Diameter of the filament was measured with a micrometer. Fiber diameters were measured using a Zeiss Axioscope Optical Microscope. Moisture content of the filaments were determined immediately following each fiber spinning trial.

Characterization Methods

Since moisture content plays an important role in the mechanical behavior of the fibers, it was necessary to condition the fibers to known moisture levels. Thus, the fibers were placed in closed chambers at room temperature and varying relative humidity (produced from solutions of differing ratios of glycerin to water) for at least one week [36]. Humidity and temperature were recorded using a Testoterm 6100 thermohygrometer. Moisture content of fiber samples was determined using a Mettler DL18 Karl Fischer Titration System.

Mechanical properties of the filaments and fibers were determined by using a Model 4501 Instron Tensile Testing Instrument equipped with either a 10N or 5kN load cell. Rubber coated grip faces were used to clamp the fibers securely in the instrument.

Trials were performed according to the ASTM standard D3822 and at least 10 tests were performed per sample. Data points were collected at a sampling interval of 2.5 pts/sec using the Instron System IX software. Values for ultimate stress, strain at maximum load, breaking stress and strain, tensile modulus, and toughness (energy to break) were computed.

To analyze sample orientation, an Enraf Nonius Delft Diffractis 593 sealed-tube x-ray system using CuK_{α} radiation at 40 kV and 26 mA was utilized. A Nickel filter and 0.2 mm collimator were employed for the point source. Flat film wide-angle x-ray exposures were taken at a distance of 50 mm using a Statton camera. Typical exposure times 8 hours for pellets (which were cut to 1 mm thicknesses) and 48 hours for single fiber samples.

Fiber surfaces and fracture surface structure were examined using a Cambridge Stereoscan Scanning Electron Microscope. Samples were placed on aluminum stubs and sputter-coated with gold palladium. The microscope was operated at 10 kV.

Certain samples were examined in transmission electron microscopy (TEM). Fibers were embedded in MedCast, Medium Grade, Quik-Cast Epoxy (Ted Pella, Inc., Redding, CA) and allowed to cure overnight at 60°C. Samples were microtomed, stained with iodine, and examined with a JEOL 200 CX TEM according to the procedures described in Chapter 4.

RESULTS AND DISCUSSION

In this study, starch exists as a plasticized blend of its polymer constituents, amylose and amylopectin, with poly(ethylene-vinyl alcohol), and not as a filler particle within a synthetic polymer matrix as previously studied, for example, in starch/polyethylene systems [37 - 41]. The extent to which these "destructurized" starch blends are spinnable as function of starch type and composition and their resulting mechanical properties are of interest. We seek to explain these results using

information gained from the morphology study of these blends already presented in Chapters 2 and 3 and from a structural examination of the fibers themselves.

Fiber Spinning Results

Initial fiber spinning conditions (T ~ 150°C, $\bar{\dot{\gamma}}$ ~ 10 - 150 s^{-1}) were chosen to allow for comparison of results with a capillary viscometry experiment conducted on these blends [2]. However, conditions were varied to eliminate foaming of plasticizer and produce a consistent flowing filament before extensional flow was applied to the blend. Drawing conditions were also optimized through the use of air flow to cool the fiber, and to attempt to stabilize it from melt flow instabilities such as draw resonance. Since the amount of moisture in a blend will affect its flow and elongational properties, moisture content before and after spinning was measured for the blends. In addition, each sample was tested under two conditions, at the moisture content of the blend as stored after compounding and after conditioning at a constant humidity level of 50% RH. Optimum spinning conditions as well as the moisture content before and after spinning for the blends are shown in Table 5.1 (for the 'as stored' blends) and in Table 5.2 (for the 50% RH conditioned blends). Blends with draw ratios equal to or less than one did not spin draw.

In general, the blends which were conditioned at 50% RH possessed less moisture than the blends after they were compounded (exceptions are WM100, WM70, and WM40 blends in which the amount of water added during compounding was limited) (Tables 5.1a, 5.2a). Differences between the pellet and filament moisture content were less than 2% for all of the blends indicating that moisture loss through vaporization of the water was not significant. Sample temperatures (129 to 176 °C) and spinnerette temperatures (97 to 148°C) were consistently lower than the melt head temperatures which ranged from 145 to 201°C. Hylon VII blends required higher temperatures to flow which may be due to the presence of the V-amylose complexes

that increase the melt viscosity [42] and which require higher temperatures and pressures to melt. It should be noted that the HY100 and HY85 blends were not able to flow after conditioning their pellets to 50% RH even at high temperature. Fused, compressed, dark brown pellets were observed in the barrel of the fiber spinner after these trials which indicate that these systems (with moisture contents of 5.8 and 5.5 wt%, respectively) did not form a fluid melt before degradation set in.

The piston velocity at a constant actuator setting for the fiber spinner motor was found to vary depending upon the flow properties of the blend tested (~ 0.04 to 0.3 cm/min). This variation resulted in different values for the apparent shear rate of the blends (40 to 445 s^{-1}) (see Tables 5.1b and 5.2b). Significant differences between the three starch varieties were not observed in the flow properties of the blends through the spinnerette. Overall, blends higher in EVOH content, which possess lower viscosities [2][42], exhibited higher volumetric and mass flowrates, and higher apparent rates of shear. This shear rate became lower at decreased moisture levels; a phenomena which is consistent with capillary rheology measurements that also show increases in viscosity with decreasing moisture content [2]. After correcting the apparent shear rates using the power law viscosity dependence for select starch blends, the calculated shear rates were not correlatable to starch content for the 'as stored' blends. However, for the 50% RH conditioned blends, the corrected shear rate was found to increase with starch content even though blends higher in starch possessed higher moisture contents. These corrected shear rates ranged from 83 to 381 s^{-1} and fall in the range for which previous capillary rheometry data was taken [2].

Die swell of the blends were determined by measuring the diameter of the filament extruded from the spinnerette before any take-up force was applied (Tables 5.1b and 5.2b). Die swell is a phenomena in which a polymer system undergoes a delayed elastic strain recovery such that the extrudate is larger than the size of the die [31]. Die swell increases with increasing shear rate, decreasing viscosity, decreasing

temperature, increasing molecular weight distribution, and decreasing l_o/d_o ratio, due to the lower residence time in the flow conduit respective to the relaxation time of the polymer chains. Ratios of the filament diameter to spinnerette size (d_F/d_o) are plotted in figure 5.5. WM blends, the least viscous of the three starch blends, undergo higher degrees of die swell (d_F/d_o approaches 1.8 for WM100). The residence time in the spinnerette, t*, for the WM blends ranges from 85 to 140 msec. NC blends show slight extrudate swelling (up to 1.2) at higher starch contents, and the HY blends undergo little or no swelling. Overall, die swell for these blends decreases as the starch content decreases, which is consistent with exposure to the increasing shear rates as EVOH constitutes more of the blends. Die swell does not significantly vary with moisture content differences in the 'as stored' and conditioned blends.

The spinnability of the blends was next examined by imparting an extensional force on the filament exiting the spinnerette. Conditions were optimized (by the use of air flow and varying take-up velocity) such that the fibers could be spun without fracture or significant draw resonance (i.e. more than 10% variation in the fiber diameter). Maximum spin draw ratios are listed in Tables 5.1b and 5.2b, and plotted in figure 5.6 to illustrate the dependence of the spinnability on starch content. Draw ratios ranged from less than one for the neat starch blends to 215 for the EVOH/GLY control. Blends exhibiting draw ratios of less than one do not draw and also exhibit die swell (thus, the 'contraction paradox' [33] in the draw ratio number). From Figure 5.6, it is clearly evident that the EVOH component is responsible for all of the extensional properties (i.e. drawability) of the blends. The 'as stored' blends exhibited higher values of spin draw ratio than did the '50% RH conditioned' blends indicating that spinnability generally improves with higher moisture levels. Blends with more amylopectin were able to draw at the highest starch contents (albeit at low draw ratios; e.g. WM70, $\lambda_S \sim 3$; NC60, $\lambda_S \sim 6$) while the HY blends exhibited no spinnability until starch contents reached 40% or less. At compositions below 50% starch, NC blends exhibited the best

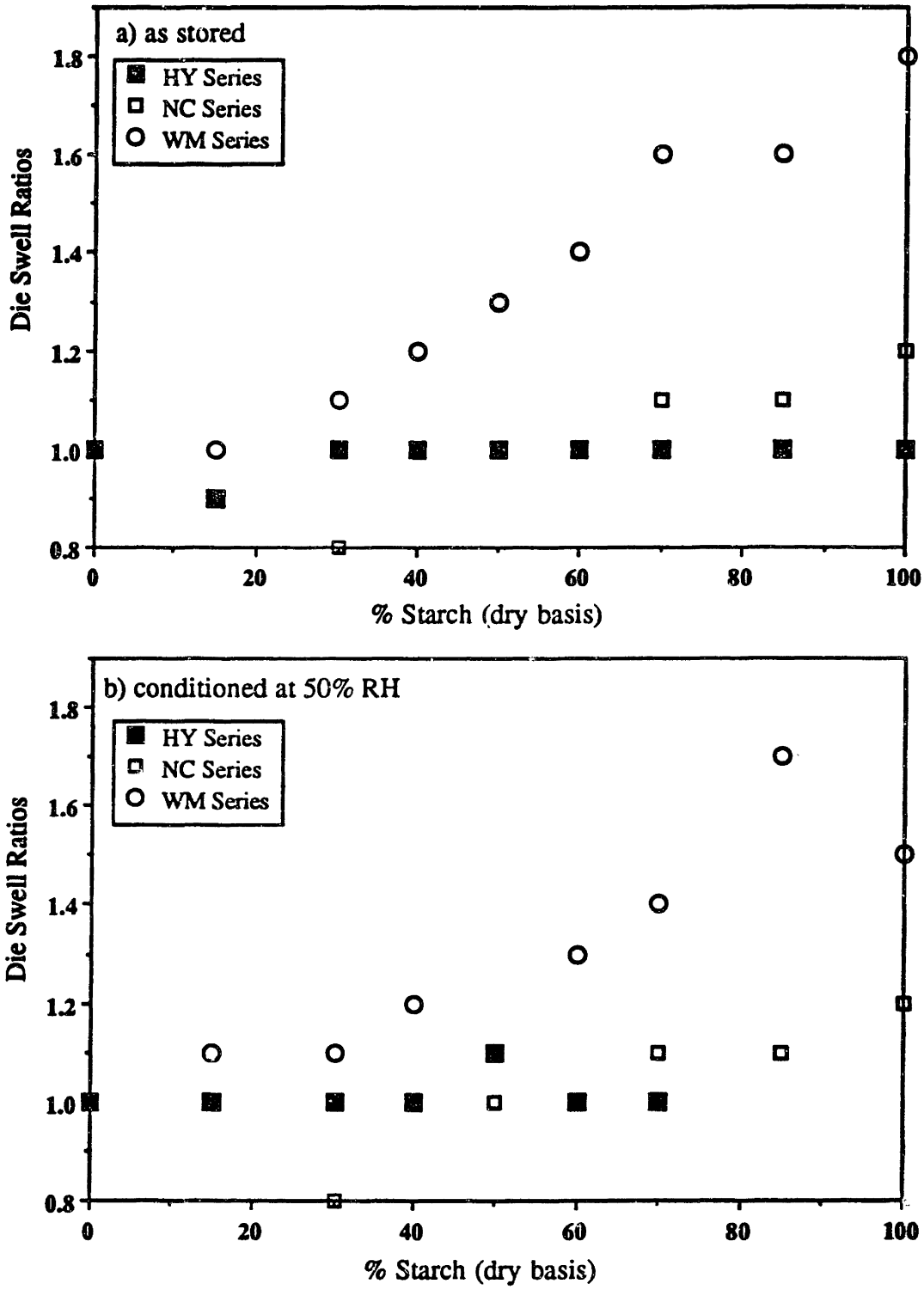

Figure 5.5. Die Swell ratios as determined for the starch/EVOH blends: a) as stored b) after conditioning at 50% RH.

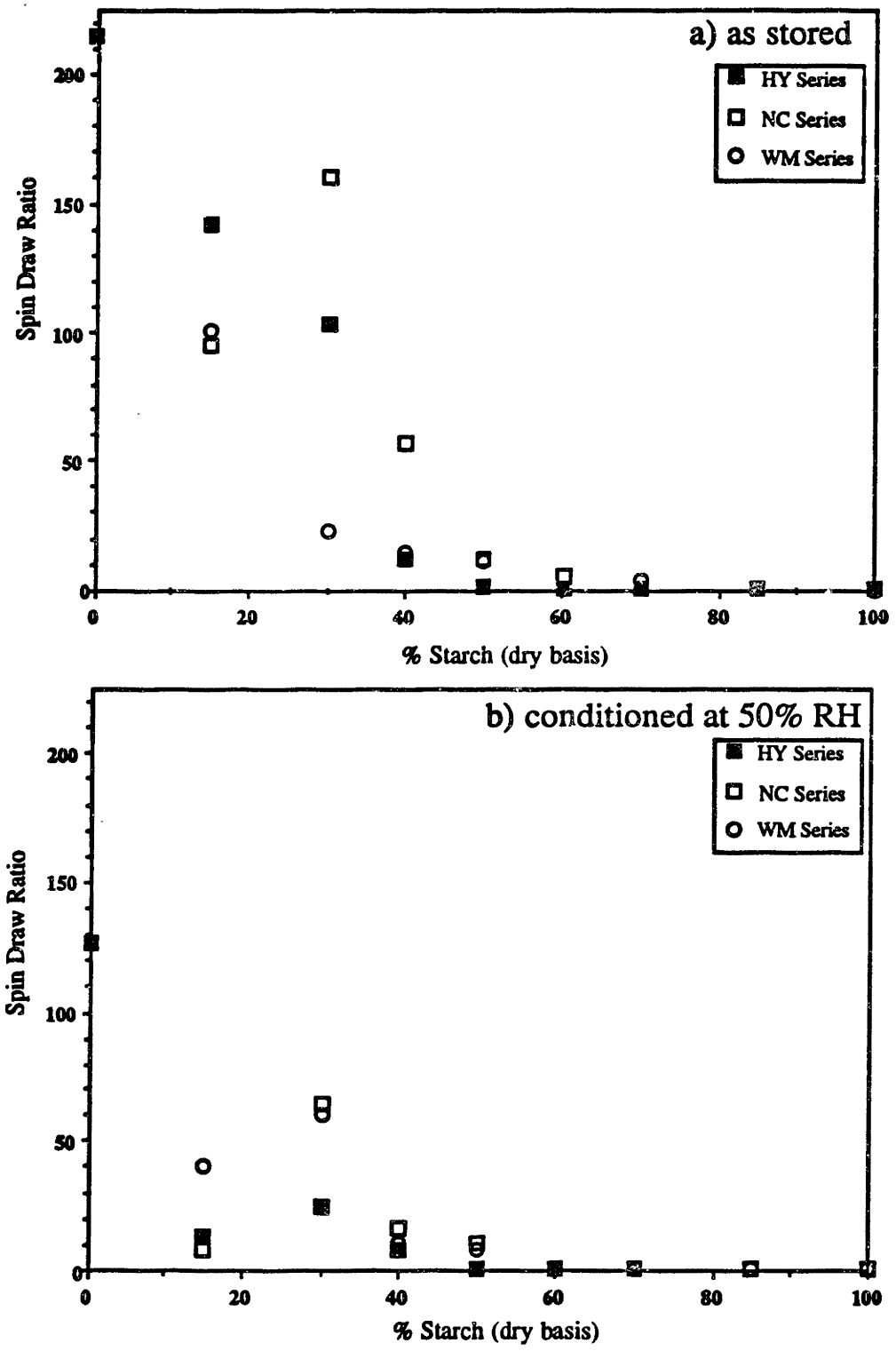

Figure 5.6. Maximum spin draw ratios as determined for the starch/EVOH blends: a) as stored, b) after conditioning pellets at 50% RH.

spinnability, then HY blends, followed by the WM blends. Morphological investigations presented below will be used to explain this behavior.

Morphology

Investigation of fiber structure provides further insight into the processing and properties of these blends. In the fiber spinning process, orientation can occur in both the spinnerette channel region (shear flow) and along the spinning path (elongational flow). To understand the effect of this orientation on the starch/EVOH blends, flat film wide-angle x-ray scattering was employed (see Figure 5.7). Patterns of the NC100 and EVOH/GLY blend pellets are given in figure 5.7c and d as references. Scattering from starch in the NC100 arises at 2θ equal to 12.9, 16.6, 18.3, 19.7, and 22.4° and for the EVOH in the control blend at 10.8, 20.4, and 21.7°. No orientation is observed in the WAXS patterns of the pellet samples.

Figure 5.7a depicts the scattering pattern of an undrawn filament for the NC50 blend. No preferred orientation of the polymer chains is evident from this diffraction pattern. In the spinnerette region of the fiber spinner, the melt is subjected to shear flow and should undergo some orientation. However, due to the short l_o/d_o ratio of 3 for the spinnerette, the time spent in the flow conduit, t*, is probably not sufficient to induce permanent orientation of the polymer chains (i.e. $t_{relax} > t^*$). The phenomena of die swell is a result of this difference in relaxation times. It should be noted, however, that domains do undergo orientation as evident in oblong starch domains and EVOH fibrils as observed in SEM of enzymatically etched filaments [see Chapter 3].

As elongational flow is imparted to the fiber, the polymer chains begin to undergo some orientation as evident by slight arcing at the equatorial reflections (figure 5.7b, $\lambda_S \sim 23$) at 2θ approximately equal to 20 - 22° (corresponding to the higher 2θ crystalline reflections apparent in both starch and EVOH and covering the regions of strong amorphous scattering). As in commercial fiber spinning, significant orientation

Figure 5.7. Flat film WAXS patterns for native corn/EVOH blends: a) NC50 pellet, b) NC50 'as spun' fiber (λ_s = 11), c) cold drawn fiber (T = 110°C, λ_c = 4, λ_{total} ~ 44). For reference are: d) NC100 pellet, e) EVOH/GLY control pellet, f) comparison of scattering patterns for undrawn and drawn NC50 with NC100 and EVOH/GLY pellet references. Note: no orientation in the starch crystalline component is apparent, even after cold drawing.

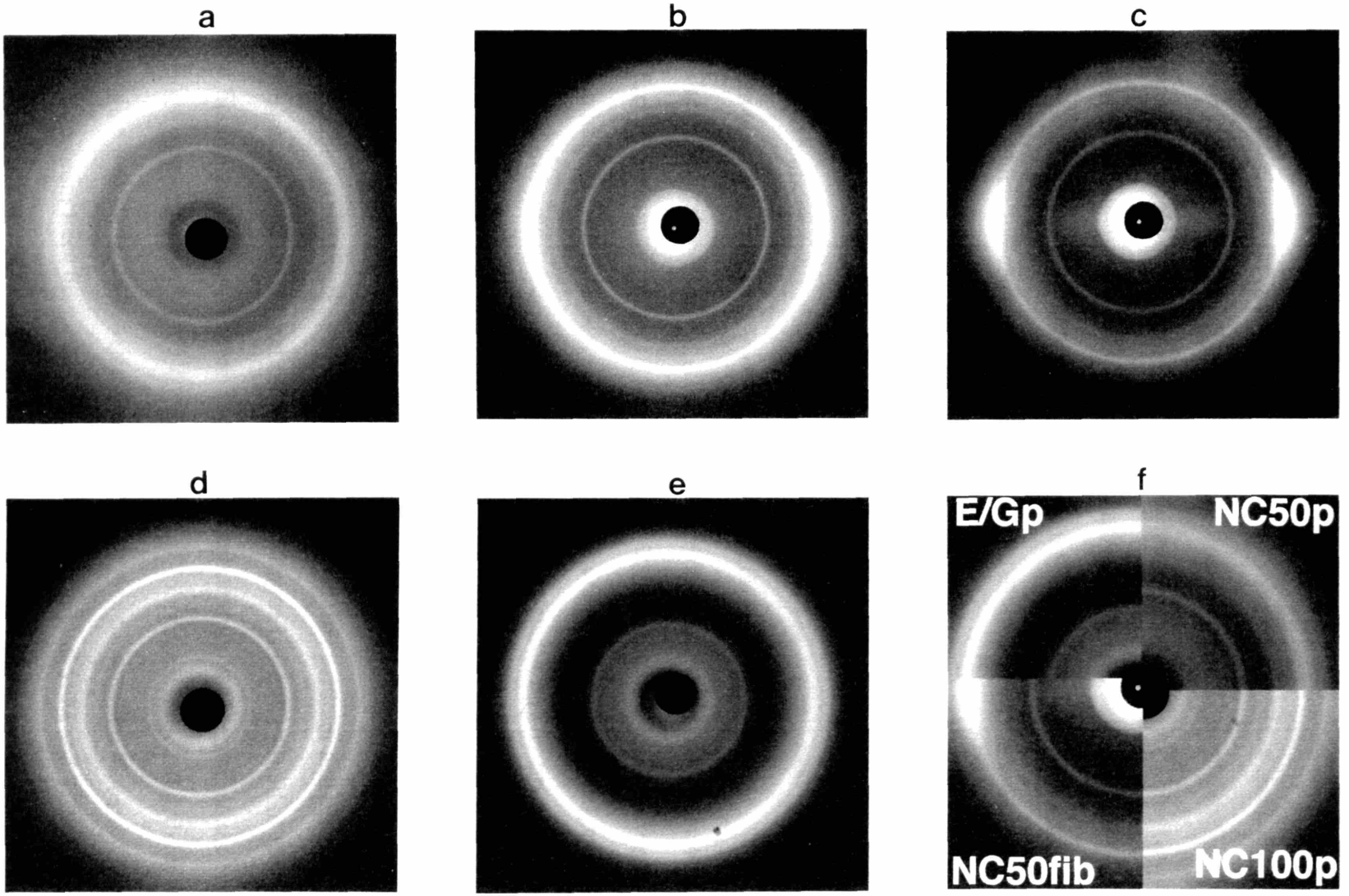
a
b
c
d
e
f
E/Gp
NC50p
NC50fib
NC100p

is not achieved in the melt-spinning processes unless high take-up velocities are employed [33]. Most molecular orientation occurs in secondary cold drawing steps that occur above the glass transition and below the melt points of the polymer samples.

For the NC50 fiber, cold drawing was performed at 110°C such that the fiber was stretched to a cold draw ratio of 3.1. The diffraction pattern of this fiber is shown in figure 5.7c. Orientation is easily observed by arcing in the equatorial reflections. No orientation associated with the crystalline starch fraction is observed, however (see figure 5.7f), which indicates that although the EVOH component is orienting, the crystallites associated with starch are randomly oriented with respect to the draw direction. This behavior is consistent with the fact the amylose and amylopectin, which are present in the blend, are high molecular weight, branched polymers which, at low moisture contents, exhibit low elongational behavior compared with the EVOH component (also, blends high in starch content show little or no drawability).

The structural appearance of the starch-based fibers was next examined to obtain further information about how structure is influenced by the processing application of melt fiber spinning. SEM micrographs are shown in figure 5.8 to allow comparison of draw ratio and surface structure for certain starch/EVOH fibers. Unlike the blend fibers, the EVOH/GLY control possessed a smooth surface at all draw ratios (fibers are shown figure 5.8b and c). In figure 5.8a, the HY50 filament (undrawn) is displayed with respect to the HY40, HY30, and HY15 fibers (drawn filaments). The filament's surface is relatively smooth except for some foreign particles and charging at tears in the gold-palladium coating (this surface appearance is similar for all of the HY undrawn filaments.). As the filament is drawn a rough texture is observed on the fiber surfaces (see magnified view of HY40 in figure 5.8a). Fibrils, cavities, and nodules are clearly visible indicating inhomogeneous blend behavior. Orientation along the draw direction is apparent from the surface features. From previous SEM and TEM studies of undrawn filaments, it was determined that the fibrils are rich in EVOH and

Figure 5.8. SEM micrographs showing the surface appearance of fibers of various starch compositions and draw ratios: a) HY series, b) NC series, c) WM series.

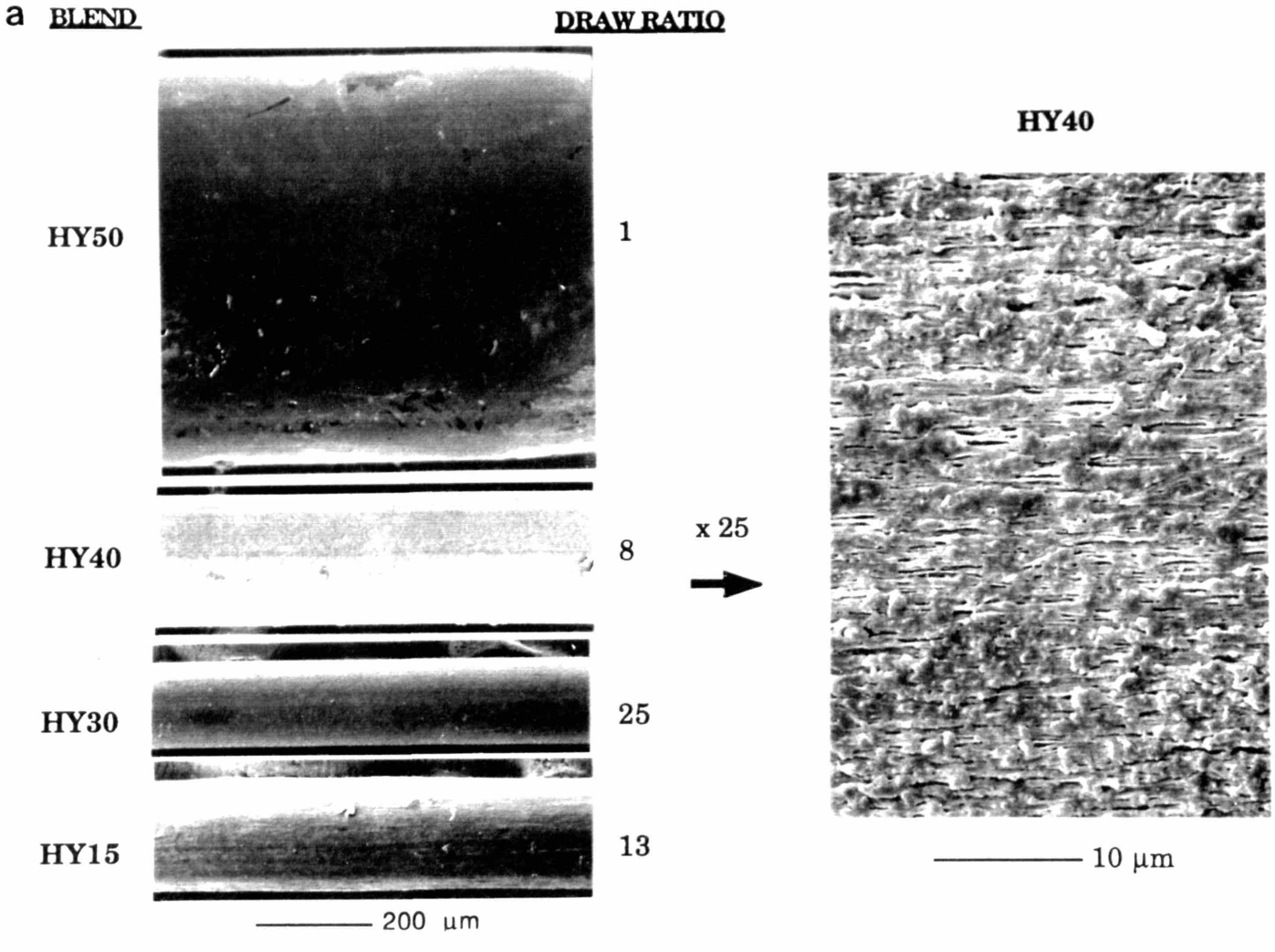
a
BLEND
DRAW RATIO
HY50
1
HY40
8
HY30
25
HY15
13
200 µm
x 25
HY40
10 µm

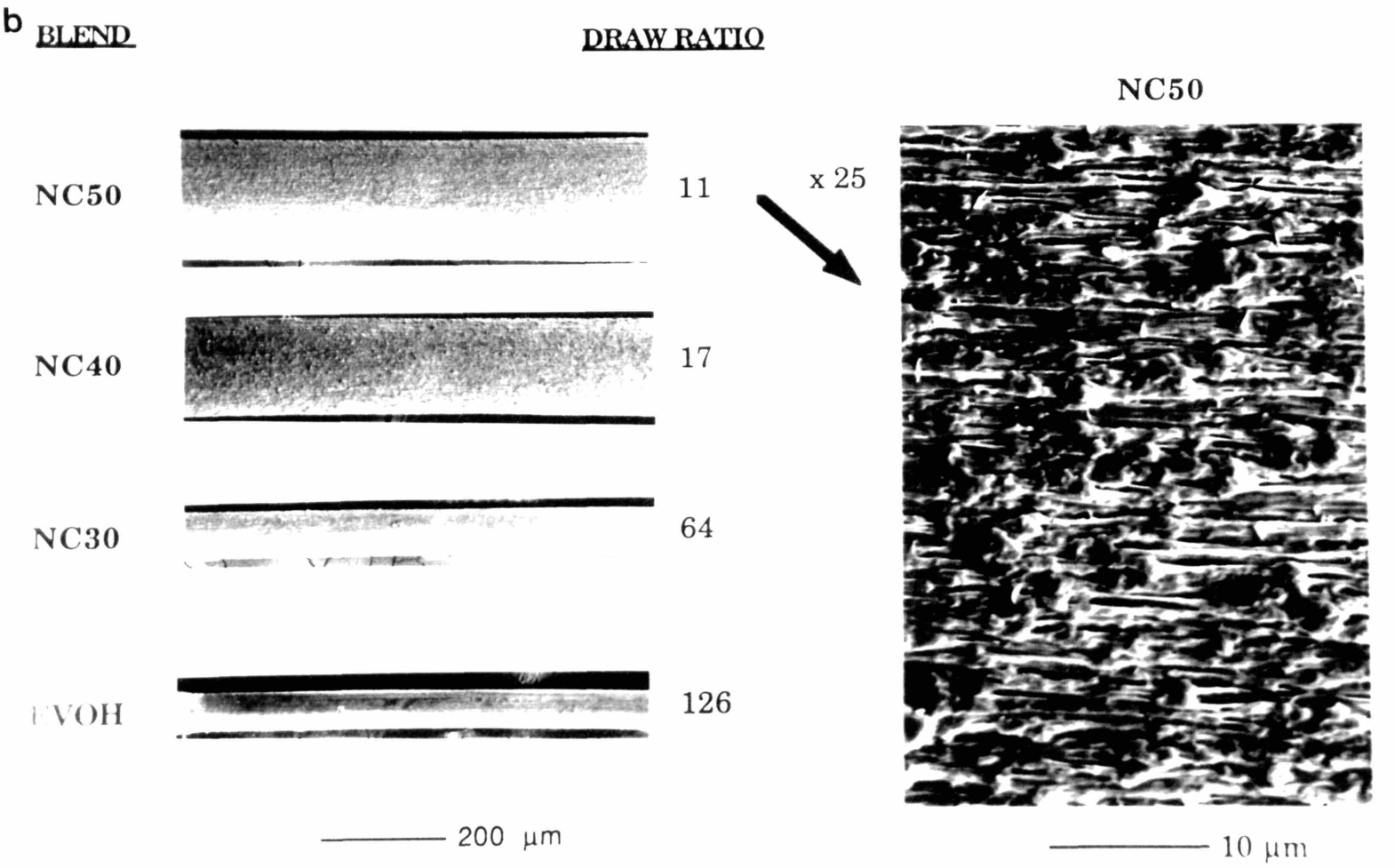
b
BLEND
DRAW RATIO
NC50
NC40
NC30
EVOH
11
17
64
126
200 µm
x 25
NC50
10 µm

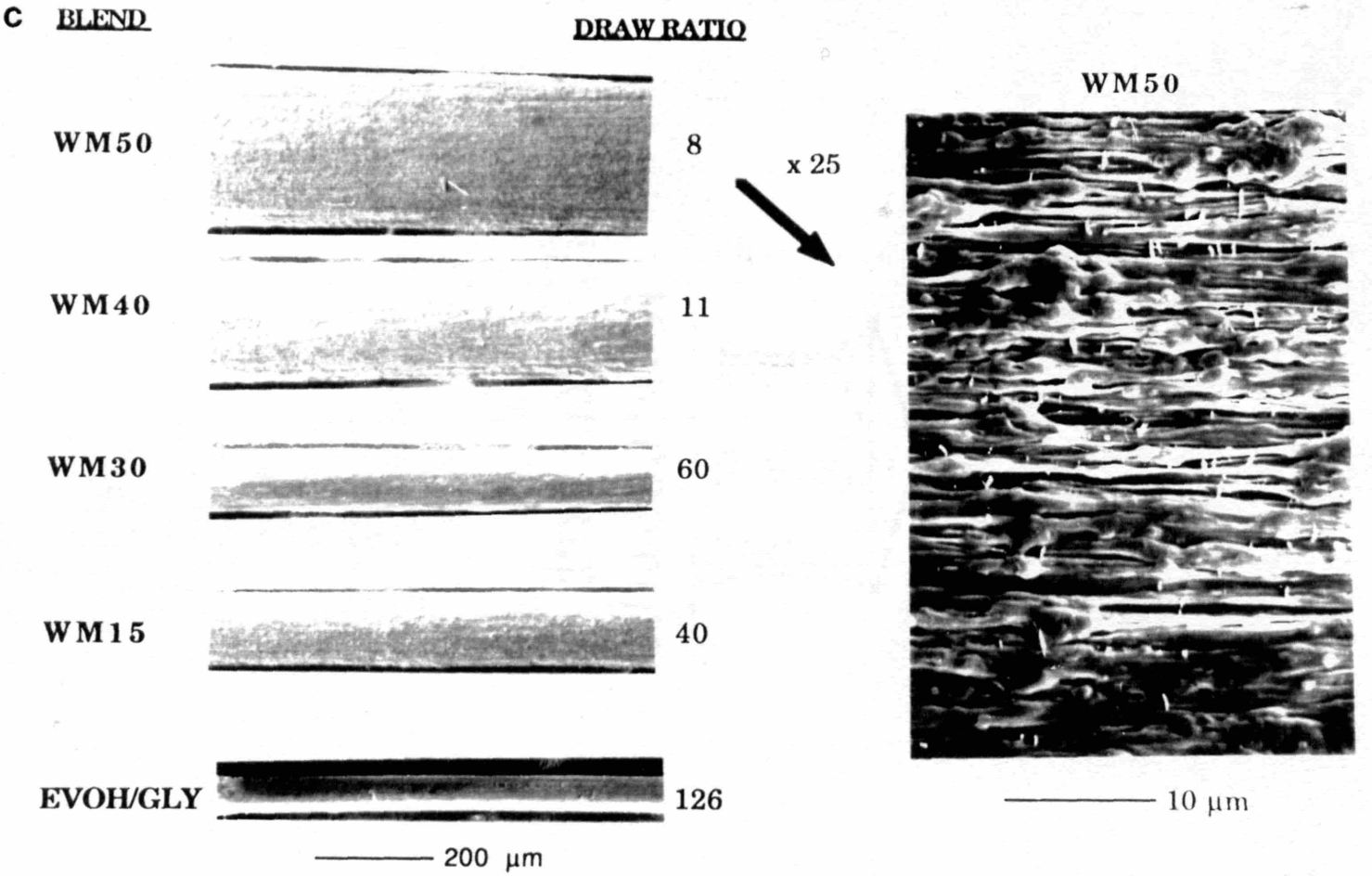
C
BLEND
DRAW RATIO
WM50
8
WM40
11
WM30
60
WM15
40
EVOH/GLY
126
200 µm
x 25
WM50
10 µm

thenodules are roughly the size of starch-rich domains. Similar surface features are observed for the NC and WM blend fibers (NC50 and WM50, figure 5.8b and c), although nodule sizes are larger than observed in the HY blends. In the magnified view of the WM50 blend fiber (figure 5.8c), additional short fibrils approximately 0.5 μm in diameter are observed perpendicular to the draw direction. These features are most likely formed when EVOH fibrils break under the extensional loads imparted in the fiber spinning process (similar behavior was observed in the NC blends for fibers spun to high draw ratios). Drawing suppresses die swell, but WM filaments showed evidence of sharking or unevenness indicating flow instabilities at the die.

The variation in surface structure as a function of composition for native corn/EVOH blend fibers is shown in figure 5.9. As in figure 5.8b, the NC50 fiber exhibits the characteristic nodular fibril structure observed for the starch-based blends at intermediate composition. Broken fibrils are evident (figure 5.9a) which is consistent with the higher spin draw ratio that this fiber experienced ($\lambda_s \sim 23$). As more EVOH is incorporated into the fiber the number of nodules per unit area decreases, the fibril width increases, and the extent of cavitation on the surface decreases. In the four blends shown, EVOH exists as the matrix component and undergoes orientation in the draw direction. The elongational properties of both the starch and EVOH are significantly different such that molten starch domains undergo only slight orientation and appear to act as small filler particles during the spinning process that adhere to the EVOH as it is melt stretched. The EVOH-rich phase begins to debond from the starch in order to undergo higher levels of elongation; hence, the formation of fibrils and cavities.

In figure 5.10, a TEM micrograph of a deformation zone in an NC50 blend is shown (similar sample as in figure 5.12). The dark, iodine stained, starch-rich inclusions show little deformation and even de-adhere from the EVOH-rich matrix as it is deformed. Eventually EVOH-rich fibrils are formed that span across the zone.

Figure 5.9. SEM micrographs depicting the change in fiber surface appearance as a function of composition: a) NC50, $\lambda_S = 23$, b) NC40, $\lambda_S = 17$, c) NC30, $\lambda_S = 63$, d) NC15, $\lambda_S = 95$. (Draw direction vertical.) Fibril formation of the EVOH-rich phase is evident on the fiber surfaces. As starch content increases, the number of nodules and cavities present at the surface also increases.

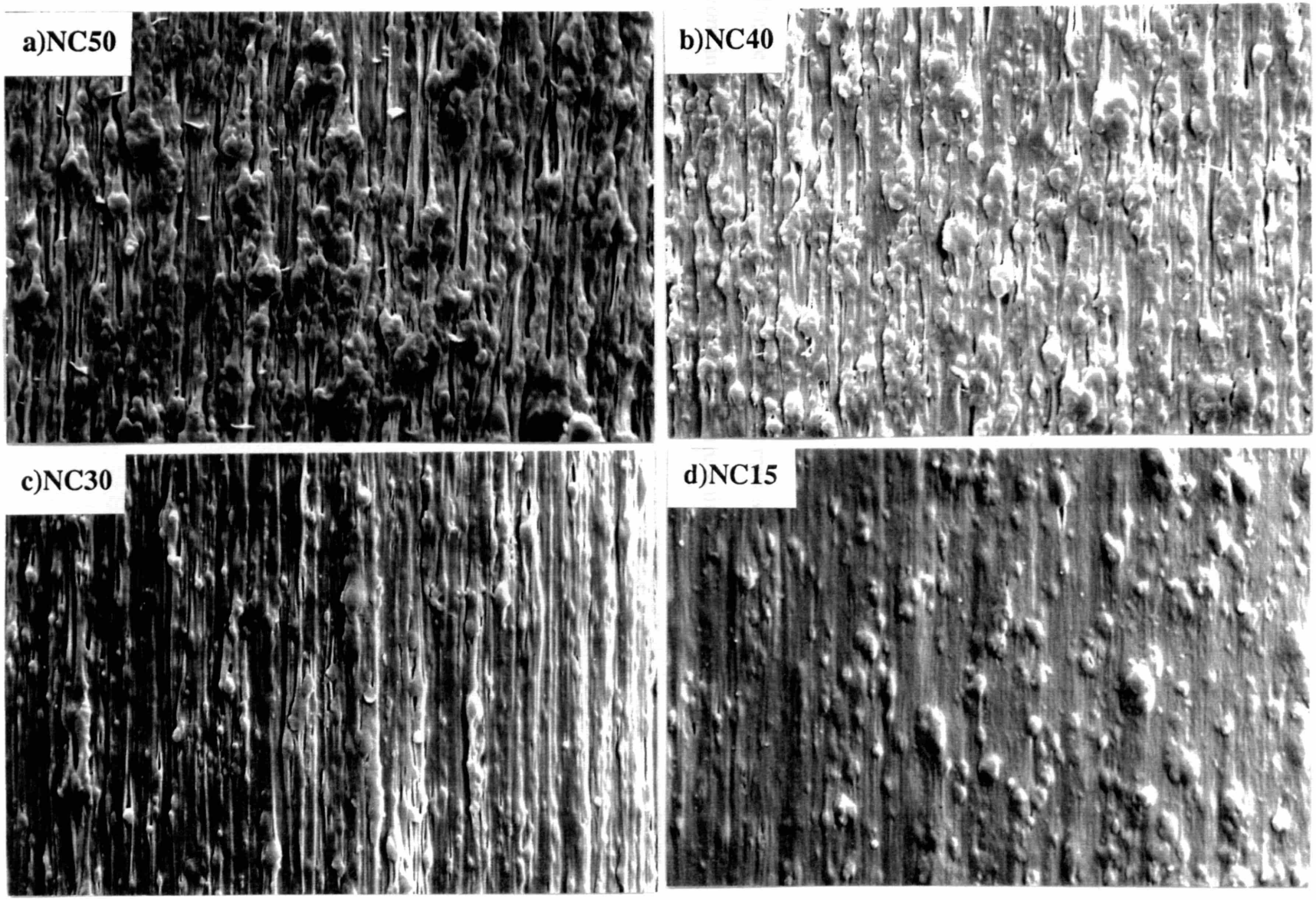
a)NC50
b)NC40
c)NC30
d)NC15

Figure 5.10. TEM micrograph of a microtomed section containing a deformation zone in a NC50 blend fiber. Starch domains are stained dark with iodine vapor.

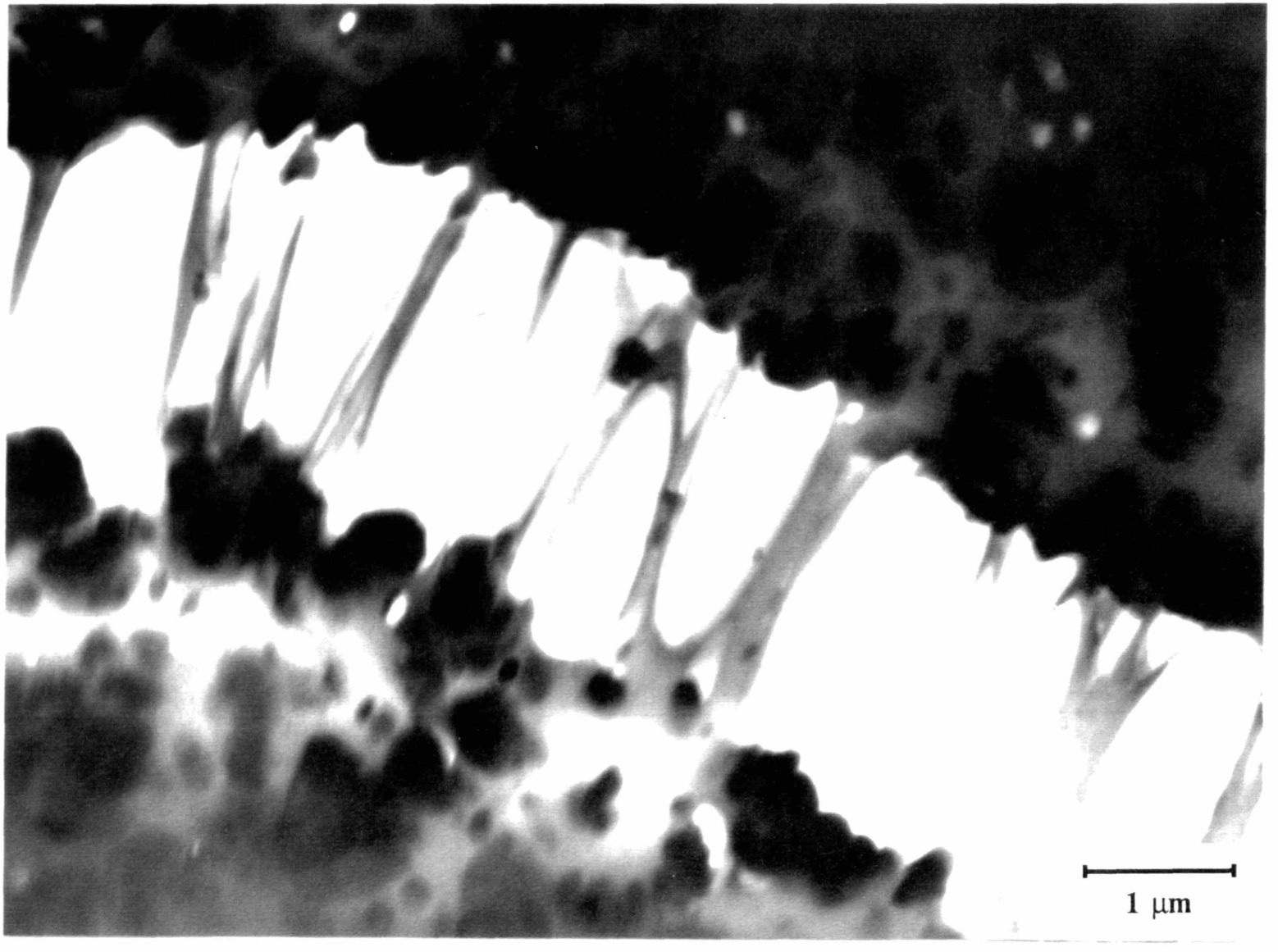
1 μm

Although the deformation that is presented in this figure occurred at room temperature, cooling of the fiber in the spin line resulted in similar behavior as depicted previously in the starch-EVOH fiber surfaces. In addition, the stress whitening observed in certain blend fibers as they were deformed may be attributed to this de-adhesion between phases (cavitation under certain loads).

The surface of an NC50 fiber as fractured at 50% RH and room temperature is shown in figure 5.11. This fiber appears to have undergone both ductile and granular fracture. The V-notch at the top of the micrograph is indicative of the ductile nature of the fracture. Granular fracture usually occurs in fibers that are not high in crystallinity and consist of components that possess relatively strong interaction [43]. Many fibers which have been prepared by solution spinning, as well as cotton and wool fibers, often exhibit granular fracture. Bicomponent and fibers made from blends can also show this behavior. Granular fracture arises when during tension, certain elements within the fiber start to break. Discontinuities in the fiber prevent the formation of a large enough stress concentration to occur across the fiber and excess stress is transferred to the remaining fiber elements. Eventually, enough elements break such that the break causes complete failure of the fiber [43]. Such fracture behavior is consistent with the previous observations of domain-size and elongational property differences between starch-rich and EVOH-rich domains which would cause variations in the local fracture behavior of the entire fiber.

As observed in figures 5.8 and 5.9, the fiber surfaces appear quite rough in SEM. A TEM cross-sectional view of the near surface region of an NC50 fiber which has been embedded in epoxy is shown in figure 5.12. A gradient structure is visible at the fiber surface as evident by the light band approximately 1 μm wide that traces the surface of the fiber and becomes progressively darker as it approaches the fiber interior. This region is predominantly unstained EVOH. Starch-rich domains are occluded by the EVOH-rich matrix and range in size from less than 0.1 μm to approximately 0.5 μm

Figure 5.11. SEM micrograph of a NC50 fiber fracture surface resulting from mechanical behavior tests (room temperature, 50% RH).

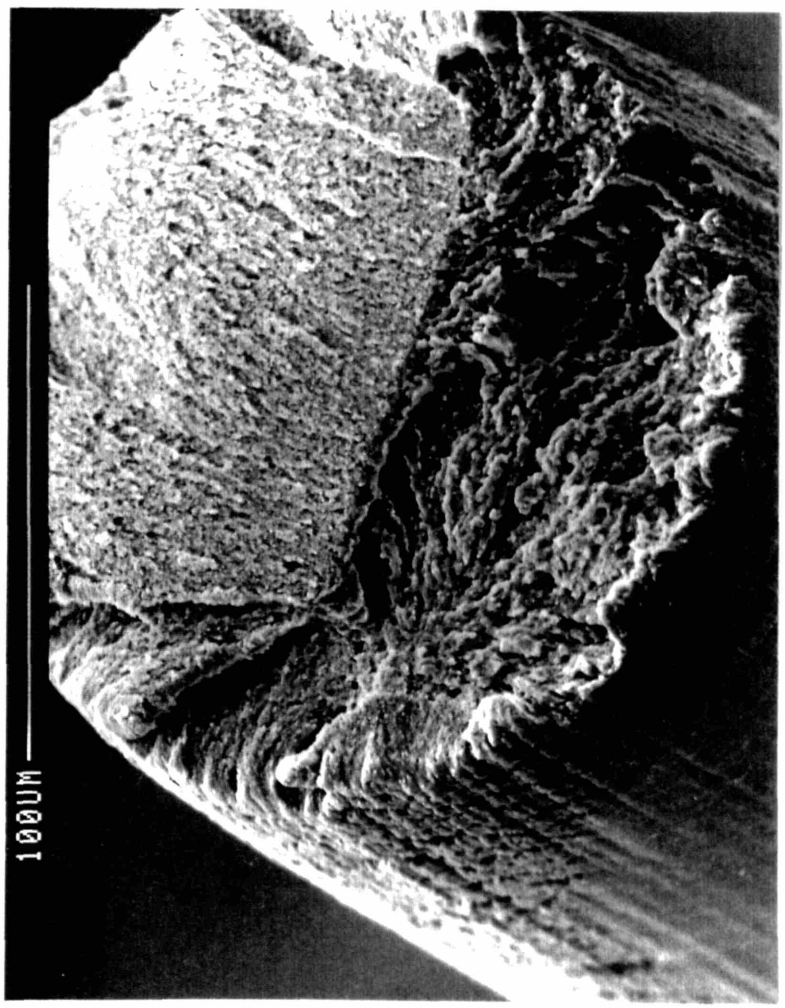
100UM

Figure 5.12. TEM micrographs depicting an axial cross-sectional view of the surface region of an NC50 fiber (d = 175 μm, $\lambda_s \sim 20$). Starch is stained dark with iodine vapor.

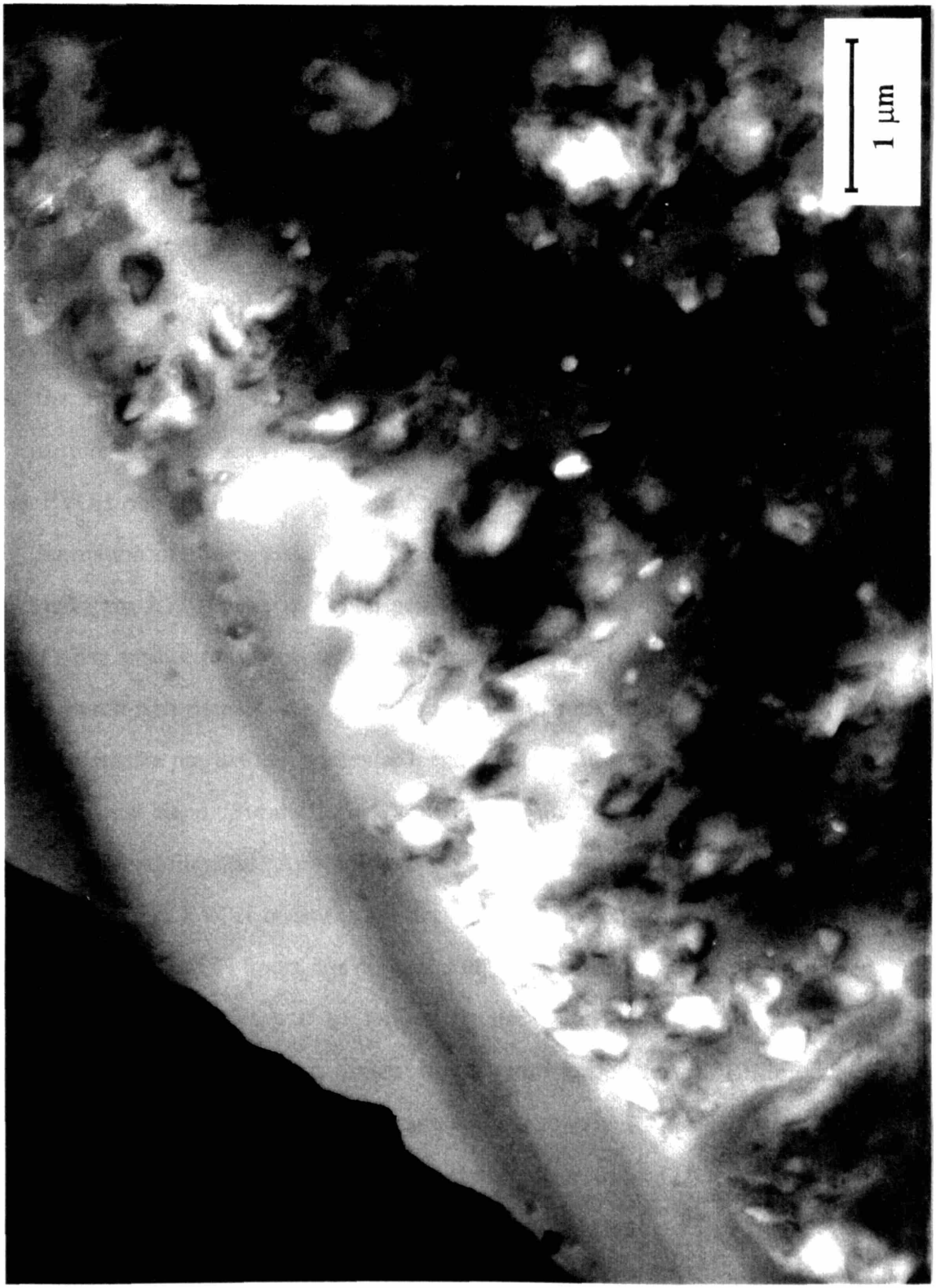
1 µm

(very light areas correspond to holes in the TEM section which may be due microvoiding). The EVOH-rich surface layer is most likely formed during flow through the spinnerette capillary when EVOH, the lower viscosity and matrix component, coats the conduit walls and, hence, the filament as it exits the spinnerette. The fiber surface cools faster than the interior, fixing the starch-rich domain structure near the surface. As the filament diameter decreases during drawing, the starch-rich domains, which do not elongate as much as the EVOH in the direction of flow, begin to project out of the surface as nodules which are coated by a thin layer of the EVOH. Thus, the two techniques, SEM and TEM, give a consistent picture of the microstructure at the surface (i.e. nodules are equivalent to starch-rich domains covered with an EVOH-rich coating).

Formation of fibrils and cavitation at the surface of this NC50 fiber is also evident in figure 5.12 (Epoxy monomer penetrates into areas where the EVOH is not present.). The surface roughness will only become greater with increasing draw ratio, since the starch-rich domains do not appear to significantly orient. The size of the starch-rich domains present in a particular blend will also limit the ultimate draw ratio attainable for that blend. Similar surface roughness is observable in biaxially oriented starch/EVOH blend films (see Appendix B).

The fact that EVOH coats the surfaces of fibers and filaments will effect the properties of starch/EVOH fibers. As discussed in Chapter 3, both biodegradability and certain transport properties will be limited by the EVOH component. At room temperature, the EVOH coating makes fibers more resistant to swelling when submersed in water (mechanical properties suffer, however, since EVOH allows transport of water molecules thus weakening the starch fraction [7]). Boiling water treatment causes significant changes to the appearance of the surface (see figure 5.13) since the temperature is now above the glass transition of EVOH (Tg ~ 55°C). For the HY50 filament, EVOH relaxes and smoothes out any surface roughness on the filament

Figure 5.13. SEM micrographs showing the effect of boiling water on the surface of starch/EVOH blends: a) an HY50 filament, b) an NC50 fiber, and c) a WM50 fiber. No change in the surface appearance of the HY50 filament is apparent. Nodules (~ 1 μm) are formed on the NC50 fiber. No oriented or nodular texture is apparent on the WM50 treated surface which initially exhibited EVOH-rich fibrils.

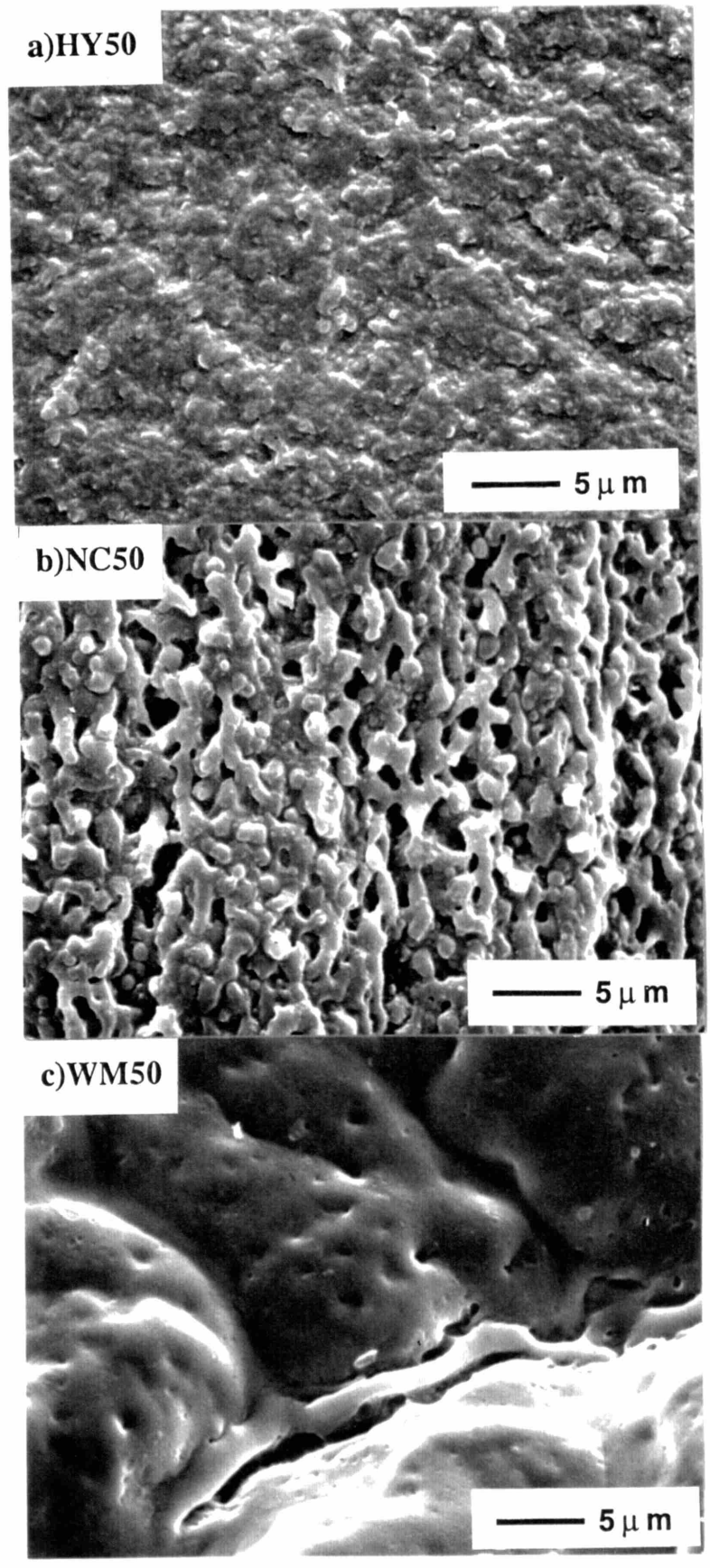
a)HY50
5 μ m
b)NC50
5 μ m
c)WM50
5 μ m

surface. For the NC50 fiber, EVOH fibrils break, EVOH flows over the starch rich-domains forming nodules approximately 1 μm in size. (Note, the appearance of these nodules are similar to those observed in commercially available Mater-Bi® blends which were attributed to the synthetic polymer component [44].) Since the WM starch disintegrates most easily in water, the fiber swells, some starch is lost, and a smoother EVOH-rich surface is observed upon drying of the filament.

Mechanical Properties

The mechanical properties of starch/EVOH blends depend on a number of factors. First, blend composition and starch type will determine the approximate behavior of these materials. Mechanical properties are also a function of storage condition since the blends undergo significant moisture uptake (8-35%) at 100% RH even with high levels of EVOH [45]. (Part of this moisture sensitivity may be attributed to the glycerin plasticizer which also absorbs moisture.) Previous studies on starch/EVOH and starch/PVOH fibers have shown that the mechanical properties vary significantly for compositions of approximately 50% starch [7]. Mechanical properties will also depend on the level of orientation (and crystallinity) within a system. In the present study, the effect of the orientation that results from fiber spinning on the mechanical properties is investigated.

Tabulated mechanical properties for blend filaments and fibers for selected blends are shown in Table 5.3. Fibers were tested immediately after spinning and after conditioning for one week at 50% RH; and the moisture contents presented represent the values at the time of testing. The mechanical behavior of starch/EVOH fibers at various compositions and draw ratios are shown in figure 5.14. The EVOH/GLY control which has been spun drawn such that the measured ratio of the spinnerette area to that of the fiber cross-section is 215 +/- 16. The EVOH/GLY control exhibits the greatest toughness and mechanical behavior profile is similar to commercially drawn

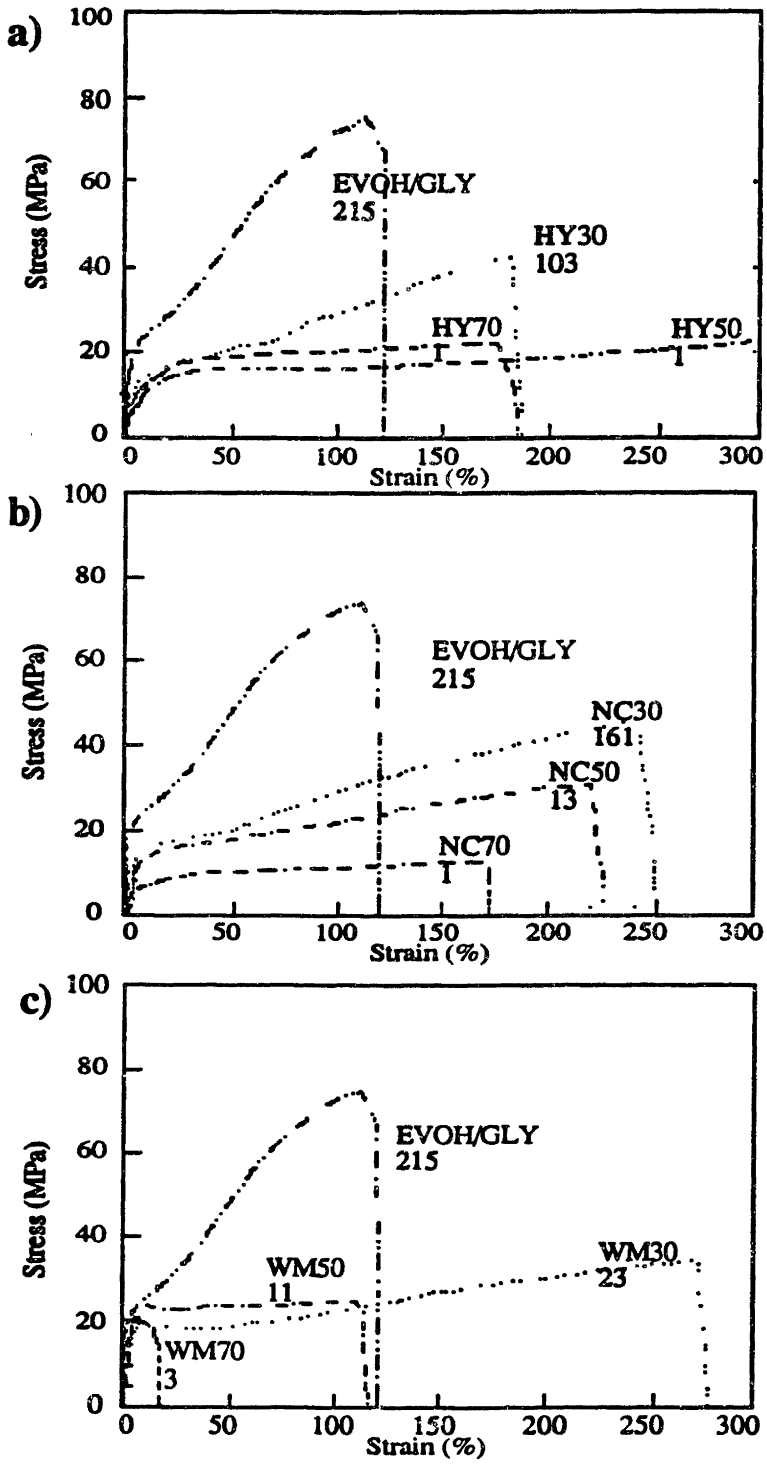

Figure 5.14. Mechanical behavior of selected starch/EVOH "fibers" with their corresponding draw ratios: a) HY series b) NC series, c) WM series. The EVOH/GLY control is shown in each plot for comparison. Testing performed after conditioning at 50% RH.

fibers except for very high strain to break (119 +/- 13%) which indicates that it can undergo significant strengthening by further fiber drawing steps. Mechanical properties of the fibers containing starch are much weaker than the synthetic polymer control sample. All exhibit lower moduli and tensile strengths, but some blends possess high elongational properties (e.g. HY50, WM30, NC30). Certain fibers undergo necking which may indicate that molecular orientation is not quite achieved at lower draw ratios (e.g. WM50, $\lambda_S = 11$). Because the mechanical properties are dependent on processing conditions, material properties for different starch types and compositions can only be compared at similar draw ratios.

Values for tensile modulus, strength, and ultimate strain for the filaments ($\lambda_S \leq 1$) are shown in figure 5.15. Overall, the mechanical properties of the undrawn filaments approximately correspond to data presented by George, Sullivan, and Park for starch/EVOH injection molded specimens [1] in that property variations with composition are similar; however, the measured values for modulus in this study are lower in magnitude. Tensile modulus increases as the amount of starch in the blend increases whereas tensile strength and strain decrease. Differences between starch types are not significant except that for starch contents, greater than 50%, waxy maize exhibits the lowest elongation. Below 50% starch, all blends possess moduli, strength, and elongational properties similar to the EVOH/GLY control.

The modulus will become higher as polymer chains become oriented and crystallize as they are spun drawn. The effect of spin draw ratio on the tensile modulus for selected starch/EVOH blends is depicted in Figure 5.16. For the 50% starch blends, the magnitude of modulus increases steeply for the WM50 as it is drawn to even low draw ratios (figure 5.16a). NC50 blends show a less sharp rise in modulus with draw, and the HY50 blend was not able to draw at all. In Chapters 2 and 3, it was shown that EVOH exists as the matrix component at this composition for all three starch blends and that the amylose and EVOH fractions are partially miscible. The WM50 blend,

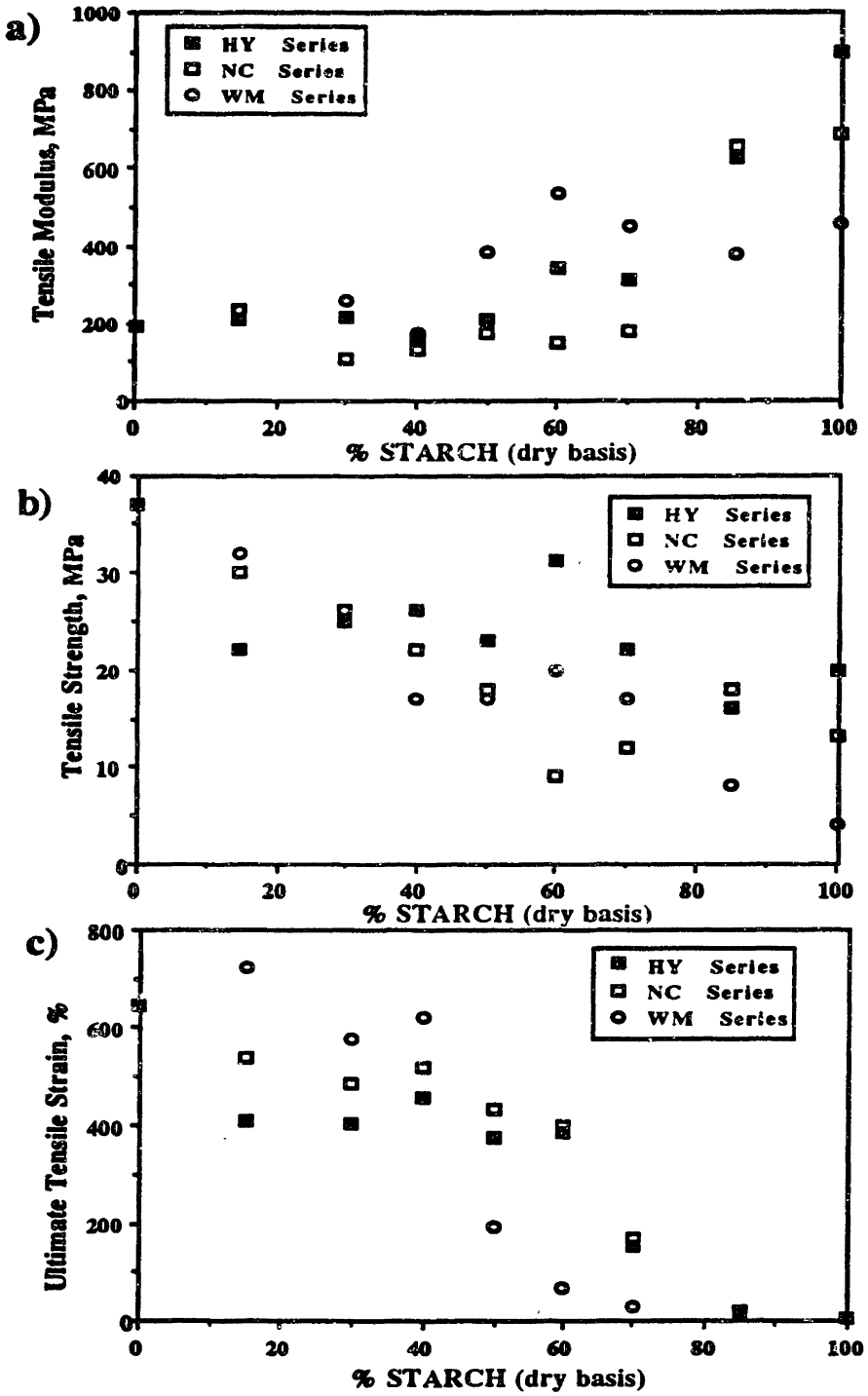

Figure 5.15. Mechanical properties of the starch/EVOH blend filaments (draw ratio ≤ 1) as a function of starch content: a) tensile modulus, b) tensile strength, and c) ultimate tensile modulus.

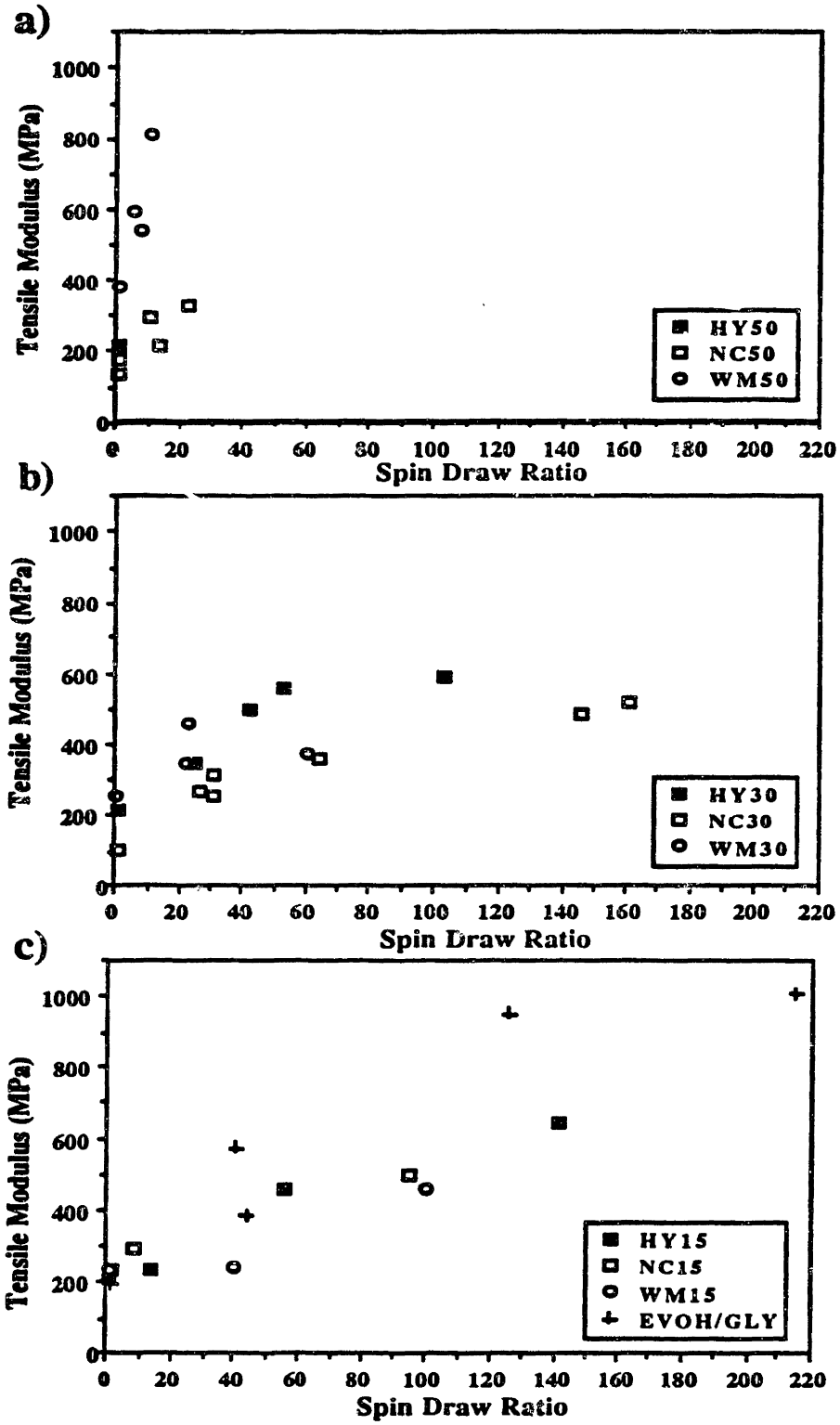

Figure 5.16. The effect of spin draw ratio on the tensile modulus for selected starch/EVOH blend fibers: a) 50% starch (dry basis), b) 30% starch, and c) 15% starch, EVOH/GLY control.

exhibiting little miscibility, would have a purer EVOH phase which is able to orient more easily and debond from the starch phase when subjected to elongational flow. In addition, the waxy maize starch domains may flow (and orient) more than the NC or HY starches as the matrix elongates since it possesses a lower viscosity. Conversely, EVOH polymer chains are inhibited from strongly orienting in HY blends due to their favorable interaction with the higher viscosity starch.

At even lower starch content (30% and 15%), the variation in modulus increases as the spin draw ratio becomes even higher (figures 5.16b and c). Values for modulus for the EVOH/GLY control are given in figure 5.16c for comparison. At 30% starch content, higher values for modulus are initially attained by the WM blend followed by HY blend. Although the NC blend undergoes the highest level of draw, its modulus is lower than the HY blends. This difference is not easily explainable, but may be due to contribution to modulus by the starch fraction ($E_{NC} < E_{HY}$). At 15% starch content, behavior of the starch types is similar since the majority EVOH component dominates the initial stiffness properties of the material. Modulus of the EVOH/GLY control is higher than the 15% starch blends even at similar draw ratios (except for the undrawn filaments). This behavior can be attributed to the larger amount of oriented crystalline EVOH in this sample.

Values for tensile strength (not plotted) are comparable among the starch/EVOH blends and the control sample at similar draw ratios indicating again EVOH is carrying most of the load in the fibers. Ultimate tensile strain, however, is higher for the starch containing blends which seems to confirm that the EVOH component is not highly oriented or crystalline in these melt-spun fibers, and can therefore undergo higher extensions before breakage (and as shown in figure 5.11). Although phase separated, interfacial adhesion between the starch-rich and EVOH-domains is sufficient for the blends to withstand loads similar to that of the EVOH/GLY control.

CONCLUSIONS

Melt fiber spinning was performed to explore the thermoplastic processability, mechanical properties, and structural characteristics of oriented filaments made from thermoplastic starch-based blends. Polymer blends of amylose and amylopectin (from three corn starch varieties) with EVOH were achieved during prior extrusion blending with glycerin and water as plasticizers (i.e. granular structure was destroyed). Thus, items made from blends of thermoplastic starch can be processed and possess relatively acceptable mechanical properties even up to intermediate starch loadings (in comparison to polyolefin films containing dry starch filler).

Overall, drawability was a strong function of EVOH composition. Blends containing a majority of EVOH had sufficient elongational properties to draw ($\lambda_S > 1$). Calculated spin draw ratios, λ_S, obtained for these materials ranged from less than 1 to 215. The extensibility of the starch-rich domains was very low, especially for any crystalline starch fraction. The high amylose (HY) blends exhibited very little drawability at compositions from 50 to 100% starch due to the high viscosity and partial miscibility of the Hylon VII starch with EVOH. Native corn (NC) blends could be spun at compositions of 50% starch or lower. Waxy maize blends, though more susceptible to melt flow instabilities, had the ability to spin at compositions with as much as 70% starch ($\lambda_S = 3$). Die swell at the spinnerette orifice was significant for the waxy maize blends, which contain only amylopectin (reaching a value of 1.8 for the WM100 blend), whereas the high amylose, HY, blends exhibited no die swell.

Blends with higher quantities of starch exhibited mechanical properties which depended more upon starch content than variety. Differences in fiber mechanical properties among the starch varieties were observed for similar draw ratios as a result of the differing starch-rich domain sizes among blends. Most of the elongational properties are due to the EVOH matrix component, and debonding of the EVOH matrix from the starch-rich domains is one route to failure in items made with starch/EVOH

blends. Fracture surfaces of starch/EVOH fibers show a combination of both ductile and granular fracture at 50% RH. Microscopic investigations reveal that the surfaces of the filaments, initially smooth and coated with EVOH, roughen significantly (± 0.5 μm thickness variations for a NC50 fiber). At high draw ratios, EVOH-rich fibrils, starch-rich nodules, and cavitated areas are observed. Overall, filaments and fibers made from the HY blends show the most resistance to swelling and surface modification in boiling water.

REFERENCES

1. E.R. George, T.M. Sullivan and E.H. Park, 'Thermoplastic Starch Blends with a Poly(Ethylene-co-Vinyl Alcohol): Processability and Physical Properties,'*Polymer Engineering and Science*, **34,** 17 (1994).

2. M.A. Villar, E.L. Thomas and R.C. Armstrong, 'Rheological Properties of Thermoplastic Starch and Starch/Poly(ethylene-co-vinyl alcohol) Blends,'*Polymer*, (submitted 1994).

3. C.E. Weigand, 'Thermoplastic Processing of Starch and Starch-Based Systems', MS Thesis, Massachusetts Institute of Technology (1992).

4. R.L. Whistler and G.E. Hilbert, 'Mechanical Properties of Films from Amylose, Amylopectin, and Whole Starch Triacetates,'*Industrial & Engineering Chemistry*, **36,** 796 (1944).

5. H.F. Zobel, 'Molecules to Granules: A Comprehensive Starch Review,'*Starch/Starke*, **40,** 44 (1988).

6. N.E. Lloyd and L.C. Kirst, 'Some Factors Affecting the Tensile Strength of Starch Films,'*Cereal Chemistry*, **40,** 154 (1963).

7. S. Simmons, C.E. Weigand, R.J. Albalak, R.C. Armstrong and E.L. Thomas, 'Thermoplastic Processing of Starch: Melt Spinning of Starch-Based Fibers', in *Biodegradable Polymers and Packaging*, D.L. Kaplan, C. Ching and E.L. Thomas, Eds. 1993, Technomic Publishing Co.: Lancaster, PA. p. 171.

8. G. Lay, J. Rehm, R.F. Stepto, M. Thoma, J.-P. Sachetto, D.J. Lentz and J. Silbiger, 'Polymer Composition Containing Destructurized Starch', in *United States Patent No. 5,095,054*, Warner-Lambert Company, 1992.

9. R.P. Westhoff, W.F. Kwoleck and F.H. Otey, 'Starch-Polyvinyl Alcohol Films - Effect of Various Plasticizers,'*Starch/Starke*, **31,** 163 (1979).

10. M. Wooton and A. Bamunuarachichi, 'Water Binding Capacity of Commercial Produced Native and Modified Starches,'*Starch*, **30,** 306 (1978).

11. F.S. Buehler, V. Baron, E. Schmid, P. Meler and H.J. Schultz, 'Procedure for Creation and Use of Starch Fibers', in *Eur Patent: 0541050A3*, EMS-INVENTA, Ed. 1993: Germany.

12. S. Akuzawa, S. Sawayama and A. Kawabata, 'Spinnability of Starch Pastes,'*Biosci. Biotech. Biochem.*, **56,** 932 (1992).

13. F.R. Senti and L.P. Withauer, 'Oriented Filaments of Amylose and Alkali Amylose,'*J. Amer. Chem. Soc.*, **68,** 2407 (1947).

14. I.A. Wolff, D.W. Olds and G.E. Hilbert, 'Triesters of Corn Starch, Amylose, and Amylopectin: Properties,'*Industrial and Eng. Chem.*, **43,** 911 (1951).

15. I.A. Wolff, H.A. Davis, J.E. Cluskey, L.J. Gundrum and C.E. Rist, 'Preparation of Films from Amylose,'*Ind. Eng. Chem.*, **43,** 915 (1951).

16. R.E. Rundle, L. Daasch and D. French, 'The Structure of the "B" Modification of Starch from Film and Fiber Diffraction Diagrams,'*J. Amer. Chem. Soc.*, **66,** 130 (1944).

17. A. Sarko and H.-C.H. Wu, 'The Crystal Structure of A-, B-, and C-Polymorphs of Amylose and Starch,'*Starch/Starke*, **30,** 73 (1978).

18. H.-C.H. Wu and A. Sarko, 'The Crystal Structure of A-Starch is it Double Helical?,'*Carbohydreate Research*, **54,** C3 (1977).

19. H.-C.H. Wu and A. Sarko, 'The Double-Helical Molecular Structure of Crystalline A-Amylose,'*Carbohydrate Research*, **61,** 27 (1978).

20. H.-C.H. Wu and A. Sarko, 'The Double-Helical Molecular Structure of Crystalline B-Amylose,'*Carbohydrate Research*, **61,** 7 (1978).

21. A.M. Mark and C.L. Mehltretter, 'Water-Soluble Films from Partially Acetylated High-Amylose Corn Starch,'*Die Starke*, **21,** 92 (1969).

22. A.M. Mark and C.L. Mehltretter, 'Acetylation of High-Amylose Corn Starch,'*1970*, **22,** 108 (1970).

23. R. Takahashi and A. Nakamura, 'Properties of Starch Films and their Improvement,'*Die Starke*, **22,** 309 (1970).

24. F.H. Otey, A.M. Mark, C.L. Mehltretter and C.R. Russell, 'Starch-based Film for Degradable Agricultural Mulch,'*I&EC Prod. Res. And Dev.*, **13,** 90 (1974).

25. F.H. Otey, R.P. Westhoff and C.R. Russell, 'Starch Graft Copolymers - Degradable Fillers for Poly(vinyl chloride) Plastics,'*I&EC Prod. Res. and Dev.*, **15,** 139 (1976).

26. F.H. Otey, R.P. Westhoff and C.R. Russell, 'Biodegradable Films from Starch and Ethylene-Acrylic Acid Copolymer,'*Ind. Eng. Chem. Prod. Res. Dev.*, **16,** 305 (1977).

27. F.H. Otey, R.P. Westhoff and W.M. Doane, 'Starch-based Blown Films,'*I&EC Prod. Res. and Dev.*, **19,** 592 (1980).

28. F.H. Otey and R.P. Westhoff, 'Starch-based Films: Preliminary Diffusion Evaluation,'*I&E Prod. Res. and Dev.*, **23,** 284 (1984).

29. F.H. Otey, R.P. Westhoff and W.M. Doane, 'Starch-based Blown Films 2,'*I&EC Research*, **26,** 1659 (1987).

30. H. Roper and H. Koch, 'The Role of Starch in Biodegradable Thermoplastic Materials,'*Starch/Starke*, **42,** 123 (1990).

31. Z. Tadmor and C.G. Gogos, *Principles of Polymer Processing*. 1979, New York: John Wiley & Sons. 521.

32. Z.K. Walczak, *Formation of Synthetic Fibers*. 1977, New York: Gordon and Breach.

33. A. Ziabicki, *Fundamentals of Fibre Formation*. 1976, London: John Wiley & Sons.

34. D.R. Paul, 'Fibers from Polymer Blends', in *Polymer Blends*, D.R. Paul and S. Newman, Eds. 1978, Academic Press: New York. p. 167.

35. H. Vanoene, 'Modes of Dispersion of Viscoelastic Fluids in Flow,'*Journal of Colloid and Interface Science*, **40,** 448 (1972).

36. 'Constant Test Atmospheres over Aqueous Solutions', in *Deutsche Normen*. 1981.

37. G.J.L. Griffin, *J. Polym. Sci. Polym. Symp.*, **57,** 281 (1976).

38. G.J.L. Griffin, *Pure Appl. Chem.*, **52,** 399 (1980).

39. S.M. Goheen and R.P. Wool, 'Degradation of Polyethylene-Starch Blends in Soil,'*J. Appl. Polym. Sci.*, **42,** 2691 (1991).

40. R.L. Evangelista, Z.L. Nikolov, W. Sung, J.-L. Jane and R.J. Gelina, 'Effect of Compounding and Starch Modification on Properties of Starch-Filled Low-Density Polyethylene,'*Ind. Eng. Chem. Res.*, **30,** 1841 (1991).

41. A.-C. Albertsson and S. Karlsson, 'Degradable Polyethylene-Starch Complex,'*Makromol. Chem., Macromol. Symp.*, **48/49,** 395 (1991).

42. J.L. Willett, B.K. Jasberg and C.L. Swanson, 'Rheology of Thermoplastic Starch: Effects of Temperature, Moisture Content, and Additives on Melt Viscosity,'*Polymer Engineering and Science*, **35,** 202 (1995).

43. J.W.S. Hearle, B. Lomas, W.D. Cooke and I.J. Duerdon, *Fiber Failure and Wear of Materials: An Atlas of Fracture, Fatigue, and Durability*. Polymer Science and Technology, ed. T.J. Kemp and J.F. Kennedy. 1989, Chichester, UK: Ellis Horwood Limited.

44. C. Bastioli. *Mater-Bi: Properties and Biodegradability*. in *Environmentally Degradable Polymers: Technical, Business, and Public Ferspectives (August 13-15, 1991)*. 1991. Chelmsford, MA.

45. T. Sullivan, personal communication (1993).

Table 5.1a. Optimum Spinning Conditions for the Starch/EVOH Blends (as stored, do = 762 μm)

Blend	Moisture Content (%) Pellets	Moisture Content (%) Fibers	Melt Head Temp. (°C)	Sample Bulk Temp. (°C)	Spinnerette Temp. (°C)
High Amylose Starch (Hylon VII) Blends:					
HY100	7.3	6.7	190	164	142
HY85	7.6	7.2	182	159	136
HY70	10.8	10.3	160	138	128
HY60	9.8	9.6	161	142	118
HY50	8.7	8.4	161	138	137
HY40	6.7	6.0	150	131	123
HY30	7.0	8.3	160	148	139
HY15	6.1	5.6	160	141	131
Native Corn Starch Blends:					
NC100	16.9	15.7	160	145	130
NC85	9.5	8.6	160	140	124
NC70	12.5	12.6	160	145	138
NC60	8.1	6.2	160	148	125
NC50	11.0	9.4	160	147	148
NC40	5.1	4.4	150	137	120
NC30	6.2	6.6	170	151	148
NC15	5.7	5.5	161	142	122
Waxy Maize Starch Blends:					
WM100	6.6	6.1	160	148	128
WM85	8.6	8.7	153	138	121
WM70	5.3	5.2	160	145	131
WM60	7.8	6.2	161	138	116
WM50	10.1	9.2	160	145	144
WM40	5.2	4.1	150	135	113
WM30	6.9	7.4	160	150	148
WM15	4.1	5.0	160	145	131
Poly(ethylene-co-vinyl alcohol) Control:					
EVOH/GLY	1.9	2.1	165	151	139

Table 5.1b. Optimum Spinning Conditions for the Starch/EVOH Blends (as stored, do = 762 μm)

Blend	Apparent Shear Rate (s^-1)	Corrected Shear Rate (s^-1)	Mass Flow Rate (g/min)	Filament Diameter (μm)	Fiber Diameter (μm)	Draw Ratio	Die Swell
High Amylose Starch (Hylon VII) Blends:							
HY100	68	194	0.27	792	792	0.9	1.0
HY85	40		0.17	775	775	1.0	1.0
HY70	100	167	0.37	772	772	1.0	1.0
HY60	128		0.54	768	768	1.0	1.0
HY50	205	318	0.61	772	742	1.1	1.0
HY40	191		0.60	740	213	13	1.0
HY30	229	284	0.77	763	75	103	1.0
HY15	286		0.75	650	64	142	0.9
Native Corn Starch Blends:							
NC100	223	381	0.91	899	899	0.7	1.2
NC85	328		0.34	850	850	0.8	1.1
NC70	427	321	1.03	823	823	0.9	1.1
NC60	445		1.32	747	303	6	1.0
NC50	229	305	0.92	752	208	13	1.0
NC40	233		0.86	730	101	57	1.0
NC30	321	374	0.90	644	60	161	0.8
NC15	158		0.41	687	78	95	0.9
Waxy Maize Starch Blends:							
WM100	197	255	0.89	1400	1400	0.3	1.8
WM85	151		0.65	1255	1255	0.4	1.6
WM70	151	194	0.73	1200	412	3.4	1.6
WM60	133		0.71	1080	1080	0.5	1.4
WM50	166	201	0.81	1012	230	11	1.3
WM40	175		0.76	912	198	15	1.2
WM30	322	367	1.14	820	159	23	1.1
WM15	294		0.71	787	76	101	1.0
Poly(ethylene-co-vinyl alcohol) Control:							
EVOH/GLY	274		0.82	745	52	215	1.0

Table 5.2a. Optimum Spinning Conditions for the Starch/EVOH Blends (pellets conditioned at 50%RH, do = 762 μm)

Blend	Moisture Content (%) Pellets	Moisture Content (%) Fibers	Melt Head Temperature (°C)	Sample Bulk Temp. (°C)	Spinnerette Temp. (°C)
High Amylose Starch (Hylon VII) Blends:					
HY100	5.8	-	201	176	140
HY85	5.5	-	200	170	136
HY70	6.0	5.0	185	163	130
HY60	5.6	6.1	160	148	147
HY50	5.9	6.6	170	143	105
HY40	5.4	6.4	160	147	148
HY30	5.1	4.5	160	138	125
HY15	4.6	4.5	160	138	137
Native Corn Starch Blends:					
NC100	8.4	8.9	160	143	118
NC85	6.0	6.7	160	141	137
NC70	7.8	6.7	160	143	115
NC60	6.2	6.3	160	136	134
NC50	5.9	6.2	155	135	104
NC40	5.0	7.6	150	136	136
NC30	5.0	4.8	150	134	127
NC15	4.9	5.3	160	143	144
Waxy Maize Starch Blends:					
WM100	7.6	7.5	145	133	111
WM85	7.1	6.7	160	142	146
WM70	6.0	5.3	160	138	108
WM60	5.8	6.4	145	135	134
WM50	5.4	5.2	145	129	97
WM40	5.4	5.9	145	136	137
WM30	5.1	4.7	160	139	122
WM15	3.8	5.0	160	144	146
Poly(ethylene-co-vinyl alcohol) Control:					
EVOH/GLY	3.7	4.6	145	141	143

Table 5.2b. Optimum Spinning Conditions for the Starch/EVOH Blends (pellets conditioned at 50%RH, do = 762 μm)

Blend	Apparent Shear Rate (s^-1)	Corrected Shear Rate (s^-1)	Mass Flow Rate (g/min)	Filament Diameter (μm)	Fiber Diameter (μm)	Draw Ratio	Die Swell
High Amylose Starch (Hylon VII) Blends:							
HY100	No flow	-	-	-	-	-	-
HY85	No flow	-	-	-	-	-	-
HY70	98	165	0.31	769	769	1.0	1.0
HY60	77		0.27	788	788	0.9	1.0
HY50	108	167	0.35	802	802	0.9	1.1
HY40	187		0.64	773	262	8	1.0
HY30	180	223	0.55	760	153	25	1.0
HY15	124		0.67	797	208	13	1.0
Native Corn Starch Blends:							
NC100	49	83	0.25	928	928	0.7	1.2
NC85	59		0.26	871	871	0.8	1.1
NC70	134	101	0.70	876	876	0.8	1.1
NC60	186		0.93	771	771	1	1.0
NC50	196	261	0.67	783	229	11	1.0
NC40	241		0.84	772	184	17	1.0
NC30	268	313	0.75	613	95	64	0.8
NC15	186		0.34	737	268	8	1.0
Waxy Maize Starch Blends:							
WM100	109	141	0.49	1122	1122	0.5	1.5
WM85	143		0.67	1267	1267	0.4	1.7
WM70	142	182	0.74	1039	1039	0.5	1.4
WM60	124		0.76	1015	1015	0.6	1.3
WM50	158	191	0.62	865	278	8	1.1
WM40	176		0.81	933	230	11	1.2
WM30	194	221	0.63	803	98	60	1.1
WM15	267		0.75	837	121	40	1.1
Poly(ethylene-co-vinyl alcohol) Control:							
EVOH/GLY	211		0.68	743	68	126	1.0

Table 5.3a. Mechanical Properties of Hylon VII/EVOH Blends

Sample	Diameter (μm)	Draw Ratio	Moisture Content (%)	Tensile Strength (MPa)	Ultimate Tensile Strain (%)	Tensile Modulus (MPa)
HY100	790 ± 7	0.9 ± 0.0	6.5	20 ± 2	4 ± 1	894 ± 38
	792 ± 4	0.9 ± 0.0	6.7	20 ± 2	4 ± 1	927 ± 46
HY85	775 ± 9	1.0 ± 0.0	7.2	16 ± 1	16 ± 2	619 ± 41
HY70	772 ± 1	1.0 ± 0.0	7.2	22 ± 0	155 ± 9	310 ± 18
	770 ± 1	1.0 ± 0.0	6.1	23 ± 0	170 ± 10	301 ± 25
	769 ± 13	1.0 ± 0.0	5.0	21 ± 1	229 ± 8	139 ± 10
HY60	788 ± 4	0.9 ± 0.0	5.3	31 ± 1	478 ± 15	341 ± 22
	768 ± 1	1.0 ± 0.0	4.8	31 ± 1	386 ± 32	422 ± 17
HY50	772 ± 2	1.0 ± 0.0	5.7	23 ± 2	400 ± 38	212 ± 14
	742 ± 1	1.1 ± 0.0	5.6	16 ± 1	374 ± 16	201 ± 17
HY40	740 ± 13	1.1 ± 0.0	8.3	26 ± 0	461 ± 36	161 ± 14
	262 ± 19	8.5 ± 0.6	6.7	31 ± 5	343 ± 49	160 ± 19
	213 ± 26	12.8 ± 1.6	7.0	29 ± 3	283 ± 48	173 ± 19
HY30	763 ± 22	1.0 ± 0.0	5.0	25 ± 5	402 ± 78	215 ± 20
	153 ± 18	24.8 ± 2.9	5.0	38 ± 7	163 ± 57	350 ± 43
	117 ± 15	42.4 ± 5.4	4.6	31 ± 5	207 ± 30	502 ± 47
	105 ± 13	52.7 ± 6.5	5.0	39 ± 2	160 ± 54	562 ± 43
	75 ± 11	103.2 ± 15.1	4.6	34 ± 5	176 ± 21	594 ± 57
HY15	797 ± 4	0.9 ± 0.0	6.7	22 ± 5	409 ± 50	208 ± 4
	208 ± 30	13.4 ± 1.9	4.4	29 ± 4	216 ± 56	237 ± 32
	102 ± 6	55.8 ± 3.3	6.1	49 ± 4	170 ± 30	456 ± 87
	64 ± 5	141.8 ± 11.1	6.7	52 ± 3	164 ± 17	643 ± 17

Table 5.3b. Mechanical Properties of Native Corn starch/EVOH Blends

Sample	Diameter (μm)	Draw Ratio	Moisture Content (%)	Tensile Strength (MPa)	Ultimate Tensile Strain (%)	Tensile Modulus (MPa)
NC100	928 ± 24	0.7 ± 0.0	8.0	6 ± 3	2 ± 1	687 ± 24
	899 ± 40	0.7 ± 0.0	8.4	13 ± 4	2.6 ± 0	798 ± 18
NC85	871 ± 8	0.8 ± 0.0	5.9	18 ± 1	22 ± 2	650 ± 33
	850 ± 3	0.8 ± 0.0	5.9	23 ± 1	29 ± 1	816 ± 44
NC70	876 ± 8	0.8 ± 0.0	6.7	12 ± 3	172 ± 26	183 ± 6
	823 ± 19	0.9 ± 0.0	7.8	11 ± 1	125 ± 17	138 ± 8
NC60	771 ± 6	1.0 ± 0.0	6.2	9 ± 1	401 ± 9	150 ± 9
	303 ± 16	6.3 ± 0.3	6.2	12 ± 3	272 ± 66	214 ± 19
NC50	783 ± 9	0.9 ± 0.0	5.9	18 ± 0	372 ± 23	174 ± 14
	752 ± 5	1.0 ± 0.0	5.9	24 ± 1	434 ± 29	134 ± 5
	229 ± 14	11.1 ± 0.7	5.3	19 ± 1	110 ± 7	296 ± 56
	208 ± 33	13.4 ± 2.1	5.8	26 ± 3	236 ± 35	212 ± 49
	160 ± 38	22.7 ± 5.4	5.9	31 ± 6	207 ± 58	325 ± 97
NC40	730 ± 14	1.1 ± 0.0	5.3	22 ± 1	523 ± 25	129 ± 12
	184 ± 31	17.2 ± 2.9	5.4	31 ± 3	280 ± 49	156 ± 30
	101 ± 10	56.9 ± 5.6	7.9	31 ± 4	131 ± 31	116 ± 87
NC30	644 ± 8	1.4 ± 0.0	5.1	26 ± 2	486 ± 68	103 ± 136
	149 ± 22	26.2 ± 3.9	4.6	35 ± 4	227 ± 57	267 ± 51
	136 ± 8	31.4 ± 1.8	5.1	44 ± 2	244 ± 25	316 ± 17
	136 ± 7	31.4 ± 1.6	5.7	43 ± 2	244 ± 20	251 ± 25
	95 ± 8	64.3 ± 5.4	4.6	47 ± 2	204 ± 15	358 ± 82
	63 ± 2	146.3 ± 4.6	5.7	44 ± 4	130 ± 22	485 ± 31
	60 ± 2	161.3 ± 5.4	5.0	47 ± 3	139 ± 13	516 ± 37
NC15	737 ± 5	1.1 ± 0.0	7.0	30 ± 2	538 ± 46	236 ± 7
	268 ± 30	8.1 ± 0.9	7.0	39 ± 1	416 ± 17	296 ± 26
	78 ± 10	95.4 ± 12.2	7.0	51 ± 2	215 ± 16	496 ± 83

Table 5.3c. Mechanical Properties of Waxy Maize starch/EVOH Blends

Sample	Diameter (μm)	Draw Ratio	Moisture Content (%)	Tensile Strength (MPa)	Ultimate Tensile Strain (%)	Tensile Modulus (MPa)
WM100	1400 ± 25	0.3 ± 0.0	7.6	4 ± 1	2 ± 1	457 ± 100
	1122 ± 52	0.5 ± 0.0	7.1	5 ± 1	2 ± 1	453 ± 24
WM85	1177 ± 26	0.4 ± 0.0	7.2	8 ± 2	5.8 ± 3	377 ± 38
	1093 ± 17	0.5 ± 0.0	7.2	2.2 ± 1	12 ± 1	172 ± 51
WM70	1054 ± 41	0.5 ± 0.0	6.8	17 ± 1	29 ± 8	452 ± 45
	436 ± 42	3.1 ± 0.3	7.0	21 ± 2	13 ± 9	685 ± 63
	410 ± 46	3.5 ± 0.4	7.2	19 ± 1	10 ± 3	690 ± 53
WM60	1080 ± 56	0.5 ± 0.0	6.6	20 ± 2	67 ± 4	534 ± 77
	1015 ± 20	0.6 ± 0.0	6.6	20 ± 1	70 ± 8	513 ± 25
WM50	865 ± 30	0.8 ± 0.0	5.7	17 ± 3	188 ± 20	380 ± 99
	314 ± 27	5.9 ± 0.5	5.7	22 ± 2	146 ± 49	593 ± 54
	278 ± 24	7.5 ± 0.6	7.5	23 ± 2	152 ± 35	538 ± 51
	230 ± 15	11.0 ± 0.7	6.0	28 ± 1	122 ± 62	808 ± 33
WM40	933 ± 70	0.7 ± 0.1	5.3	17 ± 3	620 ± 19	173 ± 30
	230 ± 14	11.0 ± 0.7	5.6	27 ± 5	173 ± 47	380 ± 62
WM30	820 ± 30	0.9 ± 0.0	5.6	26 ± 2	577 ± 50	255 ± 25
	163 ± 15	21.9 ± 2.0	6.0	34 ± 2	256 ± 21	343 ± 40
	159 ± 16	23.0 ± 2.3	4.8	39 ± 4	252 ± 21	460 ± 16
	98 ± 16	60.5 ± 9.9	5.3	39 ± 3	179 ± 32	373 ± 63
WM15	787 ± 21	0.9 ± 0.0	5.1	32 ± 3	720 ± 56	230 ± 30
	121 ± 7	39.7 ± 2.3	5.1	43 ± 1	188 ± 24	239 ± 60
	76 ± 3	100.5 ± 4.0	6.3	47 ± 4	119 ± 13	459 ± 81

Table 5.3d. Mechanical Properties of the EVOH/GLY control

Sample	Diameter (μm)	Draw Ratio	Moisture Content (%)	Tensile Strength (MPa)	Ultimate Tensile Strain (%)	Tensile Modulus (MPa)
EVOH/GLY	743 ± 48	1.1 ± 0.1	3.2	37 ± 7	645 ± 13	190 ± 9
	115 ± 7	43.9 ± 2.7	3.9	44 ± 6	121 ± 13	388 ± 34
	120 ± 3	40.3 ± 1.0	3.6	47 ± 18	139 ± 13	574 ± 107
	68 ± 4	125.6 ± 7.4	3.4	70 ± 15	31 ± 13	953 ± 40
	52 ± 4	214.7 ± 16.5	3.2	83 ± 6	19 ± 13	1006 ± 93

Chapter 6

Bubble Support Method for Preparing Thin, Equi-Biaxially Stretched Polyolefin Film for Direct TEM Observation

ABSTRACT

A model technique for preparing thin, equi-biaxially stretched polyolefin films is presented. The use of a rubber substrate is employed to support an initially dilute solution of polymer in solvent. Heat is applied to the system and the solvent evaporates leaving a thin molten polymer layer on top of the substrate. As the substrate is inflated, it forms a 'Bubble Support' for the polyolefin layer which undergoes equi-biaxial deformation. The resulting film is thin enough for direct observation in Transmission Electron Microscopy (TEM). High density polyethylene is employed to demonstrate this technique which also can be used on a wide range of semi-crystalline thermoplastics. Variation of the experimental processing conditions (i.e. temperature, inflation rate, cooling time) lead to a variety of observed morphologies that result from changes in the crystallization, relaxation, and deformation behavior of the polymer. This technique afford insight into the microstructure of semi-crystalline thermoplastics which undergo multiaxial stretching during processing.

INTRODUCTION

The physical properties of thermoplastic items such as fiber and film depend strongly on the processing history of the polymer system and its effect on the polymer microstructure. Correlation of structure/property relationships for semi-crystalline polymers and their blends under thermoplastic processing conditions has long received attention. Improvement of the property characteristics of commercially prepared blown films and thermoformed items requires an understanding of morphology development

under extensional flows. In this chapter, we seek to explore the influence of equi-biaxial extensional flow on the microstructure of semi-crystalline polyolefins using transmission electron microscopy as the key morphological probe. In particular, the effect on biaxial flow on the crystallization characteristics of linear high density polyethylene is investigated employing a small scale apparatus that requires little material (< 0.2 g.) and with which many trials under different experimental conditions can be performed. This study is complementary to the research presented in other areas of this thesis in that the effect of processing on the structure and properties of semi-crystalline polymers is the main issue, rather than the influence of blend composition.

The biaxial deformation of polyolefins has been studied in the past by several researchers. Generally, biaxially stretched films for structural analysis are made by bubble forming (film blowing) [1 - 7], by tentering (employing a stretching frame) [8 - 16], or by compression molding [3, 17 - 19]. One of the earliest studies was performed by Hopkins and co-workers [1] who used x-rays to measure the stress and orientation of polyethylene from polyethylene disks (2 - 3.5 mm thick) which were inflated until rupture at room temperature. Much of the subsequent structural changes have been characterized by bulk techniques such as x-ray and birefringence. Others [2, 12, 20, 21] have extensively used light microscopy to observe changes in the spherulitic structure of precursor films under stress. Fewer studies have been performed using transmission electron microscopy, and these generally employ surface replicas [8 - 11] or microtomed sections [16] of polymer films.

Provided that the sample is thin enough (ideally below 1000 Å for a polymer with carbon backbone), transmission electron microscopy can yield very useful information. Through amplitude and phase contrast mechanisms, the real space structure can be determined and local orientation can be detected using selected area diffraction (details about the contrast mechanisms arising in TEM were discussed in Chapter 4). This technique has been used in the past to examine melt- and gel- drawn

semi-crystalline polymer films that exhibit high levels of uniaxial orientation [22 - 34]. In these studies, films were prepared utilizing the 'Petermann method' in which high longitudinal flow gradients within an extremely short distance were employed (see figure 6.1) to yield essentially single-crystal or fiber-like textured films [22]. At low electron dose and operating the TEM at underfocus conditions to enhance phase contrast differences between crystalline and amorphous regions (For polyethylene, the mean inner potentials are 7.35 and 6.32 V, respectively.), the microstructure was revealed to consist of alternating gray (crystalline) and light (intercrystalline, amorphous) regions as shown in figure 6.2. The darkest patches correspond to crystalline areas which are oriented such that the Bragg condition is fulfilled and diffraction contrast arises in addition to phase contrast. Electron diffraction patterns taken of 'Petermann film' exhibit a fiber-like patterns resulting from alignment of the polymer molecular axes (c axis) primarily in the flow direction. Further studies examined the subsequent deformation of these films directly in the TEM [27 - 30].

The present study represents an extension of this work in which the polymer melt is not uniaxially, but equi-biaxially stretched while crystallizing. This method is similar to the Petermann technique in that very thin films are produced that can be directly examined without subsequent surface replication (which does not allow electron diffraction) or without microtoming (which introduces further deformation to the polymer film). Because very thin unsupported films were not attainable due to hole formation during film blowing, a flexible substrate is chosen to support the polymer film. This set-up also incorporates certain aspects of a technique previously employed by Haas and Geil in which they examined the room temperature deformation of polyethylene single crystals which were deposited onto a Mylar or Viton bubble support [35]. However, in this case, a molten polymer layer is formed from evaporation of a hot, dilute polymer solution which was placed on the rubber substrate. Once the molten layer is formed, the substrate is inflated, stretching the melt while it cools and

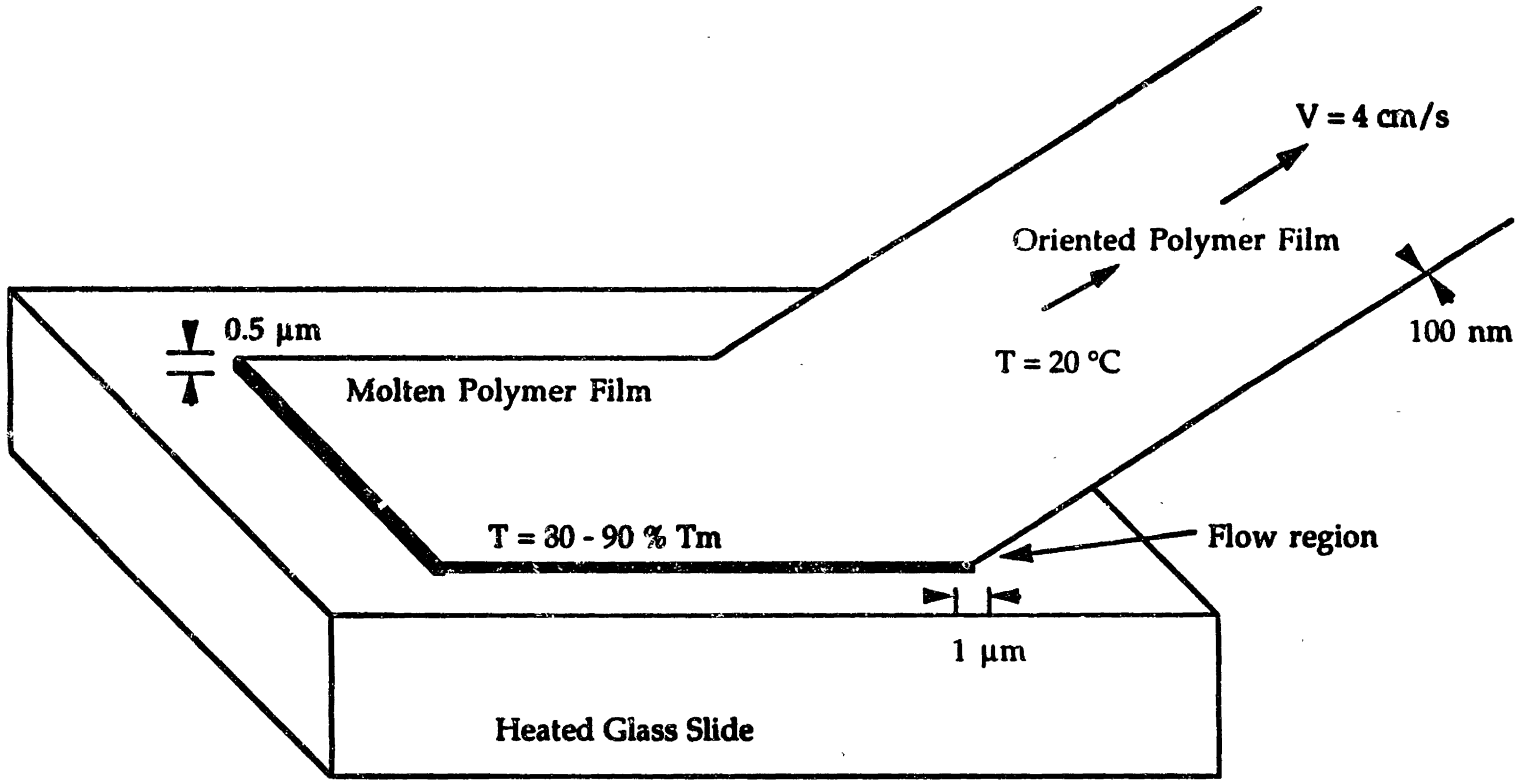

Figure 6.1. Schematic diagram of the Petermann method for preparing thin, oriented polymer films [after Petermann, 1979]

Figure 6.2. Bright field phase contrast (objective lens defocus ~ - 1.8 μm) transmission electron micrograph and electron diffraction pattern of a high density polyethylene 'Petermann' film. Draw direction is vertical.

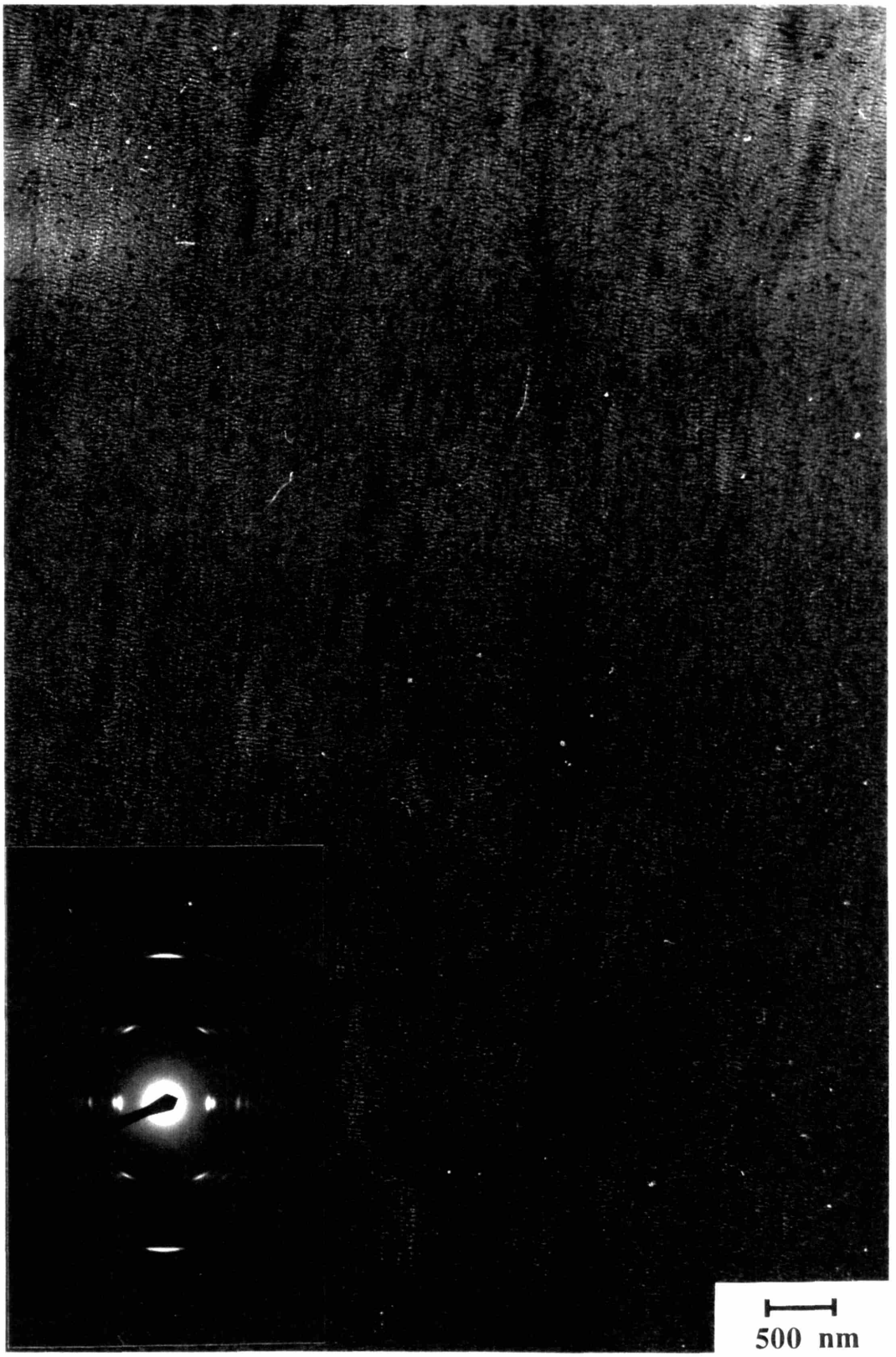
500 nm

crystallizes under the biaxial strain. The advantage of this technique is that it subjects the polymer to relatively equal biaxial tension stresses [6] and requires a very small amount of polymer (< 0.2 g.) to perform several trials.

ANALYSIS OF EXPERIMENT

An analysis of this process can be achieved by comparing it to that of a membrane with rotational symmetry (applicable to that of the film blowing processes) [36]. For a free bubble, there exists two principal radii of curvature in the longitudinal and circumferential directions (see Figure 6.3). By symmetry, the two principal directions of stress (π) and strain (ε) are in the meridian (11) and circumferential (33) directions (stress in the normal direction (22) is equal to zero). This leads to biaxial elongational flow during thermoforming operations. Equations describing the stresses in these directions (assuming incompressibility, small thickness gradients, and no body and acceleration forces) are shown below:

$$\Delta P = -\delta\left(\frac{\pi_{11}}{R_L} + \frac{\pi_{33}}{R_C}\right) \tag{6.1}$$

$$-\frac{d}{dz}\left(r\,\delta\,\pi_{11}\cos\theta\right) = r\left(\frac{dr}{dz}\Delta P - F_T\right) \tag{6.2}$$

where ΔP is the pressure difference (the net normal force/area) and F_T is the tangential (friction force, usually taken to be equal to zero for free bubbles).

Schmidt and Carley have shown that for many thermoplastics, the bubble blowing process can be approximated by assuming the deforming material to be isotropic and isothermally elastic [37]. Setting the work of deformation equal to the elastically stored free energy per unit volume ($dw = f\,dA$), they have determined an empirical expression for the strain-energy density, W:

$$W = C_{10}(I_1 - 3) + C_{02}(I_2 - 3)^2 \tag{6.3}$$

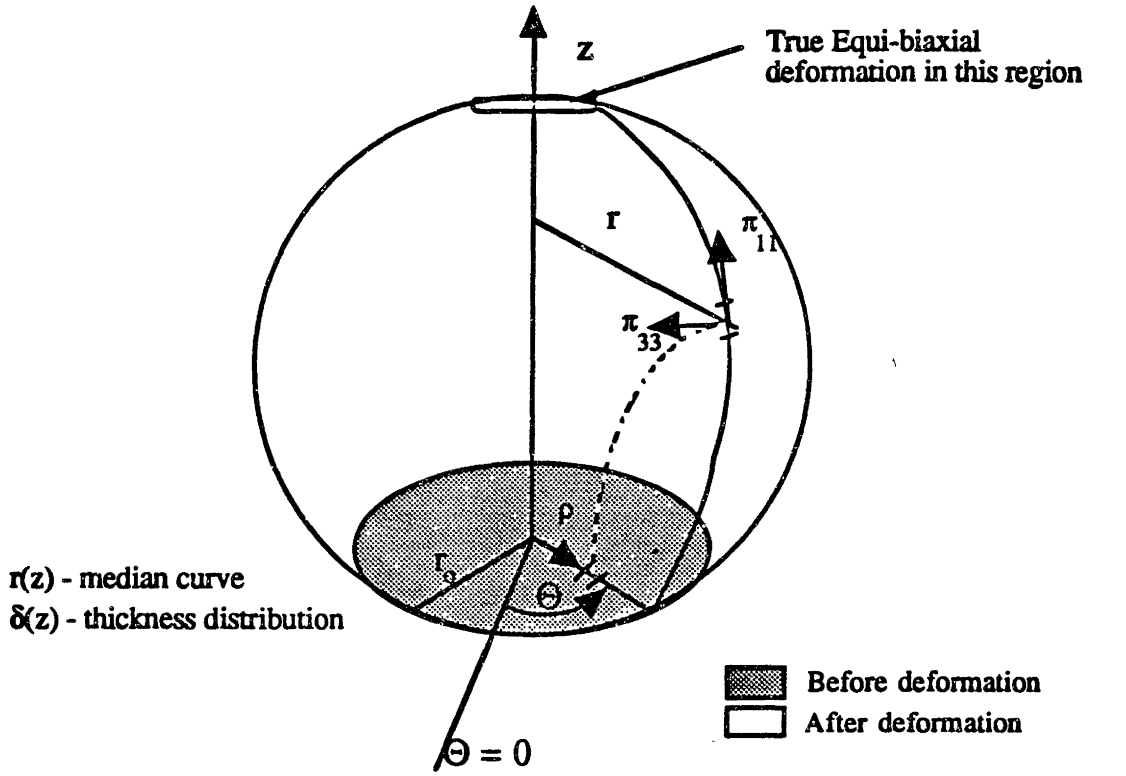

Figure 6.3. Idealized axisymmetric deformation of a free bubble. By symmetry, the two principal directions of stress, π, are in the meridian (11) and circumferential (33) directions. Stress in the normal direction (22) is equal to zero.

where I_1 and I_2 are the first and second strain invariants and C_{01} and C_{02} are coefficients corresponding to this simplified version of a power series first proposed by Treloar [38] to describe large bubbles blown from rubber sheets. Non-spherical profiles of the film blowing operation using the above expression are consistent with experimental profiles of actual polymer bubbles [37].

Establishing the extent of deformation a polymer undergoes requires the determination of extension ratios. In bubble blowing, there are three principal extension ratios: a) the meridian extension ratio, λ_1; b) the circumferential extension ratio, λ_3, and c) the normal extension ratio, λ_2 that are defined by:

$$\lambda_1 = \frac{d\varepsilon}{d\rho} \tag{6.4}$$

$$\lambda_3 = \frac{2\pi r}{2\pi\rho} \tag{6.5}$$

$$\lambda_2 = \frac{1}{\lambda_1\lambda_3} = \frac{\delta}{\delta_o} \tag{6.6}$$

Near the apex of the sphere, λ_1 approaches λ_3, the condition of equi-biaxial deformation. Experimentally, Schmidt and Crawley found significant variation in the shell thickness from the top to the bottom of the bubble [36] which yielded varying extension ratios for a particular bubble. They have reported variations in thickness from the top of the bubble to the its bottom edge by as much as a factor of 26 [37]. In this study, film samples are only obtained from the apex of the bubble where the greatest thinning of the film occurs (and $\lambda_1 \approx \lambda_3$).

Another quantity, areal elongation, is commonly used by engineers in commercial film blowing operations. This ratio is related to the normal extension ratio by:

$$AE = \frac{A_f - A_o}{A_o} \approx \frac{\delta_o}{\delta} = \frac{1}{\lambda_2} \qquad (6.7)$$

where A_f and A_o are the final and initial surface areas of the film, respectively. Normally, thickness measurements are made to determine areal elongation since density is assumed to be constant. For the set-up employed in our study, accurate thickness measurements during the time of the experiment were not easily achievable (see experimental procedure). Areal elongation was estimated by measuring the height and width of the bubble and employing Schmidt and Carley's profile analysis to compute a value for the final area of the bubble. Due to variation in the bubble support thickness and polymer film thickness, this computed areal elongation is likely to be lower than the actual elongation occurring at the bubble apex.

The inter-relationship between time and rate of crystallization, deformation, and relaxation will determine the final morphology of the film. Ideally, to mimic the commercial film blowing process, crystallization should occur on the same time scale as that of the deformation of the film:

$$\frac{\tau_{crystallization}}{\tau_{deformation}} \approx 1 \qquad (6.8)$$

The rate of crystallization and induction time to crystallization are a strong function of rate and extent of deformation [36]. As the deformation increases for the case of uniaxial flows, chain alignment favors the formation of nuclei. The rate at which crystallization occurs also varies with the degree of undercooling and molecular weight. Another kinetic parameter can be defined by the Deborah number, De, which will depend on the viscoelastic nature of the polymer system [39]:

$$De = \frac{\tau_{relaxation}}{t_{experiment}} \qquad (6.9)$$

Relaxation times are dependent on such factors as temperature, crystallization rates, orientation, molecular weight, heat transfer (h), diffusion of polymer/solvent, and for blends, macro- vs. micro- phase segregation times. A goal for this experiment is to determine the appropriate conditions underwhich simultaneous crystallization and extension occur such that molecular relaxation will not erase the effects of biaxial deformation on the microstructure (i.e. De >> 1).

EXPERIMENTAL PROCEDURE

The experimental procedure followed is shown in Figure 6.4 and can be divided into three parts. The first is very similar to the Petermann technique which was used to prepare uniaxially-oriented, melt-drawn thin films. A thin layer of hot, dilute solution of polymer in a suitable, volatile solvent was spread over a heated substrate, in this case, a flexible rubber. The polymer employed was Exxon Ziegler-Natta polymerized HDPE (M_n = 12174, M_w = 68698, Polydispersity = 5.64). The solvent used was ortho-xylene (Sigma-Aldrich, 98% HPLC grade) and heated to a temperature approximately 115 to 125°C to dissolve the polyethylene. Starting solution concentrations were 0.25 to 0.5 wt%. Nitrile® rubber (Best Manufacturing Co.), which is resistant to xylene over the course of the experiment, was employed as the flexible substrate. A heat gun was employed to maintain the polymer at a temperature above its melting point (T = 150 - 175 °C). Copper-constantan thermocouples placed on or just above the surface of the substrate were used to record temperature.

Once the solvent had evaporated and a steady state temperature was reached (T = 150 - 170 °C), the second part of the experiment was initiated by shutting off the heat gun. After waiting a certain time, t_{wait}, during which the polymer was allowed to cool, the clamped substrate was inflated using nitrogen gas (Airco) for time, $t_{inflate}$. A constant pressure of 10 psig was used, and the average areal inflation rate employed

a.

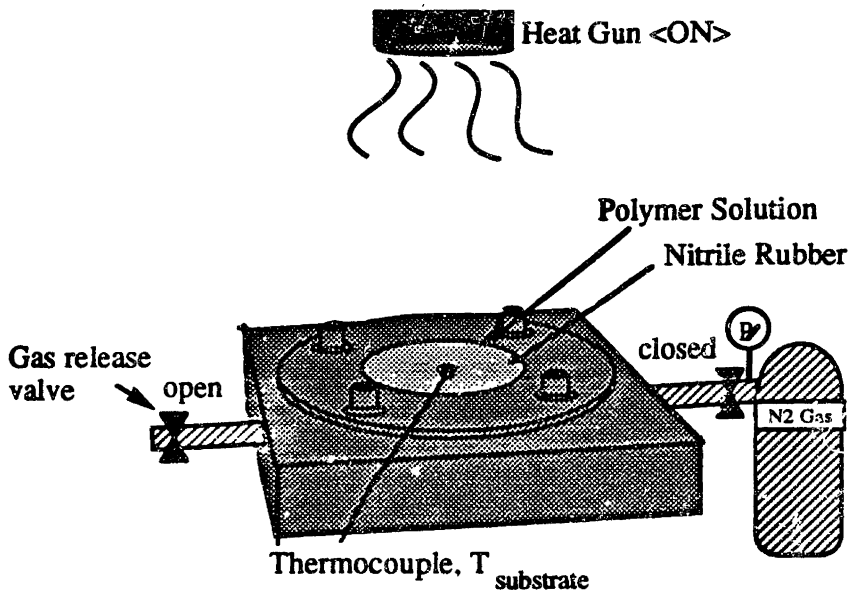

b.

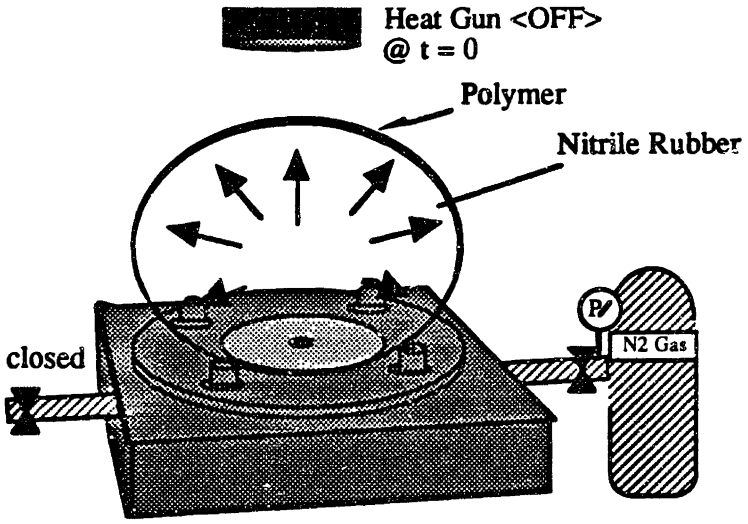

Figure 6.4. Schematic of the biaxial deformation experiment: a) Polymer melt is formed from a dilute solution deposited on a clamped flexible substrate. b) After shutting off the heat gun at t = 0, and waiting a period of time, t_{wait}; the substrate is inflated and the polymer deformed during the interval, $t_{inflate}$.

varied from 30 to 40 cm^2/sec. Because the positioning of thermocouple interfered with the substrate inflation, it was not used during the deformation step. Temperature at the time of inflation (i.e. after t_{wait}) was estimated from a series of calibration runs in which the cooling rate and polymer temperature are measured at varied starting temperatures. Usual times for t_{wait} ranged from 0 to 4 seconds which corresponds to a decrease in the surface temperature before inflation of from 0 to approximately 45°C.

Finally, in the third part, the inflated bubble was dipped into hot parrafin wax (T ~ 70°C) after the polymer film has completely solidified. The system was then immediately quenched by cold water (T ~ 4°C) to harden the wax. The substrate was then deflated, leaving the polymer adhering to the paraffin which retained the inflated shape. The area at the top of the bubble was removed, and the polyolefin thin film was separated from the wax by dissolving the paraffin with room temperature xylene. The remaining polymer film was collected on filter paper and allowed to dry. Smaller sections were cut with a razor, floated off the filter paper onto the surface of water, and collected with copper TEM grids. Samples were coated with a light layer of evaporated carbon prior to viewing in the TEM (JEOL 200CX) at 100 keV.

RESULTS AND DISCUSSION

The small size scale of this experiment allows us to vary the processing conditions such that various combinations of crystallization, deformation, and relaxation times are achieved. We now present the variations in microstructure for a particular polymer that result from changes in temperature, inflation time, and concentration.

The crystallization of a polyethylene melt under quiescent conditions usually results in the formation of spherulites. This structure usually forms in thicker thermoplastically processed specimens in which temperature gradients in the sample are such that crystallization occurs after both deformation and relaxation of the polymer chains has occurred. In thin films, crystallization is confined to roughly a two

dimensional state and temperature gradients across the film are minimized. In figure 6.5, the result of crystallization after deformation is shown as a result of a particular trial. The polymer melt was heated to a temperature of 175°C and immediately deformed over a period of 3 seconds until a total areal elongation of 9.3 (i.e. 930% increase in area) for the film on the bubble support was achieved. The resultant microstructure is that of spherulites greater than 12 μm in size. The edges of three spherulites which have impinged on each other are shown in figure 6.5 (note dark extinction bands which are indicative of twisted lamellae). During the deformation of the melt, the crystallization temperature was not reached, T ~ 140°C, after inflation. The molten polymer chains relaxed and crystallization proceeded under quiescent conditions. It should be noted that the melt completely covered the apex area of the bubble support and formed a film of constant thickness (no voids). Subsequent trials were run at lower temperatures and various holding times before inflation.

While the previous figure shows that the melt continued to form a consistent film over the substrate during deformation, it gives us little information about how deformation influences the crystallization behavior of the polymer film. In the presence of stresses, morphologies very different from those achieved by crystallization in the quiescent state are formed (i.e. row nucleated structures such as are formed in Petermann film). In figure 6.6, the final microstructure strongly suggests nearly simultaneous crystallization and biaxial deformation. The initial temperature of the melt before deformation was measured to be 158°C, after cooling for 2 seconds, the estimated temperature at the start of deformation is approximately 136°C (conc = 0.25 w/v%, $t_{inflate}$ = 3 s, AE = 8.5). Because the initial solution concentration was less, a thinner melt layer was initially formed and deformation accompanied by crystallization produced a network-like structure of fibrils and fibril clusters with cavitated areas. The size of the fibrils was approximately 50 to 70Å in diameter and extend to various lengths. Overlapping and thicker regions are observed in the film which may be a result

Figure 6.5. Bright-field transmission electron micrograph of a biaxially, melt drawn polyethylene film exhibiting an undeformed spherulitic morphology (t_{wait} = 0, $t_{inflate}$ = 3 s, AE = 9.3). Relaxation of the polymer chains prior to crystallization occurs after melt is deformed.

500 nm

Figure 6.6 Bright field micrograph of a biaxially, melt drawn polyethylene film exhibiting a network of crystallized fibrils (T_i = 158°C, T(t_{wait} = 2 s) ~ 136°C, $t_{inflate}$ = 3 sec, AE = 8.5). Biaxial deformation dominates the morphology of this particular film.

500 nm

of local regions of differing extensions.

The overall effect of this equi-biaxial extension results in local regions of highly oriented polyethylene which crystallizes in fibrils (packets of which give rise to fiber patterns via selected area electron diffraction). Thus, these fibrils possess locally uniaxially oriented polymer chains oriented with there c-axes along the length of the fibril and primarily in the plane of the film. Because the load is distributed equi-axially, the fiber themselves are oriented in many different directions which gives rise to an electron diffraction pattern, taken normal to the film surface, that indicates in-plane random orientation of the polymer chains. See figure 6.7 (inset).

The inflation rate of the substrate was such that it corresponded to inflation rates used in commercial film blowing (areal extension rate ~ 300%/sec). However, sensitivity of the polymer to temperature changes is likely to be higher than in commercial operations since the film is very thin (thickness of the molten layer is estimated to be less than 1 μm) and crystallization occurs in a pseudo-two-dimensional fashion. In addition, the interaction of the film with the substrate surface may effect the morphology. Roughness variations on the rubber substrate surface may lead to film thickness and extension variations on the final polymer film. Atomic force microscopy measurements showed that height variations on the substrate surface were approximately 0.3 μm at zero inflation. In addition, temperature and heat capacity of the substrate (heat was applied from above during the experiment to lessen this effect) will also effect the final film morphology. This variation in the substrate properties may be responsible for thickness variation in the resultant biaxially stretched, melt-crystallized polyethylene film. In addition, cold drawing of the film after crystallization may result in some further deformation, decrystallization of lamellae and recrystallization into the local uniaxially oriented regions.

In order to decrease the effect of surface roughness on the microstructure of the thin films, a more concentrated polymer solution (0.5 w/v%) was deposited on the

Figure 6.7. a) Magnified image of a selected area in figure 6.6. Note the distribution of fibrils approximately 70 Å in size extending in various directions and cavitated areas of the polymer film. b) Corresponding electron diffraction pattern taken normal to the film indicates a primarily planar isotropic texture.

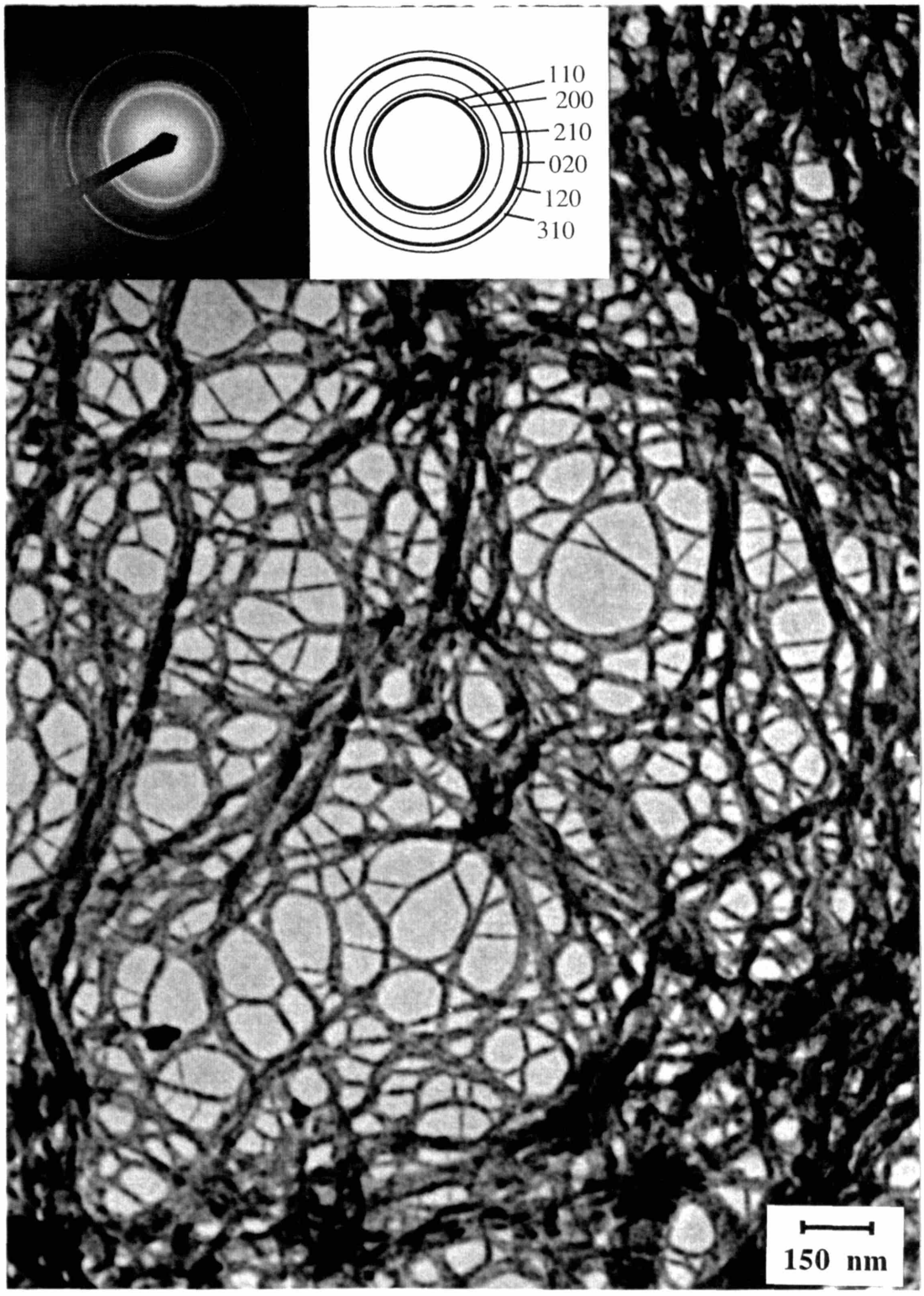
110
200
210
020
120
310
150 nm

substrate to form a thicker layer. Simultaneously deforming and crystallizing this thicker film resulted in the formation of in-plane, randomly oriented lamellae as shown in figure 6.8 ($T(t=0\ s) = 150°C$, $T(t_{wait} = 1\ s) \sim 135°C$, $t_{inflate} = 3\ s$, AE = 10.60). Although the areal elongation for this particular film is higher, the electron micrograph does not appear to show evidence of fibrils similar to those in figures 6.6 and 6.7. Some relaxation of the polymer may have occurred even during the extension process since only the polymer layer immediately adjacent to the rubber substrate would experience the highest orientation where as a molten layer above it would flow over the substrate surface. This TEM image is consistent with lamellae imaged using low voltage SEM for thicker blown films of polyethylene [40].

Previous studies of biaxial deformation of compression molded plaques of polyethylene which were heated to a temperature just below the peak melting temperature and deformed [10] yielded similar results. For the tentering operation, biaxial deformation (in rectangular coordinates) results in observed orientation of the polymer chains in two directions, easily visible in x-ray. Such techniques are generally used in film blowing in which stresses in the machine direction are different than the axial and other than random bulk orientation is attained [5, 7]. This difference in orientation in often attributed to failure of blow molded objects. For our case, we have shown that through equi-biaxial deformation (or polyaxial, depending upon the coordinate system choice), results in a film where no particular bulk area possesses a directionality associated with it; however, load is carried by very small regions of locally uniaxially oriented fibrils. Previous work by Okajima, Masuko, and Tanaka on thicker films of polypropylene using x-ray also showed such uniplanar orientation at high stretching in which the c-axis lies parallel to the film surface [3, 8, 9].

The bubble support technique is also useful in examining the effect of biaxial deformation on films in which crystallization preceded deformation. For our experiment, crystallization of the film prior to deformation was achieved by starting at

Figure 6.8. a) Bright-field electron micrograph of a thicker, biaxially oriented film. exhibiting a disordered lamellar structure formed during simultaneous equi-biaxial stretching and crystallization (conc = 0.5 w/v%, Ti = 150°C, T(t_{wait} = 1 s) ~ 135°C, $t_{inflate}$ = 3 s, AE = 10.6)

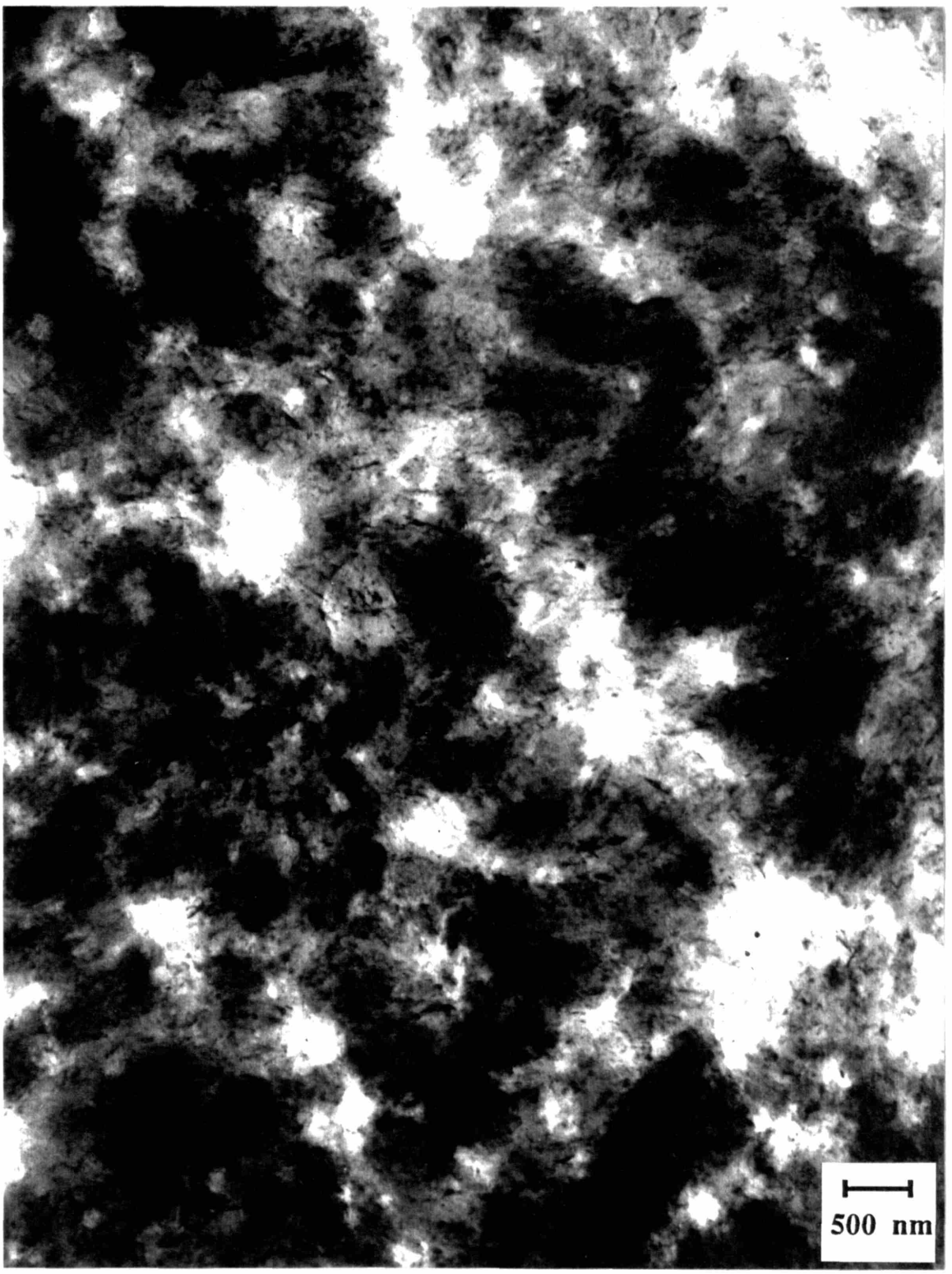
500 nm

lower temperatures and waiting longer times before the substrate was inflated. Results are shown in figure 6.9 for areal elongations of 3.1, 7.5, and 10.5, respectively. In figure 6.9a, a deformed spherulitic film is displayed. Extinction bands are no longer visible due to the imposed deformation, perhaps indicating preferred orientation of the polymer crystals in the plane of the film (reminicent cylindrite formation under high stress in uniaxial deformations [41]). Pulling out of polymer chains at the edges and near the center of the spherulites, and re-crystallization of the polymer in fibrillar form is also observed. This type of behavior was observed in thicker films using optical microscopy [2][20][21] and modeled fairly recently by T. T. Wang [42]. At higher areal elongations, a more complex structure is formed (figure 6.9b). Block-like spherulite remnants are connected by regions of uniaxially oriented fibrils (see arrows). Cavitated regions of microfibrils 50-70 Å in thickness are also present. Still further cavitation occurs at even higher extensions (figure 6.9c). Local regions of uniaxially oriented fibrils connect thicker block fragments. As the film is further stressed, weaker regions break and larger holes form, ultimately leading to sample failure.

These results demonstrate that the bubble support technique is useful in studying extremes of biaxial deformation on the structure of melt crystallized polyethylene film. Past studies have shown increases in the time and load to failure are achieved for films with smaller spherulite sizes in biaxial deformation. The preparation of films but the bubble support method that are equi-biaxially deformed during crystallization essentially show random orientation of the polymer chains in the plane of the film. This random orientation eventually breaks down to a fibrillar network as the film is further stretched (or a thinner film prepared). The final morphology either for as prepared or a spherulitic structure that is biaxially deformed results in a cavitated film with local regions of uniaxially oriented re/crystallized microfibrils and fibrillar regions (similar results were found for biaxially drawn ultrahigh molecular weight polyethylene [11]). Entanglements distribute the biaxial load over a structural network of microfibrils.

Figure 6.9. Bright-field electron micrograph of a thin polyethylene films initially exhibiting a spherulitic morphologies, but subsequently stretched to different areal elongations (T_i = 140°C, $T(t_{wait}$ = 3 s) ~ 113°C): a) $t_{inflate}$ = 1 sec., AE = 3.1; b) $t_{inflate}$ = 2 sec., AE = 7.5; c) $t_{inflate}$ = 3 sec., AE = 10.5.

a) AE = 3.1
500 nm

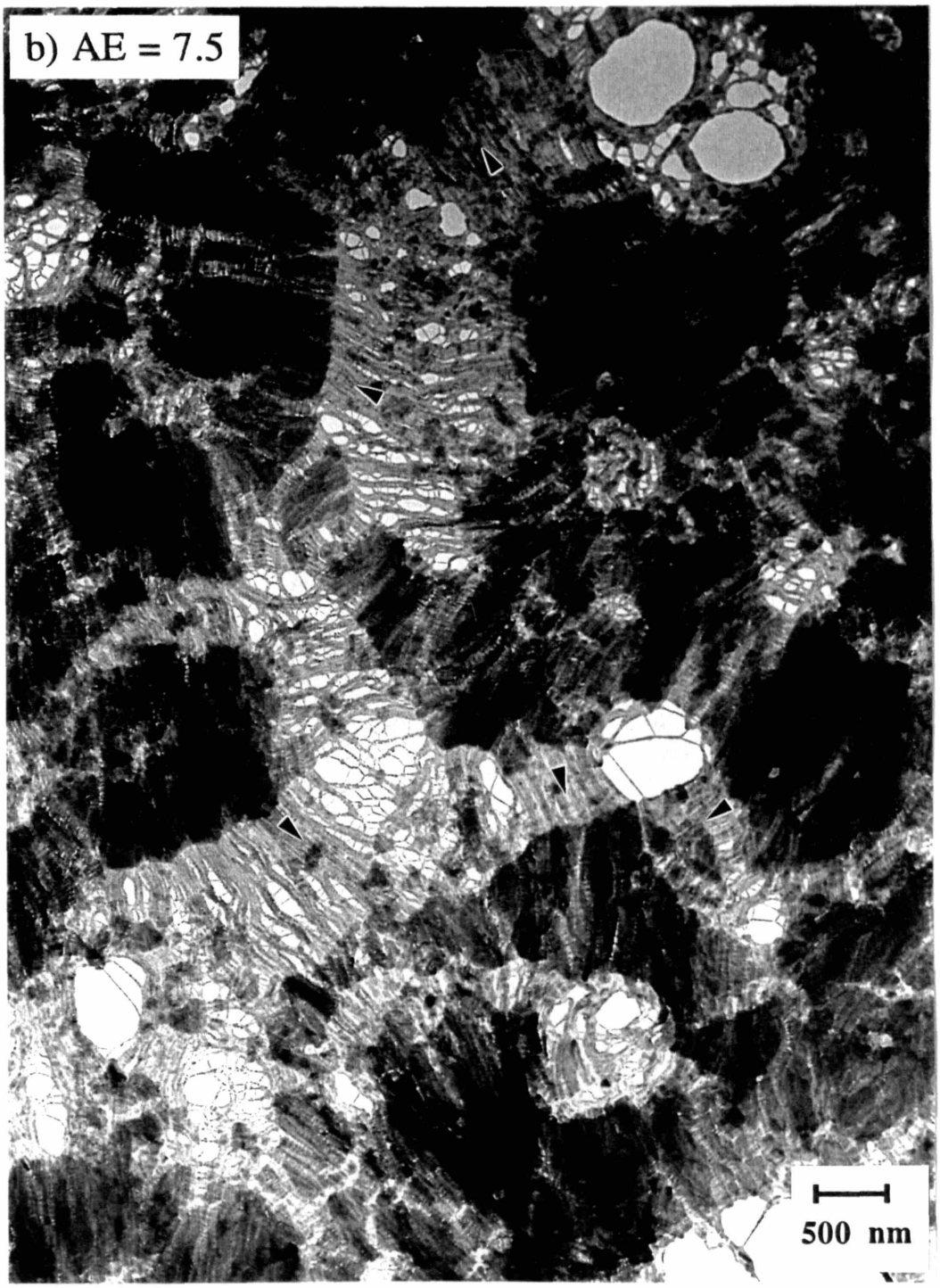
b) AE = 7.5
500 nm

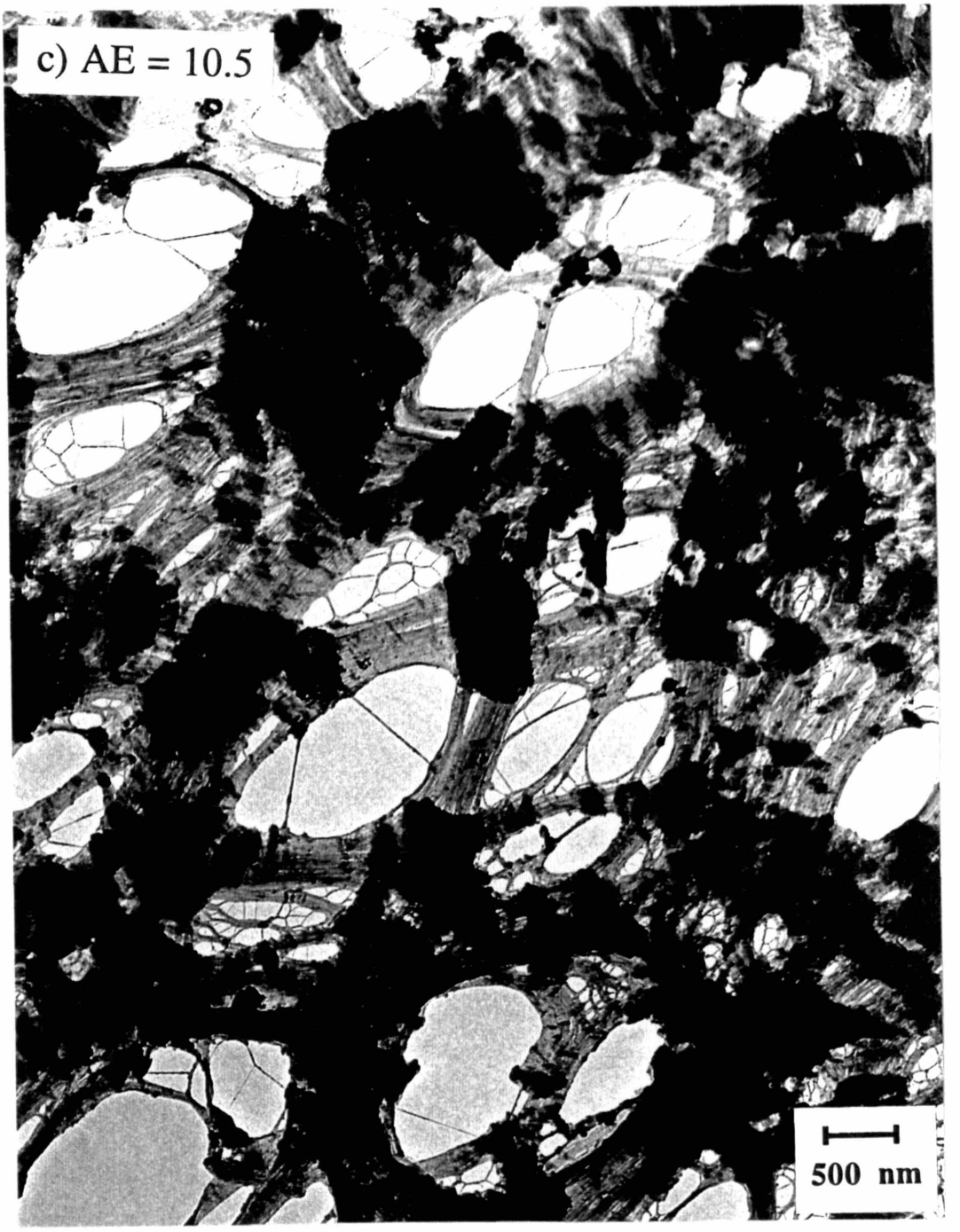
c) AE = 10.5
500 nm

Although biaxial deformation behavior for Zieglar-Natta polymerized high density polyethylene has been studied extensively, the results shown here indicate that the Bubble Support technique is advantageous for studying the mechanical behavior that would occur in more model systems (such as the Metallocene catalyzed polyolefins with lower molecular weight polydispersity [43]) or in blends of polymers used to improved mechanical properties. Using this preparation technique in combination with TEM, the deformation characteristics of new polymer systems can be evaluated even with limited, lab-scale quantities of materials.

CONCLUSIONS

A relatively simple procedure for investigating the effect of equi-biaxial deformation on melt crystallized polyolefin films which are less than 1000 Å in thickness has been demonstrated. Only very small amounts (< 0.2 g.) of polymer material is required for this technique. This preparation method allows for direct imaging of biaxially oriented films in transmission electron microscopy without the need for surface replication or microtoming. Variations in the processing conditions such as temperature and areal elongation lead to a variety of observed morphologies and give insight into the effect of kinetic variables on the formation of final film structure. Comparison of results obtained using this method were made with the existing literature on thicker films of commercially available polyolefins prepared by film blowing, tentering, and compression techniques.

REFERENCES

1. I.L. Hopkins, W.O. Baker and J.B. Howard, 'Complex Stressing of Polyethylene,'*Journal of Applied Physics*, **21,** 206 (1950).

2. J.L. Cooney, 'Effect of Morphology on Biaxial Stress Rupture of Polyethylene,'*Journal of Applied Polymer Science*, **8,** 1889 (1964).

3. S. Okajima and K. Homma, 'Studies on the Stretching of Polypropylene Film. II. Polyaxial Stretching,'*Journal of Applied Polymer Science*, **12,** 411 (1968).

4. K.-J. Choi, J.E. Spruiell and J.L. White, 'Orientation and Crystalline Morphology of Blow Molded Polyethylene Bottles,'*Polymer Engineering and Science*, **29,** 463 (1989).

5. A. Savolainen, 'Biaxially Oriented PolyPropylene Blown Films. I. Morphological Analysis of Orientation in the Machine Direction,'*Polymer Engineering and Science*, **30,** 1258 (1990).

6. D.E. Duvall and D.B. Edwards, 'Creep and Stress Rupture Testing of Polyethylene Sheet under Equal Biaxial Tensile Stress,'*Journal of Reinforced Plastics and Composites*, **12,** 285 (1993).

7. A. Gupta, D.M. Simpson and I.R. Harrison, 'Crystalline Morphology in Oriented HDPE Blown Films,'*Plastics Engineering*, 33 (1993).

8. H. Tanaka, T. Masuko, K. Homma and S. Okajima, 'Studies on the Biaxial Stretching of Polypropylene Film. III. Electron Microscopic Observation of the One-Step Biaxial Stretching of Isotactic Polypropylene Spherulites,'*Journal of Polymer Science, Pt. A-1*, **7,** 1997 (1969).

9. H. Tanaka, T. Masuko and S. Okajima, 'Studies on the Biaxial Stretching of Polypropylene Film. V. Orientation Mechanism of the One-Step Biaxially Stretched Film,'*Journal of Polymer Science Pt. A-1*, **7,** 3351 (1969).

10. G.C. Adams, 'Orientation Effects in Biaxially Stretched Linear Polyethylene,'*Journal of Polymer Science: Part A-2*, **9,** 1235 (1971).

11. A. Kaito, K. Nakayama and H. Kanetsuna, 'Microstructure of Biaxially Drawn Ultrahigh Molecular Weight Polyethylene,'*Journal of Applied Polymer Science*, **29,** 2347 (1984).

12. T. Kyu, K. Fujita and M.H. Cho, 'Structure and Orientation Development in Biaxial Stretching of Ultrahigh Molecular Weight Polyethylene Gel Films,'*Polymer Engineering and Science*, **29,** 383 (1989).

13. N.S.J.A. Gerrits and R.J. Young, 'Deformation Mechanisms in Biaxially Drawn Polyethylene,'*Journal of Polymer Science: Part B: Polymer Physics*, **29,** 825 (1991).

14. N.S.J.A. Gerrits and P.J. Lemstra, 'Porous Biaxially Drawn Ultra-High Molecular Weight Polyethylene Films,'*Polymer*, **32,** 1770 (1991).

15. N.S.J.A. Gerrits and Y. Tervoort, 'Deformation Mechanisms During Uniaxial Drawing of Melt-Crystallized Ultra-High Molecular Weight Polyethylene,'*Journal of Materials Science*, **27,** 1385 (1992).

16. R.M. Gohil, 'Morphology-Property Relationships in Oriented PET Films: A Role of In-Plane Crystalline Orientation Distribution on the Film Properties,'*Journal of Applied Polymer Science*, **48,** 1635 (1993).

17. H.G. Kilian, W. Schrodi, F. Ania, K. Bayer and F.J. Balta Calleja, 'Van der Waals Networks in the Compressive Deformation of Polyethylene,'*Colloid and Polymer Science*, **269,** 859 (1991).

18. F. Ania, F.J. Balta Calleja and R.K. Bayer, 'Structure Formation and Properties of Biaxially Oriented Polethylene Films by Compression of Injected Mouldings,'*Polymer*, **33,** 233 (1992).

19. T. Kowaleswski and A. Galeski, 'Crystallization of Linear Polyethylene from Melt in Isothermal Compression,'*Journal of Applied Polymer Science*, **44,** 95 (1992).

20. T.W. Haas and P.H. MacRae, 'Microscopic Observations of Fracture in Spherulitic Films of Linear PE,'*SPE Journal*, **24,** 28 (1968).

21. T.W. Haas and P.H. Mac Rae, 'Microscopic Observations of Fracture in Spherulitic Films of Polybutene-1,'*Polymer Engineering and Science*, **9,** 423 (1969).

22. J. Petermann and R.M. Gohil, 'A New Method for the Preparation of High Modulus Thermoplastic Films,'*J. Mater. Sci. (Letters)*, **14,** 2260 (1979).

23. J. Petermann, M. Miles and H. Gleiter, 'Growth of Polymer Crystals during Annealing', *J. Polymer Sci., Polymer Phys. Ed.*, **17,** 55 (1979).

24. J. Petermann, R.M. Gohil, M. Massud, and D. Goritz, 'Plastic Deformation of Linear Polyethylene Containing Row Structures', *J. Mater. Sci.*, **17,** 100 (1982).

25. R.M. Gohil and J. Petermann, 'Mixed Crystals in Polymer Blends: Polypropylene-Polybutene-1 Systems', *J. Macromol. Sci. Phys.*, **B18,** 217 (1980).

26. J. Petermann and R.M. Gohil, 'On the Size of Core Crystals of Isotactic Polystyrene grown from Polystyrene Blends', *J. Polymer Sci.- Polymer. Lett. Ed.*, **18,** 781 (1980).

27. W.W. Adams, 'An Electron Microscopy and X-Ray Scattering Investigation of the Deformation Morphology of Solid State Extruded Fibers and Melt-Drawn films of Polyethylene', Ph.D. Dissertation, University of Massachusetts (1984).

28. W.W. Adams, D. Yang and E.L. Thomas, 'Direct Visualization of Microstructural Deformation Processes in Polyethylene,'*Journal of Materials Science*, **21,** 2239 (1986).

29. J.M. Brady, 'Visualization of the Evolution of a Continuous Crystalline Phase in Uniaxially Drawn Polyethylene: Decrystallization and Strain-Induced (Re)Crystallization', Ph.D. Dissertation, University of Massachusetts (1987).

30. J.M. Brady and E.L. Thomas, 'Deformation of Oriented High Density

Polyethylene Shish-Kebab Films: Part I. Decrystallization at Room Temperatures,'*J. Mat. Sci.*, **24,** 3311 (1989).

31. J.M. Brady and E.L. Thomas, 'Conversion of Single Crystal Mats to Ultrahigh Modulus Polyethylene: The Formation of a Continuous Crystalline Phase,'*Polymer*, **30,** 1615 (1989).

32. V.P. Chacko, W.W. Adams and E.L. Thomas, 'Imaging of Polyethylene Films by Diffraction Contrast,'*Journal of Materials Science*, **18,** 1999 (1983).

33. D. Yang and E.L. Thomas, 'An Electron Microscopy and X-Ray Diffraction Study of the Microstructure of Melt-Drawn Polyethylene Films,'*J. Mat. Sci.*, **19,** 2098 (1984).

34. D.C. Yang, J.M. Brady and E.L. Thomas, 'Highly Oriented Single-Phase Blend Films of High- and Low-Density Polyethylene,'*Journal of Materials Science*, **23,** 2546 (1988).

35. K. Haas and P.H. Geil, 'Polymer Deformation. XI. Biaxial Deformation of Polyethylene Single Crystals,'*Journal of Polymer Science. Pt A-2*, **4,** 289 (1966).

36. Z. Tadmor and C.G. Gogos, *Principles of Polymer Processing*. 1979, New York: John Wiley & Sons. 521.

37. L.R. Schmidt and J.F. Carley, 'Biaxial Stretching of Heat-Softened Plastic Sheets: Experiments and Results,'*Polym. Eng. Sci.*, **15,** 51 (1975).

38. L.R.G. Treloar, *The Physics of Rubber Elasticity*. 1958, London: Oxford University Press.

39. F.N. Cogswell, 'Tensile Deformations in Molten Polymers,'*Rheological Acta*, **8,** 187 (1969).

40. D.L. Vezie, E.L. Thomas and W.W. Adams, 'Low-Voltage, High-Resolution Scanning Electron Microscopy: A New Characterization Technique for Polymer Microscopy,'*Polymer*, **36,** accepted (1995).

41. A. Keller and M.J. Machin, 'Oriented Crystallization in Polymers,'*J. Macromol. Sci. (Phys.)*, **B1,** 41 (1967).

42. T.T. Wang, 'Morphology and Mechanical Properties of Crystalline Polymers. 4. Behavior of Spherulites in Polyethylene Subjected to Biaxial Tension or Pure Shear,'*Macromolecules*, **25,** 933 (1992).

43. A.D. Horton, 'Metallocene Catalysis: Polymers by Design?,'*Trends in Polymer Science*, **2,** 158 (1994).

Chapter 7

Conclusions/Directions for Future Work

The influence of processing on the structure of semi-crystalline polymer systems was investigated in this thesis in order to understand and possibly improve performance properties. In particular, methods for elucidating the morphology of extruded starch/poly(ethylene-vinyl alcohol) blends were developed. The technique of transmission electron microscopy to examine starch-based systems was addressed in detail. The model application of fiber melt spinning was employed to study the effects of uniaxial shear and elongational flow on the blend morphology and mechanical properties. With the Bubble Support technique, the effects of equi-biaxial extension on the crystallization characteristics of limited amounts of semi-crystalline polymers can be studied; linear polyethylene was used as an example. The overall conclusions and directions for future work are addressed in this chapter.

Starch-based Thermoplastics

The extrusion processing of three varieties of corn starch with poly(ethylene-vinyl alcohol) to produce model systems in order to study the structural characteristics of starch-based biodegradable thermoplastics was investigated. Corn starch varieties (waxy maize, native corn, and Hylon VII) differing in branch content (amylose to amylopectin ratio) and molecular weight were blended with poly(ethylene-vinyl alcohol) containing 56 mol% VOH over a systematic compositional range from 100% starch to 0% starch (control sample). In order to plasticize the blends so that they could be used in the fiber spinning application, both glycerin and water were added during the extrusion process.

Details on the use of transmission electron microscopy for the study of such complex systems as these starch/EVOH blend were presented. Sample preparation issues specific to starch as a component were addressed, and methods of reducing artifacts in the blend morphology (e.g. avoiding water which causes the starch fraction to swell) were described. The sensitivity of both starch and EVOH to electron beam exposure was established (maximum allowable beam dosages based on the loss of the crystalline diffraction pattern were less than 3×10^{-3} C/cm^2 for starch and approximate 3.5×10^{-3} C/cm^2 for EVOH (at room temperature and 200 keV). Therefore, low dose techniques were used to image the starch/EVOH blends. Mass-thickness contrast was enhanced using iodine as a preferential stain for the starch. Due to beam damage, contrast between starch-rich and EVOH-rich domains was observed to first increase then decrease leading contrast reversal at moderate beam dosages ($> 6 \times 10^{-3}$ C/cm^2). Successful imaging and correct interpretation of TEM micrographs of semi-crystalline starch-based polymer blends is only possible when the contrast mechanisms, beam sensitivity of the sample, and optimal electron optical operating conditions of the TEM are carefully considered. In future work, cold stage transmission electron microscopy of starch-based blends (though not currently available at MIT) should be investigated. The use of this technique will limit the loss of water and organic matter as well as reduce the radiation damage of starch and other semi-crystalline polymers.

Native starch granules, when extruded with sufficient moisture and at temperatures ranging from 170 to 190°C, were observed to be destructurized in a manner similar to that observed in extrusion cooking. Polymer-polymer blending with the EVOH component was effectively achieved. Extensive phase separation occurred between amylopectin and EVOH; the morphology of the waxy maize/EVOH blends was similar to that of traditional incompatible polymer blends. TEM studies revealed EVOH to be the matrix component even up to starch concentrations of 70 wt%. At a composition of 85% starch, the EVOH component appeared to be well distributed throughout the starch-rich

matrix. Phase coarsening of the starch-rich domains for the waxy maize blends was observed as a function of time in the melt ($d \sim t^{1/8}$) although much slower than Ostwald ripening kinetics ($d \sim t^{1/3}$). This behavior is possibly due the molecular weight effects and branching on the diffusion rate, hydrogen bonding effects, and possible degradation of the starch fraction at the higher temperatures.

There is strong evidence for miscibility between the amylose and EVOH components as evident from EVOH melting point depression beyond the effects of plasticizer alone, smaller starch-rich domain sizes, and lower contrast between starch-rich and EVOH-rich phases in transmission electron microscopy for the native corn and, most noticeably, for the high amylose, Hylon VII blends. Blends containing amylose showed complexing behavior during processing, and crystallinity in both the starch and EVOH components was evident. The results of the morphological study indicate that the ultrastructural characteristics of starch/EVOH systems are quite complex. Possibly four or more phases (i.e. amorphous starch-rich, amorphous EVOH-rich, crystalline amylose-complex, crystalline EVOH) can exist for these systems. Such variation in the extent of crystallization and miscibility will lead to property differences such as the increased resistance to swelling, dissolution, and degradation in starch-based blends containing higher amounts of the crystallizable amylose.

Melt fiber spinning studies performed on the model series of blends were performed to explore the thermoplastic processability, structural characteristics, and mechanical properties of oriented blend filaments. Spin draw ratios ranged from less than 1 to 215. Overall, drawability depended upon the amount of EVOH in the blend; blends containing more than 70% starch could not be drawn. Again, increased miscibility between the starch and EVOH in the Hylon VII material was believed to decrease the spinnability characteristics of these blends at intermediate compositions due contributions of the starch component to the matrix (i.e. starch is not as extensible as EVOH). Blends of the more phase separated native corn and waxy maize starches

showed higher spinnability at higher starch contents due to the presence of EVOH as the matrix component. Melt flow instabilities were observed for waxy maize blends for which die swell at the spinnerette orifice was significant. The extent of die swell decreased as the amylose content of the starch was raised (i.e. Hylon VII blends showed little evidence of die swell, possibly due to increased hydrogen bonding in the linear starch polymer component).

Morphological observations revealed that elongational flow properties of starch/EVOH blends are primarily attributable to the EVOH component, which, when present in large enough quantities to be the matrix component, accounts for spinnability of the blends. Orientation of both starch-rich and EVOH-rich phase domains within filaments due to shear and elongational flow was observed although relaxation of individual polymer chains occurred upon exiting the capillary. EVOH domains underwent significant orientation relative to the starch as evident by the presence of EVOH-rich fibrils in blends with large amounts of starch. Wide-angle x-ray scattering studies showed that the EVOH polymer chains oriented in the direction of elongational flow and that cold drawing increased the extent of orientation of these polymer chains. The crystalline starch component did not exhibit any orientation even at high draw ratios. Strengthening of the blend by orientation of the polymer chains in a cold drawing process is solely associated with the drawing of the EVOH fraction.

Mechanical property measurements of extruded filaments and melt spun fibers confirmed morphological predictions. Overall, blends displayed mechanical properties which depended more upon starch content than variety. Again, mechanical properties were a strong function of the amount of poly(ethylene-vinyl alcohol) in a blend. Most of the elongational properties of the fibers are attributed to the EVOH matrix component, and debonding of the EVOH matrix from the starch-rich domains is one route to failure in items made with starch/EVOH blends (fracture surfaces show a combination of both ductile and granular fracture).

From enzymatic etching and cross-sectional TEM studies, the initial rate of biodegradability is predicted to be lower due to a coating, approximately 1 μm thick, of the EVOH component which was observed on the surface of extruded filaments and fibers. Once this coating is broken, biodegradation of the starch fraction will occur at a much faster rate than the EVOH. The surfaces of extruded filaments are smooth, but as a fiber is drawn, the surface roughness increases due to the presence of starch-rich domain inclusions that harden as the blend cools and do not deform in the same manner as the EVOH matrix. (Possible uses of starch/EVOH fibers in nonwoven applications might be investigated in which this surface roughness may be useful in creating mats of fibers.) The size of the starch-rich domains which range from less than 0.1 μm for Hylon VII to less than 5 μm for the waxy maize starch blends will limit the overall thickness attainable for films and fibers made with starch. Starch/EVOH fibers show very little swelling in cold water; however, surface changes, swelling, and break-up of fibers occurs when they are immersed in boiling water.

Overall, the starch/EVOH blends investigated in this study were very complex making for a difficult systematic analysis. Three polymer components, amylose, amylopectin, and poly(ethylene-vinyl alcohol), existed in combination with two plasticizers, glycerin and water. Triglyceride additives as well as naturally occurring lipids and proteins were found to further influence the morphology (forming complexes with amylose). While an ideal synthetic system consisting of monodisperse samples of pure amylose and pure amylopectin can never be attained, a simplified analysis of systems without plasticizers may be examined. For this study, attempts were made to control certain variables such as plasticizer content and processing conditions. An analysis of different starch types over a range of blend compositions was performed. Specific problems in the morphological analysis arose due to the presence of plasticizers (i.e. glycerin and water) in these systems. Glycerin is certainly not the ideal plasticizer for the starch/EVOH system in that it appears to preferentially segregate to the starch-rich

domains. Also, glycerin is very hydroscopic leading to increased moisture sensitivity of the blend. Other plasticizers, which fulfill environmental or FDA requirements, should be explored.

This work represents the first in-depth, systematic, structural analysis performed on thermoplastic starch-based blends and should provide insight into the examination of other types of starch-based systems. Morphological techniques developed for starch/EVOH blends can be readily transferred to the examination of blends of starch with other biodegradable polymers such as cellulose acetate, poly(lactic acid), poly(caprolactone), and poly(hydroxybutyrate). Higher levels of mechanical stability in humid atmospheres as well as increased overall rates of biodegradability might be attainable with these components compared with starch/EVOH blends. Again, because many of these polymers are themselves semi-crystalline, similar studies may be performed to look at the effect of microstructure (i.e. crystallization, orientation, etc.) in these systems. In addition, blends consisting of chemically modified starch (such as starch esters) have shown improved melt processability and properties; however, examination of these types of materials may require slight modification (due to differences in chemical structure) to the etching/staining methodology presented in this thesis.

Further information on thermoplastic starch/EVOH systems can be gained using structural probes that have only recently been used to study polymers. For instance, low voltage, high resolution scanning electron microscopy, which allows imaging of smaller scale features than conventional SEM, should yield further information about the ultrastructure of starch. This technique may be especially useful in re-examining the fine structure of native starch granules (i.e. growth rings, lamellae) since current microstructural models remain quite ambiguous (as discussed in Chapter 2). Modulated differential scanning calorimetry, a relatively new technique, deserves some attention since irreversible thermal transitions can be detected during the first heating cycle

(although further development of the technique on model polymer systems must first occur). Finally, the use of atomic force microscopy to observe starch-rich and EVOH-rich phase domains by detecting modulus differences should be explored. Correlation of results with biodegradability studies, which are still being developed at Army Research Laboratories, Natick, MA, should be performed.

In this study, native granules of starch were 'destructurized' forming a plasticized blend of starch polymer constituents, amylose and amylopectin, with poly(ethylene-vinyl alcohol). This is contrast to the use of starch as a dry filler particle within a synthetic polymer matrix, as previously studied, for example in starch/polyethylene (see Chapter 5). While the present study provides insights into the limits of thermoplastic starch processability (i.e. pure starch cannot be melt spun into fibers), pure or nearly pure starch resins can be and are employed in applications such as injection molded capsules for medicines or foams for packaging peanuts. In addition, a greater amount of starch can be used in blends that will form blown films and thermoformed items, since destructurization of the starch granule ensures that starch-rich domains are small and well dispersed. Unfortunately, the added cost incurred in producing thermoplastic starch (in addition to current quality control issues) presently makes starch-based resin uncompetitive with many of the commodity thermoplastics it seeks to replace (e.g. polyethylene, polypropylene, and polystyrene). Until conditions (i.e. government regulations, environmental pressure, improved marketing, etc.) make them more attractive to the consumer, the future of starch-based thermoplastics remains uncertain. The low cost of starch in relation to other biodegradable polymers and its niche applications, however, warrant additional future work in examination of the structure, properties, and processing characteristics of thermoplastic starch.

Polyolefinic Thermoplastics

The latter part of this thesis focused on examining structural changes that

arise from equi-biaxial deformation of melt crystallized polyethylene. A relatively simple procedure for investigating the effect of equi-biaxial deformation on melt crystallized polyolefin films which are less than 1000 Å thick has been demonstrated. Only very small amounts (less than 0.2 g.) of polymer material is required for this technique. This preparation method allows for direct imaging of biaxially oriented films in transmission electron microscopy without the need for surface replication or microtoming. Variation in the processing conditions such as temperature and areal elongation lead to a variety of observed morphologies and give insight into the effect of kinetic variables on the formation of final film structure. The overall effect of simultaneous equi-biaxial extension with crystallization results in local regions of highly oriented polyethylene that crystallizes in fibrils, locally uniaxially oriented, but distributed in such a way that the electron diffraction pattern, taken normal to the film surface, indicates in-plane random orientation of the polymer chains.

While this technique was demonstrated for commercially available, high density polyethylene, the Bubble Support method can be used in the preparation equi-biaxially stretched films of a wide range of polyolefinic thermoplastics and their blends for direct TEM observation. A great potential of this application is that the equi-biaxial deformation characteristics of limited quantities of model materials can be investigated. Enhancements to the bubble support set-up such as the implementation of systematic inflation and temperature controls, which would require improvements to the radiant heat source and subsequent cooling conditions, are recommended. In addition, further examination into the effect of the substrate (and possible choice of different substrate materials) on the final thin film morphology should be performed. With such modification, very detailed and controlled analyses of this aspect of polyolefinic structure, property, and processing relationships can be performed.

Appendix A.

Crystallization of Poly(ethylene-vinyl alcohol)

In the research performed in this thesis, poly(ethylene-vinyl alcohol) was blended with starch in order to investigate relationships between processing, structure, and properties and evaluate the usefulness of these systems for biodegradable thermoplastic applications. While examination of the blend morphology was the focus in the main part of this thesis, some basic points should be made about the crystallization behavior of EVOH.

Poly(ethylene-vinyl alcohol) (PVOH) is a random copolymer consisting of ethylene and vinyl alcohol repeats. Homopolymers of these repeat units crystallize into specific unit cells. For polyethylene (PE), crystalline packing occurs into an orthorhombic cell with space group, Pnam (a = 7.92 Å, b = 4.949 Å, and c = 2.546 Å); for poly(vinyl alcohol), packing occurs in a monoclinic unit cell, $P2_1/m$ (a = 7.81Å, b = 2.51 Å, c=5.51Å, and $\beta = 91.7°$). Since the hydroxyl (-OH) residue is not much larger than the H- group, the unit cell for PVOH is nearly orthorhombic and the packing along the chain axes for both PVOH and PE are quite similar (note, c = b in PVOH due to monoclinic notation). The grade of EVOH employed in the thesis work (EVALCA E105A) consisted of 56 mol% VOH repeat units and exhibits crystallinity as evident in a single melting endotherm and crystalline reflections in wide-angle x-ray scattering. At this intermediate copolymer composition, this behavior suggests that co-crystallization of the ethylene and vinyl alcohol repeats is occurring, forming a "mixed crystal" [1, 2], since the vinyl alcohol repeats are essentially randomly distributed along the polymer chain (i.e. the average sequence length of VOH groups is less than 2). This "co-crystallization" behavior is rarely seen in random copolymers. An example is poly(ethylene-propylene) for which homopolymers of ethylene and propylene are both

crystalline and exhibit very different unit cells, such that, at intermediate compositions crystallization is frustrated (i.e. the copolymer is amorphous).

DSC traces and wide-angle x-ray diffraction data for a series of EVOH compositions that are commercially available (from EVALCA Co. and Polysciences, Inc.) are shown in Figures A.1 and A.2. The broad melting behavior exhibited by EVOH copolymers has been attributed to the short vinyl alcohol and ethylene sequence distribution in commercial samples (ave. run length < 3) [3]. The degree of crystallinity measurable in commercial EVOH copolymers has been found to be limited only by branching (0 VOH% is synthetically equivalent to LDPE) and does not significantly fall off with variation in composition. Levels of crystallinity as measured by DSC, WAXS, and nuclear magnetic resonance (NMR) ranged from 30 to 50% over the entire composition range (0 to 100% VOH) [4].

This data and studies presented by others suggest that the crystal lattices of EVOH with high vinyl alcohol content are isomorphous to that of pure poly(vinyl alcohol) and copolymers high in ethylene content are isomorphous to the polyethylene crystal lattice. For commercial blends, this was found to hold true for blends greater than 60 mol% vinyl alcohol and greater than 80 mol% ethylene, respectively [5, 6]. Ethylene units incorporated into the vinyl alcohol lattice essentially act as vacancy sites and cause a contraction in the d-spacings measured for EVOH high in VOH content (e.g. (101), ($10\bar{1}$), and (200)). Vinyl alcohol units conversely act as point defects and cause an expansion in the ethylene lattice (e.g. (110), (200) lattice spacings), see figure A.3. For compositions ranging from 20 and 60 mol% vinyl alcohol, it was proposed by others that the components crystallize into an intermediate pseudo-hexagonal crystal structure [6, 7]. Since we did not have access to materials whose composition was well into this intermediate range to confirm this assertion, studies on the partitioning of ethylene and vinyl alcohol residues in modified polyethylene and poly(vinyl alcohol)

lattices were performed using solid state ^{13}C NMR. These are presented in detail in a separate paper [4] and only conclusions of this work are summarized here.

Based on differences in proton rotating frame relaxation times in solid state ^{13}C NMR data collected for EVOH samples ranging from 10 to 68 mol% VOH, spectra characteristic of the crystalline and non-crystalline regions were isolated. Composition in both regions for the EVOH samples was found to be very close to stoichiometric indicating that there was not significant partitioning of the ethylene or vinyl alcohol residues. In the composition range from 0 to 20 mol% VOH, where the polyethylene lattice dominates, substitution of a hydroxyl group for a proton appears to be only a minor perturbation, and behaves like an interstitial defect. Similar behavior was observed for incorporation of ethylene groups into the poly(vinyl alcohol) lattice (e.g. vacancy type defect). Strong exclusion of short-chain branches from the crystalline regions (i.e. butyl groups) was still observed such as occurs in LDPE. Selective partitioning of VOH-VOH sequences from melt-crystallized samples was not observed; incorporation of all VOH blocks according to statistical availability into the crystalline PE occurred. For samples which were crystallized from isopropanol, modest preference for ethylene residues was observed for the crystalline regions. This partitioning most likely results from the lower solubility of ethylene-rich versus (vinyl-alcohol)-rich segments in the alcohol solvent. These results suggest that by altering the preparation conditions, crystal size and level (and hence properties) can be controlled by changing the concentration of defects associated with the copolymer residues at certain compositions.

REFERENCES

1. C.W. Bunn and H.S. Peiser, 'Mixed Crystal Formation in High Polymers', *Nature*, **159,** 161 (1947).

2. C.W. Bunn, 'Crystal Structure of Polyvinyl Alcohol', *Nature*, **160,** 929 (1948).

3. R.J. Koopmans, R. Van Der Linden and E.F. Vansant, 'Physical Properties of High-Pressure Ethylene Vinylacetate Copolymers and Their Saponified Derivatives,'*Polymer Engineering and Science*, **23,** 306 (1983).

4. D.L. VanderHart, S. Simmons and J.W. Gilman, 'Solid State 13NMR of Ethylene/Vinyl Alcohol Copolymers: Morphological Partitioning of Hydroxyls,'*Polymer*, (submitted 1994).

5. T. Matsumoto, K. Nakamae, N. Ogoshi, M. Kawasoe and H. Oka, 'Vinyl Alcohol Copolymers', *Kobunshi Kagaku*, **28,** 610 (1971).

6. T.K. Matsumoto, H. Nakamae, H. Oka, S. Kawarai and T. Ochiumi, 'The Microstructure of Ethylene-Vinyl Alcohol Copolymer', *Sen'i Gakkaishi*, **35,** T (1975).

7. T. Matsumoto, K. Nakamae, T. Oshiuni, S. Kawarai and T. Shoioyama, 'The Microstructure and the Viscoelastic Properties of Ethylene-Vinyl Alcohol Copolymers', *Sen'i Gakkaishi*, **33,** T (1977).

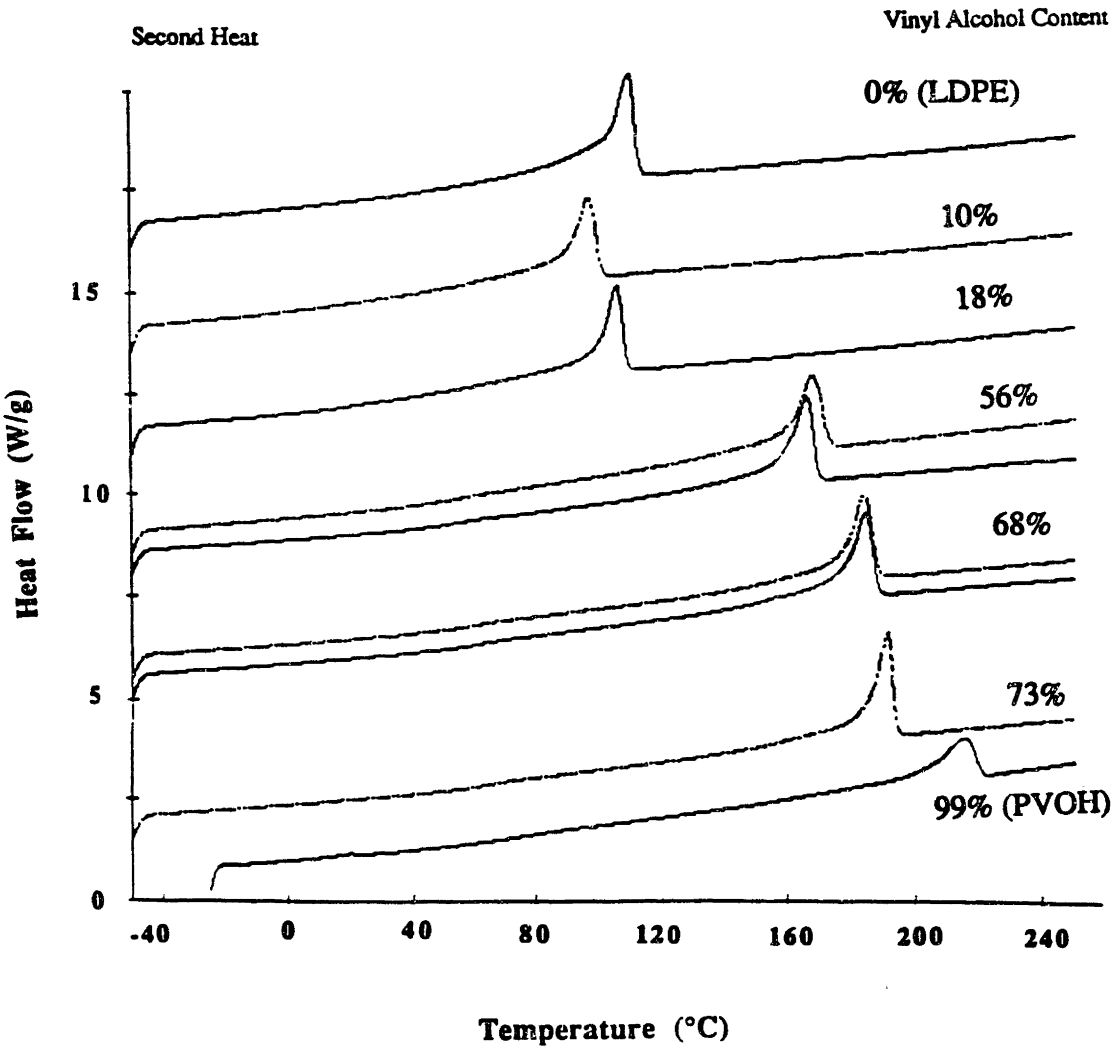

Figure A.1. Differential scanning calorimetry results (second heat) for poly(ethylene vinyl alcohol) as a function of vinyl alcohol content (0, 10, 18, 56, 68, 73, and 99+ mol% VOH). Scans were taken at a rate of 20°C/min (Al pans). Single melting endotherms are observed for all copolymer compositions.

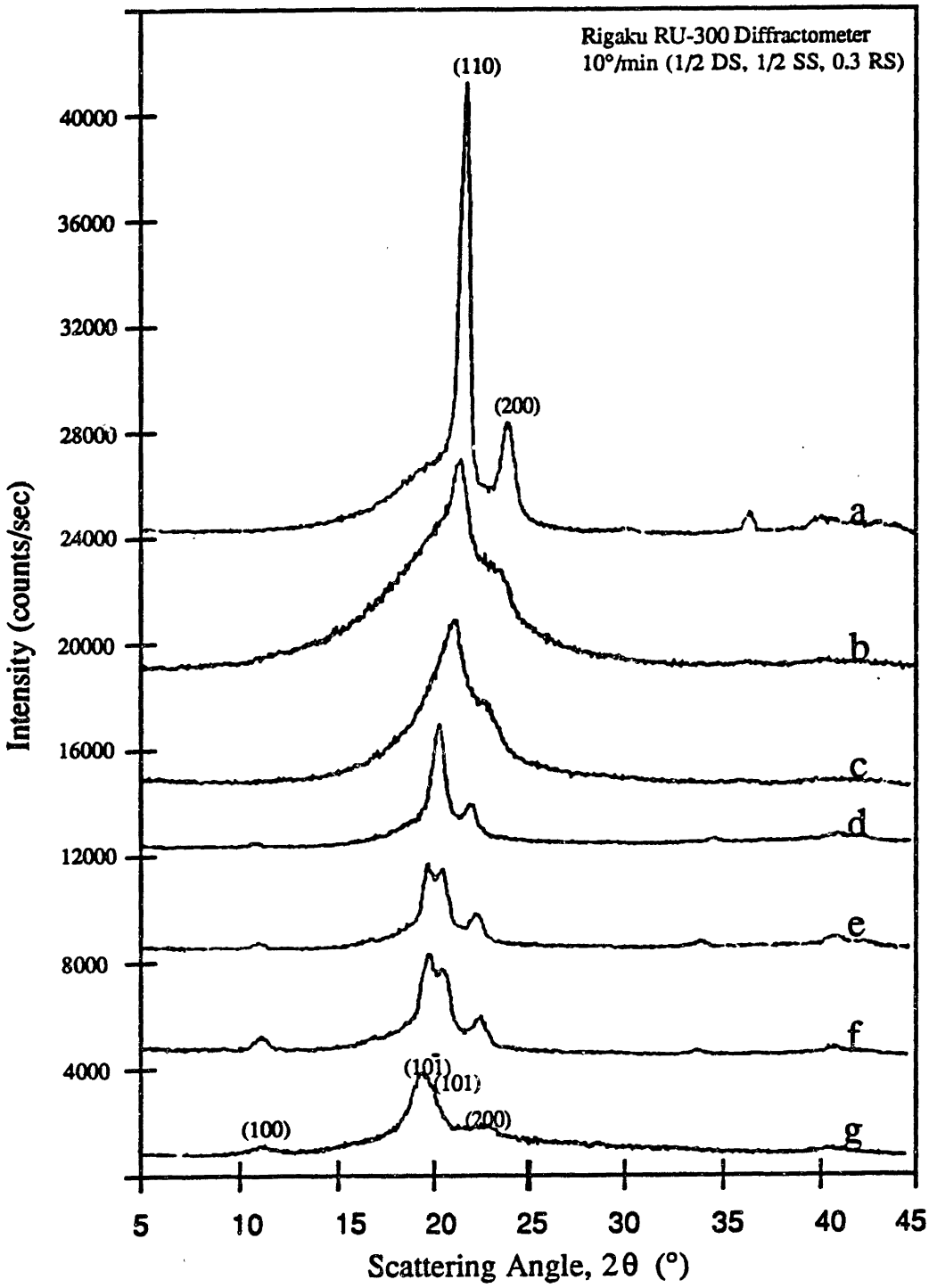

Figure A.2. Wide-angle x-ray diffractometry spectra for poly(ethylene-vinyl alcohol) of varying vinyl alcohol contents: a) 0 mol% (LDPE), b) 10 mol%, c) 18 mol%, d) 56 mol%, e) 68 mol%, f) 73 mol%, and g) 99+ mol% (PVOH). Corresponding Miller indices for LDPE and PVOH are shown in (a) and (g).

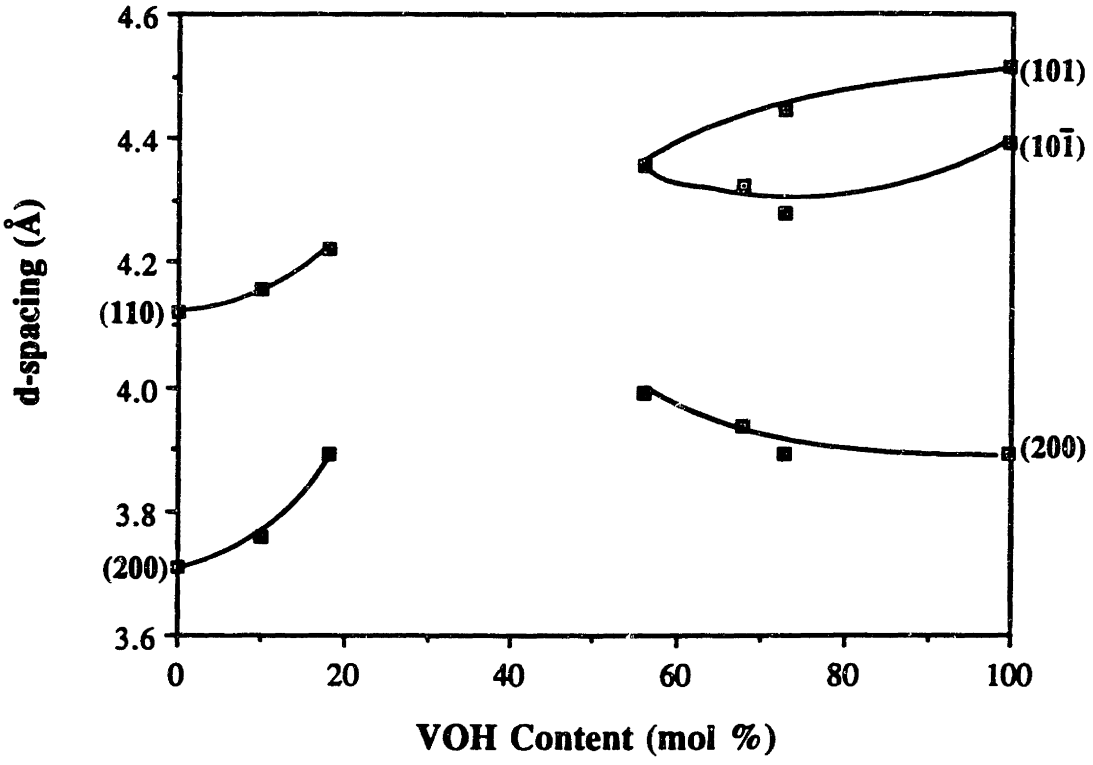

Figure A.3. Lattice spacings for poly(ethylene-vinyl alcohol) as a function vinyl alcohol content. Note: no samples were examined between 18 and 56% VOH.

Appendix B

Starch/EVOH Blown Films

While starch/EVOH processability was examined using fiber spinning as the model application in this thesis work, one of the product goals for starch-based biodegradable thermoplastics is the production of blown films to be used, for example, as packaging or as composting bags. Incorporation of higher levels of starch is desirable in order to attain faster rates of biodegradability. However, results shown in Chapter 5 indicate that both elongational flow and mechanical properties suffer as starch content is increased. Nevertheless, the film blowing of select model blends (i.e. HY50, NC50, NC30, and WM50) was investigated.

Pellets of the starch/EVOH blends were added to a C.W. Brabender single screw extruder (L/D = 24/1) fitted with a blown film die (ID = 2.54 cm, gap size = 0.05 cm). Processing conditions are given in Table B.1. Attempts at film blowing the HY50, NC50, NC30, and WM50 blends were successful. Films of thicknesses ranging from 40 to 65 μm were attainable (areal elongations, AE ~ 7.7 - 12.5). Detailed studies of the film blowing characteristics of starch/EVOH blends were performed by Dr. Peter Stenhouse at the Army Research Facility, Natick, MA. Preliminary results are presented in this Appendix in order to: 1) demonstrate that film blowing of starch/EVOH blends containing intermediate levels of starch is indeed possible and 2) illustrate the structural similarities of the blown films with melt spun fibers.

Scanning electron micrographs depicting the surface appearance of the films as blown and after submersion in boiling water for a period of 15 seconds are shown in Figures B.1 and B.2, respectively. Films prepared form Hylon VII and Native corn starch blends (figure B.1.a, b and d) exhibit a rough surface texture reminiscent of the surface textures observed for their melt spun fibers (see Chapter 5). However, in the

films starch-rich nodes are connected by EVOH-rich fibrils oriented in various directions (consistent with the biaxial extensional flows imparted on the blends). In the WM50 blend (figure B.1.c), a fibrous texture parallel to the machine direction was evident. Atomic force microscopy of the NC50 blown film revealed the surface roughness to be +/- 1.25 μm, somewhat comparable to the surface roughness evident in a NC50 melt spun fiber (see Figure 5.12). Similar to that of filaments and fibers, the surface of starch/EVOH blown films was not susceptible to enzymatic etching. This resistance may again suggest that the EVOH component also coats the surface of the blown films.

To compare the influence of hot water on the structure of starch/EVOH blends, the 'as blown' films were immersed for a period of 15 seconds in boiling water. Scanning electron micrographs displaying the film surfaces after they have been treated, dried, and coated with gold-palladium are shown in Figure B.2. For the NC50 and HY50 blends, a nodular surface is apparent (figures B.2a and B.2b). The observed surface texture of HY50 film is finer (nodules are less than 0.5 μm in size), than the surface of the NC50 on which nodules approximately 1 μm in size are observed. For the WM50 blend, the fibrous texture is lost after the boiling water treatment and larger variations in the surface structure are observed (figure B.2c). In figure B.2d, the NC30 film exhibits a more consistent coating; however, voids up to 3 μm in size are visible.

During immersion in boiling water, the film swells, some accessible starch-rich domains are dissolved, and EVOH is heated above its glass transition. EVOH-rich fibrils thus contract during this treatment and further coat the starch-rich domains that project outward on the film surface. The difference in surface microstructure between the HY50 and NC50 films is consistent with the smaller and more disperse starch-rich domains visible in the Hylon VII blends using TEM (see Chapter 4). Because EVOH is the majority component in NC30, the final surface of this film appears smoother after

hot water treatment due to the larger amount of EVOH present in the blend. The apparent difference in surface microstructure for the WM50 material compared with the NC50 and HY50 blends (i.e. no surface nodule formation) may be attributable to the increased susceptibility of the waxy-maize starch to dissolution (or dispersion) in water. The waxy maize domains, becoming saturated with the hot water that penetrates through cracks in the EVOH coating, swell and likely leach out onto the film surface. At longer times of immersion, the film integrity is destroyed (i.e. the film breaks into very small pieces). The HY and NC starch-rich domains are not as effected; both the NC and HY blends retain nodules since their starch-rich domains do not soften (flow) or swell as easily during boiling water treatment. Thus, the use starch in applications requiring some structural stability in water environments may be possible for blends at intermediate starch compositions if high amylose starches are employed.

Table B.1. Processing conditions employed during film blowing of select starch/EVOH model blends.

Sample	Max. Extrusion Temperature (°C)	Extruder Speed (rpm)	Blowing Pressure (psi)	Film Thickness (μm)
HY 50	148	30	0.47	65
NC 50	144	30	0.31	40
WM 50	134	30	0.25	50
NC 30	145	30	0.25	65

Figure B.1. Scanning electron micrographs of select starch/EVOH 'as blown' films: a) HY50, AE ~ 7.7, b) NC50, AE ~ 12.5, c) WM50, AE ~ 10; and d) NC30, AE ~ 7.7. (Specimens were coated with AuPd prior to viewing in SEM).

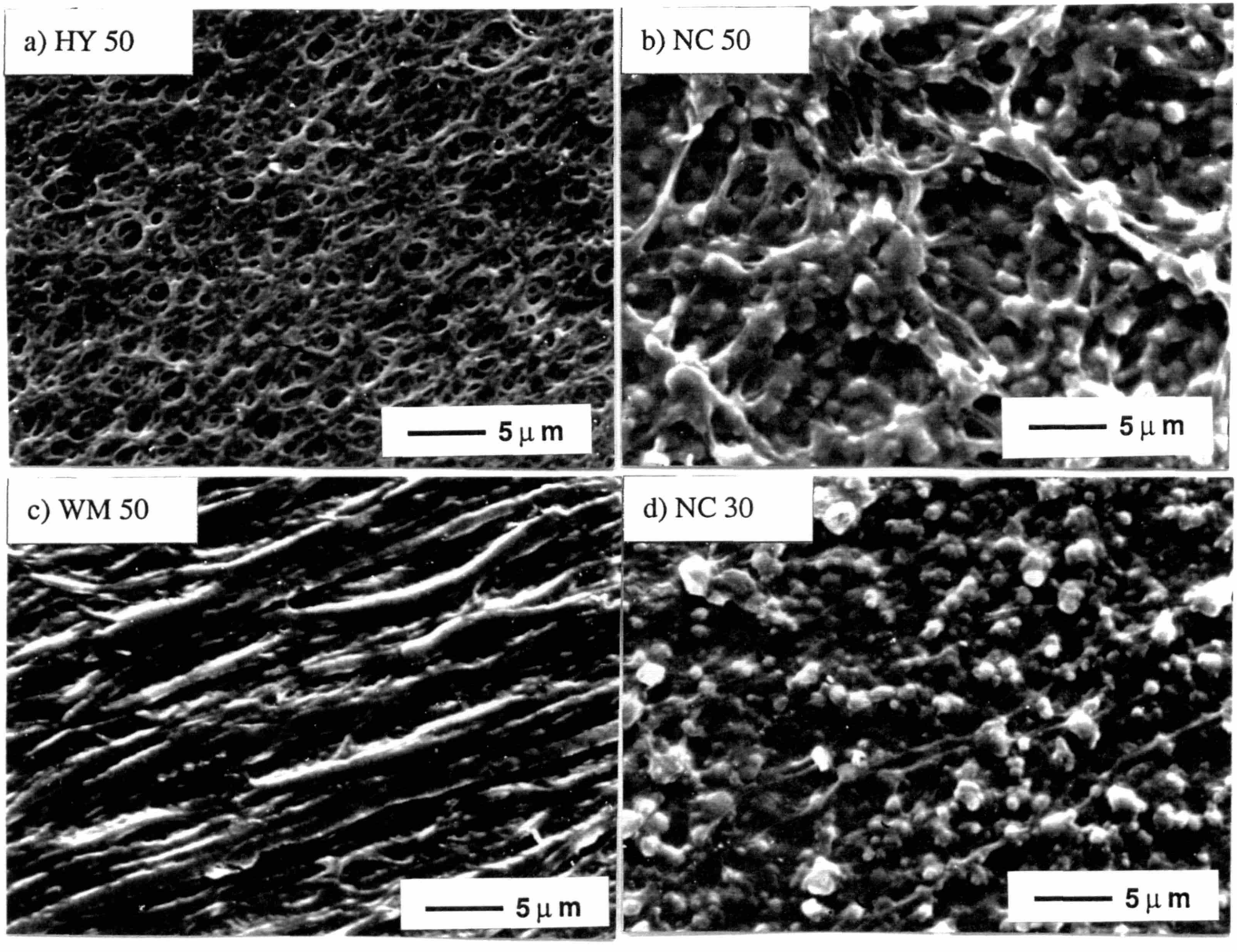
a) HY 50
5 μm
b) NC 50
5 μm
c) WM 50
5 μm
d) NC 30
5 μm

Figure B.2. Scanning electron micrographs depicting the surface structure of the starch/EVOH blown films (shown 'as blown' in figure B.1.) after immersion in boiling water for 15 seconds: a) HY50, b) NC50, c) WM50, and d) NC30. (Specimens were dried and then coated with AuPd prior to viewing in SEM.)

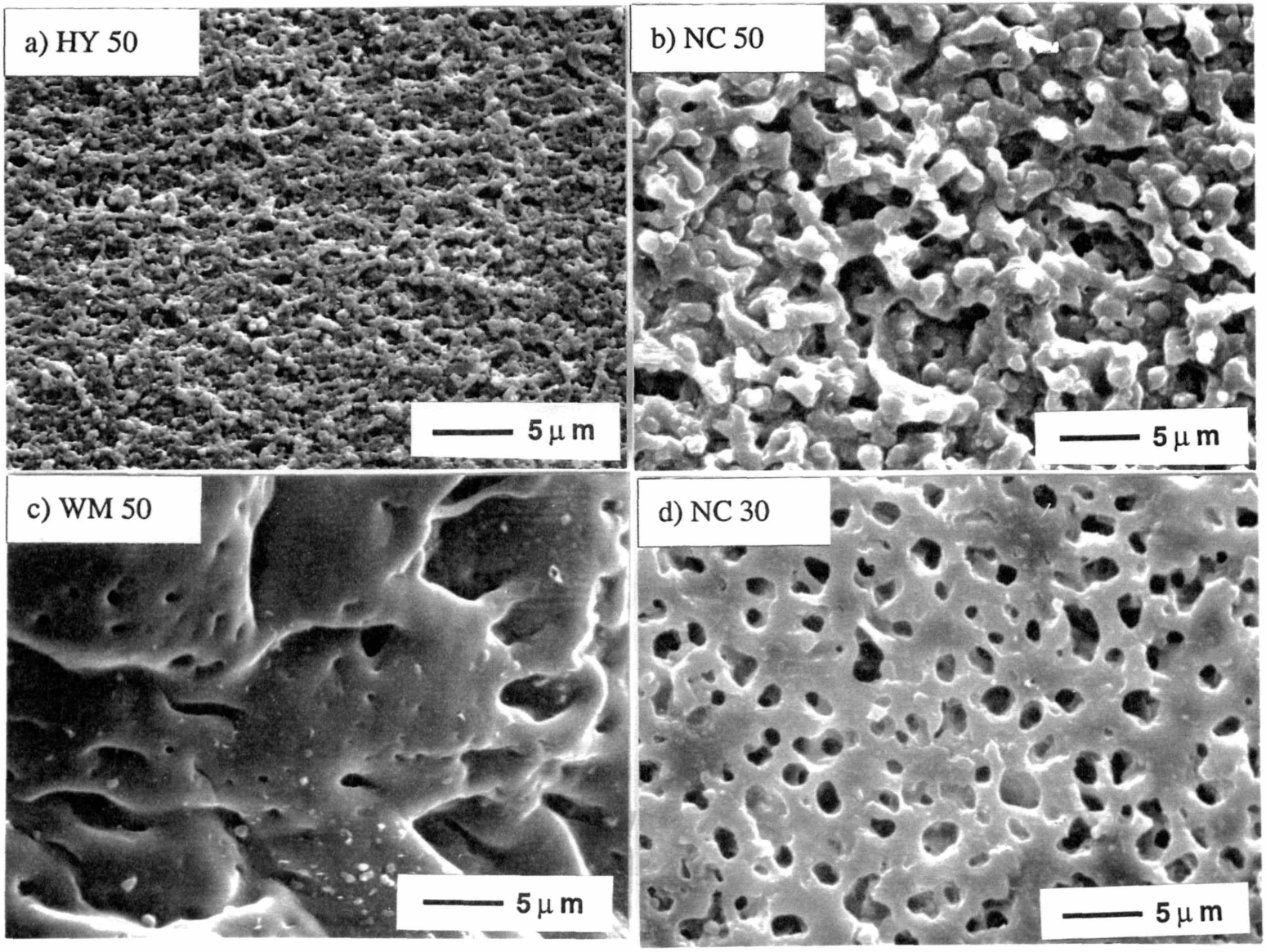
a) HY 50
5 μ m
b) NC 50
5 μ m
c) WM 50
5 μ m
d) NC 30
5 μ m